Titre: Title:	Mesohydrodynamics of suspensions of membranes
Auteur: Author:	Jian Feng Gu
Date:	2008
Type:	Mémoire ou thèse / Dissertation or Thesis
Référence: Citation:	Gu, J. F. (2008). Mesohydrodynamics of suspensions of membranes [Thèse de doctorat, École Polytechnique de Montréal]. PolyPublie. https://publications.polymtl.ca/8183/

NOTE TO USERS

UNIVERSITÉ DE MONTRÉAL

MESOHYDRODYNAMICS OF SUSPENSIONS OF MEMBRANES

JIAN FENG GU
DÉPARTEMENT DE GÉNIE CHIMIQUE
ÉCOLE POLYTECHNIQUE DE MONTRÉAL

THÈSE PRÉSENTÉE EN VUE DE L'OBTENTION
DU DIPLÔME DE PHILOSOPHIAE DOCTOR
(GÉNIE CHIMIQUE)
NOVEMBRE 2008

Your file Votre référence
ISBN: 978-0-494-47720-5
Our file Notre référence
ISBN: 978-0-494-47720-5

UNIVERSITÉ DE MONTRÉAL

ÉCOLE POLYTECHNIQUE DE MONTRÉAL

Cette thèse intitulée:

MESOHYDRODYNAMICS OF SUSPENSIONS OF MEMBRANES

présentée par: GU Jian Feng
en vue de l'obtention du diplôme de: Philosophiae Doctor
a été dûment acceptée par le jury d'examen constitué de:

M. DUBOIS Charles, Ph.D., président
M. GRMELA Miroslav, Ph.D., membre et directeur de recherche
M. FAVIS Basil, Ph.D., membre et codirecteur de recherche
M. BOUSMINA Mosto, Ph.D., membre et codirecteur de recherche
M. JOLICOEUR Mario, Ph.D., membre
M. TUCKER III Charles L., Ph.D., membre

Dedicated to my parents
and my family

ACKNOWLEDGEMENT

First of all I would like to express my deep and sincere gratitude to my research and thesis director, Professor Miroslav Grmela. Without his patience and kindness, as well as his academic experience, this thesis would not have been possible. I am thankful for his understanding and assistance to my family when my daughters were born.

I also wish to express my appreciation to my co-directors, Professor Basil Favis and Professor Mosto Bousmina. Professor Bousmina introduced me to the research project of the immiscible blends with surfactants, and gave me a lot of supports and instructions.

I am also grateful to Professor Charles Dubois and other professors in the Department of Chemical Engineering, who gave me generous help during my study in Polytechnique.

Beyond that, I am grateful to my fellow graduate students in the Department of Chemical Engineering, for their friendship and help. I would mention particular Mr. Nick Virgilio, Mr. Yunli Fang, Mr. Gang Li and Mr. Hassan Eslami.

Finally, I would like to express special thanks to my parents Qihao Gu, Yuexian Chen and my wife, Qi Qi Zheng. They helped me to concentrate on my study and completing this dissertation. Without their help and encouragement, this study would not have been completed.

RÉSUMÉ

Les fluides complexes sont omniprésents en science et en ingénierie. Les fluides biologiques, les mélanges immiscibles, les mousses et plusieurs types de suspensions sont des exemples typiques de fluides complexes. Leur structure interne (i.e. les particules en suspension dans un liquide ou les interfaces dans les mélanges immiscibles) change dans le temps sur une échelle temporelle comparable à celle de leur mouvement macroscopique. L'évolution temporelle macroscopique est donc couplée à l'évolution temporelle de la microstructure. C'est ce couplage qui cause la complexité des phénomènes d'écoulement des fluides complexes.

L'objet de cette thèse concerne les suspensions avec des interfaces ou des membranes élastiques. Elles incluent les interfaces entre deux liquides, les interfaces liquides couvertes avec des agents tensioactifs et les membranes solide-liquide des globules rouges du sang. Le point de départ généralement rencontré pour ce type d'analyse théorique des fluides complexes est la microhydrodynamique. Le formalisme peut être adapté soit pour des simulations numériques directes, soit pour une formulation de champs. Dans les deux cas, une puissance numérique significative est nécessaire pour résoudre les équations gouvernantes. Pour finalement obtenir des prédictions sur les propriétés en écoulement, il est nécessaire d'inclure des concepts physiques supplémentaires et des approximations qui permettent de transformer les solutions (qui donnent en général les trajectoires des particules individuelles ou les déformations d'une particule individuelle) en contraintes présentes dans les fluides.

L'approche que nous utilisons dans cette thèse est de type mésoscopique. Le point de départ est un modèle mésoscopique de la structure interne. La physique qui gouverne les fluides complexes est alors exprimée en équations gouvernantes du modèle rhéologique en suivant un cadre thermodynamique (GENERIC). Dans la plupart des cas, les équations gouvernantes sont une série d'équations différentielles ordinaires qui peuvent être résolues en utilisant un logiciel standard. Les prédictions de nos modèles concordent bien avec les résultats expérimentaux observés et les prédictions des modèles basés sur la microhydrodynamique.

ABSTRACT

Complex fluids are ubiquitous in science and engineering. Biological fluids, immiscible blends, foams, and many types of suspensions are familiar examples of complex fluids. Their internal structure (e.g. suspended particles in suspensions or the interface in immiscible blends) evolves in time on the time scale that is comparable with the time scale of the macroscopic motion. The macroscopic time evolution has to be therefore coupled to the microstructure time evolution. Such coupling then causes the complexity of the flow phenomena.

This thesis focuses on suspensions of interfaces or elastic membranes. They include the clean interface between two liquid bulks, liquid interfaces covered with surface active agents, and solid-liquid membranes of red blood cells. The popular point of departure of a theoretical analysis of this type of complex fluids is microhydrodynamics. The formulation can either be made into a basis for direct numerical simulations or it can be carried to a field formulation. In both cases an extensive computer power is needed to solve the governing equation. To pass finally to predictions of flow properties one needs to involve still an additional physics and approximations that allow to transform the solutions (addressing typically trajectories of individual particles or a single particle deformations) into stresses arising in the fluids.

The approach that we use in this thesis is mesoscopic. The starting point is a mesoscopic model of the internal structure and of the physics taking place in the fluid. The physics is then expressed into governing equations of the rheological model by following the thermodynamic (GENERIC) framework. In most cases, the governing equations are just a set of ordinary differential equations that can readily be solved by using a standard software. Predictions of our models are found to be in a good agreement with results of experimental observations and predictions of the models based on microhydrodynamics.

CONDENSÉ EN FRANÇAIS

Les fluides complexes sont les fluides qui possèdent une structure interne avec une longueur caractéristique mésoscopique. Ils représentent un famille nombreuse incluant, par exemple, les solutions de polymères, les polymères fondus, les fluides biologiques, les mélanges immiscibles, les mousses et une variété de suspensions. Une structure est dite mésoscopique lorsque sa longueur caractérisque est grande comparativement aux dimensions d'une molécule mais petite comparativement aux inhomogénéités macroscopiques. La structure interne mésoscopique des fluides complexes donne lieu à des écoulements aux propriétés macroscopiques inhabituelles.

Cette thèse porte sur l'étude rhéologique de suspensions de particules liquides encapsulées par une membrane. Les membranes telles que définies ici incluent les interfaces liquide-liquide dans les mélanges immiscibles et les membranes biologiques telles que rencontrées dans les fluides biologiques et biomédicaux. Les membranes biologiques incluent celles des globules rouges du sang et des microorganismes aquatiques qui existent dans la nature ou dans les bioréacteurs artificiels.

Le comportement rhéologique macroscopique d'une suspension est décrit par la relation entre les réponses en contraintes et le taux de déformation induit par le champ d'écoulement appliqué. Ce comportement est principalement contrôlé par les propriétés du matériau et la morphologie de la suspension. Les divers composants du matériau incluent entre autres les différentes phases, de même que les interfaces et membranes. Pour un mélange immiscible composé de deux liquides newtoniens, même si les deux liquides sont des liquides simples, le mélange montre un comportement non newtonien (par exemple, un comportement rhéo-fluidifiant, une différence des contraintes normales non nulle, le dépassement ou " overshoot " observé dans un écoulement transitoire et les réponses non linéaires en fréquences pour des écoulements oscillatoires. De plus, la complexité des réponses du fluide lorsque l'écoulement est imposé par une contrainte externe augmente lorsqu'un agent tensioactif est localisé à l'interface. Non seulement la valeur de la tension interfaciale diminue, elle n'est plus constante mais devient une fonction de la position à l'interface. Des gradients de la tension interfaciale, c'est-à-dire les forces de Marangoni, se développent lorsque l'agent tensioactif est non uniformément

distribué à l'interface. De plus, les forces de Marangoni modifient les perturbations du champ d'écoulement. Conséquemment, le couplage entre ces deux effets rend le comportement rhéologique de ces émulsions très complexe. L'addition d'agents "compatibilisants" dans les mélanges de polymères est la méthode la plus commune pour améliorer les propriétés physiques de ces matériaux. L'effet sur la mise en forme et l'optimisation des propriétés des matériaux finaux sont les deux questions importantes qui émergent au niveau de l'ingénierie des matériaux polymères.

Un exemple représentatif d'une membrane biologique est la membrane des globules rouges du sang. Comme les globules rouges occupent normalement environ la moitié du volume du sang, la déformabilité de la membrane a un effet critique sur la circulation du sang à travers les vaisseaux sanguins, et spécialement les vaisseaux capillaires. Parmi les facteurs qui influencent la déformabilité des globules rouges, les plus importants sont les propriétés des matériaux et la forme de la membrane qui encapsule chaque globule. La membrane des globules rouges peut être comparée à un cytosquelette recouvert par une bicouche lipidique. Elle démontre de plus un comportement solide-liquide. L'étude des suspensions de globules rouges permettra d'élucider comment ces propriétés influencent la rhéologie. À l'inverse, les mesures rhéologiques macroscopiques permettront de déterminer les propriétés des suspensions. La connaissance de la relation morphologie-rhéologie pourra ensuite être utilisée, par exemple, pour discriminer les globules anormaux ou pathologiques des globules sains ou pour tester un sang contenant des globules artificiels.

L'objectif principal de cette thèse est d'étudier théoriquement l'influence des propriétés mécaniques des membranes sur la rhéologie des suspensions. Notre but est de développer des modèles mathématiques permettant d'obtenir de meilleures prédictions par rapport aux modèles existants. Plusieurs modèles rhéologiques seront proposés pour plusieurs types de membranes retrouvées dans les suspensions.

Les méthodes de modélisation des suspensions membranaires que l'on retrouve dans la littérature peuvent être divisées en deux catégories: 1) microhydrodynamique et 2) mésohydrodynamique. Parmi les méthodes microhydrodynamiques les plus connues, citons la théorie de Taylor, la théorie de Cox, le modèle de Choi et Schowalter et la théorie de Palierne, ainsi que plusieurs types de méthodes de

simulation numérique directes. Le procédé menant aux équations gouvernantes est direct. Il consiste à écrire les équations gouvernantes et les conditions aux frontières pour ensuite les résoudre numériquement. Les équations gouvernantes sont celles de Navier-Stokes, ou équations de Stokes pour de faibles nombres de Reynolds, pour les fluides à l'intérieur et à l'extérieur de la membrane. Les conditions frontières établissent la continuité de la vitesse et l'équilibre des forces à la membrane ainsi qu'à l'infinité. Le désavantage de cette méthode réside dans la difficulté de résolution des équations gouvernantes. Les solutions analytiques ne sont possibles que pour un nombre restreint de cas limites pour des frontières simples et de petites déformations pour une seule gouttelette. Les solutions complètes et détaillées nécessaires pour prédire les propriétés en écoulement ne peuvent être obtenues qu'après des calculs numériques complexes. De plus, il existe des différences entre le comportement d'une seule gouttelette à un niveau microscopique et le comportement d'une entière population de gouttelettes à un niveau macroscopique. Pour résoudre ce problème, des simplifications additionnelles et des suppositions (par exemple la formule de la contrainte de Batchelor pour les suspensions diluées) sont nécessaires.

En comparaison, la méthode mésohydrodynamique est basée sur une description mésoscopique d'un fluide complexe. Cette méthode est apparue récemment et remonte au modèle de Doi-Ohta de 1991 et au modèle de Maffettone-Minale de 1998. Dans le modèle de Doi-Ohta, l'interface est caractérisée par deux variables: un scalaire Q et un tenseur $\boldsymbol{q}$. Elles peuvent être associées aux seconds moments des fonctions de distribution de l'orientation de la membrane. Elles donnent une image à grains grossiers des interfaces. Le modèle de Maffetone-Minale utilise un tenseur trois par trois du second ordre pour décrire la forme d'une gouttelette de forme ellipsoïde. Les deux méthodes ne décrivent pas la position et la forme exacte de l'interface.

Cette thèse est basée sur la méthode mésoscopique. Nous avons étudié de nouveaux types de suspensions (par exemple des mélanges immiscibles avec l'addition d'agents tensioactifs qui n'ont pour l'instant pas été étudiés dans un contexte mésoscopique) en utilisant une approche thermodynamique (GENERIC) qui nous a permis d'obtenir en même temps les équations d'évolution temporelle de la microstructure compatibles avec le tenseur d'extra-contraintes. L'avantage de l'approche GENERIC est qu'elle garantit la compatibilité des solutions avec cer-

taines observations expérimentales (lois de conservation, compatibilité avec la thermodynamique et compatibilité avec la mécanique), ainsi que l'émergence automatique du tenseur de contraintes. Nous n'avons pas besoin de suppositions et d'analyses additionnelles qui pourraient résulter en une expression incomplète ou incompatible des contraintes avec les équations de l'évolution temporelle de la microstructure. Un autre avantage de cette approche est que les équations gouvernantes finales sont généralement un ensemble d'équations différentielles ordinaires qui peuvent être facilement résolues avec un logiciel standard. Une comparaison quantitative des résultats expérimentaux avec les prédictions des modèles montre que cette approche est apte à prédire le comportement rhéologique des fluides complexes ayant des membranes.

Cette thèse est organisée dans un ordre progressif en terme de la complexité des membranes dispersées en solutions. Premièrement, la rhéologie des mélanges immiscibles de deux fluides newtoniens est étudiée. L'interface est à la fois déplacée par advection par l'écoulement imposé et perturbe également celui-ci. La perturbation change ensuite l'advection (elle la change en une advection non affine). Nous avons combiné une approche mésoscopique (développée avec une approche thermodynamique (GENERIC)) à l'advection active. La méthode est ensuite utilisée dans le chapitre suivant pour étendre l'applicabilité du modèle de Doi-Ohta. Par la suite, nous avons étudié une situation plus complexe dans laquelle un mélange immiscible est modifié par la présence d'un agent tensioactif. Un nouveau modèle fut développé en combinant le tenseur de forme avec la microhydrodynamique d'une gouttelette couverte de l'agent tensioactif. Même si ce modèle donne de bons résultats au niveau des prévisions, il n'est applicable que pour de petites déformations. Ensuite, un modèle mésoscopique complet est développé en utilisant une famille de tenseurs de forme à un paramètre comme variables d'état. Finalement, nous avons utilisé cette approche mésoscopique pour discuter du sujet de la rhéologie du sang humain.

Dans cette thèse, nous avons développé une approche systématique permettant de déterminer de manière analytique au moins quelques-uns des coefficients. Cette méthode consiste à combiner la solution asymptotique des modèles mésoscopiques avec l'analyse perturbatoire de la microhydrodynamique. Les modèles mésoscopiques résultants recouvrent les résultats de la microhydrodynamique pour certains cas limites et améliorent les prédictions pour les situations

plus générales.

Dans tous les chapitres, nous calculons les conséquences morphologiques et rhéologiques des nouveaux modèles et les comparons aux observations expérimentales et aux prédictions des autres types de modèles. Une revue compréhensive des travaux de recherche expérimentaux, qui constitue la base de notre compréhension physique des membranes en suspension, est présentée dans le Chapitre 1.

Parmi les travaux futurs qui peuvent être considérés, mentionnons:

1. D'autres modèles mésoscopiques rhéologiques (par exemple ceux utilisés dans la modélisation de suspension de fibres) qui peuvent être développés en adoptant l'advection active.

2. Pour la modélisation rhéologique mésoscopique de mélanges immiscibles avec interfaces couvertes avec un agent tensioactif, nous pouvons considérer des situations plus réalistes dans lesquelles la convection de l'agent tensioactif est complètement couplée avec la morphologie de la gouttelette. Un autre sujet intéressant est l'étude de l'influence de l'élasticité des phases sur la rhéologie des gouttelettes couvertes avec l'agent tensioactif.

3. L'étude des effets du rapport de viscosité des phases et de l'élasticité en flexion de la membrane sur la rhéologie des suspensions de globules rouges.

Contents

List of Tables

List of Figures

NOMENCLATURE

a	semiaxis of an ellipsoid; diameter of a sphere
b	semiaxis of an ellipsoid
c	semiaxis of an ellipsoid
$\boldsymbol{c}$	conformation tensor
Ca, $\mathcal{C}$	capillary number
C_2	$\boldsymbol{q}$-modulus
$\boldsymbol{D}$	rate of deformation tensor
E	energy
D_f	deformation parameter
D_s	diffusivity
E_s	shear modulus of membranes
$\boldsymbol{G}$	shaper tensor
G^*	complex modulus
G'	storage modulus
G''	loss modulus
$\boldsymbol{g}_\phi$	surface matric tenor
H	mean curvature; modulus
K	nK_BT; dilation modulus
K_B	Boltzmann constant
L	Poison bivector
L_{ij}	velocity gradient
$\boldsymbol{n}$	unit normal of an interface
N_1	first normal stress difference
N_1	second normal stress difference
p	hydrostatic pressure; viscosity ratio
p_{eff}	effective viscosity ratio
P_e	Peclet number
$\boldsymbol{q}$	deformation tensor of interfaces
Q	area density
R	gas constant
S	entropy
$\boldsymbol{r}$	position vector

t	time
T	temperature
$\boldsymbol{u}$	momentum
$\boldsymbol{v}$	velocity
$\boldsymbol{v}_t$	tangential interfacial velocity
$\boldsymbol{v}_n$	normal interfacial velocity
X	thermodynamic force
$\boldsymbol{W}$	vorticity tensor

ABBREVIATION

BBR	Barthes-Biesel and Rallison model
DO	Doi-Ohta model
FA	Frankel-Acrivos model
GENERIC	General Equations for Nonequilibrium Reversible-irreversible Coupling
LP	Lee-Park model
MM	Maffettone-Minale model
PIB	polyisobutene
PDMS	polydimethylsiloxane
PVP	polyvinylpyrrolidone
RBC	red blood cell
WOE	Wagner-Ottinger-Edwards model

GREEK LETTERS

β	elasticity number
γ	shear strain; property number
$\dot{\gamma}$	shear rate
Γ	interfacial tension
η	viscosity
θ, φ	orientation angle
Λ	dissipation coefficient
Ξ	dissipation potential

ρ	concentration of mass
$\boldsymbol{\sigma}$	stress tensor
τ	relaxation time
ϕ	polar angle; volume fraction
Φ	free energy
Ψ_1	first normal stress coefficient
Ψ_2	second normal stress coefficient
ω	frequency

Introduction

0.1 Suspensions of membranes

Complex fluids are the fluids that possess an internal structure with a mesoscopic length and time scales. They include, for example, polymer solutions, polymer melts, biological fluids, immiscible blends, foams, and a variety of suspensions. We say that a structure is mesoscopic when its length scale is large if compared with the length of molecules and small relative to the length scale of macroscopic inhomogeneities. The presence of the internal mesoscopic structure gives rise to unusual macroscopic flow properties of complex fluids.

This thesis focuses on the rheological studies of suspensions of liquid particles which are enclosed or separated by membranes. The membranes include both the liquid interfaces in immiscible blends and biological membranes encountered in biological fluids. The biological membranes include the membrane of red blood cells and of aquatic micro-organisms existing in the natural environment or an artificial environment created in bioreactors.

The macroscopic rheological behavior of suspensions, i.e. a relationship between the stress responses and the input deformation rates of the applied flow field, is controlled by the material properties and by the morphologies of the components of the suspension. The components include the bulk phases as well as the membranes. Even the immiscible blends composed of two Newtonian simple fluids exhibit non-Newtonian behavior (for example, they show shear thinning, nonzero first normal stress difference, an overshoots under the transient flows and nonlinear frequency responses in oscillatory flows). This is because of the presence of the interface in such fluids. The complexity of responses of fluids to externally imposed flows increases if the surface active agent, residing mainly on the interface, is added. Not only the value of the interfacial tension is reduced but also it is no longer the same on different locations of the interface. Gradient of the interfacial tension, i.e. the Marangoni stress, arises when the surface active agent is nonuniformly distributed on the interface. This always happens as a result of the driving force of the imposed flow. In addition, the Marangoni stress changes also the perturbation in the flow fields. Consequently, the coupling between these

two effects results in a very complex rheology. Addition of compatibilizers into polymer blends is the most commonly used method to improve the physical properties of the resulting materials. How does this addition influence the processing of the polymers, and how shall we optimize the properties of the final products are two important questions arising in polymer engineering.

Beside the liquid membranes or interfaces that are common in blends and emulsions composed of immiscible bulk fluids, there is another kind of membranes behaving both like a liquid and a solid. A representative example of such membranes is the membrane of red blood cells. Since the red blood cells normally occupy about 42-45% of the blood volume, their deformability has a critical effect on the circulation of the blood through the blood vessels, especially then capillary vessels. Among all the factors that influence the deformability of the red blood cells, the most important are the material properties and the shape of the membranes that encapsulate the cell. The membrane of red blood cells can be roughly looked upon as a cytoskeleton network covered by a lipid bilayer. It exhibits both the solid and the liquid behavior. The properties of the RBC membrane can be characterized by the area elasticity, shear elasticity, bending elasticity and shearing viscosity. The study on the suspension of red blood cells helps to elucidate how these properties influence the rheology and vice versa how can results of the rheological measurements determine the morphology of the cells. A knowledge of the morphology-rheology relation can be then used, for example, to discriminate between the abnormal or pathological cells and the normal healthy cells.

0.2 Objective and methodology

The objective of this thesis is to study theoretically the influences of mechanical properties of membranes on the rheology of their suspensions. Our goal is to develop mathematical models that give better predictions than the models reported in the literature. Several new rheological models are proposed for several types of membranes involved in suspensions.

The methods for the modeling of the suspension of membranes reported in literatures can be classified in two categories: microhydrodynamics and mesohydrodynamics. Among the well known microhydrodynamic theories we men-

tion in particular Taylor's theory, Cox's theory, Choi and Schowalter model and Palierne's theory, and many types of direct numerical simulation methods. The process leading to the governing equations is straightforward. It consists of writing down the classical hydrodynamic equations together with appropriate boundary conditions and then of solving them numerically (see Chapter 4). The governing equations are the Navier-Stokes equations (or Stokes equations for low Reynolds numbers) for fluids inside and outside the membrane. The boundary conditions express the continuity of the velocity and the force balance at the position of the membrane. The advantage of this method is that it is usually easy to set up the equations and to identify the material parameters involved in them. The parameters arise as a result of independent microhydrodynamic measurements. The disadvantage of this method is that the governing equations are very difficult to solve. Analytical solutions are only available for a few simple boundaries and small deformations of a single droplet. Detailed complete solutions (even for a single droplet or a small piece of the interface), needed to predict flow properties, can only be found after making complex numerical calculations. In addition, there still remains a gap between the behavior of a single droplet on the microscopic scale and the behavior of a population of droplets on the macroscopic scale. To solve this problem, additional simplifications and assumptions (e.g. Batchelor's stress formula for dilute suspension) are needed.

The mesohydrodynamic method on the other hand is based on the mesoscopic description of a complex fluid system. This method has emerged only recently and dates back to Doi-Ohta model in 1991 and Maffettone-Minale model in 1998. In the Doi-Ohta model the interface is characterized by two state variables, one scalar Q, and one traceless symmetric tensor $\boldsymbol{q}$. They can be looked upon as being second moments of the distribution functions of the membrane orientation. They give a coarse-grained picture of the interfaces. The Maffettone-Minale model uses a three by three second order tensor to express the shape of an ellipsoid-like droplet. Both methods are not concerned with the exact location and exact shape of the interface.

In this Thesis we follow the mesoscopic method. We investigate new types of suspensions (for example we investigate immiscible blends in the presence of surface active agents that have not been so far investigated in a mesoscopic setting) and use the thermodynamic (GENERIC) framework that allows us to arrive

simultaneously at the microstructure time evolution equations and a compatible with it expressions for the extra stress tensor. The GENERIC framework is presented in all chapters below. The advantage of the GENERIC framework is that it guarantees the agreement of solutions with three experimental observations: conservation laws, compatibility with thermodynamics, and compatibility with mechanics. Moreover, the stress tensor emerges automatically. We do not need additional assumptions and analysis which may possibly make the resulted expressions for the stress incomplete or incompatible with the microstructural time evolution equations. Another advantage of this approach is that the final governing equations are usually just a set of ordinary differential equations that can be readily solved with standard software packages. The disadvantage of the mesoscopic approach is that the material parameters quantifying the physics introduced into the free energy and the dissipation potential may be only partially determined analytically. The remaining parameters have to be obtained from rheological and morphological (made on the mesoscopic level) measurements.

Quantitative comparison of experimental data with the predictions of models shows the ability of this approach to predict the rheological behavior of complex fluids with membranes.

0.3 Organization of the thesis

This thesis is organized into chapters by progressively increasing complexity of the membranes.

First, the rheology of immiscible blends of two Newtonian fluids is studied. This is the simplest case of membrane suspensions. The physical property of the liquid membrane is characterized only by a single constant, namely the interfacial tension. The interface is both advected by the imposed flow and perturbs it. The perturbation then changes the advection (it changes it into a nonaffine advection). In Chapter 2 we are introducing a mesoscopic approach (developed in the thermodynamic (GENERIC) framework) to the active advection. The method is then used in Chapter 3 to extend the Doi-Ohta model. In Chapters 4 and 5 we investigate immiscible blends covered by a surface active agent. The standard microhydrodynamic approach involving only a few elements of the mesoscopic

viewpoint is presented in Chapter 4. A complete mesoscopic model is developed in Chapter 5. Finally, in Chapter 6, we use the mesoscopic approach to discuss rheology of human blood.

In all chapters we always calculate both the morphological and the rheological consequences of the new models and compare them with experimental observations and predictions of other models. The experimental investigations that we use to provide us with experimental data are reviewed in every chapter. In addition, a comprehensive review of the experimental research constituting the basis of our physical understanding of membrane suspensions is presented below in Chapter 1.

Chapter 1

Review of Experimental Observations

1.1 Immiscible blends in the absence of surface active agents

Simple fluids without a microstructure are well described by the Newtonian constitutive relation. The only material parameter that is needed to characterize the rheological behavior of an incompressible isothermal simple fluid is a constant viscosity coefficient. Immiscible blends involving an interface are examples of complex fluids. Important features of their rheological behavior are summarized below.

1.1.1 Start-up shear flows

The start-up shear flow is one of the viscometric flows that are often used to study the transient behavior. When a Newtonian droplet at rest is suddenly subjected to flow it undergoes, in general, several stages of morphological changes [1, 2]. At the first stage, the spherical droplet deforms slightly and takes an ellipsoidal-like shape. At the same time, it orients itself with a angle of approximately 45° to the flow direction. At the second stage, the droplet continues to deform into a shape resembling more a cylinder. At the third stage, the cylinder either breaks up into two droplets or grows into a long and thin fibril. The droplet morphology

is determined by the viscosity ratio ($p = \eta_d/\eta_m$, the ratio of the viscosity of the droplet to that of the matrix), the capillary number ($Ca = \frac{\eta_m \dot{\gamma} R}{\Gamma}$, with $\dot{\gamma}$ denotes the shear rate, R the radius of the droplet and Γ the interfacial tension), and the nature of the flow (shear or elongation). In the case of small capillary numbers, i.e. small droplets with large interfacial tension and viscosity under a weak flow, the interfacial morphology may just undergoes the first stage [4]. In the shear flow the droplet can break up only for viscosities are smaller than a certain value (about 3.8). On the other hand, in elongational flows the droplets can break up for any viscosity ratio [3]. The critical capillary number for a single droplet to rapture are measured by Grace [3] and formulated by de Bruijn [5].

The above three-stage morphology evolution for a single droplet does no longer exist for a non dilute emulsions. Droplet-droplet interactions lead to the coalescence. Experimental studies carried out by Wieringa et al. [6] and Jansen et al. [7] show that the critical capillary number for break up decreases by more than one order of magnitude in concentrated emulsions. Moreover, drops with viscosity ratio $p > 4$, which are known to resist the break up in single drop experiments, do show breakup at elevated emulsion concentrations. At high concentrations, the coexisted processes of breakup and coalescence can also result in a complex morphology called a co-continuous structure of interfaces [8, 9]. In this case there is no distinct definition of droplet and matrix since two bulk fluids are entangled and penetrate into each other.

As to the rheology, for Newtonian fluids a constant stress is established immediately after starting the flow. The viscosity coefficient is time independent. However, for emulsions, as flow is applied the shear stress first raises sharply to a maximum value and forms an overshoot before decreasing, sometimes showing an undershoot, and finally leveling off to a steady value [10, 11]. The magnitude of the overshoot and the undershoot are related to the capillary number. The larger the capillary number the larger the overshoot and the undershoot. Newtonian fluids do not show any elasticity. Emulsions however exhibit nonzero first normal stresses difference. It usually increases slowly with time, undergoes an overshoot for larger capillary number, and reaches eventually a steady value [10, 11]. This nonlinear and elastic behavior of immiscible blends is correlated to the morphological evolution of the interface.

1.1.2 Steady shear flows

The steady shear experiments investigate the steady-state behavior of complex fluids in dependence on the applied shear rate. Unlike the Newtonian fluid with a constant viscosity, the emulsions exhibit shear thinning, i.e. the viscosity shows a plateau at low shear rates and a decrease as the shear rate increases [14, 12]. This can be explained by the morphological changes. As the shear rate increases, the droplet attains at steady state a more deformed shape. Its cross section is reduced and the interface aligns more towards the flow direction. This then leads to a decrease in the hydrodynamic drag of droplets and consequently to a decreased viscosity. The increase in the deformation of the droplets results also in an increase of the first normal stress difference because the deformed interfaces stores some elastic energy that brings the droplet to its equilibrium spherical shape if the flow stops.

For a given shear rate, there is a unique steady-state size of a single droplet. This is not true however for emulsions. Janssen [13] observes that there exists a region of shear rate where the multiple steady-state droplet sizes can coexist. The actual sizes are dependant on the initial conditions and on the flow history. This is because of the dynamic balance between the breakup and coalescence of the droplets.

When an emulsion is sheared, the steady state droplet size does not have to always decrease. It can even increase due to the coalescence among droplets if the shear rate is small enough. Smaller droplets are more likely to coalescence than larger ones. The maximum droplet size for coalescence and the minimum droplet size for breakup coincide at a critical shear rate. Above this shear rate, since the minimum droplet size for breakup is smaller than the maximum droplet size for coalescence, a balance between the coalescence and breakup leads to a unique droplet size at a certain shear rate. However, below the critical shear rate, since the maximum droplet size for coalescence is smaller than the minimum droplet size for breakup, droplets with its size located in this region could all possibly exist. This produces the phenomenon called morphological hysteresis (Minale et al. [15, 16]).

1.1.3 Small amplitude oscillatory shear flows

This experiment measures the time dependent response of fluids to small amplitude sinusoidal shear flow with a frequency ω. The measured quantities are storage modulus (G') which describes the elasticity and loss modulus (G'') which describes the viscosity of the sample. Using a small strain ensures that: (i) the droplet remains nearly spherical, (ii) the stress response is linear in strain, and (iii) the droplet breakup and coalescence are negligible.

For the immiscible polymer blend, the observed $\log G' - \log \omega$ curve often shows a shoulder at low frequencies. This indicates that the storage modulus of blends is much larger than that of the pure components when the frequency is less than a critical value. This enhanced elasticity of the blends is contributed by the deformation and relaxation of interfaces [18, 20, 21, 19, 12]. The frequency corresponding to the shoulder is inversely proportional to the relaxation time of the droplet shape. Since this relaxation time is usually much larger for polymer blends, the presence of the shoulder makes the terminal zone shifts to very lower frequencies which makes it difficult to be observed. The experiments also show that the shoulders shifts to lower frequencies as the quantity $\frac{R}{\Gamma}$ increases [19]. The influences of the interface on the moduli are only prominent at low frequencies. At high frequencies, G' are not deviated much from the mean values of the components. While the storage modulus is influenced prominently by the presence of the interfaces, the loss modulus do not show a notable effect [17, 19].

The rheological and morphological responses of immiscible blends subjected to oscillatory shear flows are affected by the concentration. When the concentration is high, a co-continuous morphology appears. The co-continuous morphology is usually unstable, it tends to coarser, larger domains are formed. Vinckier and Laun's experiments for a blend of 40%PMMA and 60%PαMSAN [22] show that for low amplitudes the moduli are almost strain independent and decay to zero over time. For high amplitudes the moduli show a particular strain dependence and their value becomes time independent. These findings indicate that there is a critical strain below which domain growth cannot be stopped. Above the critical strain, the oscillations will hinder the coarsening process, yielding a stable morphology.

1.1.4 Other flows

The behavior of emulsions under other experimental conditions such as relaxation of stresses and shapes, fibril breakup, and shear-free flows are not listed here. Interested readers can found an excellent review of these observations in the paper of Tucker and Moldenaers (2002) [23].

1.2 Immiscible blends in the presence of surface active agents

Surface active agents, for example copolymers and surfactants, when added to the polymer blends and emulsions, cause tremendous changes in the morphology and rheology of the suspension [24, 25]. The changes are related to the three features encountered in the presence of surface active agents: (i) a local decrease of the interfacial tension proportional to its mass concentration, (ii) the mobility and diffusibility of the molecules of the surface active agent, and (iii) the steric property of surface active agent molecules.

Since the effect of the surface active agent on the morphology and rheology of emulsions is very complex, observations contradicting each other are often reported in the literature. However, there is a general agreement about the following features: (i) Decrease in the droplet size caused by the reduced interfacial tension. (ii) Large deviations from the ellipsoidal shape of droplets under strong flow field. (iii) Increased elasticity as the result of increased interfacial area. (iv) Increased overshoot in transient flows. (v) Suppression of the coalescence of the droplets.

We shall now discuss how these features appear in different types of experiments.

1.2.1 Start-up shear flows

When an emulsion is modified by a surface active agent, the modes for the deformation and breakup of droplets change if the viscosity ratio is low (for example $p < 0.1$). The extent of the change depends on the amount of the surface active agents added. If the amount is small, no prominent change is observed. If a

modest amount of the surface active agent is added, the droplet no longer undergoes an ellipsoidal and cylindrical morphology stage before breaking up into two equally sized droplets. Instead, the droplet takes a rupture mode called tip-streaming. First a shape with tip ends is developed. Then a stream of tiny droplets rupturing off the tips of the droplet[29, 30, 32] appears. Sometimes, asymmetric end pinching droplets can also be observed when a higher amount surface active agent is added [30]. However, as much larger amount of surface active agent is added, the tip streaming cannot be observed any more and the droplet could only break up via a normal rapture mode like a clean droplet [29]. Similar phenomena were observed in a plane hyperbolic flow by Janssen et.al. [31].

The tip streaming phenomenon can be interpreted by a redistribution of the surface active agent on the interface caused by the convection of the flow field. This convection leads to a much higher concentration of surface active agent and thereby a much smaller interfacial tension at the end of droplet. The reduced interfacial tension can no longer resist the drive force from the external flow. Therefore, the interfaces at the ends become more and more curved and finally the tips will be stretched out.

The experiment of Hu *et al.* [30] shows that the interfacial tension at the middle of the droplet after tip streaming increases from its initial value to the value that is the same as in the complete absence of the copolymer. This indicates that nearly all the copolymer is swept off with the small tip-streamed droplets. The convection of the copolymer on the interface of a polymer droplet has also been visualized by Jeon and Macosko [33] with confocal microscopy.

As to the shear stress responses, overshoots can still be observed in polymer blends that were compatibilized by a copolymer. The experiments of Macaubas *et al.* [34] show that both the overshoots and the steady values of the shear stress are enhanced by adding the copolymer. The overshoot for the first normal stress difference is not prominent for small shear rates both for compitibilized and uncompatibilized blends. The steady value of the compatibilized blend is greater than the one of the uncompatibilized blend. These phenomena can be explained by the reduction on the interfacial tension and the increase in the surface area with addition of the copolymers [36].

1.2.2 Steady shear flows

In steady shear flows we focus on the steady state behavior as a function of shear rates. The results of Macaubas *et al.* [34] indicate that for every shear flow history, there is a slight decrease of the volume average radius for the polymer blends without copolymer because of the break up of droplets as shear rate increases. However, after the copolymer is added into blends, no significant variation in the volume-averaged radius is observed. This suppression effect on the break up of the droplets is caused by the Marangoni stress (defined as the gradient of the interfacial tension along the interface). Similar phenomena were also observed by Filippone *et al.* [27].

The experiments of Feigl *et al.* [26] also show that the presence of a surfactant causes the drop to align more in the flow direction.

By studying the relationship between the drop deformation and capillary number Hu *et al.* [30] have discovered an interesting phenomenon. They found that the critical capillary number for breakup is largest for the sample without any copolymer. As the increasing amount of copolymer is added, the critical capillary number (defined by the interfacial tension of clean interfaces) for the droplet to break up initially decreases, then increases. The explanation for this phenomenon is that the Marangoni stress exerts a more and more important force as the concentration of the surface active agents increase. The important feature of the Marangoni stress is that it reduces the tangent interfacial velocity, thus hindering the advection of the surfactant and making the droplet looks like more viscous [40]. Van Hemelrijck *et al.* [49] also observe in their experiments that highly compatibilized blends behave as suspensions with solid spheres with the viscosity that is very close to the one predicted Einstein's formula (i.e. $\sigma_{12} \approx 1 + 0.25\phi$).

To sum up, it is clear from the observations that the presence of surface active agents at the interface has two seemingly contradictory effects. First, it reduces the interfacial tension and makes droplets easy to deform and breakup. Second, it redistributes on the interface (by the advection caused by the imposed flow) which results in the appearance of the Marangoni stress which then resists the deformation and break up of the droplets. The overall effect depends on the concentration of the surface active agent on the interface.

Another important effect on the morphology of the immiscible blends, arising

due to the presence of surface active agents, is that it inhibits the coalescence of the droplets [39, 24, 28]. The two most receipted mechanisms are: (i) repulsive steric interactions between the block copolymer layers presented at the interface, and (ii) the Marangoni stresses caused by the film drainage between two droplets [38, 37]. However, Huitric *et al.*'s study [35] show that a significant coalescence inhibition is observed only when a relatively high amount of compatibilizer is used and thus when the steric repulsions between grafted copolymer chains at the interface contribute more than the Marangoni forces to the coalescence inhibition. Experiments suggest that it is the molecular architecture of the copolymer that influences the suppression of the coalescence [41, 42, 43].

1.2.3 Small amplitude oscillatory shear flows

Small amplitude oscillatory shear flows are also a powerful tool to study the compatibilized copolymer blends. Early studies include [44, 45, 46].

In the case of compatibilized blends, the small amplitude oscillatory shear experiments of Riemann *et al.* [47, 48] show that a second relaxation mechanism is present at low frequencies. The extra shoulder in the dynamic response of the compatibilized blend is located at a frequency that is lower than that of the shape relaxation of the droplets. This indicates the existence of an extra relaxation mechanism. This behavior is also experimentally observed by Jacobs *et al.* [50] and Van Hemelrijck *et al.* [28]. The relaxation time decreases when the amount of compatibilizer increases which indicates that at a certain relatively high compatibilizer concentration it will not be possible anymore to make a distinction between the two relaxation mechanisms in the blend system since the two shoulders will appear as one. The origin of the second relaxation process is related to the Marangoni stress, i.e. to the gradient of the interfacial tension. It is possibly governed by the coupling of following factors: (i) convection caused by the imposed flow, (ii) diffusibility of the surface active agent within the interface, (iii) solubility of the surface active agent in the bulk fluids, and (iv) state equation of the surface active agent, i.e. the relationship between interfacial tension and its concentration at the surface.

Sometimes, when the compatibilizers is added to the concentrated immiscible polymer blend, especially by reactive blending, the storage modulus shows a

tremendous increase over the pure components contribution at low frequencies. The dynamic viscosity also indicates that no plateau can be observed at low shear rates [51, 52, 53, 25]. This phenomenon is commonly explained by the formation of a network structure in the blends or the enhanced elastic interactions between the graft shells of the compatibilized domains [25].

1.3 Suspensions of biological membranes

A biological membrane is an enclosing or separating amphipathic layer that acts as a barrier around a cell. A cell membrane defines a boundary between the living cell and its environment. It consists of lipids, proteins,carbohydrates and other substances. Lipids and proteins are dominant components of the membranes. The most widely accepted model for cell membranes is the fluid mosaic model proposed by Singer and Nicolson in 1972 [54]. In this model, the cell membrane is considered as a lipid bilayer where the lipid molecules can move freely in the membrane surface like fluid, while the proteins are embedded in the lipid bilayer. Beneath the lipid membrane, the membrane skeleton, a network of proteins, links with the proteins in the lipid membrane.

In this thesis we focus on one important type of biomembrane, the membrane of red blood cells. The human blood is composed of blood cells suspended in a liquid called blood plasma. Although red blood cells normally occupy about 42-45% of the blood volume, the whole blood viscosity remains low, about 4 to 5 mPas at high shear rates. The high deformability of the membrane of red blood cells causes a complex rheological behavior of suspensions of blood cells. The red blood cell has a diameter around $8\mu m$. The deformability of the red blood cells is related to following physical properties: (a) the biconcave disk shape of the RBC at equilibrium state, thus the RBC has an excess surface area as compared to a sphere with the same volume; (b) the viscosity of the internal haemoglobin solution; (c) membrane mechanical properties. The RBC membrane is easily deformed under shear but strongly resists to changes in the surface area. According to Evans and Skalak membrane model [56], the mechanical properties of the RBC membrane can be characterized by independent material constants which include area elasticity, shear elasticity, shearing viscosity and bending elas-

ticity. The most often used physical methods to measure these quantities include micropipettes and optical tweezers.

Micropipettes method was developed by Evens and Yeung [57, 59, 58, 55]. It consists of drawing the cells into a smallcalibrated micropipette (diameter around $2 \sim 8mm$) at different suction pressures ($0.1 \sim 105Pa$). The value of shear modulus of human red blood cell measured by micropipette at room temperature is typically $6 \sim 9 \times 10^{-3}$ mN/m [60]. By aspirating a preswollen cell into a micropipette, the area elasticity can also be measured. Evans et al [62] report the area elasticity to be $450mN/m$. By measuring the recovery process of a deformed red cell elongated by micropipette aspiration, the viscosity of the membrane can be obtained. The experiments of Evens and Hochmuth [61] give a value of viscosity around $10^{-3}mNs/m$. Micropipettes can also be used to measure the bending elasticity of the cell membrane. The value of the corresponding modulus is around $1.8 \times 10^{-19}Nm$ [65, 66].

Optical tweezer method has been discovered about fifteen years ago (Ashkin and Dziedzic [63], Sheetz [64]). The power of a laser source is focused on the cell observed under the microscope. Under the influence of the light, the cell becomes trapped. The measured value of shear elastics modulus is about $2.5muN/m$ [67] which is smaller than the values obtained by micropipette methods.

The blood cell shows some striking behavior under the shear flow. It can exhibit ellipsoidal shape like the droplet with the liquid interface does [68, 69]. A high shear rates is needed to attain a ellipsoidal shape. Moreover, the RBC deforms without changes in its surface area. RBCs exhibit tank treading motion when its viscosity ratio of the inner fluid viscosity to that of the suspending fluid is low [69]. This behavior can also be observed for a droplet. It makes the inner fluid rotates while still keeping a stable orientation of the cell. The RBC exhibits a tumbling motion when the viscosity ratio is above a critical value, just like the behavior of a high viscous droplet or solid particle. Another observed phenomenon is the vacillating-breathing. The vesicle long axis oscillates (or vacillates) around the flow direction, whereas its shape undergoes a breathing motion [70, 71]. These microscopic dynamic phenomena have an effect on the macroscopic suspension rheology.

The rheology of RBC suspensions is influenced by the following three factors: (a) volume fraction of RBC, (b) cell deformability, and (c) aggregation of RBCs.

RBCs tend to pile up into rod-shaped aggregates, called "rouleaux". Rouleaux formation results in an increased viscosity of blood but is often avoided in the experimental studies.

Suspensions of normal cells show shear thinning behavior at low shear rates, and become Newtonian at high shear rates. [72, 73, 76, 74, 75] The decrease in RBC deformability result in an increase in blood apparent viscosity. Carr and Cokelet [75] studied the steady-flow rheological properties of suspensions of mixtures of normal and glutaraldehyde-hardened human red blood cells in albumin-containing saline. The total cell volume concentrations (hematocrits) are between 30% and 43.5%. They found that suspensions of hardened cells are Newtonian at lower shear rates, and become dilatant (shear-thickening) at high shear rates.

These observations give an opportunity to determine the deformability of the RBC from the macroscopic rheological measurements of the suspensions. Drochon et al. [77] carried out a study on the feasibility of using rheology models to quantify the elastic models of the membranes. Later, Drochon [78] refined the method. The resulting elastic moduli of RBC are found to be in a good agreement with those obtained by micropipettes measurements.

Bibliography

[1] M. Iza, M. Bousmina, Nonlinear rheology of polymer blends: Relaxation result, J. Rheol. 44 (2000) 1363-1384.

[2] P. H. M. Elmans, H. L. Bos, J. M. H. Janssen, H. E. H. Meijer, Transient Phenomena in dispersive mixing, Chemical Engineering Scince 48 (1993) 267-276.

[3] H. P. Grace, Dispersion phenomena in high viscosity immiscible fluid systems and applications of static mixers as dispersion devices in such systems, Chem. Eng. Commun. 14 (1982) 225-277.

[4] S. Guido, M. Villone, Three-dimensional shape of a drop under simple shear flow, J Rheol. 42 (1998) 395-415.

[5] R. A. de Bruijn, Deformation and breakup of drops in simple shear flows. PhD thesis, Technische Universiteit Eindhoven (1989).

[6] J. A. Wieringa, F. van Dieren, J. J. M. Janssen, W. G. M. Agterof, Droplet breakup mechanisms during emulsification in colloid mills at high dispersed phase volume fractions, Trans. Inst. Chem. Eng. 74A (1996) 554-561.

[7] K. M. B. Jansen,W. G. M. Agterof, J. Mellema, Droplet breakup in concentrated emulsions, J. Rheol. 45 (2001) 227-236.

[8] N. Mekhilef, B. D. Favis, P. J. Carreau, Morphological stability, interfacial tension, and dual-phase continuity in polystyrene-polyethylene blends, Journal of Polymer Science: Part B: Polymer Physics 35 (1997) 293-308.

[9] P. Potschke, D. R. Paul, Formation of co-continuous structures in melt-mixed immiscible polymer blends, J. Macromol. Sci.-Pol. R. 1 (2003) 87-141.

[10] I. Vinckier, P. Moldenaers, J. Mewis, Transient rheological response and morphology evolution of immiscible polymer blends, J. Rheol. 41 (1997) 705-718.

[11] T. Jansseune, I. Vinckier, P. Moldenaers, J. Mewis, Transient stresses in immiscible model polymer blends during start-up flows, J. Non-Newtonian Fluid Mech. 99 (2001) 167-181.

[12] N. C. Das, H. Wang, J. Mewis, P. Moldenaers, Rheology and microstructures formation of immiscible model polymer blends under steady state and transient flows, Journal of Polymer Science: Part B: Polymer Physics, 43 (2005) 3519-3533.

[13] J. Janssen, Dynamics of liquid-liquid mixing, Ph.D. thesis, Eindhoven University (1993).

[14] I. Vinckier, P. Moldenaers, J. Mewis, Relationship between rheology and morphology of model blends in steady shear flow, J Rheol 40 (1996) 613-631.

[15] M. Minale, P. Moldenaers, J. Mewis, Effect of shear history on the morphology of immiscible polymer blends, Macromolecules 30 (1997) 5470-5475.

[16] M. Minale, P. Moldenaers, Study of the morphological hysteresis in immiscible polymer blend, AIChE J 44 (1998) 943-950.

[17] P. Scholz, D. Froelich, R. Muller, Viscoelastic properties and morphology of two-phase polypropylene/polyamide 6 blends in the melt. Interpretation of results with an emulsion model, J. Rheol. 33 (1989) 481-499.

[18] D. Graebling, D. Froelich, R. Muller, Viscoelastic properties of polydimethylsiloxane-polyoxyethylene blends in the melt. Emulsion model, J Rheol. 33 (1989) 1283-1291.

[19] D. Graebling, R. Muller, J. F. Palierne, Linear viscoelastic behavior of some incompatible polymer blends in the melt. Interpretation of data with a model of emulsion of viscoelastic liquids, Macromolecules 26 (1993) 320-329.

[20] D. Graebling, R. Muller, Rheological behavior of polydimethylsiloxane/polyoxyethylene blends in the melt. Emulsion model of two viscoelastic liquids, J. Rheol. 34 (1990) 193-205.

[21] H. Gramespacher, J. Meissner, Interfacial tension between polymer melts measured by shear oscillations of their blends, J Rheol. 36 (1992) 1127-1141.

[22] I. Vinckier, H.M. Laun, Assessment of the Doi-Ohta theory for co-continuous blends under oscillatory flow, J. Rheol. 45 (2001) 1373-1385.

[23] C. L. Tucker III, P. Moldenaers, Microstructural evolution in polymer blends, Annu. Rev. Fluid Mech. 34 (2002) 177-210.

[24] C. W. Macosko, P. Guegan, A. K. Khandpur, A. Nakayama, P. Marechal, T. Inoue, Compatibilizers for melt blending: Premade block copolymers, Macromolecules 29 (1996) 5590-5598.

[25] C. Sailer and U. A. Handge, Melt Viscosity, Elasticity, and Morphology of Reactively Compatibilized Polyamide6/Styrene-Acrylonitrile Blends in Shear and Elongation, Macromolecules 40 (2007) 2019-2028.

[26] K. Feigl, D. Megias-Alguacil, P. Fischer, E. J. Windhab, Simulation and experiments of droplet deformation and orientation in simple shear flowwith surfactants, Chemical Engineering Science 62 (2007) 3242-3258.

[27] G. Filippone, P. A. Netti, D. Acierno, Microstructural evolutions of LDPE/PA6 blends by rheological and rheo-optical analyses: Influence of flow and compatibilizer on break-up and coalescence processes, Polymer 48 (2007) 564-573.

[28] E. Van Hemelrijck, P. Van Puyvelde, S. Velankar, C. W. Macosko, P. Moldenaers, Interfacial elasticity and coalescence suppression in compatibilized polymer blends, J. Rheol. 48 (2004) 143-158.

[29] R. A. de Bruijn, Tipstreaming of drops in simple shear flows, Chemical Engineering Science 48 (1993) 277-284.

[30] Y. T. Hu, D. J. Pine, L. G. Leal, Drop deformation, breakup, and coalescence with compatibilizer, Phys. Fluids 12 (2000) 484-489.

[31] J. J. M. Janssen, A. Boon, W. G. M. Agterof, Influence of dynamic interfacial properties on droplet breakup in plane hyperbolic flow, AIChE Journal 43 (1997) 1436-1447.

[32] S. Velankar, P. Van Puyvelde, J. Mewis, P. Moldenaers, Effect of compatibilization on the breakup of polymeric drops in shear flow, J. Rheol. 45 (2001) 1008-1019.

[33] H. K Jeon, C. W. Macosko, Visualization of block copolymer distribution on a sheared drop, Polymer 44 (2003) 5381-5386.

[34] P. H. P. Macaubas, N. R. Demarquette, J. M. Dealy, Nonlinear viscoelasticity of PP/PS/SEBS blends, Rheol. Acta 44 (2005) 295-312.

[35] J. Huitric , M. Moana, P. J. Carreau, N. Dufaure, Effect of reactive compatibilization on droplet coalescence in shear flow, J. Non-Newtonian Fluid Mech. 145 (2007) 139-149.

[36] J. Huitric, M. Moana, M. -H. Klopffer, Modelling of the nonlinear behavior of compatibilized polyethylene/polyamide blends in shear and extensional flows, Canadian J. Chem. Eng. 80 (2002) 1051-1056.

[37] J. W. Ha, Y. Yoon, L. G. Leal, The effect of compatibilizer on the coalescence of two drops in flow, Phys. Fluids 15 (2003) 849-867.

[38] P. Van Puyvelde, S. Velankar, J. Mewis, P. Moldenaers, K. U. Leuven, Effect of Maragoni stress on deformation and coalescence in compatibilized immiscible polymer blends, Polymer Eng. Sci. 42 (2002) 1956-1964.

[39] U. Sundararaj, C. W. Macosko, Drop breakup and coalescence in polymer blends-the effects of concentration and compatibilization, Macromolecules 28 (1995) 2647-2657.

[40] S. Velankar, P. Van Puyvelde, J. Mewis, P. Moldenaers, Steady shear rheological properties of model compatibilized blends, J. Rheol. 48 (2004) 725-744.

[41] S. Lyu, T. D. Jones, F. S. Bates, C. W. Macosko, Role of block copolymers on suppression of droplet coalescence, Macromolecules 35 (2002) 7845-7855.

[42] E. Van Hemelrijck, P. Van Puyvelde, C. W. Macosko, P. Moldenaers, The effect of block copolymer architecture on the coalescence and interfacial elasticity in compatibilized polymer blends, J. Rheol. 49 (2005) 783-798.

[43] J. D. Martin, S. S. Velankar, Effects of compatibilizer on immiscible polymer blends near phase inversion, J. Rheol. 51 (2007) 669-692.

[44] B. Brahimi, A. Ait-Kadi, A. Ajji, R. Jerome, R. Fayt, Rheological properties of copolymer modified polyethylene/polystyrene blends, J. Rheol. 35 (1991) 1069-1090.

[45] Y. Germain, B. Ernst, 0. Genelot, L. Dhamani, Rheological and morphological analysis of compatibilized polypropylene/polyamide blends, J. Rheol. 38 (1994) 681-697.

[46] M. Bousmina, Bataille, S. Sapieha, H. P. Schreiber, Comparing the effect of corona treatment and block copolymer addition on rheological properties of polystyrene/polyethylene blends, J. Rheol. 39 (1995) 499-517.

[47] R. -E. Riemann, H, -J. Cantow, C. Friedrich, Rheological investigation of form relaxation and interface relaxation processes in polymer blends, Polymer Bulletin 36 (1996) 637-643.

[48] R. -E. Riemann, H, -J. Cantow, C. Friedrich, Interpretation of a new interface-governed relaxation processes in compatibilized polymer blends, Macromolecules 30 (1997) 5476-5484.

[49] E. Van Hemelrijck, P. Van Puyvelde, P. Moldenaers, Rheology and morphology of highly compatibilized polymer blends, Macromol. Sym. 233 (2006) 51-58.

[50] U. Jacobs, M. Fahrlander, J. Winterhalter, C. Friedrich, Analysis of palierne's emulsion model in the case of viscoelastic interfacial properties, J. Rheol. 43 (1999) 1495-1509.

[51] M. Moan, J. Huitric, P. Mederic, J. Jarrin, Rheological properties and reactive compatibilization of immiscible polymer blends, J. Rheol. 44 (2000) 1227-1245.

[52] S. H. Jafaria, P. Potschkea, M. Stephana, H. Warthb, H. Alberts, Multicomponent blends based on polyamide 6 and styrenic polymers: morphology and melt rheology, Polymer 43 (2002) 6985-6992.

[53] R. T. Tola, G. Groeninckxa, I. Vinckierb, P. Moldenaersb, J. Mewis, Phase morphology and stability of co-continuous (PPE/PS)/PA6 and PS/PA6 blends: effect of rheology and reactive compatibilization, Polymer 45 (2004) 2587-2601.

[54] S. J. Singer, G. L. Nicolson, The fluid mosaic model of the structure of cell membranes, Science 175 (1972) 720-731.

[55] C. Verdier, Rheological Properties of Living Materials. From Cells to Tissues, Journal of Theoretical Medicine 5 (2003) 67-91

[56] E. A. Evans, R. Skalak, Mechanics and Thermodynamics of Biomembranes, CRC, Boca Raton, FL, (1980).

[57] E. A. Evans, New membrane concept applied to the analysis of fluid shear and micropipette-deformed red blood cells, Biophys. J. 13 (1973) 941-954.

[58] E. Evans, A. Yeung, Apparent viscosity and cortical tension of blood granulocytes determined by micropipette aspiration, Biophys. J. 56 (1989) 151-160.

[59] A. Yeung, E. Evans, Cortical shell-liquid core model for passive flow of liquid-like spherical cells into micropipets, Biophys. J. 56 (1989) 139-149.

[60] R. M. Hochmuth, R. E. Waugh, Erythrocyte membrane elasticity and viscosity. Ann. Rev. Physiol. 49 (1987) 209-219.

[61] E. A. Evans, R. M. Hochmuth, Membrane viscoelasticity, Biophys. J. 16 (1976) 1-11.

[62] E. A. Evans, R. E. Waugh, L. Melnik, Elastic area compresibility modulus of red cell membrane, Biophys. J. 16 (1976) 585-595.

[63] A. Ashkin, J. M. Dziedzic, Internal cell manipulation using infrared laser traps, Proc. Natl Acad. Sci. USA 86 (1989) 7914-7918.

[64] M. Sheetz, Laser Tweezers in Cell Biology, Academic Press, San Diego (1998).

[65] E. Evans, Minimum energy analysis of energy deformation applied to pipette aspiration and surface adhesion of red blood cells, Biophys. J. 30 (1980) 265-284.

[66] E. Evans, Bending elastic modulus of red blood cell membrane derived from buckling instability in micropipette aspiration test, Biophys. J. 43 (1983) 27-30.

[67] S. Henon, G. Lenormand, A. Richter, F. Gallet, A new determination of the shear modulus of the human erythrocyte membrane using optical tweezers, Biophys. J. 76 (1999) 1145-1151.

[68] T. Fischer, H. Schmid-Schnbein, Blood Cells, Mol. Dis. 3 (1977) 351-365.

[69] T. Fischer, M. Stohr-Liesen, H. Schmid-Schonbein, The red cell as a fluid drop: Tank treading-like motion of human erythrocyte membrane in shear flow, Science 202 (1978) 894-896.

[70] V. Kantsler, V. Steinberg, Transition to Tumbling and Two Regimes of Tumbling Motion of a Vesicle in Shear Flow, Phys. Rev. Lett. 96 (2006) 036001.

[71] M. Mader, V. Vitkova, M. Abkarian, A. Viallat, T. Podgorski, Dynamics of viscous vesicles in shear flow, Eur. Phys. J. E. 19 (2006) 389-397.

[72] S. Chien, S. Usami, R. J. Dellenback, M. I. Gregersen, Am. J. Physiol. 219 (1970) 136-142.

[73] D. E. Brooks, J. W. Goodwin, G. V. F. Seaman, Interactions among Erythrocytes under Shear, J. Appl. Physiol., 28 (1970) 172-177.

[74] G. R. Cokelet, The Rheology of Human Blood, in Biomechanics: Its Foundations and Objectiues, Y. C. Fung, N. Perrone, and M. Anliker, Eds., Prentice-Hall, Englewood Cliffs, NY, (1972) 63-104.

[75] R. Carr, G. R. Cokelet, Rheology of Suspensions of Normal and Hardened Erythrocytes and their Mixtures, J. Rheol. 25 (1981) 67-82.

[76] S. Chien, S. Usami, R. J. Dellenback, C. A. Bryant, M. I. Gregersen, Changes of Erythrocyte Deformability During Fixation in Acetaldehyde, in Theoretical

and Clinical Hemorheology, H. H. Hartert, A. L. Copley, Eds. Springer-Verlag, Berlin (1971).

[77] A. Drochon, D. Barthès-Biesel, C. Lacombe, L. C Lelievre, Determination of the Red Blood Cell Apparent Membrane Elastic Modulus From Viscometric Measurements, J. Biomech. Eng. 112 (1990) 241-249; Erratum, 113 (1991) 103.

[78] A. Drochon, Rheology of dilute suspensions of red blood cells: Experimental and theoretical approaches, Eur. Phys. J.: Appl. Phys. 22 (2003) 155-162.

Chapter 2

GENERIC Models of Active Advection

Jian Feng Gu, Miroslav Grmela [1]

Ecole Polytechnique de Montreal, C.P.6079 suc. Centre-ville,
Montreal, H3C 3A7, Quebec, Canada

J. Non-Newtonian Fluid Mech. 152 (2008) 12-26.

[1]corresponding author: e-mail: miroslav.grmela@polymtl.ca

abstract

Solutions to the Stokes problem for particles suspended in a moving fluid express mathematically their active (nonaffine) advection. A mesoscopic model of the microhydrodynamic formulation of the advection is developed and its rheological consequences are investigated. The model is constructed as a particular realization of a framework (GENERIC) guaranteeing the compatibility of dynamics with thermodynamics.

2.1 Introduction

Let the system under investigation be an incompressible and isothermal suspension of particles or molecules in a Newtonian fluid. The state variables x used in the microhydrodynamic formulation [1] of the time evolution of this system are $x = (\boldsymbol{u}, x_{int})$, where $\boldsymbol{u}$ is the momentum of the suspension as a whole and $x_{int} = (x_{particles}, \widetilde{\boldsymbol{u}}, x_{interface})$ are the state variables characterizing the internal structure of the suspension; $x_{particles}$ are the coordinates describing states of the particles (alternatively, $x_{particles}$ can also be distribution functions of the particle coordinates), $\widetilde{\boldsymbol{u}}$ is the micro-scale momentum of the matrix fluid influenced by the presence of the suspended particles, and $x_{interface}$ are the coordinates needed to express the physics taking place on the interface of the particles and the matrix fluid. The governing equations are the following:

(i) The Navier-Stokes equation for the momentum field $\widetilde{\boldsymbol{u}}$ supplemented by two boundary conditions. One boundary is the region far from the suspended particles. On this boundary $\widetilde{\boldsymbol{u}}$ is required to be identical with the overall momentum field $\boldsymbol{u}$. This is how the coupling with $\boldsymbol{u}$ is introduced. The other boundary is the particle-fluid interface. This boundary condition is in fact an equation (or a system of equations) governing the time evolution of $x_{interface}$. The terms involving $\widetilde{\boldsymbol{u}}$ play in these equations a role of external forces. The boundary value problem involving $\widetilde{\boldsymbol{u}}$ and $x_{interface}$ is known as the Stokes problem.

(ii) Newton's equations governing the time evolution of $x_{particles}$.

(iii) The time evolution equation for $\boldsymbol{u}$ (a local conservation law) involving an extra stress tensor $\boldsymbol{\sigma}$ that depends on x_{int}.

It has been noted in [2-9] that mesoscopic models of the time evolution of

macroscopic systems share a common mathematical structure guaranteeing agreement of model predictions with results of certain basic experimental observations like for example global conservations of mass, momentum end energy, and the compatibility with thermodynamics. The structure has been called in [7,8] GENERIC. We use here the term a *mesoscopic level* to denote any level that lies between the level of classical hydrodynamics and the level on which state are described by coordinates and momenta (or alternatively by the wave function in quantum mechanics) of all atoms composing the system under consideration. In particular, if we append to the classical hydrodynamic fields any field or distribution function and consider them all as independent state variables, we are placing ourselves on a mesoscopic level of description. The microhydrodynamic formulation of advection recalled above is a formulation on a mesoscopic level since the state variables involve the fields or distribution functions included in x_{int}.

Among the gains that we expect from formulating the suspension dynamics in the GENERIC framework we mention three:

(i) Solutions to the governing equations are proven to possess properties expressing agreement with certain experimental observations.

(ii) The expression for the extra stress tensor $\boldsymbol{\sigma}$ arising in the GENERIC formulation is guaranteed to be consistent with the time evolution of the internal structure. This is not the case in the standard formulation where $\boldsymbol{\sigma}$ is obtained by calculating forces acting on a surface (i.e. by using directly the physical interpretation of $\boldsymbol{\sigma}$). Approximations used in these calculations are not necessarily compatible with the approximations used in the construction of the equations governing the time evolution of the internal structure. In the GENERIC formulation the compatibility of the expression for $\boldsymbol{\sigma}$ with the rest of the dynamics is guaranteed and it is shown to be closely related to the compatibility of the dynamics with thermodynamics [10].

(iii) It is very difficult to find solutions to the Stokes problem. Even for a simple case of one deformable particle and a very particular choice of fluid parameters, the process of finding solutions involves extensive numerical calculations [11-17]. An analytical solution has been found by Eshelby [18] for droplets with no interfacial tension. A particular case of the Eshelby solution is Jeffery's equation [19] for the advection of rigid ellipsoids (see also [20,21]). Difficulties

encountered in the process of finding solutions to the microhydrodynamic equations make then also difficult the process of reaching an understanding of the physics involved. It is very important therefore to attempt to construct simpler, more macroscopic, formulations. The requirement that these mesoscopic models share with the microhydrodynamic formulation the GENERIC structure offers a strategy to construct them.

In one particular case the GENERIC formulation of the suspension dynamics is known. It is the case in which the particles are seen as completely imbedded in the fluid. In this case $x_{int} = x_{particles}$ and the Stokes problem is absent. The particles passively follow the overall flow. There is no microscale momentum $\widetilde{\boldsymbol{w}}$ that is different from the overall momentum $\boldsymbol{u}$. The advection is called in this case a passive (or affine) advection. For example, the advection of macromolecules in polymeric fluids is often considered to be an affine advection.

We shall not attempt to discuss in this paper the general case. We shall limit ourselves only to constructing a GENERIC mesoscopic model in which $x_{int} = (\boldsymbol{c}, \boldsymbol{w})$, where $\boldsymbol{c}$ is a second order tensor playing the role of $x_{particles}$ ($\boldsymbol{c}$ is a state variable used to characterize the morphology of the suspension), and $\boldsymbol{w}$ is another second order tensor playing the role of $\widetilde{\boldsymbol{u}}$ ($\boldsymbol{w}$ is the thermodynamic conjugate to the velocity gradient participating in the advection).

One of the results of our analysis is an observation that the phenomenological modification of the passive advection of $\boldsymbol{c}$, introduced by Gordon and Schowalter in [22], arises as an approximation of the time evolution of $(\boldsymbol{u}, \boldsymbol{c}, \boldsymbol{w})$. It has been noted in [9] that such modification cannot be expressed as a modification of the kinematics of $\boldsymbol{c}$ (i.e. as a modification of the Poisson bracket) but it can be incorporated into the GENERIC formulation by allowing in it appearance of a new term that is time reversible, entropy preserving, skew symmetric but not Hamiltonian. It is not our intention to discuss in this paper what should and should not be included in the formulation of the abstract GENERIC structure. Our objective is simply to carry the physics that is behind the active advection from microhydrodynamics, where it is expressed in the Stokes problem, to more macroscopic levels of description. We shall see that this route leads to regarding a different advection as a different kinematics (i.e. a different Poisson bracket).

2.2 Mesoscopic Model

To begin the construction of the model, we take two different and mutually independent views of the suspension. To the first one we shall refer as Level 1 and to the second as Level 2. We present them in the following two subsections. The model is then constructed in Section 2.2.3 by combining the two viewpoints.

2.2.1 Level 1

On Level 1 we see the suspension as a whole. We do not see explicitly any internal structure in it. Implicitly it is there but it is averaged (coarse-grained) and we are thus unable to see it. Since we assume the incompressibility and the constant temperature, the only state variable is the momentum

$$x^{(1)} = \boldsymbol{u} \tag{2.1}$$

The framework, known as GENERIC, collects the mathematical structure of the time evolution equations whose solutions are guaranteed to agree with results of some basic observations as for example the compatibility with thermodynamics. For isothermal systems, the GENERIC framework has the following form:

$$\dot{x} = L\Phi_x \; + \; \textit{an appropriate dissipation} \tag{2.2}$$

where $\dot{x}$ denotes the time derivative of x, $\Phi(x)$ is the free energy, Φ_x is a shorthand notation for $\partial\Phi/\partial x$, and L is an operator expressing kinematics of x. We shall discuss the dissipation later. Now we turn to the operator L that transforms the covector Φ_x to a vector.

Motion of fluids is seen in classical hydrodynamics as a continuous sequence of transformations $\boldsymbol{R}^3 \rightarrow \boldsymbol{R}^3$. Lie group of these transformations represents mathematically the kinematics. In terms of $\boldsymbol{u}$ (that is an element of the dual of the Lie algebra corresponding to the Lie group of transformations $\boldsymbol{R}^3 \rightarrow \boldsymbol{R}^3$) this kinematics is expressed in the Poisson bracket [23]

$$\{A, B\}^{(1)} = \int d\boldsymbol{r} u_i \left(\partial_j(A_{u_i})B_{u_j} - \partial_j(B_{u_i})A_{u_j}\right) \tag{2.3}$$

where A and B are sufficiently regular real valued functions of $\boldsymbol{u}(\boldsymbol{r})$, $\boldsymbol{r}$ denotes the position vector. We use hereafter the shorthand notation $\partial_i = \frac{\partial}{\partial r_i}$ and the summation convention. The operator L is related to the Poisson bracket $\{A, B\}$ by $\{A, B\} =< A_x, LB_x >$, where $<, >$ is the inner product. We can immediately verify that the equation $\dot{x} = L\Phi_x$ with the bracket (2.3) is indeed the Euler equation provided $\Phi(\boldsymbol{u}) = \boldsymbol{u}^2/2\rho$, where ρ is the constant mass density.

It is not surprising to see the Hamiltonian (or more precisely the Poisson since L is typically degenerate) nature of the kinematics. This is because the classical Euler equation governing the time evolution of $\boldsymbol{u}$ in the absence of dissipation is Newton's law and thus an equation that, as we may expect, can be rendered to the Hamiltonian form.

2.2.2 Level 2

Level 2 is more microscopic. We are able to see explicitly at least some features of the internal structure. There are still however details that remain hidden. For example in microhydrodynamics we can follow the suspended particles and we can locate the interface. This we cannot do on Level 2. Following the mesoscopic viewpoint employed for instance in the Doi-Ohta [24] discussion of immiscible blends, we regard on Level 2 the internal structure as being uniformly spread throughout the suspension. Let $(\boldsymbol{r}_1, \boldsymbol{v}_1, \boldsymbol{r}_2, \boldsymbol{v}_2)$ be position coordinates and momenta of two points in the suspension. We shall choose the two-point distribution function

$$x^{(2)} = f(\boldsymbol{r}_1, \boldsymbol{r}_2, \boldsymbol{v}_1, \boldsymbol{v}_2) \tag{2.4}$$

as the state variable on Level 2. The kinematics of two point distribution function is well known [20,2,5]:

$$\begin{aligned} \{A, B\}^{(2)} &= \sum_{i=1}^{2} \int d\boldsymbol{r}_i \int d\boldsymbol{v}_i \, f[\frac{\partial}{\partial r_{ij}}(A_f)\frac{\partial}{\partial v_{ij}}(B_f) \\ &\quad -\frac{\partial}{\partial r_{ij}}(B_f)\frac{\partial}{\partial v_{ij}}(A_f)] \end{aligned} \tag{2.5}$$

The Lie group is in this case the group of canonical transformations of $(\boldsymbol{r}_1, \boldsymbol{v}_1, \boldsymbol{r}_2, \boldsymbol{v}_2)$; the two-point distribution function is an element of the dual of the Lie algebra

associated with this group.

2.2.3 Combination of Level 1 and Level 2

We can see suspensions on Level 1 and independently on Level 2. We can also see them simultaneously on Level 1 and Level 2. If we take this viewpoint, the state variables are

$$x^{(12)} = (x^{(1)}, x^{(2)}) = (\boldsymbol{u}(\boldsymbol{r}), f(\boldsymbol{r}_1, \boldsymbol{r}_2, \boldsymbol{v}_1, \boldsymbol{v}_2)) \tag{2.6}$$

Because of the independence of $\boldsymbol{u}$ and f, their kinematics is expressed in the Poisson bracket

$$\{A, B\} = \{A, B\}^{(1)} + \{A, B\}^{(2)} \tag{2.7}$$

where $\{A, B\}^{(1)}$ is given in (2.3) and $\{A, B\}^{(2)}$ in (2.5)

Now, we combine the two levels in such a way that the two-point distribution function describes only the details superposed on the information expressed already on Level 1 in terms of $\boldsymbol{u}$. From the state variables $(x^{(1)}, x^{(2)}) = (\boldsymbol{u}(\boldsymbol{r}), f(1,2))$ we pass to $(\hat{x}^{(1)}, \hat{x}^{(2)}) = (\hat{\boldsymbol{u}}(\boldsymbol{r}), \hat{f}(1,2))$ by the transformation

$$\begin{aligned} \hat{\boldsymbol{u}}(\boldsymbol{r}) &= \boldsymbol{u}(\boldsymbol{r}) + \int d1 \int d2 f(1,2)[\boldsymbol{v}_1 \delta(\boldsymbol{r}_1 - \boldsymbol{r}) + \boldsymbol{v}_2 \delta(\boldsymbol{r}_2 - \boldsymbol{r})] \\ \hat{f}(1,2) &= f(1,2) \end{aligned} \tag{2.8}$$

where $(1,2)$ is a shorthand notation for $(\boldsymbol{r}_1, \boldsymbol{v}_1, \boldsymbol{r}_2, \boldsymbol{v}_2)$. The momentum field $\hat{\boldsymbol{u}}$ is now the overall momentum field of the suspension and $\hat{f}$ is the distribution function characterizing only the internal structure of the suspension. To simplify the notation, we shall omit hereafter the hat over $\boldsymbol{u}$ and f.

In addition, we make in f the following change of coordinates

$$\boldsymbol{r} = \frac{1}{2}(\boldsymbol{r}_1 + \boldsymbol{r}_2);\ \boldsymbol{R} = \boldsymbol{r}_2 - \boldsymbol{r}_1;\ \boldsymbol{v} = \boldsymbol{v}_1 + \boldsymbol{v}_2;\ \boldsymbol{V} = \frac{1}{2}(\boldsymbol{v}_2 - \boldsymbol{v}_1), \tag{2.9}$$

Because of the assumption of spatial inhomogeneity of the suspension, we can omit the dependence of f on $\boldsymbol{r}$ and $\boldsymbol{v}$. Consequently, the new state variables are: $(\boldsymbol{u}(\boldsymbol{r}), f(\boldsymbol{R}, \boldsymbol{V}))$.

Finally, we reduce the description of the internal structure. Instead of the

distribution function f, we shall use only its two moments $\boldsymbol{c}$ and $\boldsymbol{w}$ defined by

$$\begin{aligned} c_{ij} &= \int d\boldsymbol{R} \int d\boldsymbol{V} R_i R_j f(\boldsymbol{R}, \boldsymbol{V}) \\ w_{ij} &= \int d\boldsymbol{R} \int d\boldsymbol{V} V_i R_j f(\boldsymbol{R}, \boldsymbol{V}) \end{aligned} \tag{2.10}$$

From (2.10) we see that $\boldsymbol{c}$ is a tensor characterizing the conformation of the internal structure in the suspension, and $\boldsymbol{w}$ a tensor related to the gradient of the local (microscopic) velocity. Below, we shall see how $\boldsymbol{c}$ and $\boldsymbol{w}$ enter the time evolution equations and the free energy. This will further clarify their physical interpretation.

The final set of state variables is thus

$$x = (\boldsymbol{u}(\boldsymbol{r}), \boldsymbol{c}, \boldsymbol{w}) \tag{2.11}$$

Their kinematics is found easily from the kinematics of $x^{(12)}$ (see (2.6) expressed in the Poisson bracket (2.7)). We use in the derivation a well known property of the Poisson bracket, namely that one-to-one transformations carry one Poisson bracket into another Poisson bracket. We note that the transformations (2.8) and (2.9) are one-to-one. The transformation (2.10) is not one-to-one but we simply pass from a bracket for $(\boldsymbol{u}(\boldsymbol{r}), f(\boldsymbol{R}, \boldsymbol{V}))$ to a bracket for (2.11) by restricting the functions A and B appearing in the bracket for $(\boldsymbol{u}(\boldsymbol{r}), f(\boldsymbol{R}, \boldsymbol{V}))$ to those that depend on $(\boldsymbol{u}(\boldsymbol{r}), f(\boldsymbol{R}, \boldsymbol{V}))$ only through their dependence on the moments (2.10). After making the transformations, we arrive at

$$\{A, B\} = \{A, B\}^{(1)} + \{A, B\}^{(c,w)} \tag{2.12}$$

where $\{A, B\}^{(1)}$ is given in (2.3) and

$$\begin{aligned} \{A, B\}^{(c,w)} = \; & c_{jk} \left(A_{c_{mj}} B_{w_{mk}} - B_{c_{mj}} A_{w_{mk}} \right) \\ & + c_{mk} \left(A_{c_{mj}} B_{w_{jk}} - B_{c_{mj}} A_{w_{jk}} \right) \\ & + w_{ij} \left(A_{w_{im}} B_{w_{mj}} - B_{w_{im}} A_{w_{mj}} \right) \\ & + c_{ij} \left(\partial_m (A_{c_{ij}}) B_{u_m} - \partial_m (B_{c_{ij}}) A_{u_m} \right) \\ & + c_{ki} \left(A_{c_{im}} \partial_k (B_{u_m}) - B_{c_{im}} \partial_k (A_{u_m}) \right) \end{aligned}$$

$$
\begin{aligned}
&+c_{km}\left(A_{c_{im}}\partial_k(B_{u_i}) - B_{c_{im}}\partial_k(A_{u_i})\right)\\
&+w_{ik}\left(A_{w_{im}}\partial_k(B_{u_m}) - B_{w_{im}}\partial_k(A_{u_m})\right)\\
&-w_{kj}\left(A_{w_{mj}}\partial_m(B_{u_k}) - B_{w_{mj}}\partial_m(A_{u_k})\right)\\
&+w_{ij}\left(\partial_m(A_{w_{ij}})B_{u_m} - \partial_m(B_{w_{ij}})A_{u_m}\right)
\end{aligned}
\tag{2.13}
$$

The time evolution equations corresponding to the Poisson bracket (2.12), (2.13) can be obtained as follows: We write the time evolution equation $\dot{x} = L\Phi_x$ as $\dot{A} - \{A, \Phi\} = 0$ *holds for all* A. By equating the terms standing by A_u, A_c and A_w to zero we arrive at

$$
\begin{aligned}
\frac{\partial u_i}{\partial t} &= -\partial_j\left(\frac{u_i u_j}{\rho}\right) - \partial_i p - \partial_j \sigma_{ij}\\
\frac{dc_{ij}}{dt} &= c_{ki}(\partial_k(\Phi_{u_j}) + \Phi_{w_{jk}}) + c_{kj}(\partial_k(\Phi_{u_i}) + \Phi_{w_{ik}})\\
\frac{dw_{ij}}{dt} &= +w_{ik}(\partial_k(\Phi_{u_j}) + \Phi_{w_{jk}}) - w_{kj}(\partial_i(\Phi_{u_k}) + \Phi_{w_{ki}})\\
&\quad -2c_{kj}\Phi_{c_{ik}}
\end{aligned}
\tag{2.14}
$$

where p is the scalar pressure given by

$$
p = -\varphi + u_k\Phi_{u_k} + c_{kl}\Phi_{c_{kl}} + w_{kl}\Phi_{w_{kl}} \tag{2.15}
$$

$\varphi(\boldsymbol{r})$ is the density of the free energy (i.e. $\Phi = \int d\boldsymbol{r}\varphi(\boldsymbol{r})$), and $\boldsymbol{\sigma}$ is the extra stress tensor

$$
\sigma_{ij} = -2c_{ik}\Phi_{c_{kj}} - w_{kj}\Phi_{w_{ki}} + w_{ik}\Phi_{w_{jk}} \tag{2.16}
$$

We see clearly from the way the tensor $\boldsymbol{w}$ appears on the right hand side of the equation governing the time evolution of $\boldsymbol{c}$ that the thermodynamic conjugate of $\boldsymbol{w}$, i.e. Φ_w, is the gradient of velocity that combines in the advection with the gradient of the overall velocity $\partial_i(\Phi_{u_j})$ and makes thus the advection active.

In order to complete the discussion of the time evolution of the state variables (2.11), we have to supplement the time reversible equations (2.14) with time irreversible terms. As it is obvious from the construction of (2.14), the free energy Φ remains unchanged during the time evolution governed by (2.14). Indeed, $\dot{\Phi} = \{\Phi, \Phi\} = 0$. The irreversible time evolution has to be constructed in such a

way that $\dot{\Phi} \leq 0$. This will be achieved if we add to the the right hand sides of the three equations in (2.14) three terms: $-\Xi_{\Phi_{u_i}}$ in the first equation, $-\Xi_{\Phi_{cij}}$ in the second equation, and $-\Xi_{\Phi_{wij}}$ in the third equation, where Ξ is a real valued function of (Φ_u, Φ_c, Φ_w) satisfying:

$$\begin{aligned} &\Xi(0,0,0) = 0 \\ &\Xi \textit{ reaches its minimum at } (0,0,0) \\ &\Xi \textit{ is convex in a neighborhood of } (0,0,0) \end{aligned} \tag{2.17}$$

Indeed, for the time evolution equations (2.14) modified in this way we have $\dot{\Phi} = -(\Phi_{u_j}\Xi_{\Phi_{u_j}} + \Phi_{c_{ij}}\Xi_{\Phi_{c_{ij}}} + \Phi_{w_{ij}}\Xi_{\Phi_{w_{ij}}}) \leq 0$.

What remains is to specify the two potentials Φ and Ξ. To do it, we shall use our physical insight. The free energy will be chosen as follows:

$$\Phi = \int d\boldsymbol{r} \left[\frac{\boldsymbol{u}^2}{2\rho} + K \left(-\frac{1}{2} \ln \det \boldsymbol{c} + \beta tr \boldsymbol{c} + \frac{1}{2} \alpha w_{ik} c^{-1}_{kj} w_{ij} \right) \right] \tag{2.18}$$

The first term represents the kinetic energy associated with the overall motion. The remaining three terms represent the contribution of the internal structure to the free energy. The parameter $K = n_{mem} k_B T$, where n_{mem} is the number density of the suspended particles, k_B is the Boltzmann constant, and T is the temperature. The second resp. the third terms represent the entropy resp. the potential energy associated with the internal structure. For the sake of simplicity, we are making the simplest choice corresponding to the particles modeled as Hookean elastic dumbbells. The parameter β is the elastic modulus divided by $k_B T$. The fourth term is the contribution of the motion of the internal structure to the kinetic energy. As we see from (2.10) that $\boldsymbol{w} \cdot \boldsymbol{c}^{-1} \cdot \boldsymbol{w}^T$ has indeed the dimension of the square of momentum. The parameter α is proportional to the inverse of the mass density associated with the internal structure.

At equilibrium, the free energy reaches its minimum. We see immediately that solutions to

$$\Phi_u = 0; \;\; \Phi_c = 0; \;\; \Phi_w = 0 \tag{2.19}$$

are

$$\boldsymbol{u} = 0; \;\; \boldsymbol{c} = \frac{1}{2\beta}\boldsymbol{\delta}; \;\; \boldsymbol{w} = 0 \tag{2.20}$$

which means that at equilibrium there is no overall flow, no internal velocity gradient and no deformations of the suspended particles.

Now, we turn to the dissipation potential Ξ. If we limit ourselves to states that are not very far from equilibrium, the conjugate state variables Φ_u, Φ_c, Φ_w are small and thus, if we keep only terms that are quadratic in Φ_u, Φ_c, Φ_w, the dissipation potential is given by

$$\begin{aligned}\Xi &= \frac{1}{2}\Phi_{c_{ij}}\frac{\Lambda}{K}c_{jk}\Phi_{c_{ki}} \\ &\quad +\frac{1}{2}\begin{pmatrix} \Phi_{w_{ij}}, & D_{ij} \end{pmatrix}\begin{pmatrix} \frac{\lambda}{K}c_{jk} & \xi c_{jk} \\ \xi c_{jk} & \eta\delta_{jk} \end{pmatrix}\begin{pmatrix} \Phi_{w_{ik}} \\ D_{ki} \end{pmatrix}\end{aligned} \tag{2.21}$$

where $D_{ij} = \frac{1}{2}(\partial_i(\Phi_{u_j}) + \partial_j(\Phi_{u_i}))$. Below, we shall limit ourselves only to simple rheometric flows in which the gradient of the overall velocity is independent of $\boldsymbol{r}$. We thus consider $\boldsymbol{D}$ appearing in (2.21) to be a constant symmetric tensor. The coefficients Λ, λ, ξ and η, called kinetic coefficients, are phenomenological parameters in which the particular nature of the suspension under consideration is expressed. Their choice is restricted only by the requirement that (2.21) satisfies (2.17) which means that

$$\begin{aligned}\frac{\Lambda}{K}\boldsymbol{c} \quad &is \quad positive\ definite \\ \begin{pmatrix} \frac{\lambda}{K}\boldsymbol{c} & \xi\boldsymbol{c} \\ \xi\boldsymbol{c} & \eta \end{pmatrix} \quad &is \quad positive\ definite\end{aligned} \tag{2.22}$$

The additional term $-\Xi_{\Phi_{u_i}}$ added to the right hand side of the first equation in (2.14) can be absorbed into the term $-\partial_j\sigma_{ij}$ if we add to the extra stress tensor $\boldsymbol{\sigma}$ two terms: $-\frac{1}{2}\xi\left(c_{ik}\Phi_{w_{jk}} + c_{jk}\Phi_{w_{ik}}\right) - \eta D_{ij}$. We note that the second term is the classical Navier-Stokes contribution to the viscosity, η is the Navier-Stokes viscosity coefficient.

This completes the construction of the time evolution equations of the model. We now turn to the investigation of their solutions. Rheological predictions will be presented in Section 2.3. Here we make only three observations.

(i) We have seen that the free energy Φ serves as the Lyapunov function (it is convex function of (2.11), and $\dot{\Phi} < 0$). Solutions to (2.14) approach equilibrium (2.20) as $t \to \infty$.

(ii) In the particular case when $\boldsymbol{w}$ is absent, the internal structure characterized by $\boldsymbol{c}$, is passively advected by the overall flow. This is clearly seen in (2.14). If we regard the fluid motion as a Lie group of transformations $\mathbf{R}^3 \to \mathbf{R}^3$, then the passive advection is seen as a Lie drag and the additional terms to the Poisson bracket expressing the kinematics of a fluid with a Lie dragged internal structure are obtained with the use of the concept of the semi-direct product [19]. The fourth and the fifth terms in (2.13) , that are the only terms that remain in (2.13) if $\boldsymbol{w}$ is absent, are exactly the terms arising in the construction that uses the concept of the semi-direct product (see more in [20]).

(iii) Let us assume that the kinetic coefficients λ is large relative to the other kinetic coefficients introduced in (2.22). This means that $\boldsymbol{w}$ approaches rapidly equilibrium. We can thus assume that $d\boldsymbol{w}/dt$ is small. Since $\boldsymbol{w}$ is already close to equilibrium (see (2.20)), $\boldsymbol{w}$ itself is small and thus the dominant terms in the time evolution equation for $\boldsymbol{w}$ are $-\Xi_{\Phi_w} - 2\Phi_c \cdot \boldsymbol{c}$. The third equation in (2.14) can be thus approximated by the equation $\Xi_{\Phi_w} + 2\Phi_c \cdot \boldsymbol{c} = 0$ which, in view of (2.21), becomes $\frac{\lambda}{K} c_{jk}\Phi_{w_{ik}} = -\xi c_{jk} D_{ki} - 2c_{kj}\Phi_{c_{ik}}$. If we insert this relation to the second equation in (2.14) we obtain

$$\begin{aligned} \frac{dc_{ij}}{dt} &= c_{ki}\left(\partial_k(\Phi_{u_j}) - \zeta D_{jk}\right) + c_{kj}\left(\partial_k(\Phi_{u_i}) - \zeta D_{ik}\right) \\ &\quad - \left(\frac{\Lambda}{K} + \frac{4K}{\lambda}\right) c_{kj}\Phi_{c_{ik}} \end{aligned} \tag{2.23}$$

where

$$\zeta = \frac{K\xi}{\lambda} \tag{2.24}$$

The question now arises of what is the expression for the extra stress tensor that is compatible with (2.23). For the time evolution equations that arise from Poisson brackets (e.g. Eqs.(2.14)), the expression for the extra stress tensor (e.g. (2.16)) appear automatically as a part of the equations. But Eq.(2.23) has arisen as an approximation of (2.14) and does not possess anymore the Poisson structure. In such a case we can turn to the method developed in [10]. We look for $\boldsymbol{\sigma}$ for which the first equation in (2.14) together with Eq.(2.23) without the last term on its right hand side imply $\frac{d\Phi}{dt} = 0$. From this requirement we then easily obtain

$$\sigma_{ij} = -2(1-\zeta)c_{ik}\Phi_{c_{ik}} \tag{2.25}$$

Indeed, if $\zeta = 0$ the expression (2.25) reduces to the expression (2.16) without the terms involving $\boldsymbol{w}$.

We note that the first two terms on the right hand side of (2.23) have the same form as the nonaffine advection arising for example in Jeffery's equation or in the phenomenological modification of the advection introduced in [19]. In Jeffery's theory the coefficient ζ arises from solving the Stokes problem of advection of a solid object. The coefficient appears to be related to the shape of the object. In [22], the coefficient ζ is a phenomenological parameter expressing a slip occurring on the molecule-fluid interface. In our analysis, ζ is a coefficient (2.24) involving parameters entering the time evolution of $(\boldsymbol{c}, \boldsymbol{w})$. Since (2.23) is a valid approximation of (2.14) only when λ is large relative to the other kinetic coefficients, the parameter ζ given in (2.24) is less than one. This is then in agreement with the phenomenological considerations reported in [19].

Hereafter, we shall use the following terminology. The advection with $\boldsymbol{w}$ absent (i.e. the advection in (2.23) with $\zeta = 0$) is called *passive* or also *affine*. The advection expressed in (2.23) with $\zeta \neq 0$ is called *nonaffine*, and the advection expressed in (2.14) is called *active*. We recall that that there are in fact two typaes of affine advections, namely the upper convected and dual to it that is called lower convected. In this paper, we consider only the upper convected advection and its modifications.

In the next two sections we calculate rheological and morphological predictions of the active advection and compare them, in Section 2.3, with predictions calculated with passive and nonaffine advections (for the Maxwell fluid discussed above), and, in Section 2.4, with predictions of the microhydrodynamic analysis, the Maffettone-Minale model, and with experimental observations (for deformations of dispersed droplets).

2.3 Maxwell Fluid with Affine, Nonaffine, and Active Advections

The free energy Φ and the dissipation potential Ξ have been chosen in Section 2.2 in such a way that in the absence of $\boldsymbol{w}$, the model (2.14) becomes the classical Maxwell model (i.e. the intramolecular potential is Hookean and the advection

is affine). We shall keep the Hookean intramolecular potential and show how changes in advection change the rheological and morphological predictions.

We thus turn to the problem of solving Eqs.(2.14),(2.16). First, we write them explicitly. With the free energy and dissipative potential given in (2.18) and (2.21) they become

$$\begin{aligned}
\frac{dc_{ij}}{dt} &= -W_{ki}c_{kj} + D_{ki}c_{kj} + K\alpha w_{ij} \\
&\quad -W_{kj}c_{ki} + D_{kj}c_{ki} + K\alpha w_{ji} \\
&\quad +\Lambda\left(\frac{1}{2}\delta_{ij} - \beta c_{ij} + \frac{\alpha}{4}\left(w_{lk}c_{ik}^{-1}w_{lj} + w_{lk}c_{jk}^{-1}w_{li}\right)\right) \\
\frac{dw_{ij}}{dt} &= -W_{kj}w_{ik} - W_{ki}w_{kj} + K\alpha w_{ik}c_{kl}^{-1}w_{jl} \\
&\quad +D_{kj}w_{ik} - D_{ki}w_{kj} + K\left(\delta_{ij} - 2\beta c_{ij}\right) \\
&\quad -\lambda\alpha w_{ij} - \xi c_{jk}D_{ik} \qquad (2.26) \\
\sigma_{ij} &= K\left(\delta_{ij} - 2\beta c_{ij} + \alpha w_{ik}c_{lk}^{-1}w_{jl}\right. \\
&\quad \left.-\frac{1}{2}\alpha\xi(w_{ij} + w_{ji})\right) \qquad (2.27)
\end{aligned}$$

where $W_{ki} = \frac{1}{2}(\partial_i\Phi_{u_k} - \partial_k\Phi_{u_i})$ is the vorticity tensor.

The imposed flow is chosen to be the simple shear flow with

$$\boldsymbol{D} = \dot{\gamma}\begin{pmatrix} 0 & \frac{1}{2} & 0 \\ \frac{1}{2} & 0 & 0 \\ 0 & 0 & 0 \end{pmatrix} \qquad (2.28)$$

and

$$\boldsymbol{W} = \dot{\gamma}\begin{pmatrix} 0 & \frac{1}{2} & 0 \\ -\frac{1}{2} & 0 & 0 \\ 0 & 0 & 0 \end{pmatrix} \qquad (2.29)$$

where $\dot{\gamma}$ is a scalar parameter called shear rate. The initial conditions are the equilibrium values (2.20).

We begin the process of solving (2.26) by assuming that the shear rate $\dot{\gamma}$ is small and use the perturbation method with $\dot{\gamma}$ playing the role of the small

parameter. We obtain in this way:

$$\eta_0 = \lim_{\dot{\gamma}\to 0}\left(-\frac{\sigma_{12}}{\dot{\gamma}}\right) = \frac{K(4\lambda - 8K\xi - \xi^2\Lambda)}{4\beta(\Lambda\lambda + 4K^2)} \tag{2.30}$$

and

$$\begin{aligned}\Psi_{10} &= \lim_{\dot{\gamma}\to 0}\left(-\frac{\sigma_{11}-\sigma_{22}}{\dot{\gamma}^2}\right) \\ &= \frac{K}{\beta(\Lambda\lambda+4K^2)^2}\left[\frac{2(\lambda - K\xi)^2}{\beta} - \frac{(\xi\Lambda + 4K)^2}{2\alpha}\right] \qquad (2.31)\\ \Psi_{20} &= \lim_{\dot{\gamma}\to 0}\left(-\frac{\sigma_{22}-\sigma_{33}}{\dot{\gamma}^2}\right) \\ &= \frac{K(4K+\xi\Lambda)\left[3\beta(4K+\xi\Lambda) - 2\alpha\xi(\lambda - K\xi)\right]}{8\alpha\beta^2(\Lambda\lambda+4K^2)^2} \qquad (2.32)\end{aligned}$$

where we use the standard notation for the viscosity coefficient η and the first (resp. the second) normal stress difference Ψ_1 (resp. Ψ_2).

We continue with numerical solutions. First, we transform (2.26) to a dimensionless form. We choose the following dimensionless variables: $\tilde{\boldsymbol{c}} = \boldsymbol{c}/a^2$, $\tilde{\boldsymbol{w}} = \boldsymbol{w}/\eta_m$, $\tilde{\sigma} = \sigma/(\dot{\gamma}\eta_m)$, $\tilde{t} = \dot{\gamma}t$, $\tilde{\boldsymbol{D}} = \boldsymbol{D}/\dot{\gamma}$, and $\tilde{\boldsymbol{W}} = \boldsymbol{W}/\dot{\gamma}$, where a is the diameter of the sphere and η_m the viscosity coefficient of the matrix fluid. In these new variables, Eqs.(2.26),(2.27) become (to simplify the notation we omit hereafter the tilde)

$$\begin{aligned}\frac{d\boldsymbol{c}}{dt} &= (\boldsymbol{D}+\boldsymbol{W})\cdot\boldsymbol{c} + \boldsymbol{c}\cdot(\boldsymbol{D}-\boldsymbol{W}) + \mu_2(\boldsymbol{w}+\boldsymbol{w}^T) \\ &\quad + \frac{1}{2}\kappa_2\boldsymbol{\delta} - \frac{\kappa_1\kappa_2}{\kappa_3}\boldsymbol{c} + \frac{1}{4}\frac{\kappa_2\mu_2}{\kappa_3}\left(\boldsymbol{c}^{-1}\cdot\boldsymbol{w}^T\cdot\boldsymbol{w} + \boldsymbol{w}^T\cdot\boldsymbol{w}\cdot\boldsymbol{c}^{-1}\right) \qquad (2.33)\\ \frac{d\boldsymbol{w}}{dt} &= \boldsymbol{w}\cdot(\boldsymbol{D}-\boldsymbol{W}) - (\boldsymbol{D}-\boldsymbol{W})\cdot\boldsymbol{w} \\ &\quad + \mu_2\boldsymbol{w}\cdot\boldsymbol{c}^{-1}\cdot\boldsymbol{w}^T + \kappa_3\boldsymbol{\delta} - 2\kappa_1\boldsymbol{c} \\ &\quad - \mu_1\boldsymbol{w} - \mu_3\boldsymbol{D}\cdot\boldsymbol{c} \qquad (2.34)\\ \boldsymbol{\sigma} &= \kappa_3\boldsymbol{\delta} - 2\kappa_1\boldsymbol{c} + \mu_2\boldsymbol{w}\cdot\boldsymbol{c}^{-1}\cdot\boldsymbol{w}^T \\ &\quad - \frac{1}{2}\mu_2\mu_3(\boldsymbol{w}+\boldsymbol{w}^T) \qquad (2.35)\end{aligned}$$

where $(\kappa_1, \kappa_2, \kappa_3)$ and (μ_1, μ_2, μ_3) are dimensionless numbers defined as follows:

$$\kappa_1 = \frac{K\beta a^2}{\eta_m \dot{\gamma}}; \quad \kappa_2 = \frac{\Lambda}{a^2\dot{\gamma}}; \quad \kappa_3 = \frac{K}{\eta_m \dot{\gamma}}$$
$$\mu_1 = \frac{\lambda\alpha}{\dot{\gamma}}; \quad \mu_2 = \frac{K\alpha\eta_m}{a^2\dot{\gamma}}; \quad \mu_3 = \frac{\xi a^2}{\eta_m} \tag{2.36}$$

In the same dimensionless variables, the model that does not involve $\boldsymbol{w}$ (i.e. the Maxwell model) has the form

$$\begin{aligned} \frac{d\boldsymbol{c}}{dt} &= (\boldsymbol{D}+\boldsymbol{W})\cdot\boldsymbol{c}+\boldsymbol{c}\cdot(\boldsymbol{D}-\boldsymbol{W}) \\ &\quad +\frac{1}{2}\kappa_2\boldsymbol{\delta}-\frac{\kappa_1\kappa_2}{\kappa_3}\boldsymbol{c} \\ \sigma &= \kappa_3\boldsymbol{\delta}-2\kappa_1\boldsymbol{c} \end{aligned} \tag{2.37}$$

and the model of nonaffine advection (2.23) (representing an approximation of the active advection)

$$\begin{aligned} \frac{d\boldsymbol{c}}{dt} &= (\boldsymbol{D}+\boldsymbol{W})\cdot\boldsymbol{c}+\boldsymbol{c}\cdot(\boldsymbol{D}-\boldsymbol{W})-\frac{\mu_2\mu_3}{\mu_1}(\boldsymbol{D}\cdot\boldsymbol{c}+\boldsymbol{c}\cdot\boldsymbol{D}) \\ &\quad -\left(4\frac{\kappa_1\mu_2}{\mu_1}+\frac{\kappa_1\kappa_2}{\kappa_3}\right)\boldsymbol{c}+\left(\frac{1}{2}\kappa_2+2\frac{\kappa_3\mu_2}{\mu_1}\right)\boldsymbol{\delta} \\ \sigma &= \left(1-\frac{\mu_2\mu_3}{\mu_1}\right)(\kappa_3\boldsymbol{\delta}-2\kappa_1\boldsymbol{c}) \end{aligned} \tag{2.38}$$

The initial conditions for Eqs.(2.33),(2.34), Eq.(2.37), and Eq.(2.38) are the equilibrium states (2.20) that, in the dimensionless variables, take the form: $\boldsymbol{c} = \frac{\kappa_3}{2\kappa_1}\boldsymbol{\delta}$; $\boldsymbol{w} = 0$. The governing equations (2.37) of the affine advection model involve only three parameters $(\kappa_1, \kappa_2, \kappa_3)$, the governing equations (2.38),(2.33),(2.34) of the models of the nonaffine and the active advection involve all six parameters $(\kappa_1, \kappa_2, \kappa_3)$ and (μ_1, μ_2, μ_3). The μ-parameters characterize the active part of the advection.

2.3.1 Results

We proceed to solve Eqs.(2.37), representing the classical Maxwell model with the affine upper convected advection, Eqs.(2.38), representing the Maxwell model

with the nonaffine advection, and Eqs.(2.33), representing the Maxwell model with the active advection. The imposed flow is the simple shear flow Eq.(2.28) and(2.29). On the figures below we present the viscosity coefficient η, the first normal stress coefficient Ψ_1, the second normal stress coefficient Ψ_2, and the morphology characterized by the conformation tensor $\boldsymbol{c}$ and, in the case of the active advection, by $\boldsymbol{c}$ and the extra velocity gradient Φ_w. The conformation tensor $\boldsymbol{c}$ is presented on some of the figures as a projection on the x, y plane of the ellipsoid represented by the algebraic equation $< \boldsymbol{r}, \boldsymbol{cr} >= 1$. On all figures we present always one result (η, Ψ_1, Ψ_2 and/or the morphology) calculated for the three types of advection. All figures thus show how the change in advection changes the rheology and/or morphology.

Figure (2.1) shows the time evolution of the viscosity coefficient η and the first and the second normal stress difference coefficient Ψ_1 and Ψ_2 for the three types of advection. The affine advection model leads to the highest values of both η and Ψ_1. On the other hand, Ψ_2 is identically zero for the affine advection but different from zero (and negative, $|\Psi_1/\Psi_2| \sim 10^1$) for the nonaffine and active advections. The overshoots, that are absent in the affine advection, appear in both the nonaffine and the active advections. This means that the modified advection (i.e. an appearance of a slip) makes the fluid more elastic. We also see that the values of the viscosity and the first normal stress coefficients are smaller for the active and nonaffine than for the passive.

Steady-state values of η, Ψ_1, and Ψ_2 as functions of the shear rate for the three types of advection are shown on Figure(2.2). For the classical Maxwell model we see, as it is well known, that all η, Ψ_1, and $\Psi_2 = 0$ are independent of the shear rate. The shear thinning appears in the modified advections because of the occurrence of the slip.

Figure (2.3) and Figure (2.4) display the influences of the coefficients μ_1 and μ_2 on the time evolution of η, Ψ_1, and Ψ_2 for the active advection. The ellipses display the conformation tensor $\boldsymbol{c}$. As μ_1 increases or μ_2 decreases, we see that the results for the active advection approaches the results calculated for the affine advection.

$\boldsymbol{\Phi_w}$ is the extra velocity gradient (see (2.14)) participating in the active advection. Together with $\boldsymbol{c}$, it characterizes the morphology in the active advection. Figure (2.5) shows the nonzero components of $\boldsymbol{\Phi_w}$. We see that the increase in

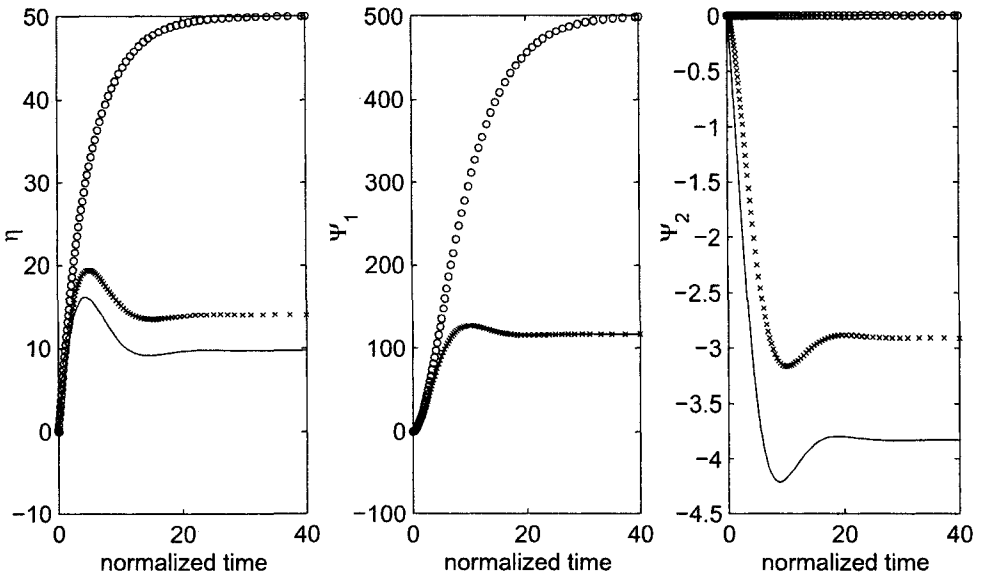

Figure 2.1: Comparison of the time evolution of η, Ψ_1 and Ψ_2 for the three types of advection in the start-up simple shear flow with $\kappa_1 = 2$, $\kappa_2 = 10^2$, $\kappa_3 = 10^3$, $\mu_1 = 10^3$, $\mu_2 = 5$, $\mu_3 = 10$. (o) affine, (x) nonaffine, (-) active

μ_2 (i.e. the increase of the slip parameter ζ) causes $|\Phi_{\boldsymbol{w}}|$ to increase. We recall that $\Phi_{\boldsymbol{w}} = 0$ in passive and nonaffine advections.

Figure (2.6) illustrates the influence of μ_2 on the time evolution of the conformation tensor $\boldsymbol{c}$. L, W and B are the three eigenvalues of $\boldsymbol{c}$, and θ is the orientational angle (the angle between the longest axis and the flow direction). While L and B show important variations, the angle θ is almost independent of μ_2.

2.4 Droplet Deformations in Emulsions

The fluid investigated in the previous section was a model fluid (Maxwell fluid). We have seen how changes in the advection change its rheology and morphology. In order to be able to compare predictions of the active advection with experimental results and also with theoretical results obtained on more microscopic levels (in particular then on the level of microhydrodynamics), we have to adapt the viewpoint of the active advection developed in the previous section to a specific

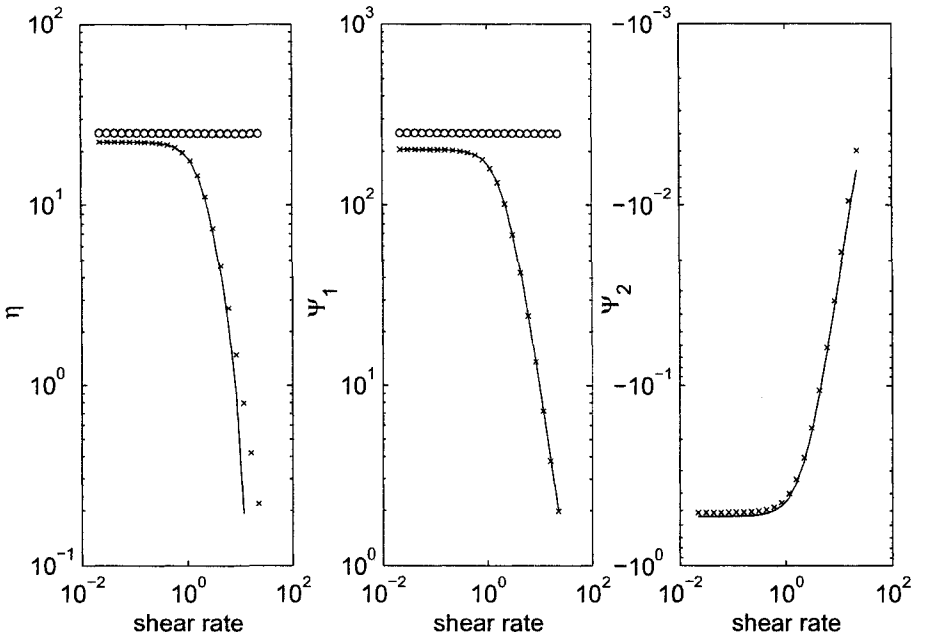

Figure 2.2: The steady-state value of η, Ψ_1, and Ψ_2 as a function of the shear rate for the three advections with $\dot{\gamma} = 1, a = 10^{-4}, \eta_m = 10^{-2}, \alpha = 5 \times 10^{-7}, K = 5, \Lambda = 10^{-6}, \beta = 2 \times 10^5, \lambda = 10^9, \xi = 10^6$. (o) affine, (x) nonaffine, (-) active

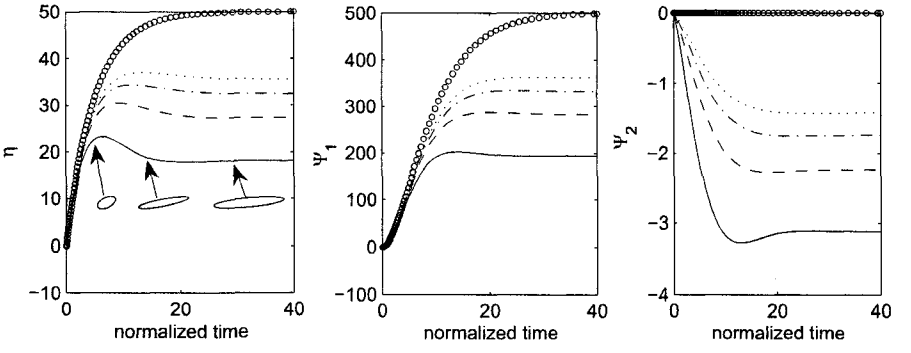

Figure 2.3: The influence of μ_1 on the time evolution of η, Ψ_1, and Ψ_2 for the active advection in the start-up simple shear flow with $\kappa_1 = 2$, $\kappa_2 = 10^2$, $\kappa_3 = 10^3$, $\mu_2 = 5$, $\mu_3 = 10$. The parameter μ_1 has different values: $(-)2 \times 10^3$, $(--)4 \times 10^3$, $(-.)6 \times 10^3$, $(...)8 \times 10^3$. The mark (o) denotes the affine advection

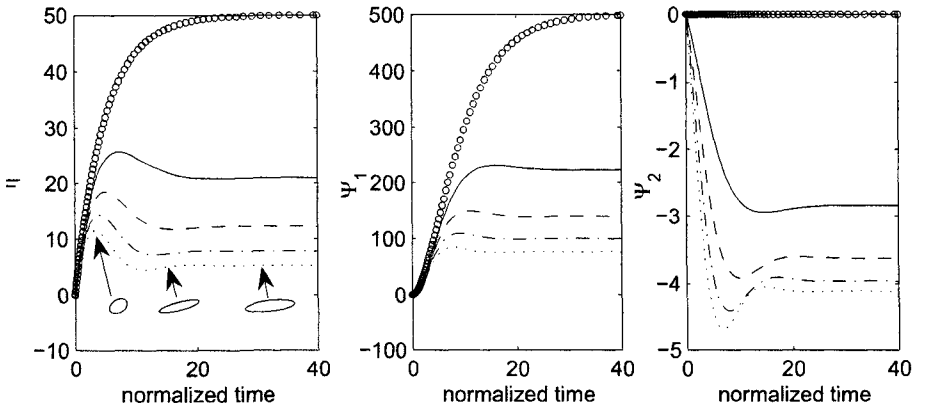

Figure 2.4: The influence of μ_2 on the time evolution of η, Ψ_1, and Ψ_2 for the active advection in the start-up simple shear flow with $\kappa_1 = 2$, $\kappa_2 = 10^2$, , $\kappa_3 = 10^3$, $\mu_1 = 5$, $\mu_3 = 10$. The parameter μ_2 has different values: $(-)2 \times 10^3$, $(--)4 \times 10^3$, $(-.)6 \times 10^3$, $(...)8 \times 10^3$. The mark (o) denotes the affine advection

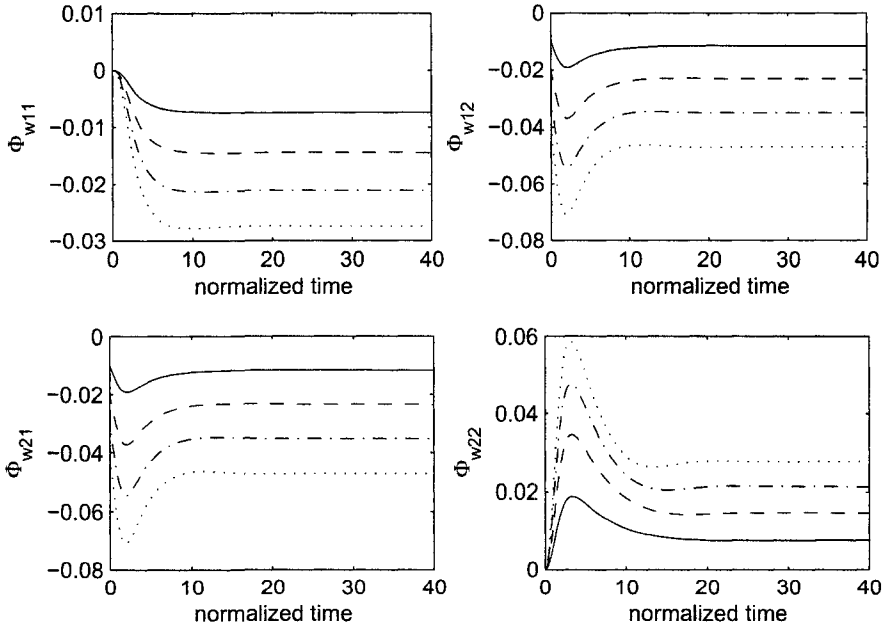

Figure 2.5: The influence of μ_2 on the time evolution of the extra velocity gradient $\Phi_{\boldsymbol{w}}$ for the active advection with the same parameters and notations as the ones used on Figure (2.4).

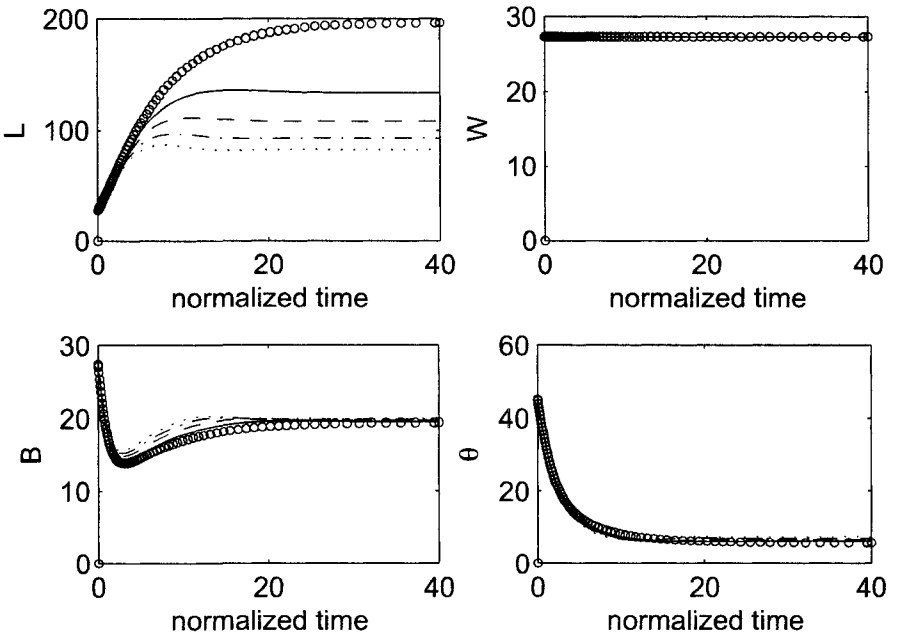

Figure 2.6: The influence of μ_2 on the time evolution of the conformation tensor $\boldsymbol{c}$ for the active advection with the same parameters and notations as the ones used on Figure (2.4). $L > W > B$ denote the three axes of $\boldsymbol{c}$, the orientational angle θ is the angle between the longest axis to the flow direction. The mark (o) denotes the affine advection

fluid that can be investigated experimentally and theoretically on other levels of description. In this section we choose a mixture of two immiscible Newtonian fluids. Deformable droplets of the miner fluid are dispersed in the matrix fluid. This type of emulsion has been indeed investigated extensively both experimentally [25-27] and theoretically on the level of microhydrodynamics [15-17,28-32]. We shall be able therefore to make the comparison.

We begin the process of adapting the governing equations (2.14) to emulsions by selecting state variables. We choose them to be same as the ones chosen in the previous section (see (2.11)). However, the conformation tensor $\boldsymbol{c}$ has now a specific physical interpretation. The ellipsoid associated with the conformation tensor $\boldsymbol{c}$ (i.e. graph of $< \boldsymbol{r}, \boldsymbol{cr} >= 1$) represents the droplet. Since both the minor and the matrix fluids are assumed to be incompressible, the volume of the droplet (i.e. $\det \boldsymbol{c}$) remains unchanged in deformations. Consequently, the state variables chosen in this section are:

$$x = (\boldsymbol{u}(\boldsymbol{r}), \boldsymbol{c}, \boldsymbol{w}); \quad det(\boldsymbol{c}) = const. \tag{2.39}$$

Due to the constraint $\det \boldsymbol{c} = const.$, the kinematics of (2.39) changes. The Poisson bracket (2.13), expressing the kinematics of (2.11), changes [33] into

$$\begin{aligned}
\{A,B\}^{(2)} \;=\; & c_{ki}\left(A_{c_{im}}\partial_k(B_{u_m}) - B_{c_{im}}\partial_k(A_{u_m})\right) \\
& + c_{km}\left(A_{c_{im}}\partial_k(B_{u_i}) - B_{c_{im}}\partial_k(A_{u_i})\right) \\
& + c_{jk}\left(A_{c_{mj}}B_{w_{mk}} - B_{c_{mj}}A_{w_{mk}}\right) \\
& + c_{mk}\left(A_{c_{mj}}B_{w_{jk}} - B_{c_{mj}}A_{w_{jk}}\right) \\
& - \frac{2}{3}c_{kl}\left(A_{c_{kl}}\partial_j B_{u_j} - B_{c_{kl}}\partial_j A_{u_j}\right) \\
& - \frac{2}{3}c_{kl}\left(A_{c_{kl}}B_{w_{jj}} - B_{c_{kl}}A_{w_{jj}}\right) \\
& + w_{ik}\left(A_{w_{im}}\partial_k(B_{u_m}) - B_{w_{im}}\partial_k(A_{u_m})\right) \\
& - w_{kj}\left(A_{w_{mj}}\partial_m(B_{u_k}) - B_{w_{mj}}\partial_m(A_{u_k})\right) \\
& + w_{ij}\left(A_{w_{im}}B_{w_{mj}} - B_{w_{im}}A_{w_{mj}}\right)
\end{aligned} \tag{2.40}$$

The time evolution equations (2.2) corresponding to the Poisson bracket (2.40)

are the following:

$$\begin{aligned}
\frac{\partial u_i}{\partial t} &= -\partial_j\left(\frac{u_i u_j}{\rho}\right) - \partial_i p - \partial_j \sigma_{ij} \\
\frac{\partial c_{ij}}{\partial t} &= c_{ki}(\partial_k(\Phi_{u_j}) + \Phi_{w_{jk}}) + c_{kj}(\partial_k(\Phi_{u_i}) + \Phi_{w_{ik}}) - \frac{2}{3}c_{ij}\Phi_{w_{kk}} \\
&\quad -\Xi_{\Phi_{c_{ij}}} \\
\frac{\partial w_{ij}}{\partial t} &= w_{ik}(\partial_k(\Phi_{u_j}) + \Phi_{w_{jk}}) - w_{kj}(\partial_i(\Phi_{u_k}) + \Phi_{w_{ki}}) \\
&\quad -2c_{kj}\Phi_{c_{ik}} + \frac{2}{3}\delta_{ij}c_{kl}\Phi_{c_{kl}} \\
&\quad -\Xi_{\Phi_{w_{ij}}}
\end{aligned} \tag{2.41}$$

where p is the scalar pressure, and $\boldsymbol{\sigma}$ is the extra stress tensor

$$\sigma_{ij} = -2c_{jk}\Phi_{c_{ki}} + \frac{2}{3}\delta_{ij}c_{kl}\Phi_{c_{kl}} - w_{kj}\Phi_{w_{ki}} + w_{ik}\Phi_{w_{jk}} \tag{2.42}$$

Since the constraint $\det \boldsymbol{c} = const.$ has to be preserved also in the dissipative part of the time evolution, we have to modify also the dissipation potential. Following [33], we choose

$$\begin{aligned}
\Xi &= X^{(1)}_{ij}\frac{1}{2}\Lambda^{(1)}c_{jk}X^{(1)}_{ik} \\
&\quad + \begin{pmatrix} X^{(2)}_{ij}, & X^{(3)}_{ij} \end{pmatrix} \frac{1}{2} \begin{pmatrix} \eta_0\delta_{jk} & \Lambda^{(2)}_{12}c_{jk} \\ \Lambda^{(2)}_{12}c_{jk} & \Lambda^{(2)}_{22}c_{jk} \end{pmatrix} \begin{pmatrix} X^{(2)}_{ik} \\ X^{(3)}_{ik} \end{pmatrix}
\end{aligned}$$

where

$$\begin{aligned}
X^{(1)}_{ij} &= \Phi_{c_{ij}} - \frac{1}{3}c^{-1}_{ij}tr(\boldsymbol{c}\Phi_c) \\
X^{(2)}_{ij} &= \frac{1}{2}(\partial_i(\Phi_{u_j}) + \partial_j(\Phi_{u_i})) \\
X^{(3)}_{ij} &= \Phi_{w_{ij}}
\end{aligned} \tag{2.43}$$

are (in the terminology of nonequilibrium thermodynamics) thermodynamic forces. It is easy to verify that the time evolution equations (2.41) imply indeed $\frac{d\det \boldsymbol{c}}{dt} = 0$.

Next, we turn our attention to the free energy Φ. We have to express in it the physics of droplet deformations. We shall modify (2.18) as follows. We leave the kinetic energy (i.e. the first and the last term in (2.18)) unchanged. The parameter α appearing in (2.18) is now equal to $1/\rho$. The second term in (2.18) (representing there the entropy) represents now the constraint $det\boldsymbol{c} = const.$. The third term in (2.18) represents the energy. In the case of deformable droplets, it will be thus the surface energy associated with the stress on the interface. Let Γ be the interfacial tension. The surface area of the droplet is approximated by the second invariant $\frac{1}{2}\left((tr\boldsymbol{c})^2 - tr\boldsymbol{cc}\right)$. The surface energy is thus $\frac{\Gamma}{2a^5}\left((tr\boldsymbol{c})^2 - tr\boldsymbol{cc}\right)$. Consequently, the free energy Φ, replacing in this section the free energy (2.18), is given by

$$\Phi = \int d\boldsymbol{r}\left[\frac{\boldsymbol{u}^2}{2\rho} - \frac{\chi\Gamma}{2a^5}\ln\det\boldsymbol{c} + \frac{\Gamma}{2a^5}\left((tr\boldsymbol{c})^2 - tr\boldsymbol{cc}\right) + \frac{w_{ij}c^{-1}_{jk}w_{ik}}{2\rho}\right] \quad (2.44)$$

where a is the radius of the undeformed droplet and χ is the Lagrange multiplier. If the constraint is $\det\boldsymbol{c} = a^6$ then $\chi = 4$ and $(\boldsymbol{c}_{eq}, \boldsymbol{w}_{eq})$ describing the thermodynamic equilibrium state (i.e. the state at which the free energy Φ reaches its minimum) is given by

$$\boldsymbol{c}_{eq} = a^2\boldsymbol{\delta};\ \boldsymbol{w}_{eq} = 0 \quad (2.45)$$

2.4.1 Results

By inserting (2.44) and (2.43) into (2.41) we obtain

$$\begin{aligned}
\frac{d\boldsymbol{c}}{dt} &= (\boldsymbol{D}+\boldsymbol{W})\cdot\boldsymbol{c} + \boldsymbol{c}\cdot(\boldsymbol{D}-\boldsymbol{W}) + \frac{1}{\rho}\left[\boldsymbol{w} + \boldsymbol{w}^T - \frac{2}{3}\boldsymbol{c}tr\left(\boldsymbol{w}\cdot\boldsymbol{c}^{-1}\right)\right] \\
&\quad -\frac{1}{2}\Lambda^{(1)}\left[2\frac{\Gamma}{a^5}(tr\boldsymbol{c}\cdot\boldsymbol{c} - \boldsymbol{c}\cdot\boldsymbol{c}) - \frac{1}{2\rho}\left(\boldsymbol{c}^{-1}\cdot\boldsymbol{w}^T\cdot\boldsymbol{w} + \boldsymbol{w}^T\cdot\boldsymbol{w}\cdot\boldsymbol{c}^{-1}\right)\right. \\
&\quad \left. -\frac{2}{3}[\bullet]\boldsymbol{\delta} - \frac{2}{3}\boldsymbol{c}\left(2\frac{\Gamma}{a^5}tr\boldsymbol{c} - \frac{1}{2\rho}tr\left(\boldsymbol{c}^{-1}\cdot\boldsymbol{w}^T\cdot\boldsymbol{w}\cdot\boldsymbol{c}^{-1}\right) - \frac{1}{3}[\bullet]tr\boldsymbol{c}^{-1}\right)\right] \\
\frac{d\boldsymbol{w}}{dt} &= \boldsymbol{w}\cdot(\boldsymbol{D}-\boldsymbol{W}) - (\boldsymbol{D}-\boldsymbol{W})\cdot\boldsymbol{w} + \frac{1}{\rho}\boldsymbol{w}\cdot\boldsymbol{c}^{-1}\cdot\boldsymbol{w}^T \\
&\quad -2\frac{\Gamma}{a^5}(tr\boldsymbol{c}\cdot\boldsymbol{c} - \boldsymbol{c}\cdot\boldsymbol{c}) + \frac{2}{3}[\bullet]\boldsymbol{\delta} - \Lambda^{(2)}_{12}\boldsymbol{D}\cdot\boldsymbol{c} - \Lambda^{(2)}_{22}\frac{1}{\rho}\boldsymbol{w}
\end{aligned}$$

$$\sigma = \int_0^1 ds \left[-2\frac{\Gamma}{a^5}(tr\boldsymbol{c}\cdot\boldsymbol{c} - \boldsymbol{c}\cdot\boldsymbol{c}) + \frac{2}{3}[\bullet]\boldsymbol{\delta} + \frac{1}{\rho}\boldsymbol{w}\cdot\boldsymbol{c}^{-1}\cdot\boldsymbol{w}^T \right] \tag{2.46}$$

where

$$[\bullet] = \frac{\Gamma}{a^5}\left((tr\boldsymbol{c})^2 - tr(\boldsymbol{c}\cdot\boldsymbol{c})\right) - \frac{1}{2\rho}tr\left(\boldsymbol{w}^T\cdot\boldsymbol{w}\cdot\boldsymbol{c}^{-1}\right) \tag{2.47}$$

In the dimensionless variables: $\boldsymbol{c}^* = \boldsymbol{c}/a^2$, $\boldsymbol{w}^* = \boldsymbol{w}/\eta_m$, $\boldsymbol{D}^* = \boldsymbol{D}/\dot{\gamma}$, $\boldsymbol{W}^* = \boldsymbol{W}/\dot{\gamma}$, $\sigma^* = \sigma/\dot{\gamma}\eta_m$, $t^* = t/\tau$, where $\tau = a\eta_m/\Gamma$ is the relaxation time of the interface, Eqs.(2.46) become (to simplify the notation, we omit hereafter the star)

$$\begin{aligned}
\frac{d\boldsymbol{c}}{dt} &= Ca\left[(\boldsymbol{D}+\boldsymbol{W})\cdot\boldsymbol{c} + \boldsymbol{c}\cdot(\boldsymbol{D}-\boldsymbol{W})\right] + \kappa\left[\boldsymbol{w} + \boldsymbol{w}^T - \frac{2}{3}\boldsymbol{c}tr\left(\boldsymbol{w}\cdot\boldsymbol{c}^{-1}\right)\right] \\
&\quad -\frac{1}{3}\xi_1\left[\boldsymbol{c}tr\boldsymbol{c} - 3\boldsymbol{c}\cdot\boldsymbol{c} - \left((tr\boldsymbol{c})^2 - tr(\boldsymbol{c}\cdot\boldsymbol{c})\right)\left(\boldsymbol{\delta} - \frac{1}{3}\boldsymbol{c}tr\boldsymbol{c}^{-1}\right)\right] \\
&\quad -\frac{1}{6}\kappa\xi_1\left[tr\left(\boldsymbol{w}^T\cdot\boldsymbol{w}\cdot\boldsymbol{c}^{-1}\right)\left(\boldsymbol{\delta} - \frac{1}{3}\boldsymbol{c}tr\boldsymbol{c}^{-1}\right) + \boldsymbol{c}tr\left(\boldsymbol{c}^{-1}\cdot\boldsymbol{w}^T\cdot\boldsymbol{w}\cdot\boldsymbol{c}^{-1}\right)\right. \\
&\quad \left. -\frac{3}{2}\left(\boldsymbol{c}^{-1}\cdot\boldsymbol{w}^T\cdot\boldsymbol{w} + \boldsymbol{w}^T\cdot\boldsymbol{w}\cdot\boldsymbol{c}^{-1}\right)\right] \\
\frac{d\boldsymbol{w}}{dt} &= Ca\left[\boldsymbol{w}\cdot(\boldsymbol{D}-\boldsymbol{W}) - (\boldsymbol{D}-\boldsymbol{W})\cdot\boldsymbol{w}\right] - 2(\boldsymbol{c}tr\boldsymbol{c} - \boldsymbol{c}\cdot\boldsymbol{c}) \\
&\quad +\frac{2}{3}\left((tr\boldsymbol{c})^2 - tr(\boldsymbol{c}\cdot\boldsymbol{c})\right)\boldsymbol{\delta} + \kappa\left(\boldsymbol{w}\cdot\boldsymbol{c}^{-1}\cdot\boldsymbol{w}^T - \frac{1}{3}tr(\boldsymbol{w}^T\cdot\boldsymbol{w}\cdot\boldsymbol{c}^{-1})\delta\right) \\
&\quad -Ca\,\xi_2\boldsymbol{D}\cdot\boldsymbol{c} - \xi_3\boldsymbol{w}
\end{aligned} \tag{2.48}$$

$$\begin{aligned}
\sigma &= Ca^{-1}\left[-2(\boldsymbol{c}tr\boldsymbol{c} - \boldsymbol{c}\cdot\boldsymbol{c}) + \frac{2}{3}\left((tr\boldsymbol{c})2 - tr(\boldsymbol{c}\cdot\boldsymbol{c})\right)\boldsymbol{\delta}\right. \\
&\quad \left. +\kappa\left(\boldsymbol{w}\cdot\boldsymbol{c}^{-1}\cdot\boldsymbol{w}^T - \frac{1}{3}tr(\boldsymbol{w}^T\cdot\boldsymbol{w}\cdot\boldsymbol{c}^{-1})\boldsymbol{\delta}\right)\right]
\end{aligned} \tag{2.49}$$

where

$$Ca = \frac{\eta_m a\dot{\gamma}}{\Gamma};\ \kappa = \frac{\eta_m^2}{a\Gamma\rho};\ \xi_1 = \frac{\eta_m\Lambda^{(1)}}{a^2};\ \xi_2 = \frac{a^2\Lambda_{12}^{(2)}}{\eta_m};\ \xi_3 = \frac{a\eta_m\Lambda_{22}^{(2)}}{\Gamma\rho} \tag{2.50}$$

are dimensionless numbers, Ca is the capillary number. The initial conditions are the equilibrium states (2.45) (i.e. $\boldsymbol{c}_{eq} = \boldsymbol{\delta}$ and $\boldsymbol{w} = 0$ if the dimensionless variables are used).

Given values of the material parameters (2.50), solutions to (2.48) can be found easily with the assistance of standard software packages. The solution consists of the morphology (droplet deformations expressed in the conformation tensor $\boldsymbol{c}$ and the perturbed velocity field expressed in the velocity gradient $\Phi_{\boldsymbol{w}}$) and the rheology expressed in the extra stress tensor $\boldsymbol{\sigma}$.

The data with which we shall compare our predictions come from three sources: (1) the Maffettone-Minale model [34], (2) the microhydrodynamic modeling, and (3) experiments. Due to limitations in the availability of data, we shall limit the comparison to droplet deformations in weak flows (i.e. to the case of small capillary numbers Ca).

First, we recall the Maffettone-Minale model. The structural state variable chosen in [34] is the conformation tensor $\boldsymbol{c}$. It is exactly the same tensor appearing in (2.39). Phenomenological considerations lead Maffettone and Minale to the following equation governing its time evolution:

$$\begin{aligned}\frac{d\boldsymbol{c}}{dt} &= Ca(\boldsymbol{D}+\boldsymbol{W})\cdot\boldsymbol{c}+\boldsymbol{c}\cdot(\boldsymbol{D}-\boldsymbol{W})-Ca(1-f_2)(\boldsymbol{D}\cdot\boldsymbol{c}+\boldsymbol{c}\cdot\boldsymbol{D}) \\ &\quad -f_1(\boldsymbol{c}-\frac{6\det\boldsymbol{c}}{((tr\boldsymbol{c})^2-tr(\boldsymbol{c}\cdot\boldsymbol{c}))}\boldsymbol{\delta})\end{aligned} \tag{2.51}$$

where $f_1=\frac{40(p+1)}{(2p+3)(19p+16)}$, $p=\eta_d/\eta_m$, η_d and η_m are viscosity of droplet and matrix fluids, and $f_2=\frac{5}{2p+3}$ or alternatively $f_2=\frac{5}{2p+3}+\frac{3Ca^2}{2+6Ca^2}$. We shall refer to the Maffettone-Minale model with the first choice of f_2 as MM-1 model and with the second choice as MM-2 model.

We have seen in Section 2.3 that (2.38), representing nonaffine advection, is an approximation (valid when the relaxation time of $\boldsymbol{w}$ is very small) of the active advection represented by Eqs.(2.33) and (2.34). Similarly, we can see that (2.51) represents the Gordon-Schowalter type nonaffine advection and that it is an approximation of the time evolution equations (2.48)representing the active advection. We shall make the relation between (2.48) and (2.51) explicit for small Ca. We look for solutions of (2.48) in the form

$$\begin{aligned}\boldsymbol{c} &= \boldsymbol{\delta}+Ca\,\boldsymbol{c}^{(1)}+O(Ca^2) \\ \boldsymbol{w} &= Ca\,\boldsymbol{w}^{(1)}+O(Ca^2)\end{aligned} \tag{2.52}$$

By inserting Eq.(2.52) into Eq.(2.48), we get the time evolution equations for $\boldsymbol{c}$ and $\boldsymbol{w}$ to the first order in Ca. If we make in addition the assumption that $\boldsymbol{w}$ reaches its steady state much faster than $\boldsymbol{c}$, we arrive at

$$\frac{d\boldsymbol{c}^{(1)}}{dt} = -\left(\frac{4\kappa}{\xi_3} + \xi_1\right)\boldsymbol{c}^{(1)} + 2(1 - \frac{\kappa\xi_2}{\xi_3})\boldsymbol{D} \tag{2.53}$$

and

$$\boldsymbol{w}^{(1)} = -\frac{1}{\xi_3}(2\boldsymbol{c}^{(1)} + \xi_2\boldsymbol{D}) \tag{2.54}$$

By comparing (2.53) and the first order in Ca approximation of (2.51), we see that both equations are the same provided

$$\frac{4\kappa}{\xi_3} + \xi_1 = \frac{40(p+1)}{(2p+3)(19p+16)} \tag{2.55}$$

and

$$1 - \frac{\kappa\xi_2}{\xi_3} = \frac{5}{2p+3} \tag{2.56}$$

Next, we turn our attention to microhydrodynamics where deformations of droplets suspended in a fluid subjected to a flow are investigated by formulating and solving the corresponding Stokes problem (see the first two paragraph of Introduction). Extensive numerical calculations are typically needed to find the solutions. An exception is the particular case of weak flows (i.e. small capillary number Ca) where the perturbation method (with Ca playing the role of small parameter) [30] provides sufficiently accurate approximation to the solutions. We present the results in Figures (2.7) and (2.8).

Finally, the experimental data are taken from Guido and Villone [27] and Torza et al. [26].

Figure (2.7) compares predictions of four models (the model of active advection developed in this paper, the MM-1 model, the MM-2 model and the microhydrodynamic investigation) with the experimental data reported in [27]. The imposed flow in [30] is a start-up simple shear flow, the viscosity ratio is $p = 1.4$, and capillary number 0.24. The deformation of the droplet is expressed by the Taylor's deformation parameter $D_f = \frac{L-B}{L+B}$, where L and B are the longest and shortest length of its main axes. We can see that the MM-1 model under-

estimates the droplet deformation. The Cox microhydrodynamic analysis gives a good prediction on the steady deformation parameter but underestimates the evolution time needed for reaching the steady state. The MM-2 model and the model of active advection developed in this paper with the parameters

$$k = 10^6,\ \xi_1 = 0.385,\ \xi_2 = 10,\ \xi_3 = 2 \times 10^8 \tag{2.57}$$

provide a good agreement. The parameters (2.57) are close to but not identical with those calculated from (2.55),(2.56).

Figure (2.8) compares predictions of four models (the model of active advection , the MM-1 model, the MM-2 model and the microhydrodynamic investigation) with the experimentally observed deformation parameter D_f and orientational angle θ for different capillary numbers Ca. The orientation angle is the angle between the orientation of the longest axis L of the droplet and the direction of the imposed flow. The experimental data are taken from Torza et al. [26] for fluids with the viscosity ratio $p = 3.6$. Predictions of the MM models as well as the Cox analysis for both D_f and θ show a good agreement with experimental results for small Ca. As Ca increases, important deviations arise. Both the MM-1 model and the Cox analysis underestimate the deformation, while MM-2 model overestimates it. The unsatisfactory prediction of the Cox analysis at this regime is explained by the fact that Ca is too large for the perturbation method to be applicable. The model of active advection with the parameters

$$k = 10^6,\ \xi_1 = 0.26,\ \xi_2 = 5 \times 10^3,\ \xi_3 = 1.7 \times 10^{10} \tag{2.58}$$

gives a good fit throughout the whole range of $0 < Ca < 1$. As in the case of the set of parameters (2.57), the parameters (2.58) are close but not identical to those calculated from (2.55),(2.56). In this figure we see very clearly that the active advection represents the observed behavior more faithfully than the nonaffine advection expressed in the Maffettone-Minale model.

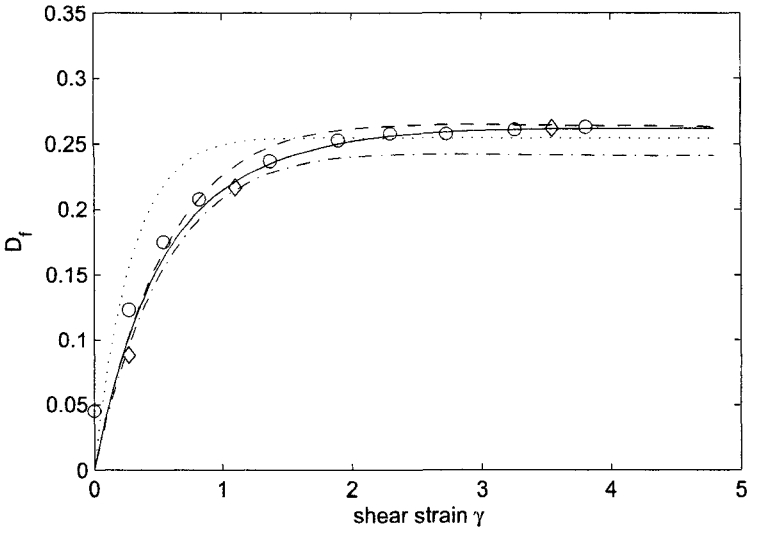

Figure 2.7: Comparison of model predictions with experimental data of the time evolution of the deformation parameter D_f for a droplet under start-up simple shear flow, with shear strain γ as the normalized time: (-.-) correspond to the MM-1 model, (- -) to the MM-2 model, (...) to the Cox analysis, (—) to the present model with the parameters (2.57), and (o, $\diamond$) to the experimental data taken from Guido and Villone [27] with $Ca = 0.24$ and $p = 1.4$.

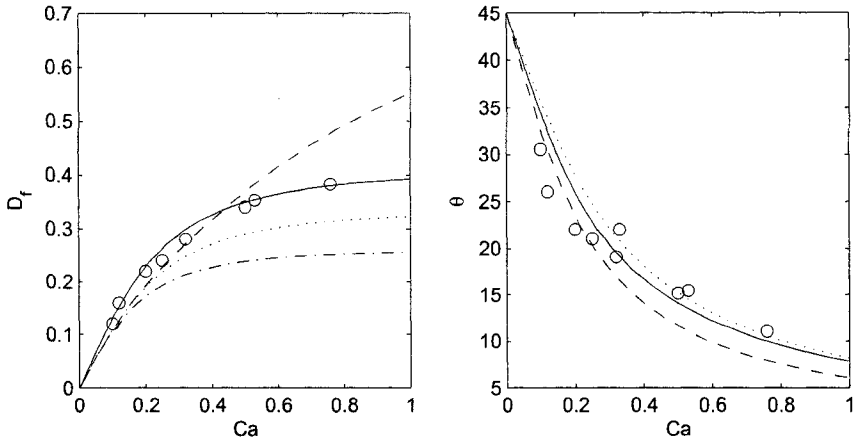

Figure 2.8: Comparison of model predictions with experimental data for the steady-state deformation parameter D_f and orientation angle θ as functions of the capillary number Ca for a droplet subjected to a simple shear flow: (-.-) corresponds to the MM-1 model, (- -) to the MM-2 model, (...) to the Cox analysis, (—) to the present model with the parameters (2.58), and (o) experimental data taken from Torza et al. [26] with $p = 3.6$.

2.5 Concluding remarks

Microhydrodynamics [1] offers a formulation of the suspension dynamics involving a detailed analysis of the physics taking place on the particle-fluid interface. The complex particle-fluid interactions induce interaction among the particles (hydrodynamic interactions) and make their advection active. The problem with this approach is that the governing equations can be solved only with a considerable effort. The mathematical complexity is then an obstacle in applications and also in getting an understanding of the physics involved. Our objective in this paper is to discuss the active advection on a mesoscopic level on which the governing equations are much easier to solve. The mesoscopic level used in this paper is of the same type as for example the level used by Doi and Ohta [24] in their investigation of rheology of immiscible blends. Fluids involving an interface are regarded in this type of theories as fluids with an internal structure that is spread throughout the fluid. In our formulation of mesoscopic theories we also use systematically the requirement of the compatibility of the time evolution with thermodynamics.

The microscale fluid velocity, i.e. the fluid velocity influenced by the presence of particles, that is one of the state variables used in the microhydrodynamic formulation is replaced in our model by a tensor field $\boldsymbol{w}$ having the physical interpretation of the thermodynamic conjugate of the velocity gradient participating in the advection. With this state variable we are then expressing the same physics as the one expressed in microhydrodynamics. The governing equations of the model consist of the time evolution equations for the distribution and shape of the advected particles expressed in our model in the conformation tensor $\boldsymbol{c}$, the tensor field $\boldsymbol{w}$, and the overall momentum field that involves the extra stress tensor $\boldsymbol{\sigma}$ expressed in terms of $(\boldsymbol{c}, \boldsymbol{w})$. The complete set of the time evolution equations possesses the GENERIC structure guaranteeing the compatibility of the model with thermodynamics. The change from the passive advection of $\boldsymbol{c}$ to the active advection of $(\boldsymbol{c}, \boldsymbol{w})$ is expressed in the change of kinematics (i.e. the Poisson bracket). In the particular case when $\boldsymbol{w}$ approaches rapidly the states at which $\boldsymbol{w} = 0$, the equations governing the time evolution of $(\boldsymbol{c}, \boldsymbol{w})$ can be approximated by an equation governing the time evolution of $\boldsymbol{c}$ involving a modified (nonaffine) advection. Such advection has been introduced phenomenologically in [22]. This type of modification of the advection cannot be expressed as a modification of kinematics (i.e. as a modification of the Poisson bracket) but, it can be expressed, as shown in [9], as an appearance of a new term on the right hand side of the time evolution equations. The new term is time reversible, entropy preserving, skew symmetric (i.e. the properties that the Hamiltonian term has) but it is non Hamiltonian since the Jacobi identity is not satisfied.

The general mesoscopic theory of active advection is illustrated in this paper on two examples. In the first example we take the most classical rheological model, namely the Maxwell model, and modify it by changing the passive advection involved in it into the nonaffine and the active advections. Rheological and morphological consequences of the modifications are displayed on Figures 1-6. In order to be able to compare predictions of the model of active advection developed in this paper with results arising in other theoretical approaches to active advection and in experiments, we turn in the second example to a model of a concrete fluid, namely the immiscible blends with droplet morphology. The comparison of predictions of the model developed in this paper with the Maffettone-Minal model, microhydrodynamic analysis and experiments is shown on Figures 7 and

8.

Acknowledgment

This research has been partially supported by the Natural Sciences and Engineering Research Council of Canada

References

[1] S. Kim, S.J. Karilla, Microhydrodynamics, Butterworth-Heinemann (1991)

[2] M. Grmela, Particle and bracket formulations of kinetic equations, Contemp. Math. 28 (1984) 125-132.

[3] M. Grmela, Hamiltonian dynamics of incompressible elastic fluids, Phys. Lett A 130 (1988) 81-86.

[4] M. Grmela, Bracket Formulation of Diffusion-Convection Equation, Physica D 21 (1986) 179-212.

[5] M. Grmela, Mesoscopic dynamics and thermodynamics: appliocations to polymeric fluids, in: J. Casas-Vazquez, D. Jou (Eds.), Rheological Modelling: Thermodynamic and Statistical Approaches, Lecture Notes in Physics, vol. 381, Springer, Berlin, 1991, pp. 99-125.

[6] A.N. Beris, B.J. Edwards, The Thermodynamics of Flowing Systems , Oxford Univ. Press (1994)

[7] M. Grmela, H.C. Oettinger, Dynamics and thermodynamics of complex fluids. Part I. Illustration of a general formalism, Phys. Rev. E 56 (1997) 6620-6632.

[8] H.C. Oettinger,M. Grmela, Dynamics and thermodynamics of complex fluids. Part II. Development of a general formalism, Phys. Rev. E 56 (1997) 6632-6655.

[9] H.C Oettinger, Beyond Equilibrium Thermodynamics, Wiley-Interscience (2005)

[10] M. Grmela, Stress Tensor in Generalized Hydrodynamics, Phys. Letters A 111 (1985) 41-44.

[11] H.A. Stone, L.G. Leal, Relaxation and breakup of an initially extended

drop in an otherwise quiescent fluid, J. Fluid Mech. 198 (1989) 399-427.

[12] J. Blawzdziewicz, P. Vlahovska, M. Loewenberg, Rheology of dilute emulsion of surfactant-covered spherical drops, Physica A 276 (2000) 50-85.

[13] P.M. Vlahovska, M. Loewenberg, J. Blawzdziewicz, Deformation of a surfactant-covered drop in a linear flow, Phys. Fluids 17 (205) 103103-1-18.

[14] J. Lee, C. Pozrikidis, Effect of surfactants on the deformation of drops and bubbles in Navier-Stokes flow, Computers and Fluids, 35 (2006) 43-60.

[15] J.M. Rallison, A. Acrivos, A numerical study of the deformation and burst of a viscous drop in general shear flows. J. Fluid Mech. 89 (1978) 191-200.

[16] H.A. Stone, Relaxation and breakup of an initially extended drop in an otherwise quiescent fluid. J. Fluid Mech. 198 (1989) 399-427.

[17] I.B. Bazhlekov, P.D. Anderson, H.E.H. Meijer, Nonsingular boundary integral method for deformable drops in viscous flows, Phys. Fluids 16 (2004) 1064-1081.

[18] J.D. Eshelby, The determination of the elastic field of an ellipsoidal inclusion, and related problems, Proc. R. Soc. Lond. A 241 (1957) 376-396; J.D. Eshelby, The elastic field outside of an ellipsoidal inclusion, Proc. R. Soc. London A 252 (1959) 561-569.

[19] G.B. Jeffery, The motion of ellipsoidal particles immersed in a viscous fluid, Proc. R. Soc. Lond. A 102 (1922) 181-179.

[20] E.D. Wetzel, C.L. Tucket III, Droplet deformation in dispersions with unequal viscosities and zero interfacial tension, J. Flui Mech. 426 (2001) 199-228.

[21] M. Junk, R. Illner, A new derivation of Jeffery's equation, J. math, fluid mech. 8 (2006) 1-34.

[22] R.J. Gordon, W.R. Schowalter, Anisotropic fluid theory: A different approach to the dumbbell theory of dilute polymer solutions, Trans. Soc. Rheol. 16 (1972) 79-97.

[23] J.E. Marsden, T.S. Ratiu, Introduction to mechanics and symmetry, 2nd ed. in: Texts in Applied Mathematics, vol 17, Springer-Verlag (1999).

[24] M. Doi, T. Ohta, Dynamics and rheology of complex interfaces, J. Chem. Phys. 95 (1991) 1242-1248.

[25] G.I. Taylor, The formation of emulsions in definable field of flow, Proc. Roy. Soc. A 146 (1934) 501-523.

[26] S.Torza, R.G. Cox, S.G. Mason, Particle motions in sheared suspensions. XVII. Transient and steady deformation and burst of liquid drops, J. Colloid Interface Sci. 38 (1972) 395-411.

[27] S.Guido, M. Villone, Three-dimensional shape of a drop under simple shear flow, J.Rheol. 42 (1998) 395-415.

[28] N.A. Frankel, A. Acrivos, The constitutive equation for a dilute emulsion. J. Fluid Mech. 44 (1970) 65-78.

[29] G.I. Taylor, The viscosity of a fluid containing small drops of another fluid, Proc. Roy. Soc. A 138 (1932) 41-48.

[30] R.G. Cox, The deformation of a drop in a general time-dependent fluid flow, J. Fluid Mech. 37 (1969) 601-623.

[31] D.Barthès-Biesel, A. Acrivos, Deformation and burst of a liquid droplet freely suspended in a linear shear field, J. Fluid Mech. 61 (1973)1-21.

[32] S.J. Choi, W.R. Schowalter, Rheological properties of non-dilute suspensions of deformable particles, Phys. Fluids 18 (1975) 420-427.

[33] B.J. Edwards, M. Dressler, M. Grmela and A. Ait-Kadi, Rheological models with microstructural constraints, Rheol. Acta 42 (2003) 64-72.

[34] P.L.Maffettone, M.Minale, Equation of change for ellipsoidal drops in viscous flow, J.Non-Newtonian Fluid Mech., 78 (1998) 227-241.

Chapter 3

Flow Properties of Immiscible Blends: Doi-Ohta Model with Active Advection

Jian Feng Gu, Miroslav Grmela [1]

Ecole Polytechnique de Montreal, C.P.6079 suc. Centre-ville,
Montreal, H3C 3A7, Quebec, Canada

Physical Review E 78 (2008) 056302

[1]corresponding author: e-mail: miroslav.grmela@polymtl.ca

abstract

The interface between two immiscible fluids is both influenced (advected) by the imposed flow and influences (perturbs) it. The perturbation then changes the advection. This phenomenon is taken into account in an extended Doi Ohta model of rheological behavior of immiscible blends. The agreement of rheological predictions with experimental data is improved.

3.1 Introduction

Macroscopic flow behavior of immiscible blends cannot be described with only classical hydrodynamic fields serving as state variables. This is because the immiscible blends contain an interface that evolves in time on the time scale comparable with the time scale on which the hydrodynamic fields evolve. In order to model flows of immiscible blends we have to therefore, first, choose a way to describe states of the interface (we shall call it an interface morphology) and, second, find equations governing the time evolution of the morphology and the hydrodynamic fields.

As for the the mathematical characterization of the morphology, we follow in this paper Doi and Ohta [1]. Immiscible blends are assumed to be isothermal, incompressible and spatially homogeneous. The interface is seen as being uniformly distributed throughout the fluid. Its states are characterized by one tensor $\boldsymbol{q}$ and one scalar Q. The latter is the surface area per unit volume and the former is a symmetric traceless tensor characterizing the orientation of the interface. Other important characteristics of the morphology, as for example the curvature and, more generally, the global shape of the interface, are out of the reach of the Doi Ohta description. Consequently, the strong points of the Doi Ohta theory are: mathematical simplicity, and rheological (rather than morphological) predictions. Below, we shall extend the Doi Ohta model in order to be able to account for the flow perturbations caused by the presence of the interface. The extension will not however provide a more detailed description of the morphology.

For the imposed overall flow the interface is an obstacle that moves and deforms in response to the forces generated in the fluid-interface interactions and also modifies the flow in its neighborhood. If all the details of: (i) the shape of

the interface, (ii) interface-fluid interactions (boundary conditions), and (iii) rheological properties of both fluids involved are known then both the modification of the flow and the modification of the advection can be obtained as a solution to the corresponding Stokes problem. Due to the lack of knowledge of all three point (i)-(iii) mentioned above as well as the enormous mathematical (numerical) complexity involved in the process of solving the Stokes problem, we cannot take this microhydrodynamic path. We only recall that the microhydrodynamics investigation implies that the flow in the vicinity of the interface remains unperturbed (and thus the interface follows passively the flow - a passive advection), only if both fluids in the mixture are identical and the interface is completely structureless and does not interact with the bulk fluid. Otherwise, the flow of the fluid surrounding the interface is always perturbed and the advection of the interface is never passive (we shall call it an active advection). Even if the mechanical properties of the interface as well as the bulk fluid-interface interactions are ignored, just the "rheological inhomogeneity" (i.e. the appearance of regions with different viscosities) is sufficient to create flow perturbations and thus a non passive (active) advection.

Doi and Ohta have assumed in [1] that the interface is advected passively (i.e. its presence does not perturb the the flow around it). A mesoscopic investigation of the advection that takes into account the active role of the interface in its advection but does not enter into all details needed in the complete microhydrodynamic analysis has been introduced in [2]. Our goal in this paper is to replace the passive advection in the Doi Ohta model by the active advection introduced in a general form in [2].

The paper is organized as follows. In Section 3.2 we recall the concept of mesoscopic active advection and the Doi Ohta model. The governing equations of the Doi Ohta model with the active advection are developed in Section 3.3. Predictions of the extended model are compared with predictions of other models and with some published experimental data in Section 3.4.

3.2 Active Advection

States of isothermal, incompressible and homogeneous immiscible blends are described in the Doi Ohta theory by the field of the overall momentum $\boldsymbol{u}(\boldsymbol{r})$ and by the interface morphology characterized by $\boldsymbol{q}$ and Q; $\boldsymbol{r}$ denotes the position vector, $\boldsymbol{q}$ is a symmetric traceless tensor characterizing the orientation of the interface and Q is the surface area per unit volume. In order to be able to deal with the active role that the interface plays in the advection, we introduced another tensor $\boldsymbol{w}$ that is closely related to the gradient of the perturbed velocity.

The governing equations of the extended Doi Ohta theory (a coupled set of equations governing the time evolution of $(\boldsymbol{u}, \boldsymbol{q}, Q, \boldsymbol{w})$) will be constructed in this paper by filling the thermodynamic framework (called GENERIC) with the mesoscopic version of the physics involved in the microhydrodynamic formulation of the Stokes problem. The framework itself guarantees the compatibility of the time evolution with mechanics in the inviscid limit and the compatibility with thermodynamics of externally unforced fluids. The process of filling the framework is called *GENERIC constitutive relations* similarly as the process of filling the framework of local balance laws (representing the general framework for governing equations of classical hydrodynamics) is called *constitutive relations.* In order to prepare the construction of the governing equations of the extended theory we shall recall the GENERIC framework ([3] - [10])(in Section 3.2.1), GENERIC formulation of the active advection developed in [2] (Section 3.2.2), and the GENERIC formulation of the Doi Ohta theory ([11],[12]) (Section 3.2.3).

3.2.1 Thermodynamic (GENERIC) framework

The abstract framework for the governing equations of classical hydrodynamics (the balance laws) arises from requiring the mass momentum and energy conservation. The filling the framework, i.e. the specification of the fluxes introduced in the balance laws) is called a constitutive relation. In addition to the mass, momentum and energy conservation, solutions to the hydrodynamic equations are also required to agree with the experimental observations constituting the basis of equilibrium thermodynamics (a fluid that is left undisturbed reaches a state at which its behavior is found to be well described by equilibrium thermodynamics).

Consequences of this requirement are explored in nonequilibrium thermodynamics. Still another general aspect of hydrodynamics is its mechanical origin. The balance of momentum has also an alternative interpretation as a continuum version of Newton's law. This mechanical aspect is used in classical hydrodynamics only in providing the part of the momentum flux with the physical interpretation of the force acting on surface. A general framework for the mesoscopic time evolution based on the requirements of the conservation of mass, momentum and energy, and with equal importance also on the requirement of the compatibility with thermodynamics and mechanics is called GENERIC. Its main advantage is its applicability for complex fluids whose states have to be characterized not only by the classical hydrodynamic fields but also with extra fields characterizing the internal structure. If compared with classical hydrodynamics, the GENERIC viewpoint is particularly new and powerful in requiring the compatibility with mechanics. Newton's law enters the analysis not only in providing an alternative physical interpretation to the balance of momentum but also in the discussion of the time evolution of the internal structure. Below, we shall recall the GENERIC framework in the special context of isothermal fluids.

Let x denote the state variables. If we limit ourselves to isothermal and incompressible fluids then the compatible with thermodynamics and mechanics time evolution of x is governed by ([3] - [10])

$$\dot{x} = L\Phi_x - \frac{\partial \Xi}{\partial \Phi_x} \tag{3.1}$$

called in [7], [8] GENERIC. By $\dot{x}$ we denote the time derivative of x. The first term on the right hand side of (3.1) expresses the compatibility with mechanics, the second the compatibility with thermodynamics. The symbols appearing in (3.1) have the following meaning.

Free energy

$\Phi(x)$, a real valued function of x, has the physical meaning of the total free energy. By Φ_x we denote the derivative of Φ with respect to x.

Kinematics

The operator L, hereafter called a Poisson bivector, transforms a covector (a

gradient of a potential) into a vector. From the physical point of view, L expresses kinematics of the state variables x. In the particular case of classical mechanics of particles (the state variables in this case are $x = (p, q)$, where q are position vectors and p the momenta of the particles), $L = \begin{pmatrix} 0 & 1 \\ -1 & 0 \end{pmatrix}$. This is the Poisson bivector transforming in classical mechanics the gradient of energy $E(q, p)$ into a vector field. In the general setting, L is required to satisfy the following properties: $\{A, B\} =< A_x, LB_x >$ is a Poisson bracket, i.e. $\{A, B\} = -\{B, A\}$, and satisfies the Jacobi identity $\{A, \{B, C\}\} + \{B, \{C, A\}\} + \{C, \{A, B\}\} = 0$; A, B, C are sufficiently regular real valued functions of x, $<, >$ denotes the inner product. The Poisson bracket corresponding to $L = \begin{pmatrix} 0 & 1 \\ -1 & 0 \end{pmatrix}$ is thus $\{A, B\} = A_q B_p - B_q A_p$.

Dissipation

$\Xi(\Phi_x)$, called a dissipation potential, is a sufficiently regular real valued function of Φ_x satisfying the following properties:

$$\begin{aligned} &\Xi(0) = 0, \\ &\Xi \textit{ reaches its minimum at } 0, \\ &\Xi \textit{ is convex in a neighborhood of } 0 \end{aligned} \tag{3.2}$$

Properties of solutions of (3.1)

The properties required from L, Ξ appearing in (3.1) imply that solutions to (3.1) satisfy the following inequality:

$$\frac{d\Phi}{dt} \leq 0 \tag{3.3}$$

The free energy Φ can thus only remain unchanged or decrease during the time evolution. To see that (3.3) indeed holds, we note that $\frac{d\Phi}{dt} =< \Phi_x, L\Phi_x > - < \Phi_x, \frac{\partial \Xi}{\partial \Phi_x} >\leq 0$. The last inequality follows from $< \Phi_x, L\Phi_x >= 0$ and from the properties required from the dissipation potential Ξ. The inequality (3.3) together with the thermodynamic stability requirement (i.e. Φ is a convex function of x) allows us to consider Φ as a Lyapunov function. This then means that solutions

to (3.1) tend, as $t \to \infty$, to states that minimize the free energy (i.e. the states, called equilibrium states, that are solutions of $\Phi_x = 0$). Since the first term on the right hand side of (3.1) leaves Φ unchanged, we shall also write (3.1) as

$$\frac{\partial}{\partial t} = \left(\frac{\partial}{\partial t}\right)_{nondiss} + \left(\frac{\partial}{\partial t}\right)_{diss} \tag{3.4}$$

where

$$\left(\frac{\partial x}{\partial t}\right)_{nondiss} = L\Phi_x \tag{3.5}$$

and

$$\left(\frac{\partial x}{\partial t}\right)_{diss} = -\frac{\partial \Xi}{\partial \Phi_x} \tag{3.6}$$

The framework (3.1) is filled by specifying the state variables x, the potentials Φ, Ξ, and the operator $L(x)$. A specification of x, Φ, Ξ, L is called a GENERIC constitutive relation. Below, we shall recall two examples (in Sections 3.2.2 and 3.2.3) and in Section 3.3 we shall develop a third one as the main result of this paper.

3.2.2 GENERIC formulation of active advection

In this subsection we shall gradually develop the time evolution equations introduced in [2].

One component complex fluid

We begin with a one component incompressible and isothermal complex fluid whose internal structure (morphology) is chosen to be characterized by a conformation tensor $\boldsymbol{c}$ (a three-by-three symmetric and positive definite matrix). We assume that the complex fluid is homogeneous and thus we consider $\boldsymbol{c}$ to be independent of $\boldsymbol{r}$. Depending on what type of complex fluid and the internal structure we consider, the conformation tensor $\boldsymbol{c}$ can have many different physical interpretations. Typically, it is seen as a deformation tensor of the internal structure. In Section 3.2.3 we shall interpret it in the context of the Doi Ohta characterization of the interface.

We proceed to specify the GENERIC constitutive relations.

State variables

The state variable x in this subsection is thus

$$x = (\boldsymbol{u}(\boldsymbol{r}), \boldsymbol{c}) \tag{3.7}$$

where $\boldsymbol{u}(\boldsymbol{r})$ is the field of the overall momentum and $\boldsymbol{c}$ is the conformation tensor.

Kinematics

Next, we need the Poisson bracket expressing kinematics of (3.7)(see [13],[14],[15] and Section 3.3.1):

$$\begin{aligned} \{A, B\}^{(u,c)} &= \int d\boldsymbol{r} u_i (\partial_j (A_{u_i}) B_{u_j} - \partial_j (B_{u_i}) A_{u_j}) \\ &+ \int d\boldsymbol{r} c_{kl} (A_{c_{lm}} \partial_k B_{u_m} - B_{c_{lm}} \partial_k A_{u_m}) \\ &+ \int d\boldsymbol{r} c_{km} (A_{c_{lm}} \partial_k B_{u_l} - B_{c_{lm}} \partial_k A_{u_l}) \end{aligned} \tag{3.8}$$

In the above two equations we use the following notation: $i, j = 1, 2, 3$; $\partial_i = \partial / \partial r_i$; repeated indices mean summation; A and B are sufficiently regular real valued functionals of $(\boldsymbol{u}(\boldsymbol{r}), \boldsymbol{c})$; $A_{u_i} = \delta A / \delta u_i(\boldsymbol{r})$; δ / δ denotes the Volterra functional derivative.

The equations $(\dot{x})_{nondiss} = L \Phi_x$ corresponding to the bracket (3.8) are:

$$\begin{aligned} \left(\frac{\partial \boldsymbol{u}}{\partial t} \right)_{nondiss} &= \nabla(\boldsymbol{u}\boldsymbol{v}) - \nabla p - \nabla \boldsymbol{\sigma}^{(nd)} \\ \left(\frac{d\boldsymbol{c}}{dt} \right)_{nondiss} &= \boldsymbol{c} \cdot \nabla \boldsymbol{v} + \nabla \boldsymbol{v}^T \cdot \boldsymbol{c} \end{aligned} \tag{3.9}$$

where

$$\boldsymbol{\sigma}^{(nd)} = -2 \Phi_{\boldsymbol{c}} \cdot \boldsymbol{c} \tag{3.10}$$

p is the hydrostatic pressure, $\boldsymbol{v} = \Phi_{\boldsymbol{u}}$ and the superscript ^{T} denotes the transpose. The time derivative in the second equation in (3.9) is the ordinary derivative (not the partial derivative as in the first equation) since $\boldsymbol{c}$ is, according to our assump-

tion, independent of $\boldsymbol{r}$.

Dissipation

We recall that $\Phi_{\boldsymbol{c}} = 0$ at equilibrium. The thermodynamic force driving the internal structure to its equilibrium is thus $\boldsymbol{X} = \Phi_{\boldsymbol{c}}$. If we limit ourselves to states for which $(\Phi_{\boldsymbol{c}})^k; k \geq 3$ can be neglected, we choose

$$\Xi = \frac{1}{2}\Lambda \operatorname{tr}(\boldsymbol{X} \cdot \boldsymbol{c} \cdot \boldsymbol{X}) \tag{3.11}$$

where $\Lambda > 0$ is a phenomenological coefficient. The equation $(\dot{x})_{diss} = -\frac{\partial \Xi}{\partial \Phi_x}$ becomes thus

$$\begin{aligned} \left(\frac{\partial \boldsymbol{u}}{\partial t}\right)_{diss} &= 0 \\ \left(\frac{d\boldsymbol{c}}{dt}\right)_{diss} &= -\frac{1}{2}\Lambda\left(\boldsymbol{c} \cdot \Phi_{\boldsymbol{c}} + \Phi_{\boldsymbol{c}} \cdot \boldsymbol{c}\right) \end{aligned} \tag{3.12}$$

The individual nature of the complex fluid under consideration is expressed in the free energy Φ and the dissipation potential Ξ. In this paper the complex fluid under investigation is an immiscible blend. We shall discuss Φ and Ξ in Section 3.3 after completing the presentation of the advection.

Active advection

As we have already explained in Introduction, the advection is formulated in the context of microhydrodynamics as the Stokes problem. Existence of a nontrivial solution to the Stokes problem implies that the advection is not passive (i.e. it is active in our terminology). How can we discuss the active advection on a mesoscopic level on which we cannot formulate the Stokes problem? We shall follow here the approach developed in [2]. In this section we shall recall the mathematical formulation. The physics behind it is discussed in Section 3.3.1.

In order to be able to account for changes in the imposed flow caused by the flow-interface interaction, we introduce a new state variable $\boldsymbol{w}$ that is a three by three tensor whose relation to the perturbed flow will become clear later (see Eq.(3.14)and also Section 3.3.1) when its role in the time evolution is revealed.

State variables

$$x = (\boldsymbol{u}(\boldsymbol{r}), \boldsymbol{c}, \boldsymbol{w}) \tag{3.13}$$

The kinematics of the conformation tensor $\boldsymbol{c}$ is assumed to be given by the bracket (3.8). Otherwise, its physical interpretation is left unspecified.

Kinematics

The Poisson bracket expressing the kinematics of (3.13) is derived in [2]. The resulting from it equations governing the nondissipative time evolution of $(\boldsymbol{c}, \boldsymbol{w})$ are the following:

$$\begin{aligned}
\left(\frac{d\boldsymbol{c}}{dt}\right)_{nondiss} &= \boldsymbol{c}\cdot(\nabla\boldsymbol{v} + \Phi^T_{\boldsymbol{w}}) + (\nabla\boldsymbol{v}^T + \Phi_{\boldsymbol{w}})\cdot\boldsymbol{c} \\
\left(\frac{d\boldsymbol{w}}{dt}\right)_{nondiss} &= \boldsymbol{w}\cdot(\nabla\boldsymbol{v} + \Phi^T_{\boldsymbol{w}}) - (\nabla\boldsymbol{v} + \Phi^T_{\boldsymbol{w}})\cdot\boldsymbol{w} - 2\Phi_{\boldsymbol{c}}\cdot\boldsymbol{c} \\
\boldsymbol{\sigma}^{(nd)} &= -2\Phi_{\boldsymbol{c}}\cdot\boldsymbol{c} - \Phi^T_{\boldsymbol{w}}\cdot\boldsymbol{w} + \boldsymbol{w}\cdot\Phi^T_{\boldsymbol{w}}
\end{aligned} \tag{3.14}$$

By comparing (3.9) with the first equation of (3.14) we see that $\Phi_{\boldsymbol{w}}$ has indeed the physical meaning of the extra velocity gradient emerging due to the flow-interface interaction.

The above formulation of the active advection has been applied so far only for one specific physical interpretation of $\boldsymbol{c}$: the ellipsoid $r_i c_{ij} r_j = 1$; $\boldsymbol{r} = (r_1, r_2, r_3) \in \mathbf{R}^3$ represents a droplet ([2],[16]). Below, we shall apply it to the Doi Ohta characterization of the interface morphology.

3.2.3 GENERIC formulation of the Doi Ohta model

The Doi Ohta model developed in [1] has been put into the form (3.1) in [11], [12]. We shall recall it here.

State variables

The state variables in the Doi Ohta theory are

$$x = (\boldsymbol{u}(\boldsymbol{r}), \boldsymbol{q}, Q) \tag{3.15}$$

Kinematics

Doi and Ohta have derived in [1] the equations representing the passive advection of $(Q, \boldsymbol{q})$ from kinetic theory. It has been shown then in [11] that these equations can be cast into the form (3.5) with the Poisson bracket (3.8) transformed into new state variables $(\boldsymbol{u}, \boldsymbol{q}, Q)$ by the following transformation

$$\begin{aligned} \boldsymbol{u} &= \boldsymbol{u} \\ \boldsymbol{b} &= \boldsymbol{c}^{-1} \\ \boldsymbol{b} &= Q\boldsymbol{q} + \frac{1}{3}Q^2\boldsymbol{\delta} \\ \mathrm{tr}\boldsymbol{q} &= 0 \end{aligned} \tag{3.16}$$

The inverse of the relation between $\boldsymbol{b}$ and $(\boldsymbol{q}, Q)$ given in the second and third equations in (3.16) is

$$\begin{aligned} \boldsymbol{q} &= \frac{\boldsymbol{b}}{Q} - \frac{1}{3}Q\boldsymbol{\delta} \\ Q &= (\mathrm{tr}\boldsymbol{b})^{1/2} \end{aligned} \tag{3.17}$$

The transformation $\boldsymbol{c} \leftrightarrow (\boldsymbol{q}, Q)$ introduced in (3.16) is one-to-one so that the Poisson bracket (3.8) expressing kinematics of $(\boldsymbol{u}, \boldsymbol{c})$ transforms into a Poisson bracket expressing kinematics of $(\boldsymbol{u}, \boldsymbol{q}, Q)$ (see more in [11]).

Free energy and dissipation

Doi and Ohta did not introduce in [1] the free energy. By casting their equations into the form (3.1), the free energy that they in fact used was identified in [11], [12]. In the next section we shall combine the Doi Ohta model with the model of active advection recalled in Section 3.2.2. The free energy, the equations governing the nondissipative time evolution as well as the dissipative potential and the implied by it dissipative time evolution developed there will reduce to the corresponding quantities in the Doi Ohta theory by simply omitting the extra variable $\boldsymbol{w}$. We do not have to therefore write down here explicitly the GENERIC form of the governing equations of the original Doi Ohta theory and we can pro-

ceed directly to the extended model.

3.3 Doi Ohta Model with Active Advection

The Doi Ohta model is extended by taking into account the active role that the interface and the "rheological inhomogeneity" play in the flow-interface interaction. To formulate the extended model, we combine the state variables (3.15) of the original Doi Ohta theory and the state variables used in the active advection model (3.13). We thus use in this section the following set of state variables:

State variables

$$x = (\boldsymbol{u}(\boldsymbol{r}), \boldsymbol{q}, Q, \boldsymbol{w}) \tag{3.18}$$

Kinematics

By applying the transformation (3.16) on the Poisson brackets expressing the kinematics of the Doi Ohta model [11] (i.e. the bracket (3.8) transformed into the state variables $(\boldsymbol{u}, Q, \boldsymbol{q})$ by (3.16)) and the active advection model [2] we arrive at the Poisson bracket expressing kinematics of (3.18). The corresponding to it equations governing the nondissipative time evolution of (3.18) are the following:

$$\begin{aligned}
\left(\frac{d\boldsymbol{b}}{dt}\right)_{nondiss} &= -\boldsymbol{b}\cdot(\nabla\Phi^T_{\boldsymbol{u}} + \Phi_{\boldsymbol{w}}) - (\nabla\Phi_{\boldsymbol{u}} + \Phi^T_{\boldsymbol{w}})\cdot\boldsymbol{b} \\
\left(\frac{d\boldsymbol{w}}{dt}\right)_{nondiss} &= \boldsymbol{w}\cdot(\nabla\Phi_{\boldsymbol{u}} + \Phi^T_{\boldsymbol{w}}) - (\nabla\Phi_{\boldsymbol{u}} + \Phi^T_{\boldsymbol{w}})\cdot\boldsymbol{w} + 2\boldsymbol{b}\cdot\Phi_{\boldsymbol{b}} \\
\boldsymbol{\sigma}^{(nd)} &= 2\boldsymbol{b}\cdot\Phi_{\boldsymbol{b}} - \Phi^T_{\boldsymbol{w}}\cdot\boldsymbol{w} + \boldsymbol{w}\cdot\Phi^T_{\boldsymbol{w}}
\end{aligned} \tag{3.19}$$

and finally (we use the free energy (3.21); note that $\Phi_Q = \Gamma - \frac{\Gamma\beta_q}{Q^2}\mathrm{tr}(\boldsymbol{q}\cdot\boldsymbol{q}) + \frac{\alpha}{2}\mathrm{tr}(\boldsymbol{w}^T\cdot\boldsymbol{w}\cdot(\boldsymbol{q}+\frac{2}{3}Q\boldsymbol{\delta}))$, $\Phi_{\boldsymbol{q}} = \frac{2\Gamma\beta_q}{Q}\boldsymbol{q} + \frac{\alpha Q}{2}\boldsymbol{w}^T\cdot\boldsymbol{w}$, and $\Phi_{\boldsymbol{w}} = \alpha\boldsymbol{w}\cdot\boldsymbol{b}$)

$$\begin{aligned}
\left(\frac{dQ}{dt}\right)_{nondiss} &= -\mathrm{tr}(\boldsymbol{q}\cdot\nabla\boldsymbol{v}^T) - \frac{\alpha}{Q}\mathrm{tr}(\boldsymbol{b}\cdot\boldsymbol{w}\cdot\boldsymbol{b}) \\
\left(\frac{d\boldsymbol{q}}{dt}\right)_{nondiss} &= \left(\frac{\boldsymbol{q}}{Q} + \frac{2}{3}\boldsymbol{\delta}\right)\left[\mathrm{tr}\left(\boldsymbol{q}\cdot\nabla\boldsymbol{v}^T\right) + \frac{\alpha}{Q}\mathrm{tr}(\boldsymbol{b}\cdot\boldsymbol{w}\cdot\boldsymbol{b})\right]
\end{aligned}$$

$$
\begin{aligned}
& -\frac{1}{Q}\left[\boldsymbol{b}\cdot\left(\nabla\boldsymbol{v}^T+\alpha\boldsymbol{w}\cdot\boldsymbol{b}\right)+\left(\nabla\boldsymbol{v}+\alpha\boldsymbol{b}\cdot\boldsymbol{w}^T\right)\cdot\boldsymbol{b}\right] \\
\left(\frac{d\boldsymbol{w}}{dt}\right)_{nondiss} &= \boldsymbol{w}\cdot\left(\nabla\boldsymbol{v}+\alpha\boldsymbol{b}\cdot\boldsymbol{w}^T\right)-\left(\nabla\boldsymbol{v}+\alpha\boldsymbol{b}\cdot\boldsymbol{w}^T\right)\cdot\boldsymbol{w} \\
& +\frac{\boldsymbol{b}}{Q}\left[(\Gamma-3\Gamma\beta_q\frac{\mathrm{tr}(\boldsymbol{q}\cdot\boldsymbol{q})}{Q^2})\boldsymbol{\delta}+4\Gamma\beta_q\frac{\boldsymbol{q}}{Q}\right]+\alpha\boldsymbol{b}\cdot\boldsymbol{w}^T\cdot\boldsymbol{w} \\
\boldsymbol{\sigma}^{(nd)} &= \frac{\boldsymbol{b}}{Q}\left[(\Gamma-3\Gamma\beta_q\frac{\mathrm{tr}(\boldsymbol{q}\cdot\boldsymbol{q})}{Q^2})\boldsymbol{\delta}+4\Gamma\beta_q\frac{\boldsymbol{q}}{Q}\right]+\alpha\boldsymbol{w}\cdot\boldsymbol{b}\cdot\boldsymbol{w}^T \qquad (3.20)
\end{aligned}
$$

(where $\boldsymbol{v}=\Phi_{\boldsymbol{u}}=\boldsymbol{u}/\rho$).

Free energy

$$
\begin{aligned}
\Phi &= \Phi^{(kin)}+\Phi^{(interface)}+\Phi^{(shape)} && (3.21)\\
\Phi^{(kin)} &= \int d\boldsymbol{r}\left(\frac{\boldsymbol{u}^2}{2\rho}+\frac{\alpha}{2}\mathrm{tr}(\boldsymbol{w}^T\cdot\boldsymbol{b}\cdot\boldsymbol{w})\right) && (3.22)\\
\Phi^{(interface)} &= \int d\boldsymbol{r}\Gamma Q && (3.23)\\
\Phi^{(shape)} &= \int d\boldsymbol{r}\frac{\Gamma\beta_q\mathrm{tr}(\boldsymbol{q}\cdot\boldsymbol{q})}{Q} && (3.24)
\end{aligned}
$$

The physical meaning of the four terms and the three material parameters (α,Γ,β_q) introduced in (3.21) will be discussed in Section 3.3.1 and Section 3.3.2.

Dissipation potential

The thermodynamic forces that drive the immiscible blend to equilibrium are the following:

$$
\begin{aligned}
X^{(1)} &= \Phi_Q \\
\boldsymbol{X}^{(2)} &= \Phi_{\boldsymbol{q}} \\
\boldsymbol{X}^{(3)} &= \Phi_{\boldsymbol{w}} \\
\boldsymbol{X}^{(4)} &= \boldsymbol{D} \qquad (3.25)
\end{aligned}
$$

where $\boldsymbol{D}=\frac{1}{2}(\nabla\boldsymbol{v}+\nabla\boldsymbol{v}^T)$.

From these thermodynamic forces we now construct a dissipation potential

satisfying the general properties (3.2). If we restrict ourselves to states at which the thermodynamic forces (3.25) are not too large, it suffices to consider the following quadratic potential

$$\begin{aligned}\Xi &= \int d\boldsymbol{r}\frac{1}{2}\Big[\Lambda^{(1)}(X^{(1)})^2+\Lambda^{(2)}X^{(2)}_{ij}X^{(2)}_{ij} \\ &\quad+\begin{pmatrix} X^{(3)}_{ij}, & X^{(4)}_{ij}\end{pmatrix}\begin{pmatrix}\Lambda^{(3)}_{jk} & \Lambda^{(4)}_{jk}\\ \Lambda^{(4)}_{jk} & \eta_0\delta_{jk}\end{pmatrix}\begin{pmatrix}X^{(3)}_{ik}\\ X^{(4)}_{ik}\end{pmatrix}\Big]\end{aligned} \tag{3.26}$$

where $\Lambda^{(1)}>0, \Lambda^{(2)}>0$, and $\begin{pmatrix}\boldsymbol{\Lambda}^{(3)} & \boldsymbol{\Lambda}^{(4)}\\ \boldsymbol{\Lambda}^{(4)} & \eta_0\boldsymbol{\delta}\end{pmatrix}>0$ are dissipative phenomenological coefficients. They can depend on the state variables $(\boldsymbol{u},\boldsymbol{q},Q,\boldsymbol{w})$ but are independent of $(\Phi_{\boldsymbol{u}},\Phi_{\boldsymbol{q}},\Phi_Q,\Phi_{\boldsymbol{w}})$.

The equations governing the dissipative time evolution (3.6) implied by (3.26) are the following:

$$\begin{aligned}\left(\frac{dQ}{dt}\right)_{diss} &= -\frac{\delta\Xi}{\delta\Phi_Q}=-\Lambda^{(1)}\Phi_Q\\ \left(\frac{dq_{ij}}{dt}\right)_{diss} &= -\frac{\delta\Xi}{\delta\Phi_{q_{ij}}}=-\Lambda^{(2)}\Phi_{q_{ij}}\\ \left(\frac{dw_{ij}}{dt}\right)_{diss} &= -\frac{\delta\Xi}{\delta\Phi_{w_{ij}}}=-\Phi_{w_{ik}}\Lambda^{(3)}_{kj}-\frac{1}{2}\left(D_{ik}\Lambda^{(4)}_{kj}+\Lambda^{(4)}_{ik}D_{kj}\right)\end{aligned} \tag{3.27}$$

We now proceed to specify more the coefficients introduced in the dissipation potential (3.26):

$$\begin{aligned}\Lambda^{(1)} &= \frac{d_1Q}{\eta_0}(\mathrm{tr}(\boldsymbol{q}\cdot\boldsymbol{q}))^{1/2}\\ \Lambda^{(2)} &= \frac{d_1Q^2}{2\beta_q\eta_0}\left[(\frac{1}{\mu}-1)Q+(\mathrm{tr}(\boldsymbol{q}\cdot\boldsymbol{q}))^{1/2}\right]\\ \boldsymbol{\Lambda}^{(3)} &= \lambda\boldsymbol{b}^{-1}\\ \boldsymbol{\Lambda}^{(4)} &= \xi\boldsymbol{b}^{-1}\end{aligned} \tag{3.28}$$

The first two have been chosen in such a way that we recover with them (by ignoring $\boldsymbol{w}$) the original Doi Ohta theory; $\mu=\frac{d_1}{d_1+d_2}$, $d_1>0$ and $d_2>0$ (denoted c_1 and c_2 in the Doi Ohta paper) are phenomenological parameters, and η_0 is the

viscosity coefficient. The third and the fourth coefficients $\Lambda^{(3)}$, $\Lambda^{(4)}$ are new. We shall discuss their physical interpretation in Section 3.3.2

With the choices (3.28) and (3.21), the dissipative time evolution equations (3.27) become:

$$\begin{aligned}
\left(\frac{dQ}{dt}\right)_{diss} &= -\frac{d_1\Gamma Q}{\eta_0}(\mathrm{tr}(\boldsymbol{q}\cdot\boldsymbol{q}))^{1/2} + \frac{d_1\beta_q\Gamma}{\eta_0 Q}(\mathrm{tr}(\boldsymbol{q}\cdot\boldsymbol{q}))^{3/2} \\
&\quad -\frac{d_1\alpha Q}{2\eta_0}(\mathrm{tr}(\boldsymbol{q}\cdot\boldsymbol{q}))^{1/2}\mathrm{tr}\left[\boldsymbol{w}^T\cdot\boldsymbol{w}\cdot(\boldsymbol{q}+\frac{2}{3}Q\boldsymbol{\delta})\right] \\
\left(\frac{d\boldsymbol{q}}{dt}\right)_{diss} &= -\frac{d_1}{\eta_0}\left((\frac{1}{\mu}-1)Q + (\mathrm{tr}(\boldsymbol{q}\cdot\boldsymbol{q}))^{1/2}\right)\left(\Gamma\boldsymbol{q} + \frac{\alpha Q^2}{4\beta_q}\boldsymbol{w}^T\cdot\boldsymbol{w}\right) \\
\left(\frac{d\boldsymbol{w}}{dt}\right)_{diss} &= -\alpha\lambda\boldsymbol{w} - \xi\boldsymbol{D}\cdot\boldsymbol{b}^{-1}
\end{aligned} \tag{3.29}$$

Summing up, the governing equation of the extended Doi Ohta model are (3.4),(3.20),and (3.29). It is easy to verify that by omitting $\boldsymbol{w}$, the governing equations of the original Doi Ohta model are indeed recovered except for two additional terms (one quadratic and one third order in $\boldsymbol{q}$), appearing in our formulation, in the expression for the extra stress tensor. We emphasize at this point that all the terms in the free energy, including in particularly the term $\Phi^{(shape)}$, are essential for casting the original Doi Ohta equations into the GENERIC form. In other words we have shown that the Doi Ohta theory is compatible with thermodynamics only if the free energy is given by (3.21). Doi and Ohta did not introduce in [1] the free energy explicitly since they derived their equations in a different way than we did and they did not investigated the problem of the compatibility with thermodynamics. As shown in [11] and also in this paper, the free energy they use implicitly is (3.21) with $\boldsymbol{w} = 0$.

3.3.1 Physics expressed in the governing equations

Having written the time evolution equations, we now discuss in more detail the physics expressed in them. This discussion will also throw light on the physical interpretation of the state variables (3.18).

$(\boldsymbol{u})$

We begin with the field $\boldsymbol{u}$. The motion of a continuum is seen in all approaches to the physics of continuum as a one parameter family of transformations $\mathbf{R}^3 \rightarrow \mathbf{R}^3$. These transformation form a Lie group. The kinematics of continuum is expressed mathematically as a structure of this Lie group. The Poisson bracket associated canonically with the dual of the Lie algebra corresponding to this Lie group is given (see [14],[15]) by the first line in (3.8); $\boldsymbol{u}$ is an element of the dual of the Lie algebra. We thus conclude that the kinematics that we have used for the field $\boldsymbol{u}$ implies that $\boldsymbol{u}$ has the physical interpretation of the overall momentum field of the fluid. This interpretation is then also consistent with interpreting the first term in the (3.22) as the overall kinetic energy.

We note here that in mechanics as well as in thermodynamics, the state variables are always accompanied with their conjugates (in our case the conjugate of a state variable is a derivative of the free energy with respect to the state variables). The conjugate of the field $\boldsymbol{u}$ is thus $\Phi_{\boldsymbol{u}} = \frac{\boldsymbol{u}}{\rho} = \boldsymbol{v}$, where $\boldsymbol{v}$ the velocity field. It is the field $\boldsymbol{v}$ that is directly measured in hydrodynamic experiments and it is therefore the state variable preferred in classical hydrodynamics. We use $\boldsymbol{u}$ which has a less direct physical interpretation since it is with $\boldsymbol{u}$ that the Hamiltonian structure of fluid mechanics is clearly displayed. We recall that the same observation can be made about many other pairs of state variables. For example, the temperature is a directly measurable quantity in thermodynamics but it is advantageous to use its conjugate (i.e. the internal energy which is not directly measurable) as preferred state variable if we want to display and use the mathematical structure of thermodynamics.

$(\boldsymbol{w})$

We recall a few observations about the Stokes problem.

(i) The mathematical formulation of the Stokes problem consists of the Navier-Stokes equation for the flow velocity with the outer boundary condition being the given imposed velocity and the inner boundary condition expressing the bulk-interface interaction. The solution depends on time explicitly and implicitly. Explicitly because the Navier-Stokes equation is the time evolution equation and implicitly through the time dependence involved in the inner boundary condition.

The explicit time dependence is usually neglected by replacing the full Navier-Stokes equation with its stationary creeping flow approximation.

(ii) The advection of the interface is modified by replacing $\nabla \boldsymbol{v}$ on the right hand side of the second equation in (3.9) by $\nabla \boldsymbol{v} + \boldsymbol{\epsilon}$, where $\boldsymbol{\epsilon}$ is the gradient of the velocity perturbation.

How shall we formulate the Stokes problem in the mesoscopic setting used in this paper? We certainly cannot formulate the inner boundary condition since the knowledge of the exact shape and precise location of the interface, needed in the formulation, is outside the scope of the mesoscopic description. We shall proceed as follows: We look for a modification of the advection in which $\nabla \boldsymbol{v}$ on the right hand side of the second equation in (3.9) is replaced by $\nabla \boldsymbol{v} + \boldsymbol{\epsilon}$, where the time evolution of $\boldsymbol{\epsilon}$ is coupled to the time evolution of the rest of the state variables in such a way that together the time evolution is GENERIC. The latter requirement means that the GENERIC nature of the original formulation of the Stokes problem (and thus all the physics expressed in this structure, see Section 3.2.1) is preserved. The problem that we are facing can also be formulated (in a more mathematical language) as follows: We look for an extension (deformation) of (3.7), (3.9) in which $\nabla \boldsymbol{v}$ on the right hand side of the second equation in (3.9) deforms into $\nabla \boldsymbol{v} + \boldsymbol{\epsilon}$ and the Poisson bracket (3.8) deforms into a new Poisson bracket involving $\boldsymbol{\epsilon}$.

The setting presented in Eqs. (3.13), (3.14) provides a solution to this problem. It may not be however a unique solution. We have been unable to prove the uniqueness but we have also been unable to find another solution.

The way $\boldsymbol{w}$ appears in (3.19) shows that the transpose of the conjugate of $\boldsymbol{w}$ has the physical interpretation of the gradient of the velocity perturbation. We thus interpret the second term in (3.22) as the contribution of the velocity perturbation to the kinetic energy. We shall take the parameter α to be the inverse of the average mass of the blend.

In contrast to the microhydrodynamic formulation of the Stokes problem we keep in its mesoscopic formulation the explicit time dependence of the perturbed velocity. This is consistent with a general observation that when passing from microscopic to more macroscopic levels of description, we deal with larger objects and thus the effect of inertia becomes more important. Moreover, if we want to preserve the GENERIC structure with $\boldsymbol{w}$, we have to keep the time evolution of

$\boldsymbol{w}$.

Originally, we regard all three state variables $(\boldsymbol{u}, \boldsymbol{c}, \boldsymbol{w})$ as slow variables, their time evolution is assumed to be separated from the time evolution of the fast time evolution of irrelevant microscopic details. Let us now assume that the relaxation time of $\boldsymbol{w}$ is very small (as we do later in the comparison with results of experimental observations) and thus $\boldsymbol{w}$ becomes a fast variable. What this means is that $\boldsymbol{w}$ becomes in fact a function of the slow variables (in other words, $\boldsymbol{w}$ becomes enslaved to the remaining slow variables). It can be thus considered as a fast variable, separated from the slow variables, and omitted. The separation brings about then a change of the slow time evolution. Namely, the affine advection (i.e. the advection without $\Phi^T_{\boldsymbol{w}}$ in the first two terms on the right hand side of the first equation in (3.19)) becomes the non-affine advection (i.e. $\Phi^T_{\boldsymbol{w}}$ in the first two terms on the right hand side of the first equation in (3.19) becomes a function of $\nabla\Phi_{\boldsymbol{u}}$; see more in [2]). In this paper we shall not make the separation even in the case when the relaxation time of $\boldsymbol{w}$ is very small (see Section 3.4) because such elimination leads to the time evolution equations that do not possess anymore the GENERIC structure.

(Q,q)

It has been established in [11] that the kinematics expressed in the Poisson bracket obtained by transforming (using the transformation (3.16)) the Poisson bracket (3.8) is the same as the kinematics derived (implicitly) in [1]. Moreover, in order to interpret (3.23) as the surface tension contribution to the free energy, Q has to have the interpretation of the area of the interface per unit volume. We thus conclude that $(Q, \boldsymbol{q})$ have the same physical interpretation as $(Q, \boldsymbol{q})$ introduced in [1].

Doi and Ohta relate $(Q, \boldsymbol{q})$ to the second moment of the one particle distribution function $f(\boldsymbol{r}, \boldsymbol{n})$, where $\boldsymbol{n}$ is the unit vector perpendicular to the tangent plane of the interface at the point $\boldsymbol{r}$. The tensor $\boldsymbol{q}$ is the traceless part of the second moment in $\boldsymbol{n}$. In what sense the tensor $\boldsymbol{q}$ characterizes the shape of the interface? The tensor $\boldsymbol{q}$ is certainly related to the anisotropy of the interface distribution and thus indirectly also to its deformations. Indeed, $\boldsymbol{q} = 0$ implies that the distribution is isotropic. It is also clear that $\boldsymbol{q}$ is not directly related to

the curvature. Note that the distribution function $f(\boldsymbol{r}, \boldsymbol{n})$ itself does not contain any direct information about the curvature. For that being the case we would have to know how $\boldsymbol{n}$ changes under the infinitesimal displacement of the point to which it is attached. Indirectly however, $\boldsymbol{q}$ does characterize anisotropy of the distribution of $\boldsymbol{n}$ and thus also (very indirectly) the curvature.

Other state variables

The questions that has to be asked in any mesoscopic theory are the following: Are the state variables well chosen? Does the time evolution described in the theory represent the most pertinent part of the time evolution, does it indeed represent the slow time evolution that is well separated from the fast time evolution representing the impertinent details? These questions can be answered by either deriving the mesoscopic theory from a more microscopic theory or by comparing consequences of the mesoscopic theory with results of experimental observations. Below, we shall make only a few comments about possible additional state variables that can be adopted to improve the theory. The derivation from a more microscopic theory is out of the scope of this paper, the comparison with other theories and with experiments is presented in Section 3.4.

As shown in [17] and in the references cited therein, the free energy $\Phi^{(interface)}$ representing the surface tension contribution to the free energy should include also terms (that are added to (3.23)) involving the curvature of the interface. In order to be able to write down such terms we would have to adopt new state variables with which the curvature can be expressed. For the specific blends discussed in Section 3.4 the curvature-dependent contribution to the free energy is, as it follows from [17], very small and we therefore do not pursue this route in this paper.

In the case when the interface is a membrane with its own internal mechanical (elastic) properties then the free energy has to include new terms expressing the membrane elastic energy (see e.g. [18]). To be able to write down such terms, we would have to again enlarge the set of state variables by adopting new ones allowing to express the curvature and elastic deformations (including stretching) of the interface. We hope to follow this route in a future paper but in this paper we limit ourselves (see Section 3.4) to the interfaces with very small or totally

absent elastic deformations and we therefore do not need to make such extensions.

The morphological state variables $(Q, \boldsymbol{q})$ describe the morphology locally. We may expect that the global (shape) features of the interface (for example, the size and the distribution of droplets or the co-continuous form of the interface) play an important role in determining the overall free energy (in particular in determining its entropic part). Let the state variables through which the global shape of the interface can be expressed be denoted by the symbol $x^{(shape)}$. Let us assume that we formulate an extended theory involving $x^{(shape)}$ and thus we have equations governing the time evolution of $x^{(shape)}$. Let this time evolution be faster than the time evolution of the rest of state variables and thus $x^{(shape)}$ becomes enslaved to them (i.e. $x^{(shape)}$ becomes a function of $(Q, \boldsymbol{q})$). We suggest that the free energy (3.24) is the part of the free energy representing the global shape contribution depending after $x^{(shape)}$ on which it depends has been replaced by $x^{(shape)(Q,\boldsymbol{q})}$, on $(Q, \boldsymbol{q})$. We thus interpret (3.24) as an approximation to the shape-dependent free energy. The coefficient β_q introduced in it is considered as a (dimensionless) phenomenological material parameter (see more in Section 3.4.2, Eq(3.52)).

We recall that we have seen in Section 3.3 (see the text following Eq.(3.29)) that the part of the free energy proportional to β_q is essential for casting the original Doi Ohta equations into the GENERIC form. Specifically, it is essential for obtaining the dissipative part of the time evolution. Only with this term in the free energy the inequality $\left(\frac{\partial \Phi}{\partial t}\right)_{dissip} < 0$ is guaranteed. We note here that in order to guarantee $\frac{\partial \Phi}{\partial t} = \left(\frac{\partial \Phi}{\partial t}\right)_{nondissip} + \left(\frac{\partial \Phi}{\partial t}\right)_{dissip} < 0$ we need to guarantee that $\left(\frac{\partial \Phi}{\partial t}\right)_{nondissip} = 0$. This is indeed guaranteed provided the extra stress tensor is given by the last equation in (3.20). The terms involving β_q are however missing in the expression for the stress tensor used in the original Doi Ohta models (this has been noted already in [11]). We shall see in Section 3.4 that the missing terms improve the rheological predictions of the model.

3.3.2 Material parameters

Every theory, formulated on any level of description, needs parameters (called material parameters) expressing the individual features of the systems under consideration. For instance, in classical mechanics, it is the mass and all the parameters

entering the characterization of the forces, in hydrodynamics of simple fluids, the material parameters are the viscosity and the heat conductivity coefficients and all the parameters entering the local fundamental thermodynamic relation. The mapping: *physical systems* $\rightarrow$ *material parameters* can be obtained by following two routes: (route 1) by staying inside the level, or (route 2) by investigating relations to other levels. Below, we shall make a few brief comments about both routes.

(route 1)

Let the level on which we place ourselves be denoted by the symbol $\mathcal{L}_0$. Among all experimental observations made on the level $\mathcal{L}_0$ (we shall denote them by the symbol $\mathcal{O}_0$) we select some ($\mathcal{O}_0^{metr} \subset \mathcal{O}_0$) that will be regarded as measurements of the material parameters. The values of the parameters are obtained by fitting the results of the observations $\mathcal{O}_0^{metr}$ with predictions of the theory. The success or the failure of the theory is then seen in the comparison of the results of the remaining $\mathcal{O}_0 \setminus \mathcal{O}_0^{metr}$ observations with predictions of the theory. This route is traditionally followed on all well established levels as for example in classical thermodynamics, classical mechanics, and classical hydrodynamics.

(route 2)

Let the level $\mathcal{L}_1$ be more microscopic (i.e. involving more details) than the level $\mathcal{L}_0$. For instance, let $\mathcal{L}_0$ be the level of classical hydrodynamics and $\mathcal{L}_1$ the level of Boltzmann kinetic theory. Both levels $\mathcal{L}_0$ and $\mathcal{L}_1$ are autonomous (i.e. neither of them needs the other to be formulated and applied) but since the level $\mathcal{L}_1$ is more microscopic we can anticipate that an analysis of solutions of the governing equations on the level $\mathcal{L}_1$ can lead to a derivation of the theory on the level $\mathcal{L}_0$. The process of the derivation can be seen as a pattern recognition process in the set of solutions (trajectories) obtained on the level $\mathcal{L}_1$. For instance, in the case of $\mathcal{L}_1$ being the Boltzmann kinetic theory and $\mathcal{L}_0$ the hydrodynamics, such passage $\mathcal{L}_1 \rightarrow \mathcal{L}_0$ is provided by the famous Chapman Enskog method. Let the material parameters associated with the level $\mathcal{L}_1$ resp. $\mathcal{L}_0$ be denoted $\mathcal{P}_1$ resp. $\mathcal{P}_1$. The passage $\mathcal{L}_1 \rightarrow \mathcal{L}_0$ induces the passage $\mathcal{P}_1 \rightarrow \mathcal{P}_0$. The material parameters $\mathcal{P}_0$ can be thus obtained by independent measurements made on the level $\mathcal{L}_1$. For example, by using the Chapman Enskog method, we obtain the viscosity and the heat conductivity coefficients expressed in terms of the material parameters used in the Boltzmann kinetic theory.

Now, let the level $\mathcal{L}_0$ (we shall denote it hereafter $\mathcal{L}_{meso}$) be the level with the state variables (3.18) and the governing equations (3.20), (3.27) and the more microscopic level $\mathcal{L}_1$ (denoted hereafter $\mathcal{L}_{microhyd}$) the level of microhydrodynamics on which the interface is specified as a surface in $\mathbf{R}^3$, i.e. as an immersion $\mathbf{R}^2 \supset \Omega \hookrightarrow \mathbf{R}^3$. The material parameters used on the level $\mathcal{L}_{meso}$ are

$$(d_1, \mu, \eta_0, \Gamma, \beta_q, \lambda, \xi,) \tag{3.30}$$

The first four appear already in the original Doi Ohta theory, the last three are new. We emphasize that all these material parameters have a clear physical interpretation from the way they have appeared in the GENERIC construction of the governing equations. Essentially, they quantify the physics that we have introduced into our model. We also note that all the parameters that entered the dissipation potential (i.e. $d_1, \mu, \eta_0, \lambda, \xi$) do not have to be just numbers, they can be functions of the state variables. We have to only require that the properties of the dissipation potential (3.2) hold.

The material parameters serving on the level of microhydrodynamics are the hydrodynamic parameters characterizing the two fluids involved as well as the parameters characterizing their interface and the bulk-interface interactions.

Some material parameters included in (3.30) will be determined in Section 3.4 by following the route 2, some by following the route 1. We recall briefly the way we proceeded in [16]. The morphology of the interface in [16] is seen as a collection of droplets mathematically described as ellipsoids. If we then limit ourselves to small deformations we can solve (by using the perturbation method) both the microhydrodynamic formulation and the mesoscopic formulation analytically. By comparing the solutions we find the mapping $\mathcal{P}_{microhyd} \to \mathcal{P}_{meso}$. We shall follow the similar strategy in Section 3.4.

Before identifying the material parameters (3.30) for the blends observed in experiments we explore solutions to the governing equations for a large domain of the parameters. Already this investigation allows to identify regions in the space of material parameters that have to be excluded. For example, we find in the next section that if $\lambda < 10^8$ than the solutions are unphysical (they widely oscillate in time and do not reach stationary values).

Finally, we comment about the choice of the coefficient Λ_1 that we have made (following [1], in (3.28)). The advantage of this particular choice is that the relaxation of Q stops once the isotropic distribution of the interface (corresponding to $\boldsymbol{q} = 0$) is reached. This is indeed the behavior observed in experiments. We recall (see e.g. [19]) that in the physical systems involving an interface endowed with surface tension the extra stress (determined for example, in the case of spherical droplets, by the well known Young-Laplace formula) remains to be present even at the complete equilibrium. In the next section where we shall calculate rheological consequences of the governing equations, we shall also mention other choices for the coefficients $\Lambda^{(1)}$, $\Lambda^{(2)}$, $\Lambda^{(3)}$ and compare their consequences.

3.4 Results

Now we proceed to solve Eqs.(3.4), (3.20), (3.29). From the mathematical point of view, they represent a set of ordinary differential equations that we solve numerically by using standard software packages. In the cases when the equations are "stiff", we use the solver called ode23s in Matlab. It is based on a modified Resenbrock formula of order 2.

We solve the equations with the imposed flow being a simple shear flow. From the calculated extra stress tensor we extract the standard rheological characteristics and present them on figures.

The initial condition in our calculations is always

$$Q = Q_0; \ \boldsymbol{q} = 0; \ \boldsymbol{w} = 0 \tag{3.31}$$

where Q_0 is considered to be a parameter.

The predictions of the active DO model (i.e. on Eqs.(3.4), (3.20), (3.29)) will be compared below with predictions of some other models and some published experimental data. The other models that we shall consider are four Doi Ohta type models (denoted by the symbols DO 1, DO 2, LP, WOE) and one, (FA), based on an approximate (small deformation) microhydrodynamic analysis. The Doi Ohta type models all share the same nondissipative time evolution (governed by (3.20) with $\boldsymbol{w}$ missing) and differ in the choice of the dissipative coefficients Λ_1 and Λ_2. They are the following:

DO 1

This is the original Doi Ohta model [1] (i.e. the field $\boldsymbol{w}$ is absent) corresponding to $\Lambda^{(1)}$ and $\Lambda^{(2)}$ given in (3.28) with $\mathrm{tr}(\boldsymbol{q}\cdot\boldsymbol{q})$ is replaced by Q^2 (also used in [26] and [28]).

DO 2

This is the original Doi Ohta model [1] (i.e. the field $\boldsymbol{w}$ is absent) corresponding to Λ_1 and Λ_2 given in (3.28) (also used in [27]).

LP

This is the modification of the Doi Ohta model introduced by Lee and Park [20]. In their reinterpretation of the physics involved in the dissipative time evolution, d_1 is the rate coefficient of droplet coalescence, d_2 the rate coefficient of the shape relaxation, and a new parameter, d_3 is the rate of droplet break up and deformations.

WOE

This is the modification of the Doi Ohta model introduced in [21]. In this model the initial value of Q, namely Q_0, plays the role of the length scale. The thermodynamic force driving Q to equilibrium is proportional to $Q - Q_0$.

FA

This is not a model formulated on a mesoscopic level as the previous four are. The immiscible blend is assumed to be a colloidal suspension of spherical droplets that only slightly change their shape in the flow. With this assumption, the microhydrodynamic formulation [22] of the dynamics of the interface can be brought into closed form expressions for quantities characterizing rheological behavior ([22], [23]). In Ref.[23] the droplet radius is let to depend on the shear rate.

3.4.1 Dimensionless equations

We recall that an immiscible blend is regarded on the mesoscopic level that we have adopted in this paper as a single fluid with an internal structure. In view

of the experimental data with which we shall later compare predictions of the model, we shall hereafter restrict ourselves to the droplet morphology. The single fluid will be the fluid outside the droplets and the surface of the droplets will be the internal structure. Instead of η_0 denoting the viscosity of the single fluid we shall now use η_{out}.

We shall regard $1/Q_0$ as a characteristic length (Q_0 is the initial surface area per unit volume of the interface), and $\eta_{out}/(Q_0\Gamma)$ as the characteristic time, and Γ is the surface tension. We note that in the particular case of suspensions of spherical droplets, $Q_0 = 3\phi/r_0$, where r_0 is the initial radius of the droplet and ϕ the volume fraction of the droplets. The dimensionless state variables are introduced as follows:

$$Q^* = \frac{Q}{Q_0},\quad \boldsymbol{q}^* = \frac{\boldsymbol{q}}{Q_0},\quad t^* = t\frac{Q_0\Gamma}{\eta_{out}},\quad \nabla\boldsymbol{v}^* = \frac{\nabla\boldsymbol{v}}{\dot{\gamma}},\quad \boldsymbol{w}^* = \frac{\boldsymbol{w}}{\eta_{out}},\quad \sigma^* = \frac{\sigma}{\eta_{out}\dot{\gamma}} \tag{3.32}$$

The dimensionless time evolution equations become: (in order to simplify the notation we omit hereafter the superscript $*$, all quantities are dimensionless)

$$\begin{aligned}
\frac{dQ}{dt} &= -\mathcal{C}\,\mathrm{tr}\left(\boldsymbol{q}\cdot\nabla v^T\right) - \kappa\frac{\mathrm{tr}(\boldsymbol{b}\cdot\boldsymbol{w}\cdot\boldsymbol{b})}{Q} - d_1\left[(\boldsymbol{q}:\boldsymbol{q})^{\frac{1}{2}}Q - \beta_q\frac{(\boldsymbol{q}:\boldsymbol{q})^{\frac{3}{2}}}{Q}\right.\\
&\quad \left.+\frac{\kappa}{2}Q(\boldsymbol{q}:\boldsymbol{q})^{\frac{1}{2}}\mathrm{tr}\left(\boldsymbol{w}^T\cdot\boldsymbol{w}\cdot\left(\boldsymbol{q}+\frac{2}{3}Q\boldsymbol{\delta}\right)\right)\right]\\
\frac{d\boldsymbol{q}}{dt} &= \left(\frac{\boldsymbol{q}}{Q}+\frac{2}{3}\boldsymbol{\delta}\right)\left[\mathcal{C}\,\mathrm{tr}\left(\boldsymbol{q}\cdot\nabla v^T\right) + \kappa\frac{\mathrm{tr}(\boldsymbol{b}\cdot\boldsymbol{w}\cdot\boldsymbol{b})}{Q}\right]\\
&\quad -\frac{1}{Q}\left[\mathcal{C}\left(\boldsymbol{b}\cdot\nabla\boldsymbol{v}^T+\nabla\boldsymbol{v}\cdot\boldsymbol{b}\right)+\kappa\boldsymbol{b}\cdot\left(\boldsymbol{w}+\boldsymbol{w}^T\right)\cdot\boldsymbol{b}\right]\\
&\quad -d_1\left[\left(\frac{1}{\mu}-1\right)Q+(\boldsymbol{q}:\boldsymbol{q})^{\frac{1}{2}}\right]\left(\boldsymbol{q}+\frac{\kappa}{4\beta_q}Q^2\boldsymbol{w}^T\cdot\boldsymbol{w}\right)\\
\frac{d\boldsymbol{w}}{dt} &= \mathcal{C}\left(\boldsymbol{w}\cdot\nabla\boldsymbol{v}-\nabla\boldsymbol{v}\cdot\boldsymbol{w}\right)+\kappa\left(\boldsymbol{w}\cdot\boldsymbol{b}\cdot\boldsymbol{w}^T-\boldsymbol{b}\cdot\boldsymbol{w}^T\cdot\boldsymbol{w}\right)\\
&\quad +\frac{\boldsymbol{b}}{Q}\cdot\left[\left(1-3\beta_q\frac{\boldsymbol{q}:\boldsymbol{q}}{Q^2}\right)\boldsymbol{\delta}+4\beta_q\frac{\boldsymbol{q}}{Q}\right]+\kappa\boldsymbol{b}\cdot\boldsymbol{w}^T\cdot\boldsymbol{w}\\
&\quad -\mu_1\boldsymbol{w}-\mathcal{C}\mu_2\boldsymbol{D}\cdot\boldsymbol{b}^{-1}\\
\boldsymbol{\sigma}^{int} &= \mathcal{C}^{-1}\left\{\frac{\boldsymbol{b}}{Q}\cdot\left[\left(1-3\beta_q\frac{\boldsymbol{q}:\boldsymbol{q}}{Q^2}\right)\boldsymbol{\delta}+4\beta_q\frac{\boldsymbol{q}}{Q}\right]+\kappa\boldsymbol{w}\cdot\boldsymbol{b}\cdot\boldsymbol{w}^T\right\}
\end{aligned} \tag{3.33}$$

where

$$\boldsymbol{b} = Q\boldsymbol{q} + \frac{1}{3}Q^2\boldsymbol{\delta} \tag{3.34}$$

The dimensionless parameters appearing in (3.33) are defined as follows:

$$\mathcal{C} = \frac{\eta_{out}\dot{\gamma}}{Q_0\Gamma};\quad \kappa = \frac{\alpha Q_0\eta_{out}^2}{\Gamma};\quad \mu_1 = \frac{\lambda\alpha\eta_{out}}{Q_0\Gamma};\quad \mu_2 = \frac{\xi}{Q^2\eta_{out}} \tag{3.35}$$

The dimensionless parameter $\mathcal{C}$ is a capillary number describing the relative strength of the applied viscous force (that tends to enlarge and deform the interface) to that of the interfacial tension (that tends to resist the deformations). The dimensionless parameter κ, representing the ratio of the kinetic energy of the interface to the interfacial free energy, is a known parameter since α is the inverse of mass density of the interface. The parameters d_1 and μ are the same as those introduced in the original Doi Ohta model. The dimensionless parameters μ_1 and μ_2 characterize the dissipation of $\boldsymbol{w}$. They, as well as β_q, will be determined (see Section 3.4.2) by relating particular solutions of the present model to those arising in the the microhydrodynamic formulation.

The initial conditions are the following:

$$Q = 1;\ \boldsymbol{q} = \boldsymbol{0};\ \boldsymbol{w} = \boldsymbol{0} \tag{3.36}$$

3.4.2 Determination of the material parameters

The dimensionless parameters appearing in (3.33) are:

$$(d_1, \mu, \beta_q, \mu_1, \mu_2) \tag{3.37}$$

The first two have been introduced in the original Doi Ohta theory (see [1]), β_q, μ_1 and μ_2 are new material parameters. In this section, the new parameters will be determined, i.e. they will be expressed in terms of the remaining material parameters. The method we use is similar to the one used in [16]. We solve analytically the equations of the present model in a particular situation and compare them with the analytical solutions of the microhydrodynamic equations in the same situation. The particular situation that we consider corresponds to the weak external flow. The equations, both those arising in the mesoscopic

model and those arising in the microhydrodynamic formulation, are solve by the perturbation method with the capillary number $\mathcal{C}$ playing the role of the small parameter:

$$Q = 1 + \mathcal{C}\, Q^{(1)} + O(\mathcal{C}^2) \tag{3.38}$$

$$\boldsymbol{q} = \mathcal{C}\, \boldsymbol{q}^{(1)} + O(\mathcal{C}^2) \tag{3.39}$$

and

$$\boldsymbol{w} = \mathcal{C}\, \boldsymbol{w}^{(1)} + O(\mathcal{C}^2) \tag{3.40}$$

We assume moreover that $\boldsymbol{w}$ evolves in time much faster than Q and $\boldsymbol{q}$. To the first order in the small parameter $\mathcal{C}$, Eqs.(3.33) become

$$\frac{dQ^{(1)}}{dt} = -d_1 \left(\boldsymbol{q}^{(1)} : \boldsymbol{q}^{(1)}\right)^{\frac{1}{2}} \tag{3.41}$$

$$\frac{d\boldsymbol{q}^{(1)}}{dt} = -\frac{2}{3}\left(1 - \frac{\kappa\mu_2}{\mu_1}\right)\boldsymbol{D} - \left[\left(\frac{1}{\mu} - 1\right) d_1 + \frac{2\kappa}{27\mu_1}\left(4\beta_q + 3\right)\right]\boldsymbol{q}^{(1)} \tag{3.42}$$

$$\boldsymbol{w}^{(1)} = \frac{1}{\mu_1}\left[\left(\frac{4}{3}\beta_q + 1\right)\boldsymbol{q}^{(1)} - 3\mu_2\boldsymbol{D}\right] \tag{3.43}$$

and the interfacial excess stress tensor writes as

$$\sigma^{int} = \left(\frac{4}{3}\beta_q + 1\right)\boldsymbol{q}^{(1)} + O(\mathcal{C}) \tag{3.44}$$

From Eq.(3.42) we obtain the relaxation time of $\boldsymbol{q}$ (with dimension) as

$$\tau_q = \frac{\eta_{out}}{Q_0\Gamma}\frac{1}{\left(\frac{1}{\mu} - 1\right) d_1 + \frac{2\kappa}{27\mu_1}\left(4\beta_q + 3\right)} \tag{3.45}$$

At the steady state, with $d\boldsymbol{q}^{(1)}/dt = 0$, Eq.(3.44) leads to the following zero-shear viscosity

$$\left[-\sigma_{12}^{int}\right]_0 = \frac{\left(1 - \frac{\kappa\mu_2}{\mu_1}\right)\left(4\beta_q + 3\right)}{9\left[\left(\frac{1}{\mu} - 1\right) d_1 + \frac{2\kappa}{27\mu_1}\left(4\beta_q + 3\right)\right]} \tag{3.46}$$

Now, we turn to the analytical solutions known from microhydrodynamic theories for the problem of emulsions. First, we compare the stresses. Taylor's

small deformation theory [24] leads to

$$\left[\eta^{int}\right]_0 = \frac{5p+2}{2p+2} \tag{3.47}$$

where $p = \eta_{in}/\eta_{out}$; η_{in} resp. η_{out} is the viscosity coefficient of the fluid inside resp. outside the droplet. By equating (3.46) with (3.47) we arrive at the first equation relating the microhydrodynamic material parameters and (3.37):

$$\frac{\left(1-\frac{\kappa\mu_2}{\mu_1}\right)(4\beta_q+3)}{9\left[\left(\frac{1}{\mu}-1\right)d_1+\frac{2\kappa}{27\mu_1}(4\beta_q+3)\right]} = \frac{5p+2}{2p+2} \tag{3.48}$$

Second, we compare the morphology. The problem is that the microhydrodynamic and the Doi Ohta characterization of the morphology are not directly comparable. Nevertheless, we still can compare the relaxation times. Palierne's microhydrodynamic analysis [25] gives a relaxation time for the droplet shape at low frequencies,

$$\tau_c = \frac{\eta_{out} r_0}{\Gamma}\frac{(19p+16)(2p+3)}{40(p+1)} \tag{3.49}$$

where r_0 is the initial radius of the droplet : $r_0 = 3\phi/Q_0$, ϕ is the volume fraction of the dispersed phase. By equating (3.49) with (3.45) we obtain the second equation relating the microhydrodynamic material parameters and (3.37):

$$\frac{1}{Q_0}\frac{1}{\left(\frac{1}{\mu}-1\right)d_1+\frac{2\kappa}{27\mu_1}(4\beta_q+3)} = r_0\frac{(19p+16)(2p+3)}{40(p+1)} \tag{3.50}$$

Now we proceed to draw consequences of Eqs.(3.48) and (3.50). We note that they are two nonlinear algebraic equations relating five unknowns (3.37). Among all possible solutions we look for those satisfying the following properties: (i) $\mu_1 > 0$ (in order to satisfy the requirements put on the dissipation potential), and (ii) as $1/\mu_1$ and μ_2/μ_1 tend to zero as $p \to 1$ (the advection is expected to be passive if $\eta_{in} \sim \eta_{out}$).

From the requirement (ii) we get

$$d_1 = \frac{16\mu}{105(1-\mu)\phi} \tag{3.51}$$

$$\beta_q = \frac{3}{5\phi} - \frac{3}{4} \tag{3.52}$$

With these values of d_1 and β_q we then obtain

$$\mu_1 = \frac{7\kappa(19p+16)(2p+3)}{3\left(175(p+1) - 2(19p+16)(2p+3)\right)} \tag{3.53}$$

$$\mu_2 = \frac{7\left((19p+16)(2p+3) - 25(5p+2)\right)}{3\left(175(p+1) - 2(19p+16)(2p+3)\right)} \tag{3.54}$$

We note that the requirement (i) is satisfied if $p < 1$. But this restriction is not a loss of generality since the Doi Ohta characterization of the morphology does not distinguish between "inside" and "outside". In the comparison with experimental data we shall thus consider p to be always a ration of the smaller viscosity coefficient to the larger viscosity coefficient. The difference between the experimental data of the blend with p and $1/p$ (see Section 3.4.4) will be expressed in other parameters (in particular in the the parameter μ - arising already in the original Doi Ohta theory - that is, at this point, left undetermined).

3.4.3 Effect of μ

In the original Doi Ohta equations, the parameter μ describes the ratio of the relaxation rate of the area density (the size of the interface) to that of the deformation of the interface (the deformation of its shape). The range of μ is from 0 to 1. Although the physical meaning of the parameter μ remains the same in the present active advection model, its influence on the morphological and the rheological is different.

Fig.3.1 and Fig.3.2 illustrate the influences of μ on the transient behavior of the immiscible blend. The applied flow field is a start-up simple shear flow, Q/Q_0 is the normalized area density, $\frac{\mathrm{tr}(\boldsymbol{q}\cdot\boldsymbol{q})^{1/2}}{Q}$ describes the normalized average deformation of the interface, σ_{12}^{int}, and N_1^{int} are the interface contributions to the normalized (i.e. divided by $\eta_{out}\dot{\gamma}$) shear stress and the first normal stress difference. The calculations are made by choosing $\eta_{out} = 93Pa\,s$, $p = 0.5$, $\phi = 30\%$, $Q_0 = 5\times10^4 m^{-1}$, $\dot{\gamma} = 0.5s^{-1}$ and μ takes three different values: 0.2, 0.5 and 0.8. The results of DO1 model (symbol $\circ$) and DO2 model (symbol $\diamond$) are also displayed, with d_1 and μ taking the same values as the active DO model with $\mu =$

0.5 (dashed line). Fig.3.1 shows that when μ takes small values, for example, $\mu < 0.2$ with the above initial conditions, the area density increases monotonously with time. This corresponds to the processes of deformation or breakup of droplets. Upon increasing μ ($\mu > 0.5$ here), the interfacial area densities show monotonous decreases with time. This indicates that the coalescence of droplets takes place. The larger μ the stronger is the effect of the coalescence. As a consequence of the decrease of the area density with larger μ, the averaged deformation of the interface increases because larger droplets with the same interfacial tension are easier to deform under the same external flow. The figure also displays a larger overshoot of the deformation for larger droplets with smaller area density. The present model is the DO2 model modified with active advection. The comparison of the dashed lines (active DO model with $\mu = 0.5$) and $\diamond$ symbols (DO2 model with the same d_1 and μ) indicates that the DO2 model overestimates the area density and underestimates the global deformation of interfaces.

As to the rheological properties depicted in Fig.(3.2), it can be seen that both the shear stress and the first normal stress difference decrease as μ increases. This is in accordance with the decreased area density displayed in Fig.3.1. Since smaller Q and $\boldsymbol{q}$ results in smaller stresses. Fig.(3.2) also displays that the overshoots become more prominent as μ enhanced because the size of droplet is increased with lower area density. We can also see from these graphs that the DO2 model underestimates both the shear stress and the first stress differences. This is because the expression for the stress tensor used in the original Doi Ohta models is incomplete. The contribution due to the deformation of the interface (i.e. the terms involving β_q in the last equation of (3.33) are missing in the original Doi Ohta models.

The influences of μ on predicted steady-state values of morphological and rheological functions are displayed on Fig.3.3 and Fig.3.4. η^{int} and N_1^{int} are the interface contributions to the viscosity and the first normal stress difference. The calculations are made by choosing $\eta_m = 93Pa\,s$, $p = 0.5$, $\phi = 30\%$, $\Gamma = 1 \times 10^{-3}Nm$, $Q_0 = 1 \times 10^4 m^{-1}$ and μ takes three different values: 0.2, 0.5 and 0.8. When the shear rate varies, we observed in Fig.3.3 that an increase in μ leads to a decrease in the area density and an increase in the deformation of the interface, just as the figure of the transient states shows. Moreover, we note that the influence of μ is more pronounced at smaller shear rates, and become

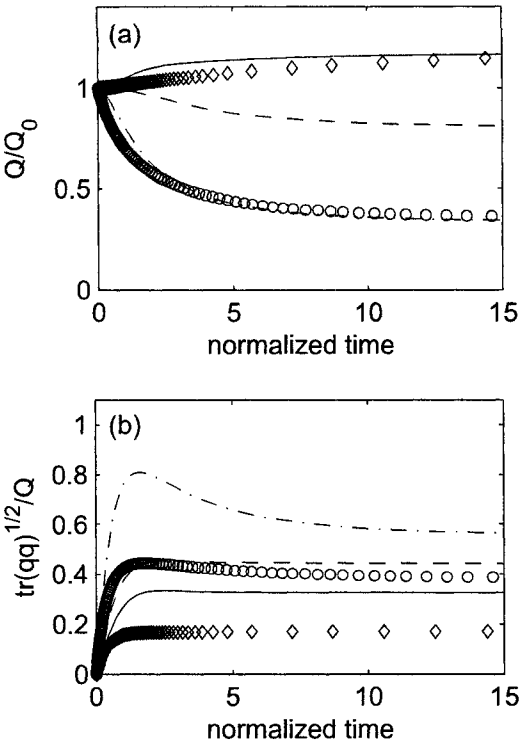

Figure 3.1: The influences of μ on the time evolution of the area density $\frac{Q}{Q_0}$ (a) and the deformation $(\mathrm{tr}(\boldsymbol{q}\cdot\boldsymbol{q}))^{1/2}/Q$ (b) of the interface of blends subjected to a start-up simple shear flow. ($\circ$) and ($\diamond$) correspond to DO1 model and DO2 model respectively; the curves (—), (- -) and (-.-) correspond to the active DO model with $\mu = 0.2$, $\mu = 0.5$ and $\mu = 0.8$ respectively.

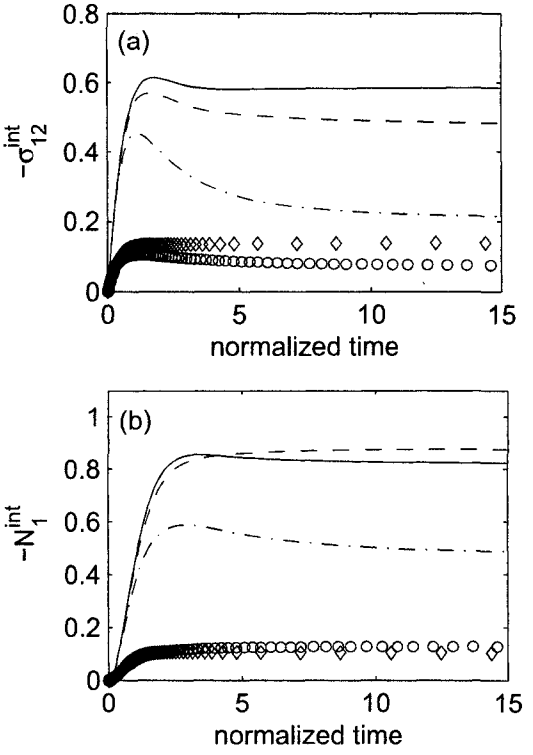

Figure 3.2: The influences of μ on the time evolution of the normalized interfacial shear stress σ_{12}^{int} and the first normal stress difference N_1^{int} of blends subjected to a start-up simple shear flow. ($\circ$) and ($\diamond$) correspond to DO1 model and DO2 model respectively; the curves (—), (- -) and (-.-) correspond to the active DO model with $\mu = 0.2$, $\mu = 0.5$ and $\mu = 0.8$ respectively.

less pronounced as the shear rate increases. Fig.3.3 also indicates that both the DO1 model and the DO2 model predict a linear relation between Q/Q_0 and $\dot{\gamma}$. These relation becomes nonlinear in the active DO model. Another difference between the DO1 and DO2 models on one side and the active DO model model on the other side is in the dependence of the steady-state value of the interface deformation on the shear rate. Both DO1 and DO2 models predict no dependence but the active DO model predicts an increase with an increase of the shear rate.

The rheological properties at steady states are displayed on Fig.3.4. We see that an increase of μ causes both the shear stress and first normal stress difference to decrease. This effect becomes less pronounced in the region of higher shear rates. The active DO model predicts a shear thinning behavior, while the viscosities predicted by the two Doi Ohta models are constant over the different shear rates. From the expression of the stress tensor, we conclude that the shear thinning is mainly caused by: (i) the decrease of the deformation part of the stress tensor (i.e., the terms involving β_q), and (ii) by the active advection. The figure shows also that N_1 predicted by the active DO model become nonlinear as a function of shear rate. Moreover, we note that η and N_1 are insensitive to changes of μ at high shear rates.

3.4.4 Effect of p and $\mathcal{C}$

The viscosity ratio p is defined as the ratio of the viscosity of the dispersed phase to that of the the matrix phase. It describes the nonuniformity of the material properties of the immiscible blends, and plays the most important role in controlling the extent of perturbation on the applied flow field. The original Doi Ohta model considers only $p = 1$, corresponding to the passive advection, which is a special case of the active advection. The capillary number $\mathcal{C}$ is another parameter that affects the properties of emulsions. In the following paragraph, we will discuss the effect of p and $\mathcal{C}$ on rheological and morphological predictions of active DO model.

Fig.3.5 and Fig.3.6 illustrate the influence of p and $\mathcal{C}$ on steady-state morphological and rheological behavior. σ_{12}^{int} and N_1^{int} are the interface contributions to the normalized (i.e. divided by $\eta_{out}\dot{\gamma}$) shear stress and the first normal stress difference. The calculations are made with: $\phi = 30\%$, $\kappa = 9.514 \times 10^7$, $\mu = 0.1$

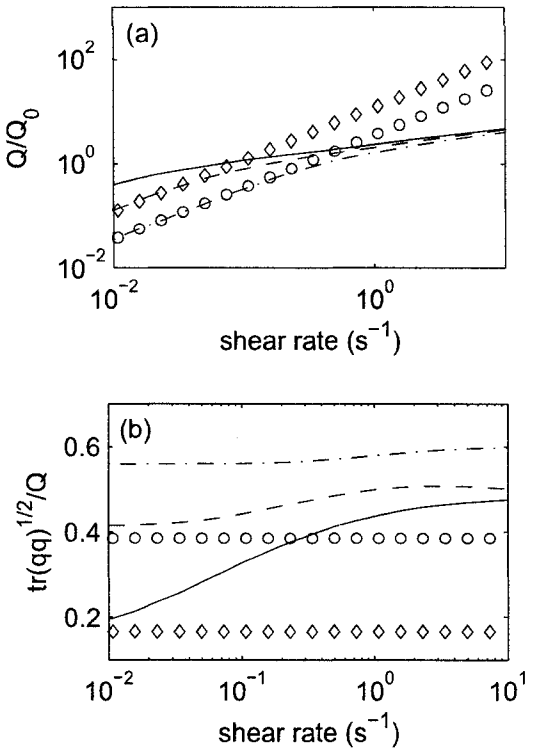

Figure 3.3: The influences of μ on steady state values of the normalized area density (a) and the deformation (b) of the interface of blends subjected to a simple shear flow. ($\circ$) and ($\diamond$) correspond to DO1 model and DO2 model respectively; the curves (—), (- -) and (-.-) correspond to the active DO model with $\mu = 0.2$, $\mu = 0.5$ and $\mu = 0.8$ respectively.

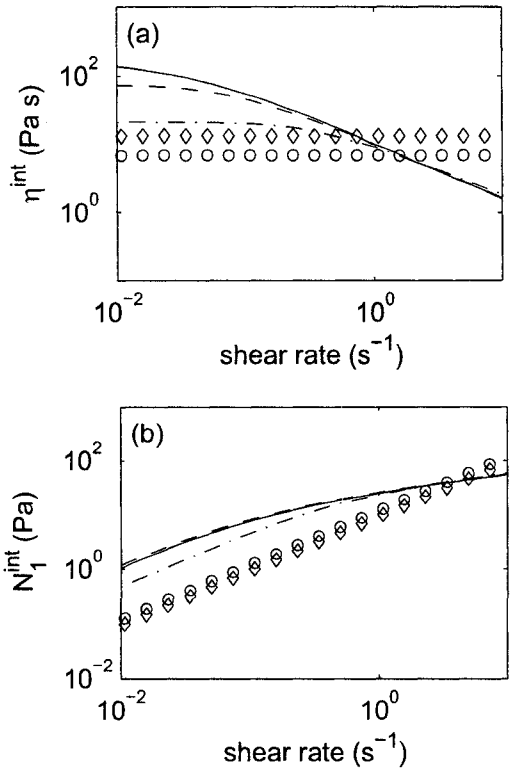

Figure 3.4: The influences of μ on steady state values of the normalized interfacial shear stress σ_{12}^{int} and the first normal stress difference N_1^{int} presented as functions of the shear rate. ($\circ$) and ($\diamond$) correspond to DO1 model and DO2 model respectively; the curves (—), (- -) and (-.-) correspond to the active DO model with $\mu = 0.2$, $\mu = 0.5$ and $\mu = 0.8$ respectively.

and p takes three different values: 0.1, 0.5, and $1 - 1 \times 10^{-5}$. It can be seen from Fig.3.5 that, if p takes a value very close to the unity, the interface is convected in active DO model just like the DO2 model does at small capillary numbers. This implies that the passive advection takes place for $p = 1$. When p deviates from unity, the predicted area density is less than that of DO2 model, which indicates a nonaffine advection. However, the global deformation, $\frac{\mathrm{tr}(\boldsymbol{q}\cdot\boldsymbol{q})^{1/2}}{Q}$, is increased because the decrease of Q is larger than the decrease of $\mathrm{tr}(\boldsymbol{qq})^{1/2}$. This means that during the nonaffine advection the break up of the droplets in deformations is less frequent than during the affine advection.

We turn now to the interfacial shear stress represented on Fig.3.6. We can see that the shear stress is largest for the passive advection with $p = 1$. We also note that in the zero shear rate limit it reaches the value 1.75 which is in agreement with Taylor's theory. The first normal stress difference shows, for the passive advection, an increase when $\mathcal{C}$ increases, but a decrease when $\mathcal{C}$ increases for the nonaffine advection.

3.4.5 Comparison with experimental data and with other models

In this section we compare the results predicted by the active DO model with experimental data. In order to facilitate the illustration, we also present predictions of other models, including the DO1, DO2 models, WOE model, LP model, and FA model. The experimental data are taken from Vinckier *et al.* [29], Grizzuti *et al.* [23] and Lacroix *et al.* [12]. All the material data and initial conditions (if reported) are the same as those in the experiments. The phenomenological parameter, μ is determined by fitting the data.

First, we consider the steady state rheological properties of semi-dilute emulsions. The experimental data are taken from Vinckier *et al.* [29] for the model system of poly(isobutene) (PIB) and poly(dimethylsiloxane) (PDMS) with $70\% PIB$ as matrix. Both components show nearly constant viscosity and a slight elasticity for the shear rates in the interval from $0.3s^{-1}$ to $6s^{-1}$. The interfacial tension is $2.8 \times 10^{-3} N/m$. Fig.3.7 shows the comparison of the contributions of the interface to the viscosity coefficient η^{int} and the first normal stress difference N_1^{int}. The experimental values are obtained by subtracting the bulk contribution by using

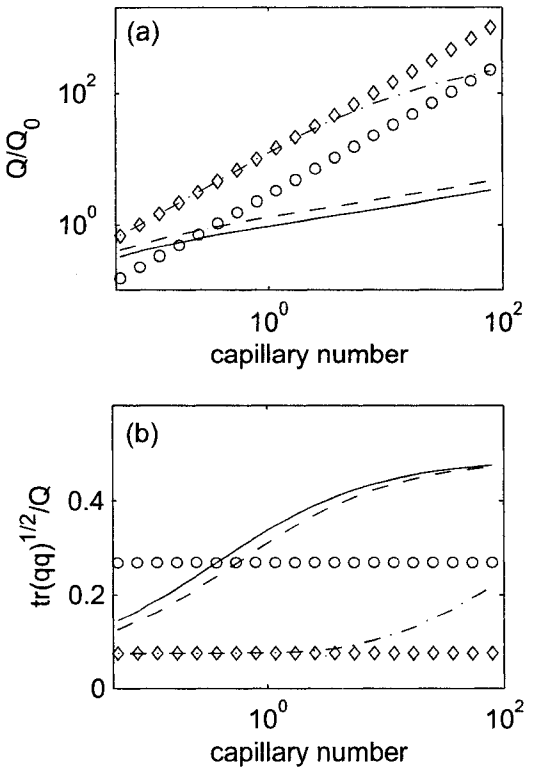

Figure 3.5: The influences of p on steady state values of the normalized area density (a) and the deformation (b) of the interface of blends presented as functions of $\mathcal{C}$. ($\circ$) and ($\diamond$) correspond to DO1 model and DO2 model respectively; the curves (—), (- -) and (-.-) correspond to the active DO model with $p = 0.1$, $p = 0.5$, and $p = 1 - 1 \times 10^{-5}$ respectively.

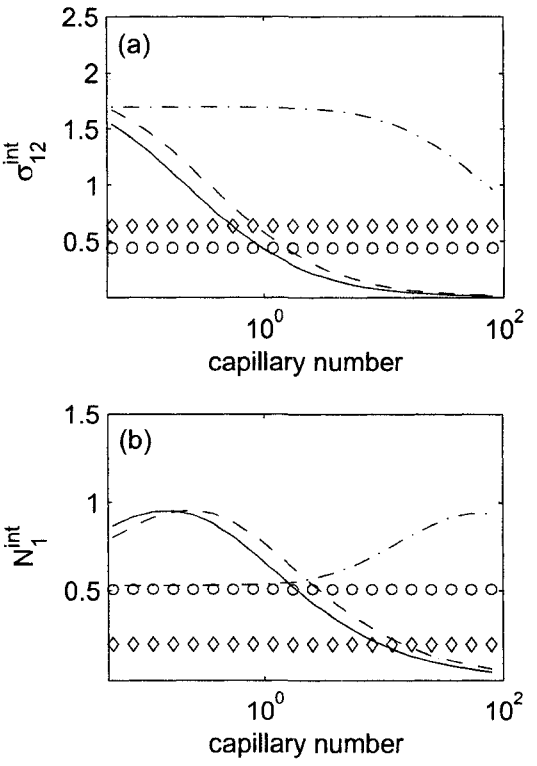

Figure 3.6: The influences of p on steady state values of the normalized interfacial shear stress σ_{12}^{int} and the first normal stress difference N_1^{int} presented as functions of $\mathcal{C}$. ($\circ$) and ($\diamond$) correspond to DO1 model and DO2 model respectively; the curves (—), (- -) and (-.-) correspond to the active DO model with $p = 0.1$, $p = 0.5$, and $p = 1 - 1 \times 10^{-5}$ respectively.

Table 3.1: Parameters used to predict the rheological properties of the immiscible blend of $PIB/PDMS(70\%30\%)$ in the experiments of Vinckier *et al.* [29]

	p	$\eta_{out}(Pa\,s)$	ϕ	$\Gamma(mN/m)$	$Q_0(m^{-1})$	d_1	μ
DO1	–	93	0.3	2.8	1.4×10^4	0.53	0.51
DO2	–	93	0.3	2.8	1.4×10^4	0.53	0.51
WOE	–	93	0.3	2.8	1.4×10^4	0.53	0.51
active DO	1.075	93	0.3	2.8	1.4×10^4	–	0.51

the following linear mixing rule:

$$\begin{aligned} \eta^{tot} &= \eta^{int} + \eta^{com} \\ N_1^{tot} &= N_1^{int} + N_1^{com} \end{aligned} \tag{3.55}$$

where η^{com} and N_1^{com} are the volume averaged values for both components. Besides the two original Doi Ohta models, DO1 and DO2, the predictions of the WOE model are also presented. Since the initial area density, Q_0, was not provided in the experimental data, we take it as another fitting parameters here. The value of parameters used in the models are listed in Table 3.1.

We first compare the two original Doi Ohta models. We can see that with the same values of the material parameters the DO2 model gives higher values for the viscosity coefficient and for the first normal stress difference. But both DO1 and DO2 models predict constant viscosity coefficients and thus fail to predict the experimentally observed shear thinning phenomena. The WOE model predicts qualitatively the right trend of the shear thinning, but the predictions are not quantitatively good enough. Predictions of the WOE model for the first normal stress difference look also worse than those of the original Doi Ohta models. We note that the active DO model does not only predict the shear thinning behavior but it gives also the best quantitative fitting to the experimental data. The improvement in prediction of the active DO model is mainly a consequence of the more realistic consideration of the advection of the interface, and the more complete expression for the stress tensor.

Figure 3.8 displays other predictions of the active DO model and compares

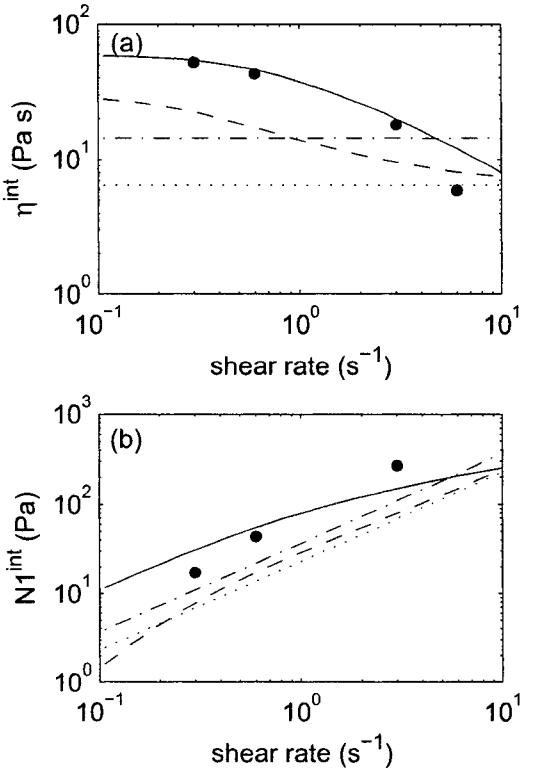

Figure 3.7: The steady state interfacial viscosity (a) and the first normal stress difference (b) for the DO1 model (...); for the DO2 model(-.-); for the WOE model (- -); for the active DO model(—); by (•) we represent the Vinckier *et al.* [29] experimental data

them with the experimental data, the LP model, and the FA model (the extended version of the FA model due to Grizzuti *et al.*)[23]. The steady-state viscosity of the emulsion in the extended FA model is written as [23]

$$\eta = \frac{\eta_{out}}{1+\theta_1}\left[1+\frac{5p+2}{2p+2}\phi+\theta_1\left(1+\frac{5p+2}{2p+2}\phi-\frac{19p+16}{2(p+1)(2p+3)}\phi\right)\right] \tag{3.56}$$

where

$$\theta_1 = \left(\frac{(2p+3)(19p+16)}{40(p+1)}\frac{\eta_m K}{\Gamma}\dot{\gamma}^{(1-\theta_2)}\right)^2 \tag{3.57}$$

Here K and θ_2 are the parameters determined by linear viscoelastic measurements. Since the extended FA model gives good predictions for semi-concentrate emulsions, we are including it in the collection of models with which we are comparing the active DO model. The experimental data are taken from Grizzuti *et al.*[23] for immiscible model polymer blend of PIB/PDMS system subjected to a simple shear flow. Figure 3.8a addresses the 30/70 system in 9^oC with the volume ratio of 30% of PIB as the droplet phase. Figure 3.8b is for the 70/30 system in 9^oC with the volume ratio of 70% of PIB as the matrix phase. The interfacial tension was reported to be $3 \times 10^{-3} N/m$. The linear mixing rule, Eq.(3.55), is used to calculate the total stress of the blends. The viscosities of both of its components are taken to be their zero shear values, that is, $\eta_{PIB} = 500(Pa\,s)$ and $\eta_{PDMS} = 310(Pa\,s)$. The values of the parameters used by the LP model and the active DO model are listed in Table 3.2 and Table 3.3. Since the initial radius, Q_0, is not known in the experiments, we use both Q_0 and μ as fitting parameters. The critical steady-state droplet radii used in the FA model are taken as $6\mu m$ for 30/70 system and $3\mu m$ for 70/30 system, corresponding to the measured values at shear rate $\dot{\gamma} = 3s^{-1}$. The parameters K and θ_2 are those used by Grizzuti *et al.*[23]. As shown on Figure 3.8a and 3.8b, the LP model, just like the original DO models, fails to predict the shear thinning behavior. Introducing more parameters does not change the steady state viscosity dependance on the shear rate. The FA model (without adjustable parameters) can only qualitatively predict the shear thinning behavior. The extended FA model, with an added relation (based on results of measurements) between the droplet radius and the shear rates, can give very good results over the lager shear rates region. However, both FA models underestimate the viscosity at low shear rates. The predictions of the

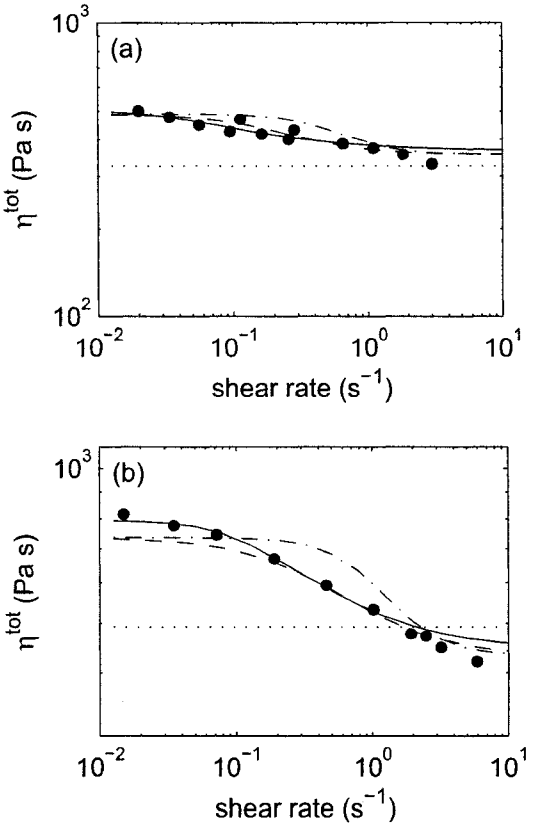

Figure 3.8: Steady state interfacial viscosity of: (a) 30/70 , (b) 70/30 blends of PIB/PDMS. The curve (...) corresponds to the LP model; (-.-) to the FA model, and (- -) to the extended FA model; (—) to the active DO model; (•) represents the experimental data taken from Grizzuti *et al.* [23]

active DO model is in good agreement with experimental data. It gives results that are better than the results for the extended FA model except at the region of large shear rates. The deviations of both models from the experimental data at high shear rates may be partially caused by the shear thinning of PDMS itself (experimental data of Grizzuti *et al.*[23] shows that the viscosity of pure PDMS has already dropped near $\dot{\gamma} = 5s^{-1}$).

In Figure(3.9) we investigate the active DO model in start-up simple shear flows. The models with which we make the comparison are selected to be: the DO1 model, DO2 model, and the WOE model. The experimental data are taken from Lacroix *et al* [12] for immiscible polymer blends of PP/(EVA-EMA) with

Table 3.2: Parameters used to predict the rheological properties of the PIB/PDMS(30/70) blend in the experiments of Grizzuti *et al.* [23]

	p	$\eta_{out}(Pa\,s)$	ϕ	$\Gamma(mN/m)$	$Q_0(m^{-1})$	ν	d_1	μ
LP	–	310	0.3	3	3×10^3	0.9	1.08	0.68
active DO	1.61	310	0.3	3	3×10^3	–	–	0.68

Table 3.3: Parameters used to predict the rheological properties of the PIB/PDMS(70/30) blend in the experiments of Grizzuti *et al.* [23]

	p	$\eta_{out}(Pa\,s)$	ϕ	$\Gamma(mN/m)$	$Q_0(m^{-1})$	ν	d_1	μ
LP	–	500	0.3	3	3×10^4	0.9	0.56	0.525
active DO	0.62	500	0.3	3	3×10^4	–	–	0.525

the volume fraction 28.5% of EVA-EMA as the droplet phase. Although the components are non-Newtonian fluids, the dependance of the steady state viscosities of the pure components on the shear rate is not important since we only consider the transient properties of the blends at a fixed shear rate. Results of the experimental observations indicate that both components do not exhibit any measurable overshoot at start-up flows. Consequently, the overshoots observed in the graphs are totally due to the presence of the interface. Again, the linear mixing rule, Eq.(3.55), is used. The data that we select in Figure 3.9a and Figure 3.9b correspond to: $\dot{\gamma} = 0.0126s^{-1}$ and $\dot{\gamma} = 0.0317s^{-1}$ respectively. The initial value of the surface area density is calculated by $Q_0 = 3\phi/r_0$, with ϕ representing volume fraction of the droplet phase and r_0 being the measured initial volume averaged droplet radius. The parameters used in the calculations are listed in Table 3.4 and Table 3.5. We can see that the two original DO models can predict well the steady state and but underestimate the overshoots observed in the experiments, while the active DO model can provide good predictions of both the steady state values and the hight of overshoots. However, the time takes for the blends to reach the maximum of the overshoot predicted by active DO model is less than the experimental observations. The WOE model, as shown on Fig. 3.9, fails to predict the overshoot. A possible explanation for this is that the mod-

Table 3.4: Parameters used to predict the rheological properties of the PP/(EVA-EMA) blend in the experiments of Lacroix *et al.* [12] for $\dot{\gamma} = 0.0126s^{-1}$

	p	$\eta_m(Pa\,s)$	ϕ	$\Gamma(mN/m)$	$r_0(\mu m)$	d_1	μ
DO1	–	11650	0.285	1.2	3.75	0.6	0.65
DO2	–	11650	0.285	1.2	3.75	1	0.65
WOE	–	11650	0.285	1.2	3.75	4.5	0.62
active DO	0.126	11650	0.285	1.2	3.75	–	0.95

Table 3.5: Parameters used to predict the rheological properties of the PP/(EVA-EMA) blend in the experiments of Lacroix *et al.* [12] for $\dot{\gamma} = 0.0317s^{-1}$

	p	$\eta_m(Pa\,s)$	ϕ	$\Gamma(mN/m)$	$r_0(\mu m)$	d_1	μ
DO1	–	11080	0.285	1.2	3.75	0.3	0.65
DO2	–	11080	0.285	1.2	3.75	0.7	0.65
WOE	–	11080	0.285	1.2	3.75	2.2	0.65
active DO	0.131	11080	0.285	1.2	3.75	–	0.92

ification introduced in the WOE model limit its applicability to, essentially, an absence of the break up and coalescence (which play likely an important role in the initial deformations in start up flows). It is worthwhile to note that in active DO model a relative larger μ is fitted out for the data of $\dot{\gamma} = 0.0126s^{-1}$ than for that of $\dot{\gamma} = 0.0317s^{-1}$. This is in agreement with the experimental observations on the relationship between the average steady droplet size and shear rate, which the droplet size is proportional to the inverse of shear rate. Since the larger μ means stronger tendency for droplet to coalescence, the smaller the shear rates the easier for droplets to collide and coalescent to form larger droplets.

To sum up, it is evident that the active DO model, although using one less free parameter, can give the best predictions among all the Doi Ohta type models.

3.5 Concluding Remarks

The most frequently used point of departure for discussing immiscible blends is microhydrodynamics [30]. The physics entering the governing equations consists

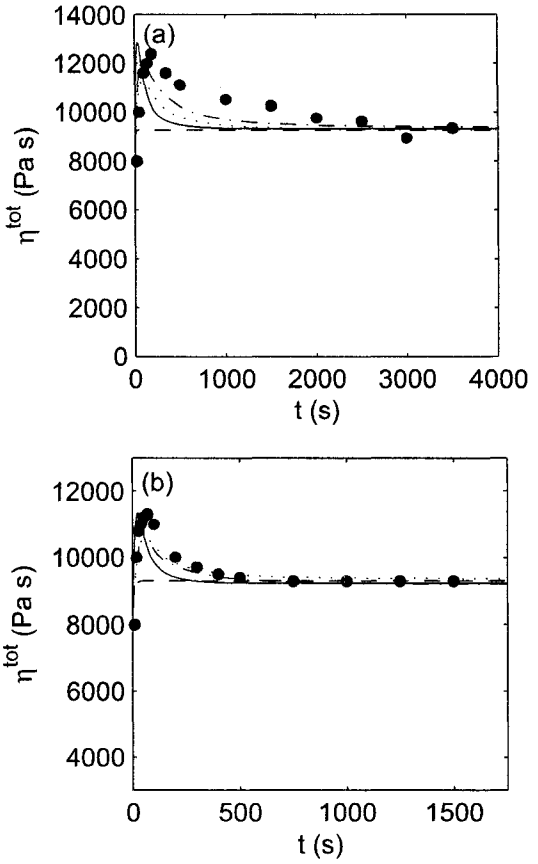

Figure 3.9: The time evolution of the total viscosity under start-up simple shear flows with: (a) $\dot{\gamma} = 0.0126s^{-1}$, and (b) $\dot{\gamma} = 0.0317s^{-1}$ (b). The curves (...) correspond to the DO 1 model; (-.-) to the DO 2 model; (- -) to the WOE model; (—) to the active DO model; (•) represent experimental data taken from Lacroix *et al.* [12]

of the rheological properties of the two fluids, mechanical properties of the interface, and the interface-bulk fluid interactions. All the material parameters involved can be, at least in principle, obtained in independent microhydrodynamic measurements. The governing equations are easily written but they are difficult to solve. Moreover, their solutions provide only the morphology. The transformation: *morphology→rheology* requires additional physical input and approximations.

In this paper we take a different (a mesoscopic) path. We regard the immiscible blend as a single fluid involving an internal structure. How do we characterize the internal structure? We follow Doi Ohta [1] and us the surface area per unit volume (Q) and the anisotropy tensor ($\boldsymbol{q}$). The new physics (relative to [1]) that we are bringing is the perturbation of the overall flow due to the presence of the interface and the "rheological inhomogeneity" of the two fluids. In order to be able to express the new physics we adopt an additional state variable (a tensor $\boldsymbol{w}$ that is a conjugate of the perturbed velocity gradient). We are taking the mesoscopic viewpoint for two reasons. First, we want to search for a new physics emerging in the overall (mesoscopic) hydrodynamics of immiscible blends. Such search is, on the microhydrodynamic path, entangled hopelessly with the enormous difficulty of solving the microhydrodynamic governing equations. Second, we want to satisfy the practical need of providing a relatively simple formulation that can be used in, say, calculations involved in polymer processing operations.

The disadvantage of the mesoscopic approach taken in this paper is that the material parameters quantifying the physics involved (mesoscopic material parameters) can be only partially determined by the comparison with microhydrodynamic theories. The remaining parameters (arising already in the original Doi Ohta theory) have to be obtained from measurements belonging to the same mesoscopic level (similarly as, for instance, the material parameters of classical hydrodynamics are usually obtained from hydrodynamic measurements and not from microscopic measurements of atoms composing the fluid under consideration).

The advantage of the Doi Ohta approach is the simplicity and transparency of the governing equations. We construct them by filling the general framework called GENERIC. The framework itself guarantees agreement of solutions with experimental observations constituting the basis of mechanics and thermody-

namics. The framework is filled by an insight into the physics taking place in the flowing immiscible blend. We call the process of filling the GENERIC framework a "GENERIC constitutive relation". We use this terminology in order to make a direct analogy with the familiar term "constitutive relations" used for the process of filling another abstract framework, namely the framework of local conservation laws (balance equations: time derivative of a field equals divergence of a flux), constituting the basis of classical hydrodynamics. If the fluids under consideration have an internal structure whose time evolution takes place on the time scale comparable with the time scale on which the hydrodynamic fields evolve the the abstract framework of local conservations laws is insufficient and has to be replaced by the framework of GENERIC.

The final output of the model that can be compared with experimental data is the following: (i) an information about morphology of the interface (namely the information expressed in the orientation tensor $\boldsymbol{q}$ and the density of the surface area of the interface Q), and (ii) the rheological behavior. In this paper we concentrate on predictions of the nonlinear rheological responses to imposed shear flows and their comparison with predictions of the original Doi Ohta model and experimental data reported in the literature. In the original Doi Ohta model we distinguish four versions: Doi Ohta 1, Doi Ohta 2, Lee-Park, and Wagner Ottinger Edwards corresponding to four variations in the selection of phenomenological quantities entering the model. In general, we find that the more faithful to reality (i.e. closer to microhydrodynamics) consideration of the physics in the active Doi Ohta model improves the agreement of predictions with the observed behavior.

Acknowledgment

This research has been partially supported by the Natural Sciences and Engineering Research Council of Canada

Bibliography

[1] M. Doi and T. Ohta, J. Chem. Phys. 95 (1991) 1242.

[2] J. F. Gu and M. Grmela, "GENERIC Model of Active Advection," J. Non-Newtonian Fluid Mech. 152 (2008) 12

[3] M. Grmela, (1984) Particle and bracket formulations of kinetic equations. Contemp Math 28 (1984) 125

[4] M. Grmela, Bracket formulation of diffusion-convection equations. Physica D 21 (1986) 177

[5] M. Grmela, Mesoscopic Dynamic and Thermodynamic: Application to Polymer Fluids. Lecture Notes in Physics 381 (1991) 99

[6] A. N. Beris and B. J. Edwards, Thermodynamics of flowing systems. 1 st edn. Oxford University Press, New York (1994)

[7] M. Grmela and H. C. Ottinger, Dynamics and thermodynamics of complex fluids. I. Development of a general formalism. Phys Rev E 56 (1997) 6620

[8] H. C. Ottinger and M. Grmela, Dynamics and thermodynamics of complex fluids. II. Illustrations of a general formalism. Phys. Rev.E 56 (1997) 6633

[9] M. Grmela, Reciprocity relations in thermodynamics. Physica A 309 (2002) 304

[10] H. C. Ottinger, Beyond Equilibrium Thermodynamics. Wiley (2005)

[11] M. Grmela and A. Ait-Kadi, J. Non-Newtonian Fluid Mech. 55 (1994) 191.

[12] C. Lacroix, M. Grmela, and P.J. Carreau, J. Rheol. 42 (1998) 41.

[13] A. Clebsch, J. Reine Angew. Math. 56 (1895) 1

[14] V. I. Arnold, Ann. Inst. Fourier 16 (1966) 319

[15] J. E. Marsden and A. Weinstein, Physica D 7 (1983) 305

[16] J. F. Gu, M. Grmela, and M. Bousmina, Physics of Fluids 20 (2008) 043102

[17] V. G. Baidakov, G. Sh. Boltachev, and G.G. Chernykh, Curvature corrections to surface tension, Phys. Rev. E 70 (2004) 011603

[18] W. Helfrich, Z. Naturforschung 29c (1974) 510

[19] J. Pellicer, J.A. Manzanares, and S. Mafe, Am.J.Phys. 63 (1995) 542

[20] H. M. Lee and O.O. Park, J. Rheol. 38 (1994) 1405.

[21] J. Wagner, H. C. Ottinger, and B.J. Edwards, AIChE. J. 45 (1999) 1169 .

[22] N. A. Frankel and A. Acrivos, J. Fluid Mech. 44 (1970) 65.

[23] N. Grizzuti, G. Buonocore, and G. Iorio, J. Rheol. 44 (2000) 149.

[24] G. I. Taylor, Proc. R. Soc. London, Ser. A 138 (1932) 41.

[25] J. F. Palierne, Rheol. Acta, 29 (1990) 204; 30 (1991) 497

[26] Y. Takahashi, N. Kurashima, I. Noda, M. Doi, J. Rheol. 38 (1994) 699.

[27] G. K. Guenther and D. G. Baird, J. Rheol. 40 (1996) 1.

[28] I. Vinckier and H. M. Laun, J. Rheol. 45 (2001) 1373.

[29] I. Vinckier, M. Minale, and J. Mewis, P. Moldenaers, Colloids Surf. A: Physicochem. Eng. Aspects 150 (1999) 217.

[30] S. Kim and S. J. Karilla, Microhydrodynamics, Butterworth-Heinemann (1991)

Chapter 4

A Shape Tensor Model for a Droplet with Its Interface Covered with Surfactants

Jian Feng Gu[1], Mosto Bousmina[2] ,Miroslav Grmela[1,3]

[1] Ecole Polytechnique de Montreal, C.P.6079 suc. Centre-ville, Montreal, H3C 3A7, Quebec, Canada

[2] Department of Chemical Engineering, Laval University, Ste-Foy, G1K 7P4, Quebec, Canada

This chapter is based on the oral presentation on PPS 2005-America's Regional Meeting of the Polymer Processing Society, Quebec City, Canada (August 14-17, 2005)

[3]corresponding author: e-mail: miroslav.grmela@polymtl.ca

abstract

A model is developed to describe the morphology of a droplet covered with surface active agents. The model combines the mesoscopic shape tensor model of Wetzel and Tucker [22] with the boundary integral formulation of microhydrodynamics of a surfactant-covered droplet [4]. The effects of the properties of the surfactant on the droplet deformation are discussed. Shape evolution of the droplet predicted by the present model agrees well with numerical simulations at small deformations. However, the deviation becomes larger when the deformation increases.

4.1 Introduction

Surfactants and copolymers are often added to the emulsion and immiscible polymer blends to improve the dispersion. These surface active agents are mainly distributed at the interfaces. They reduce the interfacial tension, change the morphology of the interfaces, and ultimately affect the rheology of the emulsions and blends.

However, the theoretical study of this problem has not yet received much attention. The first one reported in the literature is due to Flumerfelt [1]. By extending the Cox's work [2] on clean droplets, he carried out a first-order perturbation analysis of the deformation and orientation of drops in shear and extensional flow field. The approach was based on the Lamb's general solution of Stokes problem [3]. However his work is limited to smaller deformations and the overall stress responses of the emulsions was not provided.

It was until 1990 when Stone and Leal [4] extended the analysis to finite deformations and the presence of the break up of droplets. They solved the Stokes equation together with the coupled mass equation of surfactants numerically. They used the approach based on the reformulation of Stokes problem into equations involving boundary-integrals. Stone and Leal focused merely on the morphology but not on the rheology of the emulsion. The Stone and Leal paper was then followed by a large list of papers [5, 6, 7, 8, 9, 10, 11, 12, 13] that also use the boundary integral method to calculate the interfacial velocity and a finite difference method to compute surfactant concentration. Kruijt-Stegeman et al.

[17] use the finite element method for both the velocity and the concentration. Li et al. [18] and Renardy et al. [15] use a volume-of-fluid method to track the interface with a continuous surface stress formulation to describe the interfacial tension and a projection method to solve the Navier-Stokes equations. The effect of surfactant solubility has been considered in Milliken and Leal [6] and Eggleton and Stebe [9].

By means of analytical solutions for small perturbations of the drop shape and surfactant distribution, Vlahovska *et al.*[19] obtained a third-order perturbation solution of the problem. However, their solution is limited to the situation of the viscosity ratio equals one, and the diffusion of the surfactant at the interface is neglected. Although the solution agrees well with the numerical simulations under weak flows, its perturbation nature restricts its reliability only in the situations that both the deformation and concentration gradient of the surfactant are not too large.

In this article, a new method will be proposed. It combines the shape tensor tensor model of Wetzel and Tucker [22] with the boundary integral formulation of Stokes equations. Similar approach was used by Yu and bousmina for modelling emulsions without surfactants [20].

4.2 Microhydrodynamics

For a dilute emulsion with the presence of surfactant, the hydrodynamic interaction between the droplets can be neglected. We consider therefore a single droplet of a Newtonian liquid with viscosity η_d dispersed in another Newtonian liquid with viscosity η_m. The interface separating the droplet and the matrix is assumed to be characterized completely by the interfacial tension Γ. Other properties of the interface, like the surface shear viscosity and the dilatation viscosity are neglected. The surfactant which is added into the blend is assumed to be insoluble to both fluids. It resides therefore only on the interface. The concentration of the surfactant is defined as the mass of the surfactant per unit interfacial area. The matrix liquid undergoes a linear flow with velocity gradient $\nabla \boldsymbol{v}$. The surfactant is advected by the flow but remains still confined on the interface. This leads to a nonuniformlly distribution of the surfactant, with higher

concentration at the ends and lower concentration in the middle of the droplet. The resulted nonuniformity of interfacial tension greatly affect the morphology (and consequently also the rheology) of the droplet.

In the context of microhydrodynamics, since the Reynolds number is very low for a small droplet, the flow of the incompressible bulk fluids can be described by the following Stokes equations and the continuity equations,

$$-\nabla P_i + \eta_i \nabla^2 \boldsymbol{v}_i = 0 \tag{4.1}$$

$$\nabla \cdot \boldsymbol{v}_i = 0 \tag{4.2}$$

where η_i is the viscosity coefficient, $\boldsymbol{v}_i$ and P_i are the velocity field and pressure field respectively. $i = d$ denotes the droplet and $i = m$ the matrix.

The boundary conditions are

$$\boldsymbol{v} = \nabla \boldsymbol{v} \cdot \boldsymbol{r}, \quad as \ |\boldsymbol{r}| \to \infty \tag{4.3}$$

$$[\boldsymbol{v}(\boldsymbol{r})]_S = 0, \quad as \ \boldsymbol{r} \in S \tag{4.4}$$

$$[\sigma(\boldsymbol{r}) \cdot \boldsymbol{n}(\boldsymbol{r})]_S = \Gamma \boldsymbol{n}(\boldsymbol{r}) \nabla_s \cdot \boldsymbol{n}(\boldsymbol{r}) - \nabla_s \Gamma, \quad as \ \boldsymbol{r} \in S \tag{4.5}$$

where $\boldsymbol{r}$ is the position vector, S denotes the interface, and $[\ ]_s$ represents the jump across the interface from inside to outside of the droplet. ∇_s is the surface gradient operator, $\boldsymbol{\nabla_s} = (\mathrm{I} - \boldsymbol{n}) \cdot \boldsymbol{n}$, where I is the identity tensor and $\boldsymbol{n}$ is the unit normal of interface.

The interfacial tension of the interface depends locally on the concentration of surface active agents. Such relationship is referred to as the equation of state for surface active agents. For dilute surfactant, we assume (Adamson 1967 [23]) that the equation of state is linear:

$$\Gamma = \Gamma_c - \rho RT \tag{4.6}$$

where Γ_c is the interfacial tension of the clean interface (i.e. in the absence of the surfactant), R the gas constant, T is the absolute temperature.

The mass conservation of surfactant leads to a time-dependant convective-

diffusion equation that can be written as (Aris 1962 [16], Stone and Leal [4])

$$\frac{\partial \rho}{\partial t} + \nabla_s \cdot (\rho \boldsymbol{v}_t) + \rho(\nabla_s \boldsymbol{n})(\boldsymbol{v} \cdot \boldsymbol{n}) - D_s \nabla_s^2 \rho = j_n \tag{4.7}$$

where v_t is the tangential component of the interfacial velocity, i.e. $\boldsymbol{v_t} = (\mathrm{I} - \boldsymbol{n}) \cdot \boldsymbol{v}$, D_s is the diffusivity of the surfactant on the interface, and j_n is the flux between the interface and bulks. For insoluble surfactant, j_n disappears.

The evolution of the shape of the droplet is described by the kinematic equation of interfaces

$$\frac{d\boldsymbol{r}_s}{dt} = (\boldsymbol{u} \cdot \boldsymbol{n})\boldsymbol{n} \tag{4.8}$$

where $\boldsymbol{r}_s$ denotes a point at the interface.

It is clear that the difficulty of this problem stems from the movement of the interface. Thus the boundary conditions at interfaces can not applied explicitly. To add to the complexity, also the mass equation can not be solved independently, since it is coupled to the shape and the velocity of the interface.

4.3 Shape tensor model

In microhydrodynamics, the interface can be looked at as a two dimensional surface embedded in a three dimensional space. It can be described by a function of positions. From a more macroscopic or mesoscopic point of view, we can characterize an overall morphology of the interface, for example, by the Doi-Ohta variables or Maffeton-Minale tensor. These approaches give coarse-grained pictures of the morphology of the interface by averaging out some unimportant detailed information. As a consequence, the problem becomes easier to solve without loosing the most important factors.

The microscopic observations [21] show that up to moderate deformations, the steady-state drop shape can well be described by an ellipsoid having three different axes. This justifies the use of the following equation to describe the shape of a droplet,

$$G_{ij} r_i r_j = 1 \tag{4.9}$$

where $\boldsymbol{G}$ is a positive symmetric second order tensor, which was called the shape tensor by Wetzel and Tucker [22]. The shape tensor is the inverse of Maffeton-

Minale tensor [25]. The eigenvalues of $\boldsymbol{G}$ are equal to the reciprocal of the square of the semiaxes of the ellipsoid $(1/a^2, 1/b^2, 1/c^2)$. Here a, b, and c $(a > b > c)$ are the three semiaxes of the ellipsoid. The aspect ratios between the semiaxes are defined as: C=c/a, D=c/b. The orientation is defined by the corresponding eigenvectors.

Taking the material derivatives of Eq.(4.9) leads to the following time evolution equation of $\boldsymbol{G}$,

$$\frac{dG_{ij}}{dt} + L_{ki}G_{kj} + G_{ik}L_{kj} = 0 \tag{4.10}$$

To obtain Eq.(4.10) the following linear assumption on the velocity field is used,

$$v_i = L_{ij}r_j \tag{4.11}$$

where L_{ij} is the velocity gradient of the interface. By the non-slip condition, it can be assumed that L_{ij} is uniform inside the whole droplet. But it is in general different from the applied flow gradient $\nabla \boldsymbol{v}$ if the viscosities of the bulks are not equal and the interfacial tension is not zero.

For the situation of a droplet with clean interface, L_{ij} can be expressed in terms of the applied velocity gradient and the Eshelby tensors [26] which are functions of aspect ratios of the ellipsoidal droplet. See the paper of Wetzel and Tucker [22] and Jackson and Tucker [24].

4.4 Shape tensor model with surfactants

In this section we neglect the tip streaming is absent and we assume that the droplet morphology does not deviates much from the ellipsoidal shape. This usually happens in the weak flow field and the viscosity ratio of the emulsion is larger than the order of 0.1 or the the concentration of the surfactant at interface is very high [27, 28, 10, 29, 30]. Our strategy for the new model is to establish a connection between the mesoscopic tensor model and the microhydrodynamic formulation of the Stokes problem.

4.4.1 Interfacial velocity

Following the standard boundary-integral reformulation of the Stokes problem, the integral representation for the normalized (i.e. divided by $\dot{\gamma}a$) velocity $\boldsymbol{v}(\boldsymbol{r}_s)$ of interface is given by, in dimensionless form (Stone and Leal [4]),

$$\begin{aligned}\frac{1+p}{2}\boldsymbol{v}(\boldsymbol{r}_s) &= \boldsymbol{v}^A(\boldsymbol{r}_s) - \frac{1}{8\pi}\int_{S_y}\boldsymbol{J}(\boldsymbol{r}-\boldsymbol{y})\cdot\left[\frac{1-\beta\rho}{Cs(1-\beta)}\boldsymbol{n}(\nabla_s\cdot\boldsymbol{n})\right. \\ &\left. +\frac{\beta}{Cs(1-\beta)}\nabla_s\rho\right]dS_y \\ &+(p-1)\int_{S_y}\boldsymbol{n}\cdot\boldsymbol{K}(\boldsymbol{r}-\boldsymbol{y})\cdot\boldsymbol{v}(\boldsymbol{y})dS_y \end{aligned} \tag{4.12}$$

where $\boldsymbol{J}$ and $\boldsymbol{K}$ are the kernel Green functions,

$$\begin{aligned}\boldsymbol{J} &= \frac{\boldsymbol{\delta}}{|\boldsymbol{r}_s-\boldsymbol{y}|}+\frac{(\boldsymbol{r}_s-\boldsymbol{y})(\boldsymbol{r}_s-\boldsymbol{y})}{|\boldsymbol{r}_s-\boldsymbol{y}|^3}, \\ \boldsymbol{K} &= -\frac{3}{4\pi}\frac{(\boldsymbol{r}_s-\boldsymbol{y})(\boldsymbol{r}_s-\boldsymbol{y})(\boldsymbol{r}_s-\boldsymbol{y})}{|\boldsymbol{r}_s-\boldsymbol{y}|^5}\end{aligned} \tag{4.13}$$

In Eq.(4.12), $\boldsymbol{v}^A$ denotes the normalized (i.e. divided by $\dot{\gamma}a$) applied flow velocity, ρ the normalized (i.e. divided by equilibrium concentration ρ_0) surfactant concentration. The area integrals are performed over the surface of a droplet with the lengths are normalized by the undeformed droplet radius a_0. Cs is the capillary number based on the equilibrium interfacial tension with surface active agents,

$$Cs = \frac{\eta_m\dot{\gamma}a_0}{\Gamma} \tag{4.14}$$

and β is a parameter determining the sensitivity of the interfacial tension to changes in surfactant concentration,

$$\beta = \frac{\Gamma_c-\Gamma}{\Gamma_c} = \frac{\Gamma RT}{\Gamma_c} \tag{4.15}$$

By the linearity of the Stokes problem, we assume that the velocity at the interface can be separated into two parts: the contribution from the flow and the

contribution from the interfacial tension,

$$\boldsymbol{v} = [\boldsymbol{v}]_{flow} + [\boldsymbol{v}]_\Gamma \tag{4.16}$$

The similar decomposition of the velocity is also used in Yu and Bousmina model [20]. Then Eq.(4.16) leads to

$$\frac{1+p}{2}[\boldsymbol{v}(\boldsymbol{r}_s)]_{flow} = \boldsymbol{v}^A(\boldsymbol{r}_s) + (p-1)\int_{S_y} \boldsymbol{n}\cdot\boldsymbol{K}(\boldsymbol{r}-\boldsymbol{y})\cdot[\boldsymbol{v}(\boldsymbol{y})]_{flow}dS_y \tag{4.17}$$

$$\begin{aligned}\frac{1+p}{2}[\boldsymbol{v}(\boldsymbol{r}_s)]_\Gamma &= -\frac{1}{8\pi}\int_{S_y}\boldsymbol{J}(\boldsymbol{r}-\boldsymbol{y})\cdot\left[\frac{1-\beta\rho}{Ca}\boldsymbol{n}(\nabla_s\cdot\boldsymbol{n}) + \frac{\beta}{Ca}\nabla_s\rho\right]dS_y \\ &\quad +(p-1)\int_{S_y}\boldsymbol{n}\cdot\boldsymbol{K}(\boldsymbol{r}-\boldsymbol{y})\cdot[\boldsymbol{v}(\boldsymbol{y})]_\Gamma dS_y\end{aligned} \tag{4.18}$$

Yu and bousmina had shown that with respect to principle axes of the droplet, the flow termof the interfacial velocity and its gradient can be derived from Eq.(4.17) as

$$[v_i']_{flow} = \omega'^A x_j' + (B_{ijkl} + C_{ijkl})e_{kl}'^A x_j' \tag{4.19}$$

$$[L_i']_{flow} = \omega'^A + (B_{ijkl} + C_{ijkl})e_{kl}'^A \tag{4.20}$$

If the principal axes of the ellipsoid (x') are not aligned with the coordinate axes (x), the above velocity gradient tensor should be rotated by the rotation tensor R_{ij} that satisfies $x_i = R_{ij}x_j'$. Here R_{ij} is defined as

$$R = \begin{pmatrix} \cos\varphi & -\sin\varphi & 0 \\ \sin\varphi & \cos\varphi & 0 \\ 0 & 0 & 1 \end{pmatrix} \tag{4.21}$$

where φ is the inclination angle of the droplet. The interfacial tension velocity term $[\boldsymbol{v}]_\Gamma$ can be obtained by numerical integration of Eq.(4.18). Notice that the interfacial velocity itself appears in the integrand of Eq.(4.18). The iteration

should be performed during the integration. Because of the singularity of the Kernel Green functions, a careful treatment is needed at the vicinity of the singular point. We proceed as follows: (i) a small region is cut out around the singularity and the integration in it is made analytically, (ii) the result is then added to the numerically computed integral in the remaining domain (see [31, 32]).

In the present model, since we assumed that the droplet always takes the shape as a ellipsoid, the unit normal vector and the mean curvature has explicit expressions. Moreover, in order to minimize the computational cost, we do not calculate the velocity by integration method at each point at the interface. Instead, only the velocity of a few points on the interface is calculated. The velocity at other positions is then obtained by an interpolation.

4.4.2 The evolution of the droplet shape

By the assumption that the velocity gradient is uniform inside the droplet, the velocity gradient can be obtained from the interfacial velocity. Since only the normal velocity determines the change in the shape of a droplet, the velocity gradient at three apex points can be obtained by the following equations,

$$\begin{aligned} L_{11} &= v_1(a,0,0)/a \\ L_{22} &= v_2(0,b,0)/b \\ L_{33} &= v_3(0,0,c)/c \end{aligned} \tag{4.22}$$

with $L_{ij} = 0$ for $i \neq j$. In order to assure that the volume remains constant during the deformations, Eq.(4.10) is modified as follows

$$\frac{dG_{ij}}{dt} + L_{ki}G_{kj} + G_{ik}L_{kj} - \frac{2}{3}G_{ij}L_{kk} = 0 \tag{4.23}$$

It can be verified that with the new term, the condition of the volume conservation condition (i.e. $\det(\boldsymbol{G}) = 0$), is indeed satisfied.

4.4.3 Distribution of the surfactant

For a insoluble surfactant, the right-hand side term in Eq.(4.7) can be neglected. Thus the mass conservation equation in its nondimensional form can be written

as

$$\frac{\partial \rho}{\partial t} + \nabla_s \cdot (\rho \boldsymbol{v}_t) + \rho(\nabla_s \boldsymbol{n})(\boldsymbol{v} \cdot \boldsymbol{n}) - \frac{1}{P_e}\nabla_s^2 \rho = 0 \tag{4.24}$$

where P_e, the Peclet number describing the relative importance of the surfactant convection and diffusion is defined as

$$P_e = \frac{\dot{\gamma} a_0^2}{D_s} \tag{4.25}$$

The Peclet number can also be expressed in terms of Cs and another parameter γ,

$$P_e = Cs\gamma \tag{4.26}$$

where γ depends on material properties only,

$$\gamma = \frac{\Gamma a_0}{\eta D_s} \tag{4.27}$$

In order to facilitate the calculations we have to cast the above equations from their tensor form into a component form with respect to a convenient coordinates system. Here we choose a surface coordinate system which is parameterized by the azimuthal angle $\theta \in [0, 2\pi)$ and the polar angle $\phi \in [0, \pi)$, as shown in Figure 4.1. It is related to the Cartesian coordinate system (x, y, z) by

$$\begin{aligned} x &= -a\cos\phi \\ y &= b\sin\theta\sin\phi \\ z &= c\cos\theta\sin\phi \end{aligned} \tag{4.28}$$

The unit normal vector at the surface can be obtained from the coefficients of the first fundamental form as follows:

$$\boldsymbol{n} = \frac{bc\cos\phi\vec{i} - ac\sin\theta\sin\phi\vec{j} - ab\cos\theta\sin\phi\vec{k}}{\sqrt{b^2c^2\cos^2\phi + a^2(b^2\cos^2\theta + c^2\sin^2\theta)\sin^2\phi}} \tag{4.29}$$

where $\vec{i}$, $\vec{j}$ and $\vec{k}$ are unit vectors in the (x,y,z) coordinates system. The mean curvatures can be obtained from the coefficients of the second fundamental form

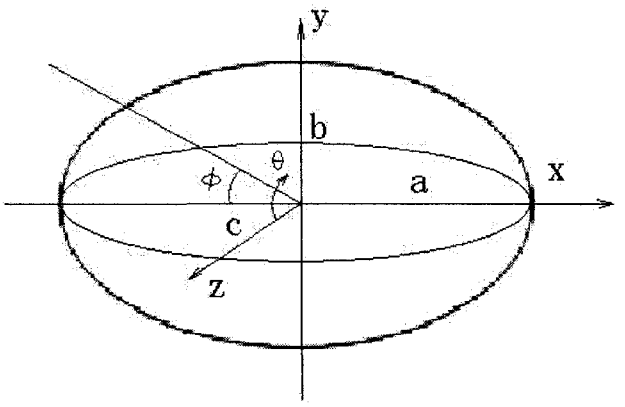

Figure 4.1: The orthogonal curvilinear coordinate system on a ellipsoidal surface

as

$$H = \frac{abc((b^2\sin^2\theta + c^2 cos^2\theta)\cos^2\phi + a^2\sin^2\phi + b^2\cos^2\theta + c^2\sin^2\theta}{2\left(b^2c^2\cos^2\phi + a^2(b^2\cos^2\theta + c^2\sin^2\theta)\sin^2\phi\right)^{3/2}} \tag{4.30}$$

Since the flow direction takes place along the x-axis, we assume that the terms containing $\frac{\partial}{\partial\theta}$ can be neglected. The mass equation (4.24) can thus be written in surface coordinates (θ, ϕ) as (Stone and Leal 1990)

$$\frac{\partial\rho}{dt} + \frac{1}{\sqrt{g}}\frac{\partial}{\partial\phi}\left(\rho\sqrt{g}v^\phi\right) - \frac{1}{P_e\sqrt{g}}\left(\frac{\partial}{\partial\phi}\sqrt{g}g^{\phi\phi}\frac{\partial\rho}{\partial\phi}\right) + 2H(\boldsymbol{v}\cdot\boldsymbol{n})\rho = 0 \tag{4.31}$$

where v^ϕ is the ϕ-component of the tangential interfacial velocity. It can be written as

$$v^\phi = \frac{\boldsymbol{v}\cdot\boldsymbol{g}_\phi}{g_{\phi\phi}} \tag{4.32}$$

where $\boldsymbol{g_\phi}$ is the covariant surface base vector of the surface coordinates,

$$\boldsymbol{g}_\phi = a\sin\phi\vec{i} + b\sin\theta\cos\phi\vec{j} + c\cos\theta\cos\phi\vec{k} \tag{4.33}$$

and g is the determinant of the surface metric tensor,

$$g = g_{\theta\theta}g_{\phi\phi} - g_{\theta\phi}^2 \tag{4.34}$$

with

$$\begin{aligned} g_{\theta\theta} &= b^2\cos^2\theta\sin^2\phi + c^2\sin^2\theta\sin^2\phi \\ g_{\phi\phi} &= a^2\sin^2\phi + b^2\sin^2\theta\cos^2\phi + c^2\cos^2\theta\cos^2\phi \\ g_{\theta\phi} &= \frac{(b^2-c^2)}{4}\sin 2\theta\sin 2\phi \end{aligned} \tag{4.35}$$

and

$$g^{\phi\phi} = \frac{g_{\theta\theta}}{g} \tag{4.36}$$

Equation(4.31) is a convective-diffusion equation. If the interfacial velocity $\boldsymbol{v}$ is known from the previous section, it can be solved numerically.

4.4.4 Numerical solution and results

The interfacial velocity and the mass distribution of surfactants are coupled. We use therefore the iteration method. The steps are as follows:
(a) Begin with an initial value of the spherical shape tensor $\boldsymbol{G}$ and with normalized equilibrium surfactant concentration $\rho = 1$.
(b) Calculate the interfacial velocity through Eq.(4.19, 4.18 and 4.16). We get $[\boldsymbol{v}]_\Gamma$.
(d) Calculate L_{ij} from Eq.(4.22).
(e) Update $\boldsymbol{G}$ with a small time increase $\triangle t$ through the solution of Eq.(4.23).
(f) The concentration of the surfactant is updated with the time increase $\triangle t$ by solving Eq.(4.31).
(g) Return to (b).

In this paper, an algorithm called the numerical method of lines [33] is used to solve the convective-diffusion equation. By this approach, the spacial derivatives are replaces by numerical approximations. Consequently, Eq.(4.31) is transformed into a system of ordinary differential equation, which can then be solved together

with Eq.(4.23) by standard ODE solvers in Matlab. The up-wind approximation for the spacial derivatives is used to improve the stability of the solutions. Because of the symmetry of the problem, only the left half droplet is calculated to save the computational cost. In the calculation, we choose 20 node points along the polar angle ϕ of the left-half of the droplet. The time step is automatically adjusted by the Matlab ODE solver, ode15s. The steady-state solution is obtained when the change rate of ρ and of length of principle axes are smaller than 0.6%. To keep the total amount of surface active agents conserved, a rescaling process is performed if the cumulative mass changes are larger than 0.2%.

Interface without a surface active agent

First, we shall consider a limiting case of a droplet with clean interfaces. Figure 4.2 displays the evolution of the length of the three axes of a droplet under a start up of simple shear flow. The calculation are based on $p = 1.4$, $Cs = 0.24$ and $\rho = 0$ which corresponding to the clean interfaces. By comparing with the results of Yu and Bousmina model [20] we found the predictions of the present model recover their results.

The influence of the property number

In this section, the influence of the diffusivity of the surface active agent on the deformation of the droplet is presented. The applied flow field is the start up elongational flow. The diffusivity is described by the Peclet number P_e or property number γ. The larger γ the smaller the diffusivity D_s. The diffusivity has a direct effect on the distribution of the surface active agent on the interface, as showed in Figure 4.3 and 4.4. The results are based on the same value of $p = 1$, $\beta = 0.3$ and $Cs = 0.08$ with different values of γ. With the start up flow, the surface active agent moves to the end of the droplet corresponding to the position of $\phi = 0$. For the surface active agents with smaller γ, a large overshoot is presented before it reaches a steady state with a smaller gradient. When γ is increased, the overshoot becomes smaller, and the smaller diffusivity leads to a lager gradient of the concentration at steady states. The steady state values of the concentration profiles for three different γ are shown in figure 4.5. It is shown that the gradient of the concentration increases as the diffusivity decreases.

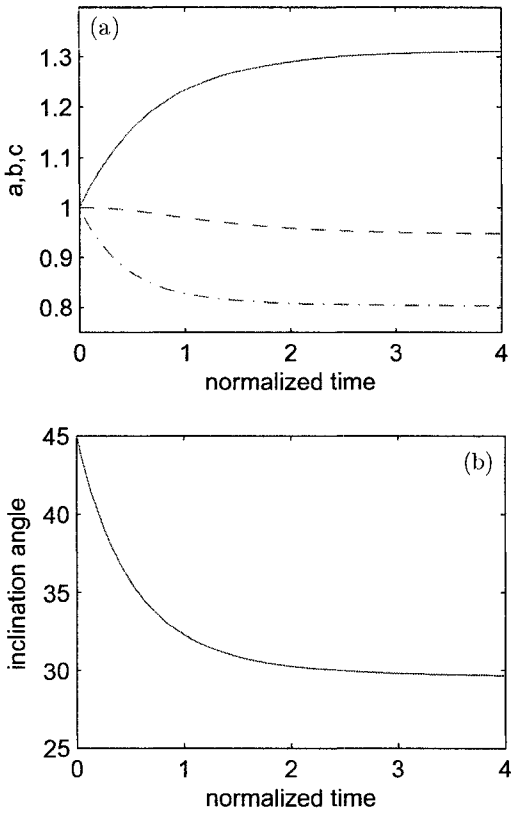

Figure 4.2: Transient morphology of a clean droplet in a simple shear flow.(a) the length of three axes. (—) a, (- -) b, (-.-) c. (b) the inclination angle.

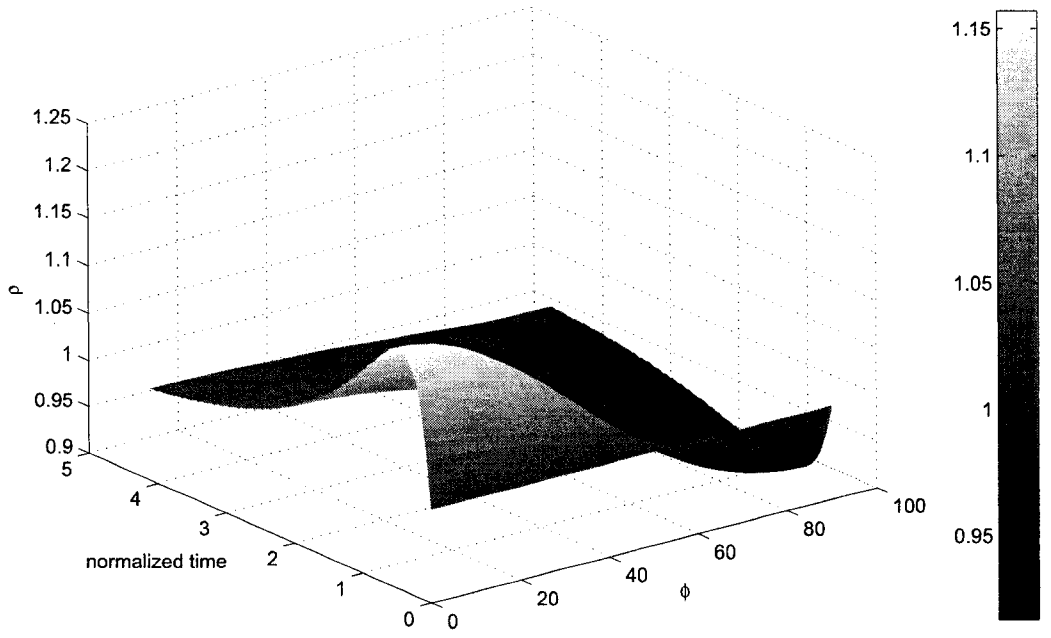

Figure 4.3: The influence of γ on the distribution of the surface active agents on the droplet at the transient state with $\gamma = 100$.

Figure 4.6 indicates the effects of the diffusivity of the surfactants on the droplet deformation number, which is defined as

$$D_f = \frac{L - B}{L + B} \tag{4.37}$$

where the actual length L and the thickness B of the droplet. The graph shows that larger γ leads to larger deformation, which is in agreement with the results of the numerical simulation of Stone and Leal [4].

The transient tangential interfacial velocity is shown in Figure 4.7 with the parameters $Cs = 0.8$, $\beta = 0.3$ and $\gamma = 1000$. We see that the interfacial velocity immediately reach its highest value as the flow started with a maximum near the position of $\phi = 45^o$, then the velocity decrease as time goes. Finally it becomes zero over the whole range of ϕ which means that the interface is totally immobilized at the steady states. This phenomenon was observed in the numerical

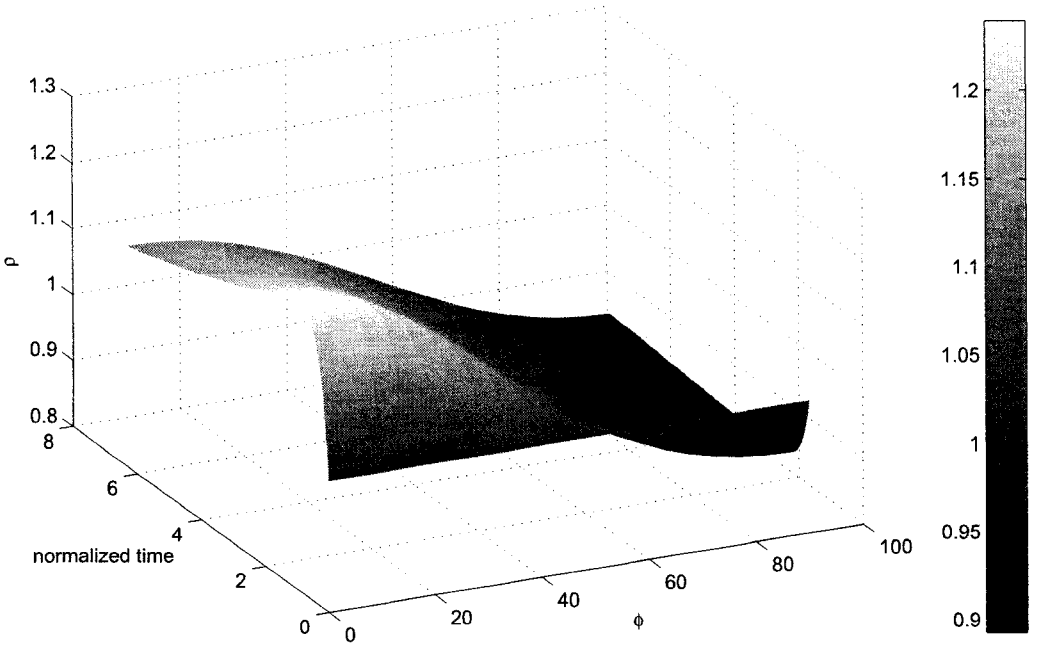

Figure 4.4: The influence of γ on the distribution of the surface active agents the droplet at the transient state with $\gamma = 1000$.

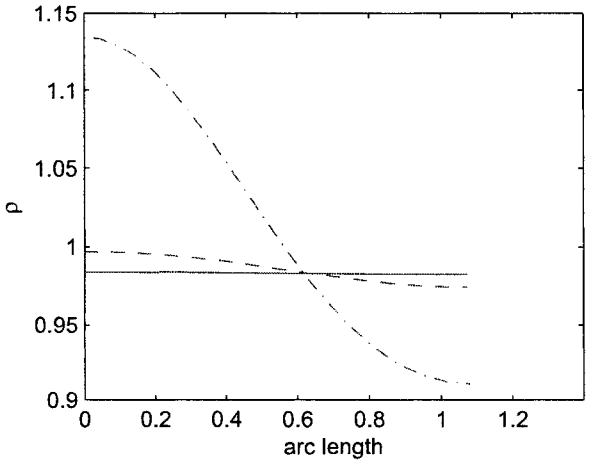

Figure 4.5: The steady state distribution of the surfactants over the arc length. (—) $\gamma = 10$, (- -) $\gamma = 100$ and (-.-) $\gamma = 1000$

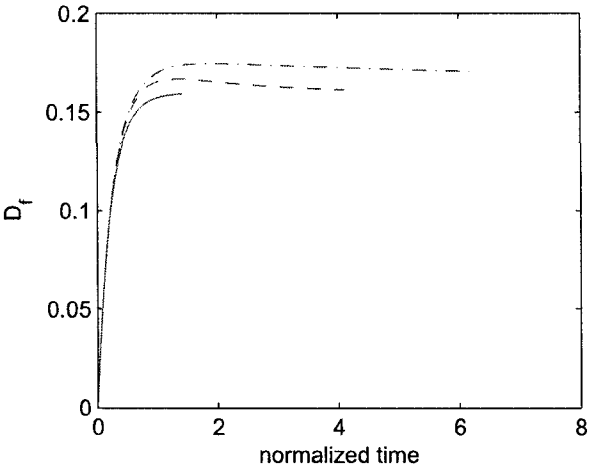

Figure 4.6: The deformation parameters for different values of γ. (—) $\gamma = 10$, (- -) $\gamma = 100$ and (-.-) $\gamma = 1000$

simulations of droplet covered by insoluble surfactant of Egglecton and Stebe [9] and Egglecton *et al.* [10]. Figure 4.8 displays the normal velocity profile. As flow starts, droplet is stretched until it reaches a steady state.

The influence of the capillary number

Figure 4.9 and Figure 4.10 indicate the effects of the capillary number Cs on the distribution of surfactant and the droplet deformation. It is shown that as Cs increase, both the gradient of the concentration and the deformation of droplet increase. This is in a qualitative agreement with the results of the numerical simulation reported in the literatures, for example reference [4]. The time for the droplet shape and concentration profile to reach steady states also increased with increased Cs. We also found that when Cs is small, for example $Cs < 0.5$, the predictions are very close to the results of Stone and Leal [4] with the same values of parameters. However, when Cs increases the deviations also increases. For example, the predicted steady state deformation parameters D_f of the present model is about 15% less than the result of Stone and Leal at $Cs = 0.8$ with $p = 1$, $\beta = 0.3$ and $\gamma = 1000$. The reason is that the ellipsoidal droplet assumption is only valid in the condition of weak flow and small droplet deformations.

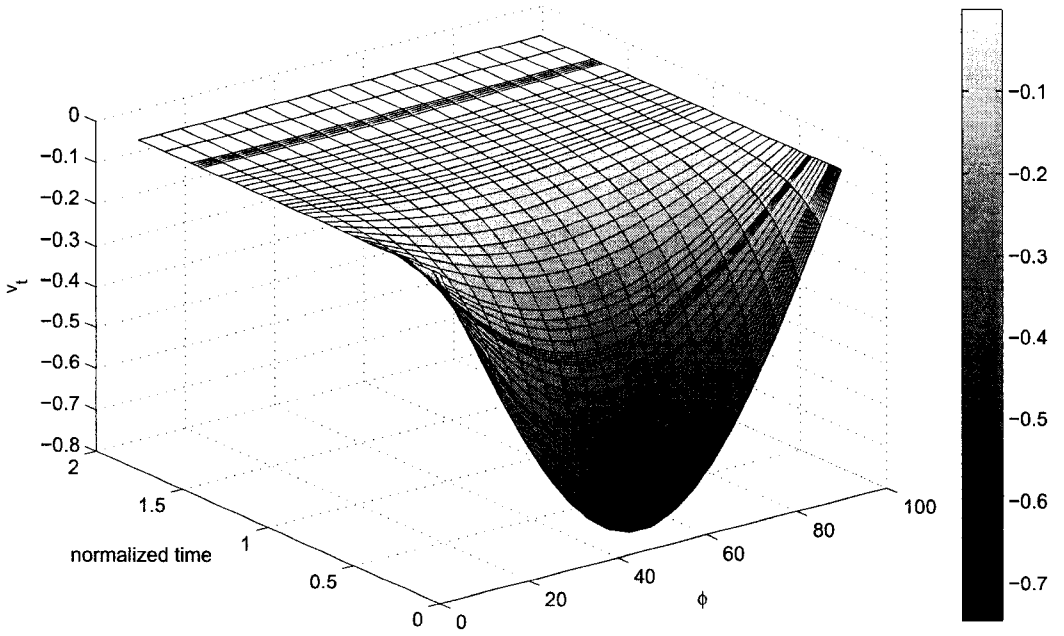

Figure 4.7: The tangential interfacial velocity profile.

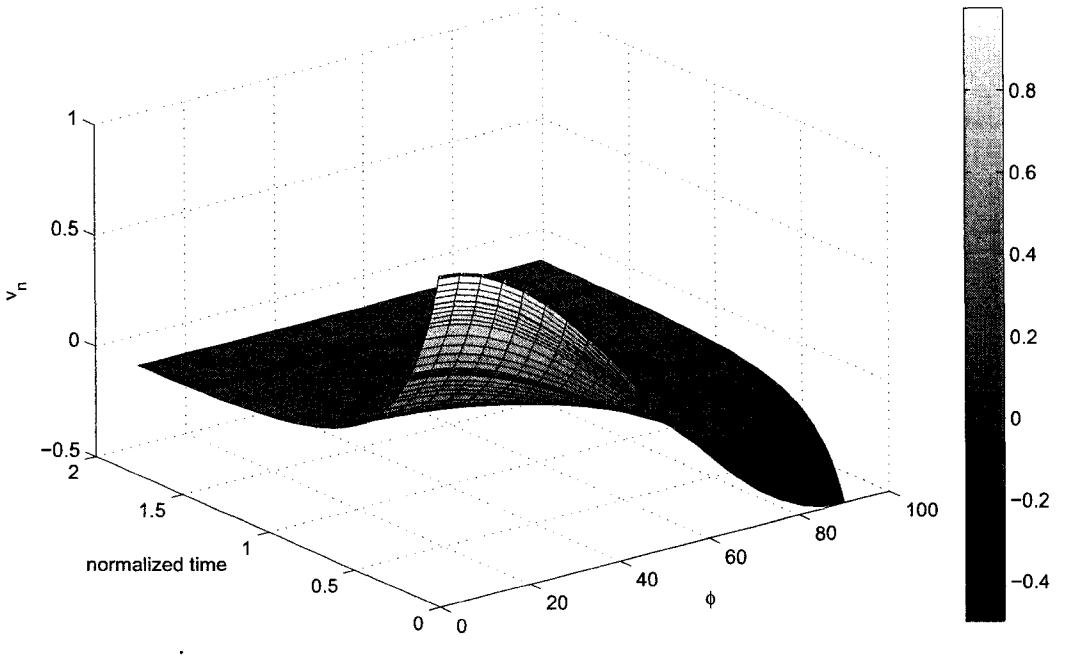

Figure 4.8: The normal interfacial velocity profile.

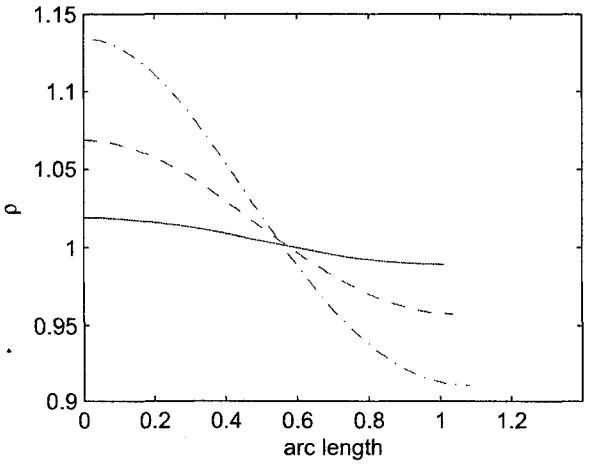

Figure 4.9: The steady state distribution of the surfactants over the arc length. (—) $Cs = 0.02$, (- -) $Cs = 0.05$ and (-.-) $Cs = 0.08$

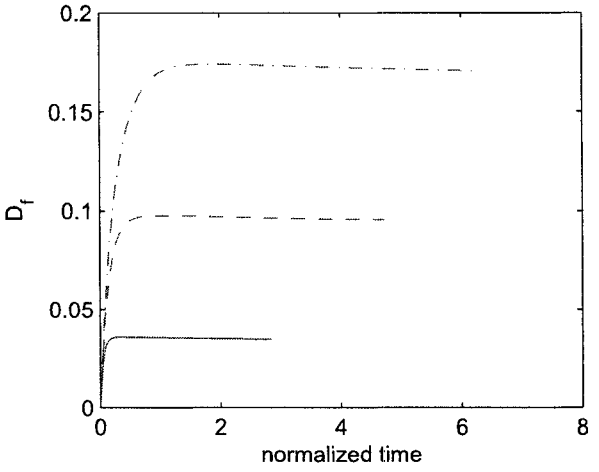

Figure 4.10: The deformation parameters for different values of Cs. (—) $Cs = 0.02$, (- -) $Cs = 0.05$ and (-.-) $Cs = 0.08$

4.4.5 Conclusion

In this paper the Yu and Bousmina model [20] for emulsions with clean interfaces is extended to the emulsions with surface active agents. The model shows good results at small deformations and under weak flows. However, when Cs increase, errors of the the model prediction increases. This is because the present model is based on the assumption that the droplet always takes the ellipsoidal shape. This assumption caused the errors of the model and thus limits its applicability.

Bibliography

[1] R. W. Flumerfelt, Effects of dynamic interfacial properties on drop deformation and orientation in shear and extensional flow fields, J. Colloid Interface Sci. 76 (1980) 330-349 .

[2] R. G. Cox, The deformation of a drop in a general time-dependent fluid flow, J. Fluid Mech. 37 (1969) 601-623.

[3] N. Lamb. Hydrodynamics, 6th ed.,Dover, New York, (1945).

[4] H. A. Stone, L. G. Leal, The effects of surfactants on drop deformation and breakup, J. Fluid Mech. 220 (1990) 161-186.

[5] W. J. Milliken, H. A. Stone, L. G. Leal, The effect of surfactant on transient motion of newtonian drops, Phys. Fluids A 5 (1993) 69-79.

[6] W. J. Milliken, L.G. Leal, The influence of surfactant on the deformation and breakup of a viscous drop: the effect of surfactant solubility. Journal of Colloid and Interface Science 166 (1994) 275-285 .

[7] Y. Pawar, K.J. Stebe, Marangoni effects on drop deformation in an extensional flow: the role of surfactant physical chemistry. I. Insoluble surfactants. Physics of Fluids A 8 (1996) 1738-1751.

[8] X. Li and C. Pozrikidis, The effect of surfactants on drop deformation and on the rheology of dilute emulsions in Stokes flow. J. Fluid Mech. 341 (1997) 165-149.

[9] C. D. Eggleton, K.J. Stebe, An adsorption-desorption-controlled surfactant on a deforming droplet. Journal of Colloid and Interface Science 208 (1998) 68-80.

[10] C. D. Eggleton, Y.P. Pawar, K.J. Stebe, Insoluble surfactants on a drop in an extensional flow: a generalization of the stagnated surface limit to deforming interfaces. Journal of Fluid Mechanics 385 (1999) 79-99.

[11] C. D. Eggleton, T.-M. Tsai, K.J. Stebe, Tip streaming from a drop in the presence of surfactants. Physical Review Letters 87 (2001) 048302 .

[12] I. B. Bazhlekov , P. D. Anderson, H. E.H. Meijer, Numerical investigation of the effect of insoluble surfactants on drop deformation and breakup in simple shear flow, Journal of Colloid and Interface Science 298 (2006) 369-394 .

[13] K. Feigl, D. Megias-Alguacilb, P. Fischerb, E. J.Windhabb, Simulation and experiments of droplet deformation and orientation in simple shear flowwith surfactants, Chemical Engineering Science. 62 (2007) 3242-3258.

[14] M. A. Drumright-Clark, Y. Renardy, The effect of insoluble surfactant at dilute concentration on drop breakup under shear with inertia. Physics of Fluids 16 (2004) 14-21.

[15] Y. Renardy, M. Renardy, V. Cristini, A new volume-of-fluid formulation for surfactants and simulations of drop deformation under shear at a low viscosity ratio. European Journal of Mechanics B/Fluids 21 (2002) 49-59.

[16] R. Aris, Vectors, Tensors, and the basic equations of fluid mechanics. Prentice-Hall. (1962).

[17] Y. W. Kruijt-Stegeman, F. N. van de Vosse, H. E. H. Meijer, Droplet behavior in the presence of insoluble surfactants. Physics of Fluids 16 (2004) 2785-2796.

[18] J. Li, Y. Renardy, M. Renardy, Numerical simulation of breakup of a viscous drop in simple shear flow through a volume-of-fluid method, Physics of Fluids 12 (2000) 269-282.

[19] P. M. Vlahovska, M. Loewenberg, J. Blawzdziewicz, Deformation of a surfactant-covered drop in a linear flow, Phys. Fluids 17 (2005) 103103.

[20] W. Yu, M. Bousmina, Ellipsoidal model for droplet deformation in Newtonian systems. J Rheol 47 (2003) 1011-1039.

[21] S. Guidoa, M. Villone, Three-dimensional shape of a drop under simple shear flow. J Rheol 42 (1998) 395-415.

[22] E. D. Wetzel, C. L. Tucker, Droplet deformation in dispersions with unequal viscosities and zero interfacial tension, J. Fluid Mech. 426 (2001) 199-228.

[23] A. W. Adamson, Physical Chemistry of Surfaces, 3rd edn. John Wiley & Sons (1967).

[24] N. E. Jackson, C. L. Tucker, A model for large deformation of an ellipsoid droplet with interfacial tension, J. Rheol. 47 (2003) 659-682.

[25] P.L.Maffettone, M.Minale, Equation of change for ellipsoidal drops in viscous flow, J. Non-Newtonian Fluid Mech., 78 (1998) 227-241.

[26] J. D. Eshelby, The determination of elastic field of an ellipsoidal inclusion, and related problems, Proc. R. Soc. London, Ser. A 241 (1957) 376-397 .

[27] R. A. De Bruijn, Tipstreaming of drops in simple shear flows, Chem. Eng. Sci. 48 (1993) 277-284 .

[28] Y. T. Hu, D. J. Pine, L. G. Leal, Drop deformation, breakup, and coalescence with compatibilizer, Phys. Fluids, 12 (2000) 484-489.

[29] P. V. Puyvelde, S. Velanker, J. Mewis, P. Moldenaers, Effect of Marangoni Stress on the Deformation and Coalescence in compatibiliaed immiscible polymer blends, Polymer Engineering and Sciece. 42 (2002) 1956-1964.

[30] Y. T. Hu, A. Lips, Estimating Surfactant Surface Coverage and Decomposing its Effect on Drop Deformation, Physical Review letters, 91 (2003) 044501-1-4.

[31] C. Pozrikidis, Boundary Integral and Singularity Methods for Linearized Viscous Flow. Cambridge: Cambridge University Press (1992).

[32] C. Pozrikidis, Numerical Computation in Science and Engineering. New York: Oxford Univ. Press (1998) .

[33] W. E. Schiesser, The numerical methods of lines. Academic press, Inc. (1991)

Chapter 5

A Mesoscopic Rheological Model of Immiscible Blends with the Interface Covered with a Surface Active Agent

Jian Feng Gu[1], Miroslav Grmela[1,4] , Mosto Bousmina[2,3]

[1] Ecole Polytechnique de Montreal, C.P.6079 suc. Centre-ville, Montreal, H3C 3A7, Quebec, Canada

[2] Department of Chemical Engineering, Laval University, Ste-Foy, G1K 7P4, Quebec, Canada

[3] Hassan II Academy of Sciences and Technology, Rabat, Marocco

Physics of Fluids 20 (2008) 043102

[4]corresponding author: e-mail: miroslav.grmela@polymtl.ca

abstract

The Maffettone-Minale mesoscopic rheological model of immiscible blends is extended to blends that include a surface active agent. Its nonuniform distribution on the interface (assumed to be the surface of droplets) and associated with it nonuniform distribution of the surface tension and the Marangoni stress are incorporated into the model. Instead of using one ellipsoid (one conformation tensor in the mathematical formulation) to characterize the shape of the droplet, we use one parameter family of ellipsoids (a "necklace" of ellipsoids) to play this role. Both rheology and morphology (including large deviations form the ellipsoidal shape of droplets) are calculated and compared with predictions of microscopic models (i.e. models based on microhydrodynamics) and with results of experimental observations.

5.1 Introduction

The fluid under consideration in this paper is an isothermal and incompressible mixture of three fluids: fluid A, fluid B, and the third fluid C that is a surface active agent (surfactant or a copolymer). We assume that the fluids A and B are, if take individually, simple fluids. We use the well established terminology according to which a fluid is termed simple if its flow behavior is found to be well described by classical hydrodynamics (defined as hydrodynamics involving only classical hydrodynamic fields - i.e. mass, momentum, and energy densities - and only local in time constitutive relations). A fluid that is not simple is called complex. For example, fluids that show viscoelastic behavior are all complex since classical hydrodynamics fails to predict such behavior. The fluids A and B are moreover immiscible. This means that the mixture involves an interface (denoted $interface_{A,B}$) between the two fluids. Even though both A and B are simple their mixture is complex because of the presence of the interface. Deformations of the interface take place on the scale that is comparable with the scale of changes of hydrodynamic fields and consequently the time evolution equations of classical hydrodynamics has to be coupled with the time evolution equation of $interface_{A,B}$. The fluid C is soluble in both fluids A and B and resides on $interface_{A,B}$ as well as in the fluids A and B. Since the surface active

agent C influences properties of $interface_{A,B}$ (in particular its surface tension), its presence makes the interface deformations more pronounced and consequently the mixture more complex.

The microhydrodynamic formulation of the time evolution of the mixture described above is straightforward and well known[1-7]. It consists of the time evolution equations for momenta of the fluids A and B in the bulk, boundary conditions on $interface_{A,B}$ that include a transport equation for the fluid C, and the chemical kinetics like rate equations describing the adsorption/desorption process of the fluid C residing on $interface_{A,B}$ and in the bulk of the fluid A and the fluid B. The advantage of this formulation is its very clear physical basis (classical hydrodynamics) and associated with it a very clear physical interpretation and an independent experimental access to the parameters representing the mixture in the mathematical formulation. All the parameters can be, at least in principle, measured by independent microhydrodynamic experiments. The disadvantage is an enormous complexity of solving the governing equations and arriving in this way to predictions that can be compared with results of macroscopic flow measurements. The complexity then also prevents a more direct understanding of the new macroscopic physics emerging in investigations of the flow behavior of the mixture.

In this paper we explore a mesoscopic formulation in which the physics is expressed on a level that is as close as possible to the level on which the macroscopic observations of our interest are made. Our objective is to develop a relatively simple formulation that provides a more direct passage between microscopic (details of the shape of $interface_{A,B}$) and macroscopic (rheological) properties of the mixture. While the microhydrodynamic analysis[(1-7)] pays most attention to morphology, our focus is put on the rheology. In order to be able to place our approach among other mesoscopic approaches, we recall briefly some of them.

Doi and Ohta[8] consider $interface_{A,B}$ as an internal structure spread throughout the fluid and characterized by one scalar (the surface area per unit volume) and one traceless symmetric tensor (expressing the orientation of $interface_{A,B}$). Maffettone and Minale[9] limit their consideration to the interface composed of ellipsoidal droplets. The droplets are described by a second order symmetric and positive definite tensor $\boldsymbol{c}$, called a conformation tensor, that serves as the morphological state variable. The ellipsoid representing the droplet is the graph of

the equation $< \boldsymbol{r}, \boldsymbol{cr} >= 1$, where $<,>$ is the scalar product and $\boldsymbol{r} \in \mathbf{R}^3$ is the position coordinate. Both approaches have been combined in Ref.10. A combination of the microhydrodynamic and the Maffettone-Minale like approaches have been explored in Refs. 11 and 12. The slender-body theory has been used in Ref. 13.

In the presence of a surface active agent C, the following physical features become particularly important: (i) transport of the fluid C on $interface_{A,B}$ leading to its nonuniform distribution, (ii) emergence of a new type of force on $interface_{A,B}$, called the Marangoni force, (iii) a complex (active) advection of droplets by the imposed flow, and (iv) large deviations from the ellipsoidal shape of droplets. The features (ii), (iii) and (iv) are direct consequences of the nonuniform distribution of the fluid C on $interface_{A,B}$. Neither the Maffettone-Minale approach nor its combinations with microhydrodynamics or the Doi-Ohta approach provide a setting suitable for discussing all four features mentioned above. Our objective in this paper is to extend the Maffettone-Minale approach so that the features (i)-(iv) can be investigated. There are still however important features, like for example droplet breakup[7,14,15] (including tip-streaming[13]) and coalescence[15] that remain outside of the scope of the setting developed in this paper.

Our strategy is the following. We represent a non ellipsoidal droplet of volume $V_{droplet}$ by a family of ellipsoidal droplets, all having the volume $V_{droplet}$. The family, parametrized by $-1 \leq s \leq 1$, is referred to as a "necklace". The parameter s is a coordinate on the string (backbone) of the necklace. To each $s \in [-1, 1]$ there is attached an ellipsoid of volume $V_{droplet}$ (represented mathematically by the graph of $< \boldsymbol{r}, \boldsymbol{c}(s)\boldsymbol{r} >= 1$, where $\boldsymbol{c}(s)$ is a symmetric positive definite tensor). As we shall explain in the next paragraph, the position on the necklace represents also position on the surface of the non ellipsoidal droplet. In the particular case when the droplet has an ellipsoidal shapes, all the ellipsoids on the necklace representing it are identical. They have all the shape of the droplet. Beside the conformation tensor $\boldsymbol{c}(s)$, we attach to each s also two scalars $\rho(s)$ and $\nu(s)$. The former has the physical meaning of the mass density of the surface active agent and the latter its momentum, both at the position s on the surface of the droplet.

How do we pass from the shape of an observed droplet $\mathcal{S}$ to its necklace representation $\mathcal{S}(s); -1 \leq s \leq 1$ and inversely, from the necklace representation to

the droplet? Details of this procedure will be presented in Section 5.2.5. Here we only sketch the idea in general terms. First, we introduce sections of an ellipsoid. We begin by providing the principal axis of the ellipsoid with a coordinate s' in such a way that the whole axis is mapped on the interval $-1 \leq s' \leq 1$. By $\delta\mathcal{S}(s')$ we denote an infinitesimal slice of the ellipsoid with thickness ds' cut perpendicularly to the principal axis at the place with the coordinate s'. We shall call it s'-th section of the ellipsoid. The whole ellipsoid is thus a union of all sections $\bigcup_{s'=-1}^{s'=1} \delta\mathcal{S}(s')$. We turn now to the necklace. By $\mathcal{S}(s)$ we denote the ellipsoid on the necklace attached at the point s. Its sections are denoted $\delta\mathcal{S}(s, s')$ and thus

$$\mathcal{S}(s) = \bigcup_{s'=-1}^{s'=1} \delta\mathcal{S}(s, s') \tag{5.1}$$

Now we are prepared to construct the shape $\mathcal{S}$ of the droplet that has the necklace representation $\mathcal{S}(s)$, $s \in [-1, 1]$. We define it as

$$\mathcal{S} = \bigcup_{s'=-1}^{s'=1} \delta\mathcal{S}(s', s') \tag{5.2}$$

In more practical terms, we formulate (5.2) as follows: We pass from the necklace representation $\mathcal{S}(s); -1 \leq s \leq 1$ to the droplet $\mathcal{S}$ by making a sequence of operations. First, we cut all the ellipsoids on the necklace into, say, ten pieces. The cutting is done perpendicularly to the principal axis with the thickness that equals one tenth of the length of the axis. From all pieces created in this way (if, for the sake simplicity, we see the necklace as consisting of, say, ten ellipsoids then we have 10×10 pieces) we assemble the droplet $\mathcal{S}$ as follows: We begin with the first piece taken from the first ellipsoid. To it we attach the second piece of the second ellipsoid. Next, we attach the third piece of the third ellipsoid. We continue in this way until we attach the tenth piece of the tenth ellipsoid. The resulting droplet, in general of non-ellipsoidal shape, is finally rescaled, uniformly in all directions, so that it has volume $V_{droplet}$.

Summing up, the necklace of ellipsoidal droplets represents a single non ellipsoidal droplet, the position on the necklace (i.e. the value of the parameter s) corresponds to the position on its surface. We can also provide the necklace morphology with an alternative "model" interpretation. Instead of considering

the suspension of droplets that are all identical (all with the same amount of the active agent that is non-uniformly distributed on them, and with the same non ellipsoidal shape) we regard the ellipsoids on the necklace as "real" suspended droplets. We thus consider a suspension of droplets that all have an ellipsoidal shape (but every droplet has, in general, a different ellipsoidal shape), and all have different amount, but uniformly distributed, of the surface active agent put on them. The sweeping of the surface active agent is seen in this interpretation as a transport among the droplets.

Finally, we comment about the advection. In the absence of the surface tension and the surface active agent, the advection of a droplet is mathematically expressed in the formula derived (by analytically solving the corresponding Stokes problem) by Eshelby[16]. A simplified version of the Eshelby advection is the non-affine advection used in the Maffettone-Minale formulation. In this paper we shall follow Gu and Grmela[17] and use an active advection in which gradient of the velocity disturbed by the presence of droplets assumes the role of an independent state variable that joins $\boldsymbol{c}(s)$, $\rho(s)$ and $\nu(s)$ to describe the morphology.

5.2 Mesoscopic Model

Our goal is to express the physical picture sketched in Introduction in governing equations of the model. We shall construct the model by following the framework (GENERIC) that helps to organize the modeling and guarantees by itself agreement of predictions of the model with observed compatibility with thermodynamics. We shall proceed in four steps. First, (Section 5.2.1), we select the state variables, second (Section 5.2.2), we find their kinematics that determines the framework for the time evolution equations. The framework is then filled with dissipation forces in the third step (Section 5.2.3), and with the free energy in the fourth step (Section 5.2.4).

5.2.1 State variables

The complete set of state variables is denoted by the symbol x. The physical picture described in Introduction leads us to the following choice:

$$x = (\boldsymbol{u}(\boldsymbol{r}), \boldsymbol{c}(s), \boldsymbol{w}(s), \rho(s), \nu(s), \rho_A(s), \rho_B(s));$$
$$det(\boldsymbol{c}(s)) = constant;\ -1 \leq s \leq 1 \tag{5.3}$$

By $\boldsymbol{u}$ we denote the overall momentum, s is the coordinate on the necklace (i.e. a parameter labeling position on the droplet interface), $\boldsymbol{w}$ is the conjugate to the gradient of the velocity perturbed by the presence of the droplet (see (5.15)), the graph of the equation $< \boldsymbol{r}, \boldsymbol{c}(s)\boldsymbol{r} >= 1$ is the ellipsoid representing the droplet at the point s on the necklace ($\boldsymbol{r}$ is the position vector and $<,>$ the scalar product), the condition $det(\boldsymbol{c}(s)) = constant$ means that all the ellipsoids have the same volume that remains a constant, $\rho(s)$ is the surface mass density of the fluid C on $interface_{A,B}$ at the point s, $\nu(s)$ its momentum at the point s on $interface_{A,B}$, and $\rho_A(s)$ (resp. $\rho_B(s)$) is the mass density per unit volume of the fluid C in the bulk of the fluid A (resp. fluid B) adjacent to $interface_{A,B}$ at the point s. In this paper we shall limit ourselves to the overall incompressibility and spatial homogeneity in the bulk (i.e. the fields (5.3) are assumed to be independent of $\boldsymbol{r}$ except for $\boldsymbol{u}$ that is a linear function of $\boldsymbol{r}$).

5.2.2 Kinematics

The next step is to specify kinematics (expressed in a Poisson bracket) of the state variables (5.3). As for $\boldsymbol{u}$, its kinematic is expressed in the well known bracket[18]

$$\{A, B\}^{(1)} = \int d\boldsymbol{r} u_i \left(\partial_j(A_{u_i})B_{u_j} - \partial_j(B_{u_i})A_{u_j}\right) \tag{5.4}$$

where A and B are real valued sufficiently regular functions of $\boldsymbol{u}$, $i, j = 1, 2, 3$, the summation convention is used throughout this paper, A_{u_j} is the functional variational derivative of A with respect to $u_j(\boldsymbol{r})$, and $\partial_j = \frac{\partial}{\partial r_j}$. To simplify the notation, we shall assume hereafter that the total volume of the fluid under consideration equals to one. The motion of a continuum is a sequence of transformation $\mathbf{R}^3 \to \mathbf{R}^3$. The bracket (5.4) is the canonical bracket corresponding to

the dual of the Lie algebra associated with the Lie group of the transformations $\mathbf{R}^3 \to \mathbf{R}^3$.

The Poisson bracket expressing kinematics of $\boldsymbol{c}(s)$ and $\boldsymbol{w}(s)$ is also well known[19,17]:

$$\begin{aligned}
\{A,B\}^{(2)} \;=\; & \int_0^1 ds\,[c_{ki}\left(A_{c_{im}}\partial_k(B_{u_m}) - B_{c_{im}}\partial_k(A_{u_m})\right) \\
& +c_{km}\left(A_{c_{im}}\partial_k(B_{u_i}) - B_{c_{im}}\partial_k(A_{u_i})\right) \\
& +c_{jk}\left(A_{c_{mj}}B_{w_{mk}} - B_{c_{mj}}A_{w_{mk}}\right) \\
& +c_{mk}\left(A_{c_{mj}}B_{w_{jk}} - B_{c_{mj}}A_{w_{jk}}\right) \\
& -\frac{2}{3}c_{kl}\left(A_{c_{kl}}\partial_j B_{u_j} - B_{c_{kl}}\partial_j A_{u_j}\right) \\
& -\frac{2}{3}c_{kl}\left(A_{c_{kl}}B_{w_{jj}} - B_{c_{kl}}A_{w_{jj}}\right) \\
& +w_{ik}\left(A_{w_{im}}\partial_k(B_{u_m}) - B_{w_{im}}\partial_k(A_{u_m})\right) \\
& -w_{kj}\left(A_{w_{mj}}\partial_m(B_{u_k}) - B_{w_{mj}}\partial_m(A_{u_k})\right) \\
& +w_{ij}\left(A_{w_{im}}B_{w_{mj}} - B_{w_{im}}A_{w_{mj}}\right)] \qquad (5.5)
\end{aligned}$$

We assume that shapes of the droplets are symmetrical and thus the interval $s \in [0,1]$ suffices to describe them. The terms involving the multiplicative factor $2/3$ arise due to the constraint $det\,\boldsymbol{c}(s) = constant$ (see Ref.19). The terms involving $\boldsymbol{w}$, representing the active advection, have been introduced in Ref.17. Finally, the kinematics of $\rho(s), \nu(s), \rho_A(s), \rho_B(s)$ is the kinematics of continuum expressed by the Poisson bracket:

$$\begin{aligned}
\{A,B\}^{(3)} \;=\; & \int_0^1 ds\left[\rho\left(\frac{\partial}{\partial s}(A_\rho)B_\nu - \frac{\partial}{\partial s}(B_\rho)A_\nu\right)\right. \\
& \left.+\nu\left(\frac{\partial}{\partial s}(A_\nu)B_\nu - \frac{\partial}{\partial s}(B_\nu)A_\nu\right)\right] \qquad (5.6)
\end{aligned}$$

and the passive advection of the four scalar fields by the overall momentum $\boldsymbol{u}$.

If $\{A,B\}$ is the Poisson bracket expressing the kinematics of (5.3) and Φ the free energy (that will be specified in Section 5.2.4) then the equations governing

the nondissipative time evolution of (5.3) are[20]

$$\frac{\partial}{\partial t}\begin{pmatrix} \boldsymbol{u} \\ \boldsymbol{c} \\ \boldsymbol{w} \\ \rho \\ \nu \\ \rho_A \\ \rho_B \end{pmatrix} = L \begin{pmatrix} \Phi_{\boldsymbol{u}} \\ \Phi_{\boldsymbol{c}} \\ \Phi_{\boldsymbol{w}} \\ \Phi_{\rho} \\ \Phi_{\nu} \\ \Phi_{\rho_A} \\ \Phi_{\rho_B} \end{pmatrix} \tag{5.7}$$

where the operator L, called a Poisson bivector, is defined as follows:

$$\{A, B\} = \int d\boldsymbol{r} \int_0^1 ds \begin{pmatrix} A_{\boldsymbol{u}} & A_{\boldsymbol{c}} & A_{\boldsymbol{w}} & A_{\rho} & A_{\nu} & A_{\rho_A} & A_{\rho_B} \end{pmatrix} L \begin{pmatrix} B_{\boldsymbol{u}} \\ B_{\boldsymbol{c}} \\ B_{\boldsymbol{w}} \\ B_{\rho} \\ B_{\nu} \\ B_{\rho_A} \\ B_{\rho_B} \end{pmatrix} \tag{5.8}$$

where $\{A, B\}$ is the Poisson bracket expressing kinematics of (5.3) and Φ is the free energy that will be specified later.

5.2.3 Dissipation

Next, we turn to the dissipative part of the time evolution. Its role is to bring the mixture to equilibrium states, i.e. to the states at which the free energy Φ reaches its minimum. If the time evolution of $(\boldsymbol{u}(\boldsymbol{r}), \boldsymbol{c}(s), \boldsymbol{w}(s), \rho(s), \nu(s), \rho_A(s), \rho_B(s))$ is governed by (5.7) then clearly $\frac{d\Phi}{dt} = 0$. This is because $\frac{d\Phi}{dt} = \{\Phi, \Phi\} = 0$. The first equality follows from (5.7) and (5.8), and the second equality from the antisymmetry of the bracket (5.8). In order to drive the mixture to equilibrium

states, the dissipative part has to therefore imply $\frac{d\Phi}{dt} < 0$. If we choose

$$\frac{\partial}{\partial t}\begin{pmatrix} \boldsymbol{u} \\ \boldsymbol{c} \\ \boldsymbol{w} \\ \rho \\ \nu \\ \rho_A \\ \rho_B \end{pmatrix} = -\begin{pmatrix} \delta\Xi/\delta\Phi_{\boldsymbol{u}} \\ \delta\Xi/\delta\Phi_{\boldsymbol{c}} \\ \delta\Xi/\delta\Phi_{\boldsymbol{w}} \\ \delta\Xi/\delta\Phi_{\rho} \\ \delta\Xi/\delta\Phi_{\nu} \\ \delta\Xi/\delta\Phi_{\rho_A} \\ \delta\Xi/\delta\Phi_{\rho_B} \end{pmatrix} \tag{5.9}$$

where δ/δ denotes the variational functional derivative then

$$\frac{d\Phi}{dt} = -\int d\boldsymbol{r}\int_0^1 ds \begin{pmatrix} \Phi_{\boldsymbol{u}} & \Phi_{\boldsymbol{c}} & \Phi_{\boldsymbol{w}} & \Phi_{\rho} & \Phi_{\nu} & \Phi_{\rho_A} & \Phi_{\rho_B} \end{pmatrix} \begin{pmatrix} \delta\Xi/\delta\Phi_{\boldsymbol{u}} \\ \delta\Xi/\delta\Phi_{\boldsymbol{c}} \\ \delta\Xi/\delta\Phi_{\boldsymbol{w}} \\ \delta\Xi/\delta\Phi_{\rho} \\ \delta\Xi/\delta\Phi_{\nu} \\ \delta\Xi/\delta\Phi_{\rho_A} \\ \delta\Xi/\delta\Phi_{\rho_B} \end{pmatrix} \tag{5.10}$$

The problem is now to find Ξ, a real valued function of $(\Phi_{\boldsymbol{u}}, \Phi_{\boldsymbol{c}}, \Phi_{\boldsymbol{w}}, \Phi_{\rho}, \Phi_{\nu}, \Phi_{\rho_A}, \Phi_{\rho_B})$ called a dissipation potential, so that the right hand side of (5.10) is positive.

It can be easily verified that if the dissipation potential Ξ satisfies the following three properties

$$\begin{aligned} &\Xi(0,0,0,0,0,0,0) = 0 \\ &\Xi \textit{ reaches its minimum at } (0,0,0,0,0,0,0) \\ &\Xi \textit{ is convex in a neighborhood of } (0,0,0,0,0,0,0) \end{aligned} \tag{5.11}$$

then indeed the right hand side of (5.10) is negative.

We are thus looking for the dissipation potential satisfying (5.11). To bring physics to its specification, we turn to nonequilibrium thermodynamics. We sug-

gest that the following six thermodynamic forces

$$\begin{aligned} X^{(1)}_{ij} &= \Phi_{c_{ij}} - \frac{1}{3}c^{-1}_{ij}tr(\boldsymbol{c}\Phi_c) \\ X^{(2)}_{ij} &= \frac{1}{2}(\partial_i(\Phi_{u_j}) + \partial_j(\Phi_{u_i})) \\ X^{(3)}_{ij} &= \Phi_{w_{ij}} \\ X^{(4)} &= \Phi_\nu \\ X^{(5)} &= -\Phi_{n_A} + \Phi_n \\ X^{(6)} &= -\Phi_{n_B} + \Phi_n \end{aligned} \tag{5.12}$$

drive the mixture to thermodynamic equilibrium. The first one drives the shape of the droplet to the equilibrium shape, i.e. to the shape of sphere (the conformation tensor describing the sphere is proportional to $\boldsymbol{\delta} = \begin{pmatrix} 1 & 0 & 0 \\ 0 & 1 & 0 \\ 0 & 0 & 1 \end{pmatrix}$). The term $-\frac{1}{3}c^{-1}_{ij}tr(\boldsymbol{c}\Phi_c)$ is added in order to keep $det\boldsymbol{c}$ constant (see more in Ref.19). The second force is the familiar Navier-Stokes viscous force, the third and fourth forces are the friction forces driving both $\boldsymbol{w}$ and ν to zero, the force $X^{(4)}$ drives moreover the diffusion on the interface, and the force $X^{(5)}$ resp. $X^{(6)}$ is the chemical affinity corresponding to the adsorption/desorption process (seen as a chemical reaction) between $interface_{A,B}$ and the fluid A resp. B. By n, n_A and n_B we denote the number of moles of the fluid C. They are related to ρ, ρ_A and ρ_B by: $\rho = Mol_C n$; $\rho_A = Mol_C n_A$; $\rho_B = Mol_C n_B$, where Mol_C is the molecular mass of the fluid C.

From the six forces (5.12) we construct the following dissipation potential:

$$\begin{aligned} \Xi = \int_0^1 ds \Bigg[& X^{(1)}_{ij}\frac{1}{2}\Lambda^{(1)}c_{jk}X^{(1)}_{ik} \\ & + \begin{pmatrix} X^{(2)}_{ij}, & X^{(3)}_{ij}, & X^{(4)}\delta_{ij} \end{pmatrix} \frac{1}{2}\mathcal{K}_{jk} \begin{pmatrix} X^{(2)}_{ik} \\ X^{(3)}_{ik} \\ X^{(4)}\delta_{ik} \end{pmatrix} \\ & + \frac{1}{2}\left(W^{(A)}(X^{(5)})^2 + W^{(B)}(X^{(6)})^2\right) \Bigg] \end{aligned} \tag{5.13}$$

where

$$\mathcal{K} = \begin{pmatrix} \eta_0\delta_{jk} & \Lambda^{(2)}_{12}c_{jk} & \Lambda^{(2)}_{13}\rho\delta_{jk} \\ \Lambda^{(2)}_{12}c_{jk} & \Lambda^{(2)}_{22}c_{jk} & \Lambda^{(2)}_{23}\rho\delta_{jk} \\ \Lambda^{(2)}_{13}\rho\delta_{jk} & \Lambda^{(2)}_{23}\rho\delta_{jk} & \Lambda^{(2)}_{33}\rho\delta_{jk} \end{pmatrix} \tag{5.14}$$

We easily verify that if $\Lambda^{(1)}\boldsymbol{c}$ and $\mathcal{K}$ are positive definite matrices and $W^{(A)}$ and $W^{(B)}$ are positive constants then (5.13) indeed satisfies (5.11) and consequently the time evolution governed by (5.9) implies $\frac{d\Phi}{dt} < 0$. The coefficients entering in (5.13) are dissipative kinetic coefficients. Their physical interpretation will be discussed in Section 5.3. The force $\boldsymbol{X}^{(1)}$ is not coupled with the forces $(\boldsymbol{X}^{(2)}, \boldsymbol{X}^{(3)}, X^{(4)})$ since they behave differently under the inversion of the sign of velocities. The dissipation potential (5.13) is constructed in such a way that it is invariant with respect to the inversion of signs of velocities and consequently the time reversible part of the time evolution is nondissipative (i.e. implying $d\Phi/dt = 0$) and the time irreversible part is dissipative (i.e. implying $d\Phi/dt < 0$). The forces $X^{(5)}$ and $X^{(6)}$ can be coupled to the force $X^{(1)}$. Such coupling would mean that the adsorption/desorption precess and evolution of the shape of the droplet are influencing one of the other. In this paper, we shall consider only a particular simplified situation (see Section 5.3) at which we shall be able to avoid a detailed consideration of the adsorption/desorption process.

In view of the assumed overall incompressibility and spatial homogeneity, the equations governing the time evolution of (5.3) become

$$\begin{aligned}
\frac{\partial u_i}{\partial t} &= -\partial_j\left(u_i\Phi_{u_j}\right) - \partial_i\pi - \partial_j\sigma_{ij} - \Xi_{\Phi_{u_i}} \\
\frac{\partial c_{ij}}{\partial t} &= c_{ki}(\partial_k(\Phi_{u_j}) + \Phi_{w_{jk}}) + c_{kj}(\partial_k(\Phi_{u_i}) + \Phi_{w_{ik}}) - \frac{2}{3}c_{ij}\Phi_{w_{kk}} \\
&\quad -\Xi_{\Phi_{c_{ij}}} \\
\frac{\partial w_{ij}}{\partial t} &= +w_{ik}(\partial_k(\Phi_{u_j}) + \Phi_{w_{jk}}) - w_{kj}(\partial_i(\Phi_{u_k}) + \Phi_{w_{ki}}) \\
&\quad -2c_{kj}\Phi_{c_{ik}} + \frac{2}{3}\delta_{ij}c_{kl}\Phi_{c_{kl}} \\
&\quad -\Xi_{\Phi_{w_{ij}}} \\
\frac{\partial \rho}{\partial t} &= -\frac{\partial}{\partial s}(\rho\Phi_\nu) \\
&\quad -\Xi_{\Phi_\rho}
\end{aligned}$$

$$\begin{aligned}
\frac{\partial \nu}{\partial t} &= -\frac{\partial}{\partial s}(\nu\Phi_\nu) - \nu\frac{\partial}{\partial s}(\Phi_\nu) - \rho\frac{\partial}{\partial s}(\Phi_\rho) \\
&\quad -\Xi_{\Phi_\nu} \\
\frac{\partial \rho_A}{\partial t} &= -\Xi_{\Phi_{\rho_A}} \\
\frac{\partial \rho_B}{\partial t} &= -\Xi_{\Phi_{\rho_B}}
\end{aligned} \tag{5.15}$$

where π is the scalar pressure (determined by the requirement of the incompressibility), and $\boldsymbol{\sigma}$ is the extra stress tensor

$$\sigma_{ij} = -2c_{jk}\Phi_{c_{ki}} + \frac{2}{3}\delta_{ij}c_{kl}\Phi_{c_{kl}} - w_{kj}\Phi_{w_{ki}} + w_{ik}\Phi_{w_{jk}} \tag{5.16}$$

5.2.4 Free energy

The physics of the mixture has been expressed so far in the choice of state variables, in their kinematics, and in the dissipative driving forces. The governing equations to which we have arrived so far ((5.15) and (5.16)) still involve the free energy Φ that remains to be specified. We turn now to its specification.

We recall that it is the equilibrium statistical mechanics that provides us with the setting and the strategy to approach this problem. As we know from thermodynamics

$$\Phi = E - k_B T S \tag{5.17}$$

where E is the energy, k_B is the Boltzmann constant, T is the (constant) temperature, and S is the entropy. The energy consists of two parts:

$$E = E_{kin} + E_{pot} \tag{5.18}$$

E_{kin} is the kinetic energy and E_{pot} the potential energy.

The kinetic energy consists of three terms

$$E_{kin} = \int d\boldsymbol{r} \int_0^1 ds \left(\frac{\boldsymbol{u}^2}{2M} + \frac{\nu^2}{2\rho} + \frac{\alpha}{2} w_{ij} c_{jk}^{-1} w_{ik} \right) \tag{5.19}$$

The first term represents the overall kinetic energy, M is the constant overall mass density. The second term is the kinetic energy of the fluid C residing on the $interface_{A,B}$. The third term represents the contribution to the kinetic energy

that arises due to the disturbance of the overall flow in the vicinity of the droplets, α is a phenomenological parameter proportional to the inverse of the mass density M. Since $\boldsymbol{w}$ has the physical interpretation closely related to the spatial gradient, the third term is a Cahn-Hilliard like term[21] but with gradients of the velocity replacing gradients of the mass density.

The potential energy is a sum of two terms

$$E_{pot} = \int d\boldsymbol{r} \int_0^1 ds \left(\mathcal{A}(\rho(s), \boldsymbol{c}(s)) + \mathcal{M}\left(\rho(s), \boldsymbol{c}(s), \frac{\partial \rho}{\partial s}(s)\right)\right) \tag{5.20}$$

The first term is the contribution of the surface tension

$$\mathcal{A}(s) = \frac{\Gamma}{a^5}\left[x_c \frac{((tr\boldsymbol{c})^2 - tr\boldsymbol{cc})}{2}\right] \tag{5.21}$$

where $\Gamma(\rho, s)$ is the interfacial tension , a is the radius of the undeformed (i.e. spherical) droplet, the term inside the bracket [] is the surface area of the droplet of unit volume. Specification of the functional dependence of the iterfacial tension Γ on ρ is called a surface equation of state[4]. In the calculations presented in Section 5.3 we shall limit ourselves to $\rho \ll \rho_\infty$ and consequently to the linear dependence (ρ_∞ is the maximum concentration of the surface active agent on the interface, a sort of "close-packing" of the surfactant molecules on the interface). The dimensional parameter x_c can either be obtained by calculating the surface of the ellipsoid corresponding to $\boldsymbol{c}(s)$ or, as we do in this paper, consider it as a phenomenological parameter that is determined (see (5.66) below) from the comparison of predictions of the model with predictions of microhydrodynamic formulations. The surface energy similar to (5.21) has been used in Dressler and Edwards[22] and also Ref.17. The second term is the Cahn-Hilliard like term[21] involving (surface) gradient (i.e. gradient with respect to s) of the mass density $\rho(s)$ of the surface active agent

$$\mathcal{M} = \frac{1}{2}\rho_{eq}\frac{-\Gamma_\rho}{a^5}\left(\frac{\partial \rho/\rho_{eq}}{\partial l}\right)^2 \left[x_c \frac{((tr\boldsymbol{c})^2 - tr\boldsymbol{c}\cdot\boldsymbol{c})}{2}\right] \tag{5.22}$$

ρ_{eq} is the equilibrium (uniform, i.e. independent of s) surface mass distribution of the surface active agent, and $\Gamma_\rho(\rho, s)$ is the derivative of Γ with respect to ρ. Note that $\Gamma_\rho(\rho, s)$ is always negative since the more surface active agent is

put on $interface_{A,B}$, the smaller is its interfacial tension. By l we denote the parameter having the interpretation of the length along the surface of the droplet normalized by the radius of the droplet. Since s is the length of the droplet by following its principal axis, there is, of course, a one-to-one relation between l and s (depending on $\boldsymbol{c}(s)$). Since the forces generated by the nonuniform distribution of the interfacial tension are called Marangoni forces, we call (5.22) a Marangoni contribution to the free energy.

The entropy contribution to the free energy is given by

$$S = \lambda \, ln \, det \, \boldsymbol{c} \tag{5.23}$$

where λ is determined by the constraint $det\,\boldsymbol{c} = constant$, i.e. it plays the role of the Lagrange multiplier.

In addition, the free energy involves a contribution depending on ρ, ρ_A, and ρ_B. Since this contribution enters our analysis only in the discussion of the adsorption/desorption process and since we shall in this paper limit ourselves (see Section 5.3) only to a particular situation which allows us to ignore this process, we shall leave here this part of the free energy unspecified.

5.2.5 Droplet shape

At this point, the governing equations are specified (with the exception of the parameters entering them - see Section 5.3.1 -). We also know how to extract from their solutions the rheology (see (5.16)). The extraction of the morphology (i.e. the shape of the droplets) is described in general terms in Introduction. Below, we shall present a detailed algorithm leading from $\boldsymbol{c}(s); s \in [-1, 1])$ to the non ellipsoidal shape of the droplet.

Because of the symmetry of the shape, it is enough to consider only right half of the droplet, i.e. we limit ourselves to the interval $s \in [0, 1]$. We assume that the right half of the droplet has been cut into N_s pieces with $N_s + 1$ parallel planes. The first plane ($i = 1$), corresponding to $s = 0$, is located at the middle of the droplet, the last plane ($i = N_s + 1$), i.e. $s = 1$, is located at the end point of the droplet. The essence of the relation between the necklace and the real shape of the droplet is that the $i - th$ cross section of the real droplet cut by the plane

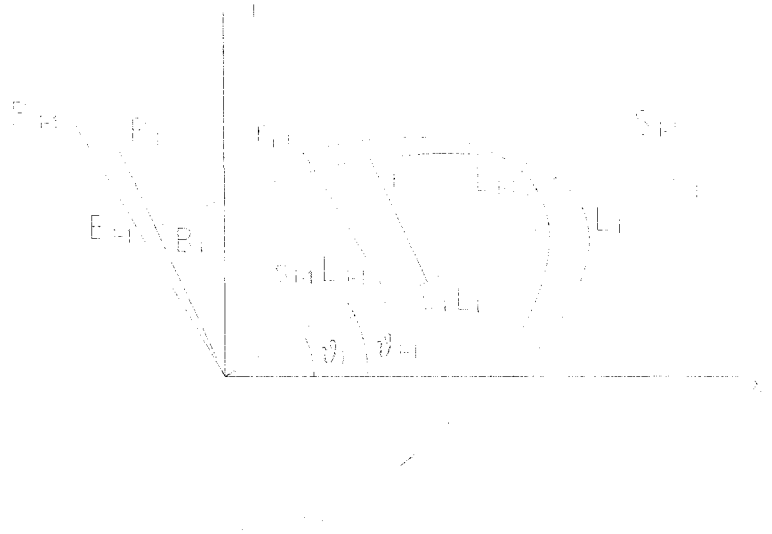

Figure 5.1: Construction of the contour of the droplet shape on equatorial plane from the necklace ellipsoids

at the location s is the same as the $i-th$ cross section of the *i-th* ellipsoid on the necklace cut at the same location. When we attach all the cross sections cut from the necklace ellipsoids, piece by piece, from $s = 0$ to $s = 1$ and let $N_s \to \infty$, the shape of the real droplet emerges.

For simplicity, we shall not plot the 3-dimensional shape. We shall be content with a 2-D contour obtained by projecting the droplet on the equatorial plane that is perpendicular to the vorticity direction of the imposed flow. We use two rectangular coordinate systems: (i) the laboratory coordinate system with coordinates (X, Y), and (ii) another coordinate system with coordinates (S_i, R_i) (see Fig.5.1). Their common origin is placed at the center of the droplet. The X-axis has the direction of the imposed flow while the S_i-axis has the direction of the largest principal axis of the $i-th$ ellipsoid. The orientation of the $i-th$ ellipsoid is described by the inclination angle θ_i between the S_i-axis and the X-axis. Different ellipsoids have different coordinates (S_i, R_i). Let L_i and B_i are the length and the thickness of the $i-th$ ellipsoid. The point $(s_i L_i, r_i)$ on the $i-th$ cross-section of the ellipsoid can be expressed in the (X, Y) frame as follows:

$$x_i = s_i L_i \cos\theta_i - r_i \sin\theta_i$$

$$y_i = s_i L_i \sin\theta_i + r_i \cos\theta_i \tag{5.24}$$

Moreover, since the point $(s_i L_i, r_i)$ are located on the ellipse on the equatorial plane, r_i can be written as

$$r_i = \pm B_i \sqrt{1 - s_i^2} \tag{5.25}$$

The positive and negative sign of r_i in Eq.(5.25) corresponds to the up and down side of the droplet respectively. The volume of the droplet can be approximated by

$$V = \pi \sum_{i=1}^{N_s+1} (r_i q_i + r_{i+1} q_{i+1}) \Delta L_{i+1} \tag{5.26}$$

where

$$q_i = W_i \sqrt{1 - s_i^2} \tag{5.27}$$

and

$$\Delta L_i = s_i L_i - s_{i-1} L_{i-1} \tag{5.28}$$

W_i is the width of the $i-th$ ellipsoid.

With Eq.(5.26), the shape can be rescaled to keep the volume of the droplet conserved. The rescaling coefficient for the three principal axes is $\left(\frac{V_0}{V}\right)^{\frac{1}{3}}$, with V_0 the volume of the initial undeformed droplet.

In addition to the contour of the droplet on its equatorial plane, providing the detailed description, the morphology of deformed droplets can also be described by two quantities providing an overall quantitative description: the deformation parameters D_f and the orientation angle θ.

The deformation parameter D_f (used first by Taylor[23]) is defined as follows:

$$D_f = \frac{L - B}{L + B} \tag{5.29}$$

where the actual length L and the thickness B of the droplet for the present model are given by

$$L = \sum_{i=1}^{N_s+1} \Delta L_i \tag{5.30}$$

$$B = B_1 \tag{5.31}$$

The averaged orientational angle θ, defined by

$$\theta = \int_0^1 \theta(s)ds, \tag{5.32}$$

can be approximately obtained from the formula

$$\theta = \sum_{i=1}^{N_s+1} \theta_i(s_i - s_{i-1}) \tag{5.33}$$

If the shape of the real droplet is exactly ellipsoidal, then D_f calculated from Eqs.(5.29),(5.30),(5.31) and θ calculated from Eq.(5.33) are exactly the same as those obtained from modeling with a single conformation tensor. In the case of droplets whose shapes deviate from the ellipsoidal shape, the larger N_s is chosen in the calculations described above the more accurate is the calculated contour, D_f, and θ.

5.2.6 Properties of solutions

The time evolution equations (5.15) have been constructed in such a way that even without specifying the free energy Φ and the dissipation potential Ξ (required only to satisfy (5.11)) their solutions satisfy the following properties:

(1) *Compatibility with thermodynamics*

As the time $t \to \infty$ solutions to (5.15) approach equilibrium states (i.e. states for which the free energy Φ reaches its minimum). This result follows from the observation that the free energy Φ plays in the time evolution the role of the Lyapunov function associated with the approach to equilibrium. Indeed, the free energy is a convex function at a neighborhood of the equilibrium state (this is the mathematical expression of the thermodynamic stability of the equilibrium state) and $\frac{d\Phi}{dt} \leq 0$. The proof remains, of course, formal since we do not say anything about the question of the existence of solutions and the topological aspects of the convergence to equilibrium states.

(2) *Conservation of the total overall momentum* $\boldsymbol{U} = \int d\boldsymbol{r}\, \boldsymbol{u}(\boldsymbol{r})$

The right hand side of the first equation in (5.15) has the form of the divergence of a flux and consequently $d\boldsymbol{U}/dt$ depends only on the situation at the boundary of the domain in which the fluid under consideration is confined.

(3) *Conservation of the total mass* $\int_{-1}^{1} ds\,(\rho + \rho_A + \rho_B)$ *of the surface active agent* C

It follows from the fourth sixth and seventh equations in (5.15) that $\frac{\partial}{\partial t}(\rho + \rho_A + \rho_B) = -\frac{\partial}{\partial s}(\rho\Phi_\nu)$. The right hand side has thus the form of the divergence of a flux and the argument made in the point (2) above applies.

(4) *Conservation of the mass fraction* $\phi = V_B/V_{tot}$ *of the minor fluid* B

The total volume V_{tot} is conserved since the mixture as a whole is assumed to be incompressible. The volume $V_B = \int_{-1}^{1} ds\, det\boldsymbol{c}(s)$ of the fluid B is also conserved since $d(det\boldsymbol{c}(s))/dt = 0$ *for all* $s \in [-1, 1]$.

(5) *Two comments*

In the particular case when $\boldsymbol{w}$ approaches equilibrium much faster than $\boldsymbol{c}$, we can approximatively solve the second and the third equations in (5.15) as follows. Instead of $\partial\boldsymbol{w}/\partial t$ on the left hand side of the third equations we put zero and solve it to obtain $\Phi_{\boldsymbol{w}}$. We insert then the solution to the second equation and obtain in this way the time evolution equation for $\boldsymbol{c}$ involving the non affine advection of the type suggested first by Gordon and Schowalter[24]. More detailed discussion of this point can be found in Ref.17.

Similarly, we can consider a particular case when ν approaches equilibrium much faster than ρ. The same procedure described above leads then to a time evolution equation for $\rho(s)$ that can be more directly compared with the surface mass transport equations developed in the microhydrodynamical formulations[2]. We hope to discuss this aspect of our model in more detail in a future paper.

To obtain a more detailed information about solutions to (5.15), we have to make all the remaining specifications and turn to numerical solutions. This is done in the next section.

5.3 Reduced Mesoscopic Model

Given the imposed flow $\boldsymbol{u}$, the governing equations (5.15) represent a system of nineteen partial differential equations for nineteen unknown functions (six components of $\boldsymbol{c}$, nine components of $\boldsymbol{w}$, and four scalars $\rho, \nu, \rho_A, \rho_B$) of two independent variables $t \in [0, \infty)$ and $s \in [0, 1]$. In order to be able to get relatively easily a first impression of results implied by the model developed above, we shall limit

ourselves in this paper to a particular situation in which the surface mass distribution $\rho(s,t); s \in [0,1]; t \in [0,\infty)$ is assumed to be known. Essentially, we assume that the last four equations in (5.15) are decoupled from the remaining equations and that their solution is known (see Appendix). We thus do not have to, in this paper, enter into details of the transport of the surface active agent (as for example its dilution due to enlargement of the surface). We intend to deal with these problems in a future paper.

If a know $\rho(s,t)$ is inserted into the second and the third equations in (5.15) then these equations become ordinary differential equations (in the time variable t) for $\boldsymbol{c}(s,t)$ and $\boldsymbol{w}(s,t)$. The variable s appears in them only as a parameter.

By using the analysis of Flumerfelt[1], we arrive in Appendix at the following expression for $\rho(s,t)$:

$$\rho/\rho_{eq} = 1 + \frac{2}{\pi}\left(1 - exp(-\frac{t/(\tau_c)_{eq}}{N_M})\right)\frac{N_M}{p_{eff}+1}(2s^2-1) \tag{5.34}$$

and the concentration gradient along arc length l writes

$$\frac{\partial\rho/\rho_{eq}}{\partial l} = \frac{2}{\pi}\left(1 - exp(-\frac{t/(\tau_c)_{eq}}{N_M})\right)\frac{4N_M}{p_{eff}+1}\, s\sqrt{1-s^2} \tag{5.35}$$

where the dimensionless number N_M (see (5.76) in Appendix) is the ratio of the strength of the imposed flow to that of the transport of the surface active agent; $(\tau_c)_{eq}$ is the relaxation time of the interface defined in Eqs.(5.80),(5.74); $p = \eta_d/\eta_m$, where η_d and η_m are viscosity coefficients of the dispersed fluid B and the matrix fluid A respectively;

$$p_{eff} = p + \frac{6N_M\beta}{5Ca} \tag{5.36}$$

where the capillary number Ca and the elasticity number β are defined below in (5.43). The effective viscosity ratio p_{eff} has been introduced in Ref.1. Its physical interpretation is discussed in Appendix. Figure 5.2 shows $\rho(s,t)$ graphically.

The second and the third equations in (5.15), if written explicitly, take the following form:

$$\frac{d\boldsymbol{c}(s)}{dt} = (\boldsymbol{D}+\boldsymbol{W})\cdot\boldsymbol{c} + \boldsymbol{c}\cdot(\boldsymbol{D}-\boldsymbol{W}) + \alpha\left[\boldsymbol{w}+\boldsymbol{w}^T - \frac{2}{3}\boldsymbol{c}tr\left(\boldsymbol{w}\cdot\boldsymbol{c}^{-1}\right)\right]$$

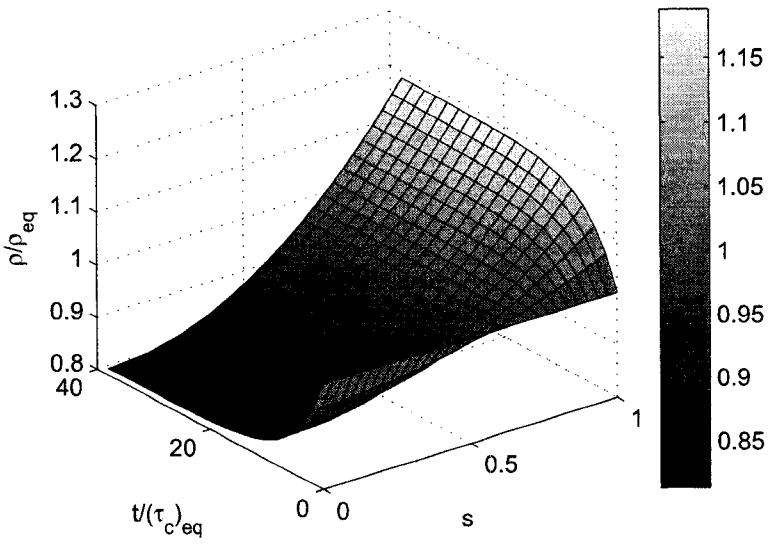

Figure 5.2: The concentration of the surface active agent $\rho(s,t)$ residing on the droplet surface; $p = 1$, $N_M = 5$, $Ca_{eq} = 0.2$ and $\beta_{eq} = 0.5$.

$$
\begin{aligned}
& -\frac{1}{2}\Lambda^{(1)}\left[2\Gamma_1(\boldsymbol{c}tr\boldsymbol{c}-\boldsymbol{c}\cdot\boldsymbol{c})-\frac{\alpha}{2}\left(\boldsymbol{c}^{-1}\cdot\boldsymbol{w}^T\cdot\boldsymbol{w}+\boldsymbol{w}^T\cdot\boldsymbol{w}\cdot\boldsymbol{c}^{-1}\right)\right. \\
& \left.-\frac{2}{3}[\bullet]\boldsymbol{\delta}-\frac{2}{3}\boldsymbol{c}\left(2\Gamma_1 tr\boldsymbol{c}-\frac{\alpha}{2}tr\left(\boldsymbol{c}^{-1}\cdot\boldsymbol{w}^T\cdot\boldsymbol{w}\cdot\boldsymbol{c}^{-1}\right)-\frac{1}{3}[\bullet]tr\boldsymbol{c}^{-1}\right)\right] \\
\frac{d\boldsymbol{w}(s)}{dt} &= \boldsymbol{w}\cdot(\boldsymbol{D}-\boldsymbol{W})-(\boldsymbol{D}-\boldsymbol{W})\cdot\boldsymbol{w}+\alpha\boldsymbol{w}\cdot\boldsymbol{c}^{-1}\cdot\boldsymbol{w}^T \\
& -2\Gamma_1(tr\boldsymbol{c}\cdot\boldsymbol{c}-\boldsymbol{c}\cdot\boldsymbol{c})+\frac{2}{3}[\bullet]\boldsymbol{\delta}-\Lambda_{12}^{(2)}\boldsymbol{D}\cdot\boldsymbol{c}-\Lambda_{22}^{(2)}\alpha\boldsymbol{w} \\
\boldsymbol{\sigma} &= \int_0^1 ds\left[-2\Gamma_1(\boldsymbol{c}tr\boldsymbol{c}-\boldsymbol{c}\cdot\boldsymbol{c})+\frac{2}{3}[\bullet]\boldsymbol{\delta}+\alpha\boldsymbol{w}\cdot\boldsymbol{c}^{-1}\cdot\boldsymbol{w}^T\right] \qquad (5.37)
\end{aligned}
$$

where

$$\Gamma_1 = \frac{x_c}{a^5}\left[\Gamma+\frac{1}{2}\rho_{eq}\varepsilon\left(\frac{\partial(\rho/\rho_{eq})}{\partial l}\right)^2\right] \qquad (5.38)$$

and

$$[\bullet] = \Gamma_1\left((tr\boldsymbol{c})^2-tr(\boldsymbol{c}\cdot\boldsymbol{c})\right)-\frac{\alpha}{2}tr\left(\boldsymbol{w}^T\cdot\boldsymbol{w}\cdot\boldsymbol{c}^{-1}\right) \qquad (5.39)$$

The parameter ε is defined below in Eq.(5.45). By $\boldsymbol{D}$ resp. $\boldsymbol{W}$ we denote the symmetric resp. antisymmetric part of the velocity gradient.

Now, we rewrite (5.37) in dimensionless form by using the following nondimen-

sional variables: $\boldsymbol{c}^* = \boldsymbol{c}/a^2$, $\boldsymbol{w}^* = \boldsymbol{w}/\eta_m$, $\boldsymbol{D}^* = \boldsymbol{D}/\dot{\gamma}$, $\boldsymbol{W}^* = \boldsymbol{W}/\dot{\gamma}$, $\boldsymbol{\sigma}^* = \boldsymbol{\sigma}/\dot{\gamma}\eta_m$, $\rho* = \rho/\rho_{eq}$, $t^* = t/\tau_c$, where τ_c is the relaxation time of the interface defined in Eq.(5.80), ρ_{eq} is the initial and also equilibrium uniform concentration of the surface active agent on $interface_{A,B}$. For simplicity, we omit hereafter the symbol * . The dimensionless governing equations read as follows

$$\begin{aligned}
\frac{d\boldsymbol{c}(s)}{dt} &= Ca\,[(\boldsymbol{D}+\boldsymbol{W})\cdot\boldsymbol{c}+\boldsymbol{c}\cdot(\boldsymbol{D}-\boldsymbol{W})]+\kappa\left[\boldsymbol{w}+\boldsymbol{w}^T-\frac{2}{3}\boldsymbol{c}\,tr\left(\boldsymbol{w}\cdot\boldsymbol{c}^{-1}\right)\right] \\
&\quad -\frac{1}{3}x_c(1+\beta')\mu_1\left[\boldsymbol{c}\,tr\boldsymbol{c}-3\boldsymbol{c}\cdot\boldsymbol{c}-\left((tr\boldsymbol{c})^2-tr(\boldsymbol{c}\cdot\boldsymbol{c})\right)\left(\boldsymbol{\delta}-\frac{1}{3}\boldsymbol{c}tr\boldsymbol{c}^{-1}\right)\right] \\
&\quad -\frac{1}{6}\kappa\mu_1\left[tr\left(\boldsymbol{w}^T\cdot\boldsymbol{w}\cdot\boldsymbol{c}^{-1}\right)\left(\boldsymbol{\delta}-\frac{1}{3}\boldsymbol{c}tr\boldsymbol{c}^{-1}\right)+\boldsymbol{c}tr\left(\boldsymbol{c}^{-1}\cdot\boldsymbol{w}^T\cdot\boldsymbol{w}\cdot\boldsymbol{c}^{-1}\right)\right. \\
&\quad \left.-\frac{3}{2}\left(\boldsymbol{c}^{-1}\cdot\boldsymbol{w}^T\cdot\boldsymbol{w}+\boldsymbol{w}^T\cdot\boldsymbol{w}\cdot\boldsymbol{c}^{-1}\right)\right] \\
\frac{d\boldsymbol{w}(s)}{dt} &= Ca\,[\boldsymbol{w}\cdot(\boldsymbol{D}-\boldsymbol{W})-(\boldsymbol{D}-\boldsymbol{W})\cdot\boldsymbol{w}] \\
&\quad -2x_c(1+\beta')\left[\boldsymbol{c}\,tr\boldsymbol{c}-\boldsymbol{c}\cdot\boldsymbol{c}-\frac{\boldsymbol{\delta}}{3}\left((tr\boldsymbol{c})^2-tr(\boldsymbol{c}\cdot\boldsymbol{c})\right)\right] \\
&\quad +\kappa\left[\boldsymbol{w}\cdot\boldsymbol{c}^{-1}\cdot\boldsymbol{w}^T-\frac{1}{3}tr(\boldsymbol{w}^T\cdot\boldsymbol{w}\cdot\boldsymbol{c}^{-1})\boldsymbol{\delta}\right]-Ca\,\mu_2\boldsymbol{D}\cdot\boldsymbol{c}-\mu_3\boldsymbol{w} \qquad (5.40)
\end{aligned}$$

The expression (5.16) for the extra stress tensor becomes

$$\begin{aligned}
\boldsymbol{\sigma} &= \int_0^1 ds\frac{1}{Ca}\left[-2x_c(1+\beta')\left(\boldsymbol{c}tr\boldsymbol{c}-\boldsymbol{c}\cdot\boldsymbol{c}-\frac{\boldsymbol{\delta}}{3}\left((tr\boldsymbol{c})^2-tr(\boldsymbol{c}\cdot\boldsymbol{c})\right)\right)\right. \\
&\quad \left.+\kappa\left(\boldsymbol{w}\cdot\boldsymbol{c}^{-1}\cdot\boldsymbol{w}^T-\frac{1}{3}tr(\boldsymbol{w}^T\cdot\boldsymbol{w}\cdot\boldsymbol{c}^{-1})\boldsymbol{\delta}\right)\right] \qquad (5.41)
\end{aligned}$$

where

$$\beta'(s)=\frac{\beta}{2}\left(\frac{\partial\rho}{\partial l}\right)^2 \qquad (5.42)$$

and

$$Ca(s)=\frac{\eta_m a\dot{\gamma}}{\Gamma(s)};\ \kappa(s)=\frac{\alpha\eta_m^2}{a\Gamma(s)};\ \beta(s)=\frac{\rho_{eq}\varepsilon}{\Gamma(s)} \qquad (5.43)$$

$$\mu_1=\frac{\eta_m\Lambda^{(1)}}{a^2};\ \mu_2=\frac{a^2\Lambda_{12}^{(2)}}{\eta_m};\ \mu_3(s)=\frac{a\eta_m\Lambda_{22}^{(2)}\alpha}{\Gamma(s)} \qquad (5.44)$$

are dimensionless numbers. Here, $Ca(s)$ is the local (i.e. dependent on s) capillary

number, and $\beta(s)$ is the local elasticity number which expresses the sensitivity of the surface tension to the variation of surfactant concentration. $\Gamma(s)$ is the local interfacial tension. As we have already discussed in Section 5.2.4, we use in this paper only the liner approximation

$$\Gamma(s) = \Gamma_c - \rho(s)\varepsilon \tag{5.45}$$

of the surface equation of state [4] (i.e. of the functional dependence of Γ on $\rho(s)$). The symbol Γ_c in (5.45) stands for the interfacial tension without the surface active agent and $\varepsilon = -\frac{\partial \Gamma}{\partial \rho}$ is a material parameter (which, in the case of a nonlinear surface equation of state, would not be a constant but an appropriate function of $\rho(s)$).

The initial conditions are the following:

$$\boldsymbol{c}(s,0) = \boldsymbol{\delta};\ \boldsymbol{w}(s,0) = 0 \ for\ all\ s \tag{5.46}$$

The material parameters entering (5.40) are: Ca, κ, β, N_M, μ_1, μ_2, μ_3, and x_c. The first four appear also in the microhydrodynamic formulation and can be thus considered to be known (from independent microhydrodynamic measurements). The remaining four are, on the other hand, phenomenological parameters. In Section 5.3.1 we shall specify the parameters μ_1, μ_2, μ_3, and x_c by relating certain particular solutions of (5.40) to some particular solutions of the governing equations arising in microhydrodynamics. We shall indeed see that μ_1, μ_2, μ_3, and x_c are related to the viscosities of the fluids A and B.

In the particular case when the surface active agent is absent, i.e. if $\rho_{eq} = 0$ and $x_c = 1$, Eqs.(5.40) become the same as those introduced in Ref.17.

5.3.1 Determination of parameters

Analytical solutions to the governing equations of the microhydrodynamical analysis of the mixture discussed in this paper are known for some particulars situations. Below, we shall use the following results: (i) droplet shape for small capillary numbers Ca in the absence of the surface active agent C [25], (ii) the first normal stress difference in the case of small volume fraction ϕ of the minor fluid B, small capillary number Ca, and absence of the surface active agent C [26], (iii)

contribution of the interface to the complex shear modulus G^* corresponding to an imposed oscillatory shear flow with small amplitudes in the absence of the surface active agent C [27,28].

We shall now solve analytically Eqs.(5.40) for the same situations and compare the results with the results coming from microhydrodynamics. The comparison will give us relations that can be used to express the parameters μ_1, μ_2, μ_3 and x_c in terms of the microhydrodynamic material parameters.

The imposed flow is in this paper assumed to be always the simple shear flow. The dimensionless rate-of strain tensor and the vorticity tensor are thus given by

$$\boldsymbol{D} = \begin{pmatrix} 0 & \frac{1}{2} & 0 \\ \frac{1}{2} & 0 & 0 \\ 0 & 0 & 0 \end{pmatrix} \tag{5.47}$$

$$\boldsymbol{W} = \begin{pmatrix} 0 & \frac{1}{2} & 0 \\ -\frac{1}{2} & 0 & 0 \\ 0 & 0 & 0 \end{pmatrix} \tag{5.48}$$

We assume that Ca is a small parameter and look for solutions of (5.40) in the form:

$$\boldsymbol{c} = \boldsymbol{\delta} + Ca\boldsymbol{c}^{(1)} + Ca^2\boldsymbol{c}^{(2)} + O(Ca^3) \tag{5.49}$$

and

$$\boldsymbol{w} = Ca\boldsymbol{w}^{(1)} + Ca^2\boldsymbol{w}^{(2)} + O(Ca^3) \tag{5.50}$$

We assume moreover that $\boldsymbol{w}$ evolves in time much faster than $\boldsymbol{c}$. To the first order in the small parameter Ca, Eqs.(5.40) become

$$\frac{d\boldsymbol{c}^{(1)}}{dt} = -\left(\frac{4\kappa}{\mu_3} + \mu_1\right) x_c(1+\beta')\boldsymbol{c}^{(1)} + 2\left(1 - \frac{\kappa\mu_2}{\mu_3}\right)\boldsymbol{D} \tag{5.51}$$

$$\boldsymbol{w}^{(1)} = -\frac{1}{\mu_3}\left(2x_c(1+\beta')\boldsymbol{c}^{(1)} + \mu_2\boldsymbol{D}\right) \tag{5.52}$$

The contribution of the interface to the zero shear viscosity, the first and the second normal stress difference are found to be

$$\eta_{s0} = 2\eta_m \frac{\mu_3 - \kappa\mu_2}{4\kappa + \mu_1\mu_3} \tag{5.53}$$

$$N_1 = -4\eta_m \dot{\gamma} Ca \frac{\mu_3(\mu_3 - \kappa\mu_2) - x_c(1+\beta')\kappa(4+\mu_1\mu_2)}{x_c(1+\beta')(4\kappa+\mu_1\mu_3)^2} \tag{5.54}$$

$$N_2 = 2\eta_m \dot{\gamma} Ca \kappa \frac{\mu_2(\mu_3 - \kappa\mu_2) + x_c(1+\beta')(4+\mu_1\mu_2)}{x_c(1+\beta')(4\kappa+\mu_1\mu_3)^2} \tag{5.55}$$

Next, we turn to the oscillatory shear flow with the shear strain given by $\gamma = -i\gamma_0 e^{i\omega t}$, where γ_0 is the amplitude and ω is the frequency. If γ_0 is small, we can limit ourselves only to linearized governing equations. By using (5.49) and (5.50), we then solve Eqs.(5.40) linearized about the equilibrium state. From the solution we then obtain the following interfacial complex shear modulus ($G^* = -\frac{\sigma_{12}}{\gamma}$):

$$G^* = i2\omega\eta_m \frac{x_c(1+\beta')[(\mu_3 - \kappa\mu_2) + i\tau_c\omega]}{[4x_c(1+\beta')\kappa + x_c(1+\beta')\mu_1\mu_3 - \tau_c^2\omega^2] + i[x_c(1+\beta')\mu_1 + \mu_3]\tau_c\omega} \tag{5.56}$$

Having found some particular solutions to (5.40), we compare them now with consequences of the microhydrodynamic analysis.

First, we consider deformations of the droplet. By comparing Eq.(5.51) with the droplet shape calculated by Rallison[25] (see also Ref.9), we find that the shapes are identical provided

$$\left(\frac{4\kappa}{\mu_3} + \mu_1\right) x_c(1+\beta') = \frac{40(p_{eff}+1)}{(2p_{eff}+3)(19p_{eff}+16)} \tag{5.57}$$

$$1 - \frac{\kappa\mu_2}{\mu_3} = \frac{5}{2p_{eff}+3} \tag{5.58}$$

We have replaced p appearing in Ref.25 by p_{eff} (recall that $p = p_{eff}$ in the absence of the surface active agent, i.e. if $\rho_{eq} = 0$, see more in Appendix). Following Maffettone and Minale[9] (see also Ref.17), we may also suggest to replace (5.58) by

$$1 - \frac{\kappa\mu_2}{\mu_3} = \frac{5}{2p_{eff}+3} + \frac{3Ca^2}{(2+6Ca)(1+\delta p^2)} \tag{5.59}$$

where δ is a small number (we use $\delta = 0.01$).

Second, we consider the first normal stress difference N_1. If the volume fraction ϕ of the minor fluid B is small, Choi and Schowalter[26] arrive at the following

expression for the first normal stress difference:

$$N_1 = -\eta_m \dot{\gamma} Ca \frac{(19p+16)^2}{40(p+1)^2}\phi \tag{5.60}$$

Since the fluids A and B are simple Newtonian fluids, the elasticity of the mixture of A and B comes only from $interface_{A,B}$. Comparison of (5.54) with (5.60) shows (if p is replaced with p_{eff}) that

$$4\frac{\mu_3(\mu_3 - \kappa\mu_2) - \kappa x_c(1+\beta')(4+\mu_1\mu_2)}{(4\kappa+\mu_1\mu_3)^2 x_c(1+\beta')} = \frac{(19p_{eff}+16)^2}{40(p_{eff}+1)^2} \tag{5.61}$$

Third, we turn to the rheological behavior in the oscillatory flow characterized by the complex shear modulus G^*. From (5.56), we see that the relaxation time of the interface at the low frequency is

$$\tau_c = \frac{\eta_m a}{\Gamma}\frac{x_c(1+\beta')\mu_1 + \mu_3}{x_c(1+\beta')(4\kappa+\mu_1\mu_3)} \tag{5.62}$$

Palierne's expression[28] for the same quantity is

$$\tau_c = \frac{\eta_m a}{\Gamma}\frac{(19p+16)(2p+3)}{40(p+1)} \tag{5.63}$$

We see that if (5.57) is satisfied and $\mu_3 \gg \mu_1$, then both expressions are identical. This observation provides an independent confirmation (from looking at rheological consequences) of the relation (5.57) obtain above by looking at the morphological consequences.

Continuing with the comparison of the dynamical moduli, we shall now specify the parameter x_c introduced in the free energy (in Eq.(5.21)). It follows from (5.56) that the plateau value of G', (where G' is defined by $G^* = G' + iG''$) in the limit $\omega \to \infty$, equals

$$G'_\infty = 2x_c(1+\beta')\frac{\Gamma}{a} \tag{5.64}$$

Palierne's expression for the same quantity (in the limit of dilute emulsions, i.e. if $\phi \to 0$), is[28]

$$G'_\infty = 20\frac{\Gamma}{a}\frac{1}{(2p+3)^2} \tag{5.65}$$

The comparison implies (p is replaced by p_{eff})

$$x_c = \frac{10}{(2p_{eff}+3)^2(1+\beta')} \tag{5.66}$$

Summing up, by focusing on several particular cases (corresponding to the absence of the surface active agent, small capillary number, small amplitude of the imposed oscillatory shear flow, and small volume fraction of the minor fluid B) in which closed form analytical expressions can be found for both the model developed in this paper and the models based on microhydrodynamics, we have arrived at the relations (5.57), ((5.58) or (5.59)), (5.61) and (5.66). The first three have arisen by comparing the morphology and the last two by comparing the rheology.

The comparison of (5.62) and (5.63) provides a rheological confirmation of the relation (5.57) obtained by looking at the morphology.

The relation (5.66) determines the parameter x_c.

The remaining three relations (5.57), ((5.58) or (5.59)), and (5.61) are three nonlinear equations for three unknowns μ_1, μ_2 and μ_3. Moreover, since we have to satisfy the properties (5.11), we know that $\mu_3 \gg \mu_2$. Guided by the experience collected in making the comparison with results of experimental observations (in Section 5.4), we proceed as follows. First, we note that the morphology and the rheology implied by (5.40) is insensitive to the choice of μ_3 provided it lies in a certain range (see Section 5.4). Second, with a given μ_3, the remaining two parameters μ_1 and μ_2 are obtained from (5.57) and (5.59). The comparison with experimental data discussed in Section 5.4.1 shows that μ_1 and μ_2 obtained in this way give a slightly better fit of the morphology and μ_1 and μ_2 obtained by solving (5.57)), (5.61) a slightly better fit of the rheology.

5.3.2 Total stress of the blend

Now we turn to the shear stress. The stress measured in rheological measurements is the total stress, i.e. the stress originated on $interface_{A,B}$ as well as in the bulk. The predictions that we make are only for the interface contribution. If we want to compare the observed and predicted rheology, we have to therefore address the "mixing rule", i.e. the questions of how to calculate the bulk contribution and how

to combine the bulk and the interfacial contributions. As for the combination, we shall use the simplest mixing rule

$$\sigma_{12}^{tot} = \sigma_{12}^{bulk} + \phi\sigma_{12} \tag{5.67}$$

where the first term on the right hand side is the bulk contribution and and σ_{12} is the contribution of the interface. This mixing has been used for example in Refs. 8,22, and 29.

Next, we address the bulk contribution σ_{12}^{bulk}. We recall that the bulk phase is composed of two simple (Newtonian) fluids A and B. The simplest way to introduce σ_{12}^{bulk} (in the dimensionless form) is by using

$$-\sigma_{12}^{bulk} = p + (1 - \phi) \tag{5.68}$$

This relation is expected to be valid for p that is close to one. If $p \to \infty$ and $p \to 0$ then (5.68) overestimates the bulk contribution. We shall therefore look for an improved relation.

We begin with well known results for the zero shear limits of the viscosity. For a dilute emulsion of Newtonian droplets in a Newtonian matrix without the surface active agent, Taylor's theory[30,23] predicts the total zero-shear viscosity to be

$$-(\sigma_{12}^{tot})_0 = 1 + \phi\frac{5p+2}{2p+2} \tag{5.69}$$

This gives the correct total shear stress $(1 + 2.5\phi)$ as $p \to \infty$ and the correct value $(1 + \phi)$ as $p \to 0$.

The zero shear viscosity implied by the present model has been calculated to be (5.53). If we insert into it (5.57),(5.58) and (5.66) we obtain

$$-(\sigma_{12})_0 = \frac{5(19p_{eff} + 16)}{2(p_{eff} + 1)(2p_{eff} + 3)^2} \tag{5.70}$$

Since for Newtonian fluids the bulk shear viscosity is independent of the shear rate, we thus arrive at the following expression for the bulk contribution (we are

replacing p by p_{eff})

$$-\sigma_{12}^{bulk} = 1 + \phi\left(\frac{5p_{eff}+2}{2p_{eff}+2} - \frac{5(19p_{eff}+16)}{2(p_{eff}+1)(2p_{eff}+3)^2}\right) \tag{5.71}$$

By substituting (5.71) into Eq.(5.67) we obtain a new mixing rule that is valid for dilute emulsions in which both bulk phases are Newtonian fluids. We use below this new mixing rule.

Now we turn to the first and the second normal stress N_1 and N_2. Here we do not need any mixing rule since the fluids A and B are simple Newtonian fluids and consequently the only contribution to N_1 and N_2 comes from $interface_{A,B}$:

$$N_1^{tot} = \phi N_1 \tag{5.72}$$

$$N_2^{tot} = \phi N_2 \tag{5.73}$$

5.4 Comparison with Experiments and Other Models

Now we are in position to solve numerically Eqs.(5.40) and obtain in this way both the morphology and the rheology predicted by (5.40). We shall compare them with other models and with results of experimental observations. In Section 5.4.1 we look at the special case when the surface active agent is absent. The general case is discussed in Section 5.4.2.

5.4.1 Without the surface active agent

Immiscible blends in the absence of the surface active agents have been studied extensively both from the experimental and the theoretical point of view. We turn therefore first to this special case. The theoretical investigations have been carried on the level of microhydrodynamics[23,25–28,30,31] and also on the mesoscopic level[8–10,17,22,29]. Below, we shall compare predictions implied by Eqs.(5.40) with predictions of the Maffettone-Minale model[9] and the experimental data reported in Refs.32-34.

The parameters β, β' and N_M equal zero in the absence of the surface active agent. The parameter κ is calculated from the expression (5.43) in which $(\alpha)^{-1}$ (having the physical meaning of the mass density - see (5.19)) is put equal to the mass density of the matrix fluid A. The parameter x_c is calculated from (5.66). The remaining parameters μ_1, μ_2, μ_3 are determined as follows. We begin by choosing a value for μ_3 and then calculate μ_1 and μ_2. Since μ_3 is proportional to the inverse of the relaxation time of $\boldsymbol{w}$ and since we know that $\mu_3 \gg \mu_1$ and $\mu_3 \gg \mu_2$(in order to satisfy (5.11)), we choose a large value for μ_3. As we have seen in Section 5.3.1, we can calculate the parameters μ_1 and μ_2 in tree different ways: (1) from Eqs.(5.57),(5.61); (2) from Eqs.(5.57),(5.58); and (3) from Eqs.(5.57),(5.59). We shall use all three methods and compare the results. As for the choice of the parameter μ_3, we note that if μ_3 is sufficiently large (in particular if $\mu_3 > 10^6$) then predictions based on (5.40) are insensitive to variations of μ_3.

On Figure 5.3 we are comparing the morphology predicted by the Maffettone-Minale model and the morphology measured by Guido and Villone[32] with predictions of the present model. The viscosity ratio $p = 1.4$, the capillary number $Ca = 0.24$. Since the choice (3) provides the best fit (see also Figure 5.4 and Figure 5.5), we use this method also in Section 5.4.2 below.

Figure 5.4 shows the comparison of steady-state values of the deformation parameter D_f and the orientational angle θ (see 5.29),(5.32)) predicted by the present model, by the Maffettone-Minale model, and observed by Torza et al.[33]. The viscosity ratio $p = 3.6$ and the capillary number Ca varies. As in Figure 5.3, we see that the best fit is obtained with the choice (3) for the calculation of the parameters μ_1 and μ_2. Variations of the values of μ_3 do not have any noticeable influences on the results if $10^9 < \mu_3 < 10^{25}$.

Figure 5.5 shows the time evolution of the total shear stress σ_{12}^{tot} and the total first normal stress difference N_1^{tot} for a dilute emulsion (without the surface active agent) subjected to a start-up shear flow. The experimental data are taken from Jansseune *et al.*[34] (the fluids A and B are not simple Newtonian fluids in Ref.34 but in the conditions in which they are observed they behave as Newtonian fluids). We also show results calculated by Yu and Bousmina[11].

Figure 5.5 shows that the method (1) for calculating the parameters μ_1 and μ_2 gives better rheological predictions than the methods (2) and (3). We also

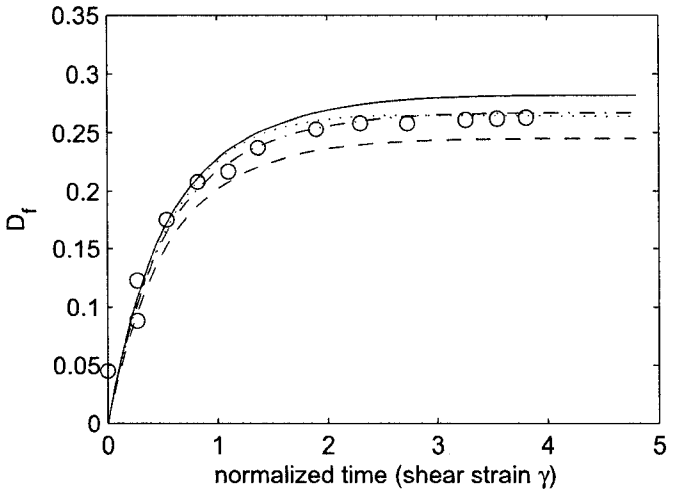

Figure 5.3: Comparison of model predictions with experimental data for the time evolution of the deformation parameter D_f of a droplet without the surface active agent (i.e. $\rho_{eq} = 0$); the normalized time is the shear strain γ. (—), (- -), and (-.-) correspond to method (1), method (2), and method (3) for calculating μ_1 and μ_2. (...) corresponds to the Maffettone-Minale model, and (o) corresponds to the experimental data taken from Guido and Villone[32] with $Ca = 0.24$ and $p = 1.4$.

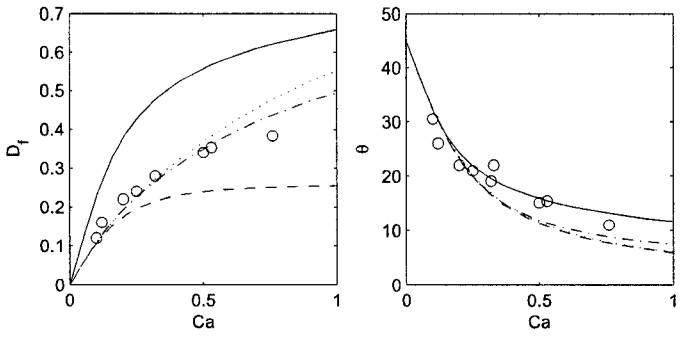

Figure 5.4: Comparison of model predictions with experimental data for the steady-state deformation parameter D_f and orientation angle θ as functions of the capillary number Ca for a droplet without surfactant. (—), (- -), and (-.-) correspond to method (1), method (2), and method (3) to relate μ_1 and μ_2 of the present model with $\rho_{eq} = 0$. (...) to the Maffettone-Minale model, and (o) to the experimental data taken from Torza *et al.*[33] with $p = 3.6$.

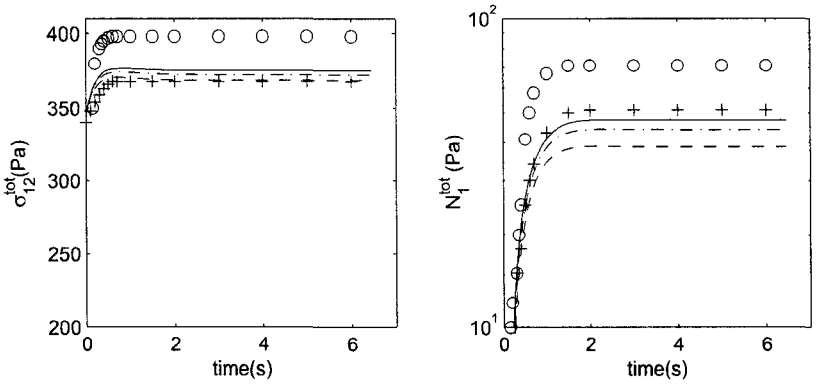

Figure 5.5: Comparison of model predictions with experimental data for the time evolution of the shear stress, σ_{12}^{tot}, and the first normal stress difference, N_1^{tot}, for a dilute emulsion without the surface active agent (i.e. $\rho_{eq} = 0$) subjected to a start-up shear flow. (—), (- -), and (-.-) correspond to method (1), method (2), and method (3) to relate μ_1 and μ_2. (+++) corresponds to the Yu-Bousmina model, and (o) corresponds to the experimental data taken from Jansseune *et al.*[34] with $\dot{\gamma} = 2.5s^{-1}$.

note that the rheological predictions made with the method (1) are very close to the ones of Yu and Bousmina[11]. We shall nevertheless use below the method (3) since with it we are getting consistently better predictions of the morphology.

5.4.2 With the surface active agent

Introduction of the surface active agent into the mixture brings the following new effects: (i) the interfacial tension is lowered, (ii) nonuniform distribution of the surface active agent on the interface brings about nonuniform distribution of the surface tension and associated with it large deviations from the ellipsoidal shape of droplets and appearance of new stresses (called Marangoni stresses).

Before solving numerically the governing equations (5.40), we shall collect all the parameters entering them.

The parameters $Ca(s), \kappa(s), \beta(s)$ depend on s only through their dependence on $\rho(s)$. We shall use hereafter the following notation: $Ca_{eq} = [Ca]_{\rho=\rho_{eq}}$; $\kappa_{eq} = [\kappa]_{\rho=\rho_{eq}}$; $\beta_{eq} = [\beta]_{\rho=\rho_{eq}}$, $(\tau_c)_{eq} = [\tau_c]_{\rho=\rho_{eq}}$ (see Eq.(5.80) for the definition of τ_c). Instead of the parameter N_M appearing in $\rho(s)$ (see (5.76)), we shall use below

the parameter

$$\chi_{eq} = \frac{\tau_\rho}{(\tau_c)_{eq}} \tag{5.74}$$

We shall call it hereafter a transport number. The relaxation times τ_c and τ_ρ are introduced in (5.80) and (5.79).

Summing up, the following six dimensionless numbers specify the mixture in the presence of the surface active agent:

1. The parameter Ca_{eq} is the capillary number defined as the ratio of the imposed shear stress to the interfacial tension. The presence of the surface active agent lowers the surface tension and thus makes the capillary number Ca_{eq} (corresponding to the uniform distribution of the surface active agent) larger. The physics that is associated with the nonuniform distribution of the surface active agent (in particular the appearance of the Marangoni stress and large deviations from the ellipsoidal shape of the droplet) is incorporated into the model developed in this paper.

2. The parameter κ_{eq} has the similar interpretation as the capillary number Ca except that the imposed shear stress is replaced by the stress created by the flow perturbation due to the presence of the obstacle (i.e. $interface_{A,B}$).

3. Diffusion on the interface and the adsorption/desorption between the interface and the bulk are two processes driving the distribution of the surface active agent to a uniform distribution. The Péclet number (the ratio of the characteristic time of diffusion to that of the convection caused by the imposed flow at the interface) measures quantitatively the diffusion and χ_{eq} the adsorption/desorption process. Contrary to the Péclet number, the parameter χ_{eq} is the intrinsic property of the mixture, independent of the imposed external influences (in particular of the imposed flow).

4. β_{eq} represents the importance of the interfacial gradient relative to the reduced uniform interfacial tension, i.e., the importance of average Marangoni free energy $\mathcal{M}$ relative to the average interfacial free energy $\mathcal{A}$.

5. $p = \eta_d/\eta_m$ is the ratio of the viscosities of the bulk phases.

6. μ_3 is a parameter proportional to the inverse of the relaxation time of $\boldsymbol{w}$ that is the dual to gradient of the velocity perturbed by the presence of the interface. As shown in Section 5.4.1, both the morphology and the rheology are insensitive to the choice of μ_3 provided it is chosen to be sufficiently large.

In the rest of this section we shall compare predictions of the present model, both morphology and rheology, with results of experimental observations and predictions of other models. We also examine how the six parameters entering the governing equations (5.40) influence the results.

Morphology

First, we turn to the morphology. Due to the lack of detailed experimental data concerning the surfactant concentration on the droplet surface and the relation between the concentration and the surface tension, the comparison with experiments shown below has a rather qualitative character.

The results are displayed on Figure 5.6. The experimental data are taken from Megias-Alguacil *et al.*[35] with both the droplet fluid B and the matrix fluid A being Newtonian. A solution of polyvinylpyrrolidone (PVP) in water is the fluid A and several silicon oils are fluids B. The interface was modified by adding two different amounts (0.1% and 1% by weight) of a nonionic surfactant (polyoxyethylene sorbitan monolaurate) with the commercial name Tween 20 (fluid C). The surfactant is soluble in the continuous phases and therefore the surfactant mass transfer from and to the interface takes place. By adding the surfactant, the equilibrium interfacial tension is reduced from $\Gamma_c = 31.2$ for the clean interface to $\Gamma_{eq} = 7.7(mN/m)$ and $\Gamma_{eq} = 6.4(mN/m)$ for 0.1% and 1% of the surfactant. Although the concentration of the surfactant located at the interface was not measured, the parameters that are needed for the calculations in the present model can be estimated. We proceed as follows. The definition of the elasticity number β_{eq} and Eq.(5.45) leads to the expression $\beta_{eq} = (\Gamma_c - \Gamma_{eq})/\Gamma_{eq}$ which gives the value of $\beta_{eq} = 0$ for the interface without the surfactant, $\beta_{eq} = 3.052$ and $\beta_{eq} = 3.875$ for 0.1% and 1% of the surfactant. The relaxation times τ_ρ and $(\tau_c)_{eq}$ can be measured in principle and used then to calculate χ_{eq} (see (5.74)). Lacking this data, we consider here the parameter χ_{eq} as a fitting parameter. The parameter κ_{eq} is calculated from (5.43) as in Section 5.4.1. We shall see below that variations in κ_{eq} have a very small effect on the results. The method (3) is used to calculate μ_1 and μ_2. Predictions of the present model are compared with predictions of Flumerfelt's theory[1,36] and with experimental data. Figure 5.6(a) displays the droplet deformation in the steady state as a function

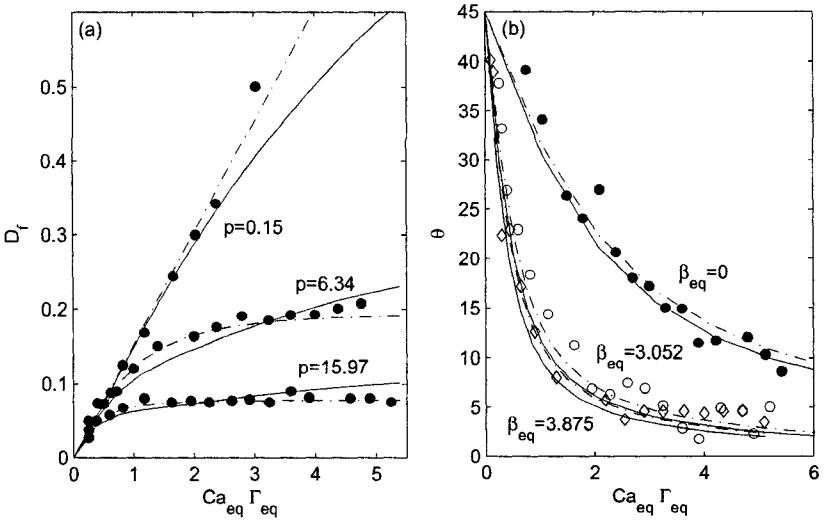

Figure 5.6: Comparison of model predictions with experimental data. (a) steady-state deformation as a function of $Ca_{eq}\Gamma_{eq}$ with 0.1% of the surface active agent for three values of p. (•) experimental data taken from Megias-Alguacil *et al.*[35]; (—) prediction of the present model with $\chi_{eq} = 0.5$ and $\kappa_{eq} = 10^3$; (-.-) predictions of Flumerfelt's theory with $\chi_{eq} = 0.5$. (b) the steady-state orientational angle θ as a function of $Ca_{eq}\Gamma_{eq}$ with $p = 15.97$. (•), (o) and ($\diamond$) are experimental data taken from Megias-Alguacil *et al.*[35] with 0%, 0.1%, and 1% of the surface active agent respectively; (—) corresponds to the present model with $\chi_{eq} = 0.3$ and $\kappa_{eq} = 10^3$; (-.-) corresponds to Flumerfelt's theory with $\chi_{eq} = 0.3$.

of $Ca_{eq}\Gamma_{eq} = \eta_m a\dot{\gamma}$ for different viscosity ratios p with 0.1% of the surfactant. Figure 5.6(b) shows steady-state values of the droplet orientational angle θ as a function of $Ca_{eq}\Gamma_{eq}$, for different amounts of the surfactant added into the continuous phase. The viscosity ratio is $p = 15.97$. The results show that although the predictions of the present model are not as good as those of Flumerflet's theory (which, we remind, is a microhydrodynamic theory), it is still satisfactory.

Next, we investigate how the parameters introduced in the present model influence the morphology. Figures 5.7, 5.8 and 5.9 display results corresponding to: (a) and (b) the steady-state deformation parameter D_f and the orientational angle θ respectively as functions of the capillary number Ca_{eq}, (c) and (d) the concentration of the surface active agent distributed on the droplet surface and the corresponding interfacial tension respectively for the capillary number $Ca_{eq} = 0.4$, (e) and (f) the shape of the droplet for different capillary numbers with other

parameters remaining the same.

Figures 5.7 and 5.8 represent the influences of the transport number χ_{eq}, the capillary number Ca_{eq} and the elasticity number β_{eq} on the steady-state droplet morphology with the viscosity ratio p and κ_{eq} fixed. We choose $p = 1$ and $\kappa_{eq} = 10^3$. Figure 5.7 displays results for $\chi_{eq} = 0.3$ and Figure 5.8 for $\chi_{eq} = 2$. Figure 5.9 displays the influences of the viscosity ratio p on the steady-state droplet morphology. We use here $\chi_{eq} = 2$ and $\kappa_{eq} = 10^3$. The method (3) is used to calculate μ_1 and μ_2. The calculation of the shape of the droplet is made with $N_s = 60$ pieces of the ellipsoids (see Section 5.2.5)

Effect of χ_{eq} and Ca_{eq}

When χ_{eq} is small (i.e. τ_ρ is small), the surface active agent moves easily between the droplet surface and the bulk phases. Consequently, as it is seen on Figure 5.7c, the surface active agent tends to be uniformly distributed on the droplet surface. This implies small gradients of the interfacial tension and small differences in the morphology as β_{eq} changes. The larger is $\dot{\gamma}$ the larger is Ca_{eq} and consequently the more nonuniform is ρ (as it is seen from (5.34)). As shown on Fig.5.8, the larger is χ_{eq} the more pronounced is the impact of the surfactant on the morphology of the droplet. The magnitude of the variations, both in the concentration and in the interfacial tension, increases along the surface. The role of χ_{eq} is similar to the role of the Péclet number when the diffusion process rather than the adsorption/desorption process dominates the relaxation. The influence of the Péclet number on the morphology has been investigated by Stone and Leal[2]. The main difference between the diffusion and the adsorption/desorption control of the relaxation is that the change of the Péclet number does not influence the total amount of the surface active agent located on the interface while the χ_{eq} does. By making χ_{eq} smaller, the surfactant in the bulk passes more easily to the interface and thus the total amount of the surface active agent on the interface increases during the deformation. Consequently, as indicated on Figures 5.7 and 5.8, in the limit of the uniform distribution of the surface active agent, deformations of the droplet with soluble surface active agent are larger than with the insoluble one (i.e. $\chi_{eq} \to \infty$) with the same nonzero elasticity number. This phenomenon was also observed in the numerical solutions of the

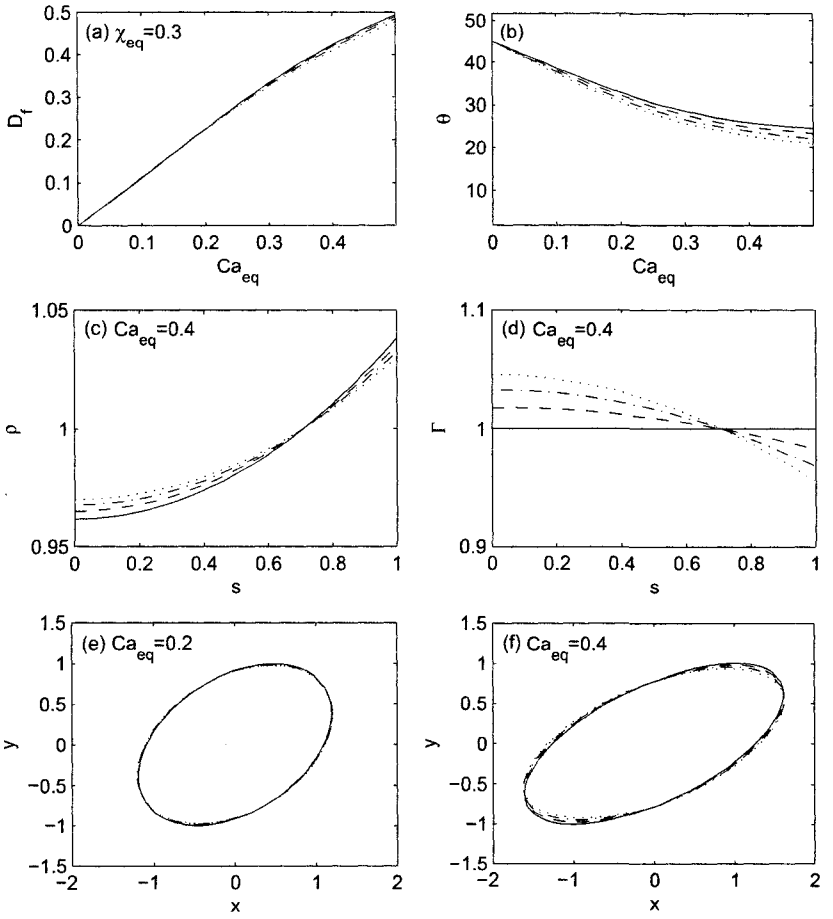

Figure 5.7: Influence of β_{eq} on the steady-state morphology for a droplet covered with a surface active agent with $p = 1$ and $\chi_{eq} = 0.3$. (—) corresponds to $\beta_{eq} = 0$, (- -) corresponds to $\beta_{eq} = 0.5$, (-.-) corresponds to $\beta_{eq} = 1$, and (...) corresponds to $\beta_{eq} = 1.5$. (a) D_f vs Ca_{eq}, (b) θ vs Ca, (c) ρ vs s at $Ca_{eq} = 0.4$, (d) Γ vs s at $Ca_{eq} = 0.4$, (e) droplet for $Ca_{eq} = 0.2$, (f) droplet for $Ca_{eq} = 0.4$.

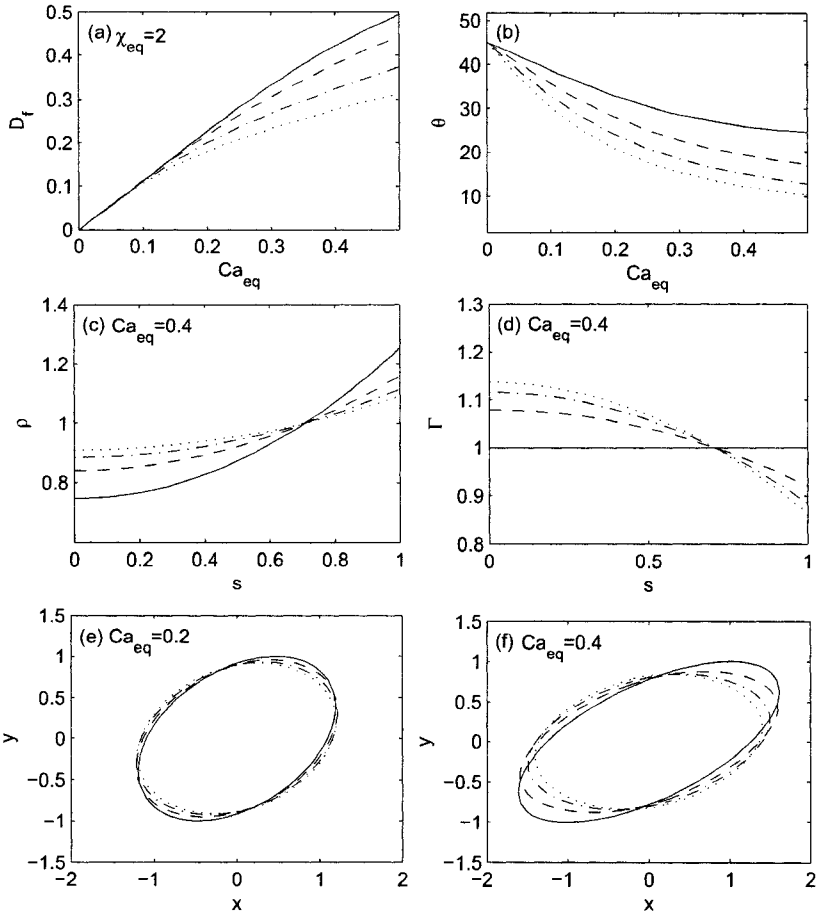

Figure 5.8: The same as Fig.5.7 except that $\chi_{eq} = 2$.

microhydrodynamic equations by Milliken and Leal[14] for blends with a soluble surfactant.

An increase in the capillary number Ca_{eq} has two opposite effects on deformations of the droplet. On the one hand, it makes the droplet more deformed because of the stronger imposed flow, on the other hand, the gradient of the surfactant concentration $\rho(s)$ becomes larger which then tends to suppress the deformation due to the Marangoni force. The similar effect has then also the surface dilution due to the increase of the surface of the droplet. Which of these two influences prevail depends then on the transport number χ_{eq}. This is shown on Figures 5.7(e,f) and 5.8(e,f).

We also note that when $\beta_{eq} \neq 0$, a larger χ_{eq} leads to a smaller deformation of the droplet and a smaler orientation angle, which is the same behavior as if the droplet were more viscous.

Effect of the elasticity number β_{eq}

The elasticity number β_{eq} (see (5.43)) represents the importance of the interfacial gradient relative to the reduced uniform interfacial tension. Given the surfactant, the coefficient ε (see (5.45)) is fixed. An increase of β_{eq} corresponds to an increase of the concentration of the surfactant. The solid lines on Figures 5.7 and 5.8 represent the case when $\varepsilon = 0$ (see (5.45)), i.e. the case when the surfactant has no effect on the interfacial tension. The surfactant distribution becomes very nonuniform while the distribution of the surface tension is completely uniform. The deformation parameter D_f and the orientational angle θ are the same as if the interface were clean.

If $\varepsilon \neq 0$ then an increase in β_{eq} increases the Marangoni force which then inhibits the convection of the surfactant. This in turn yields a decrease in the slope of $\rho(s)$ as displayed on Figures 5.7(c) and 5.8(c). Since the Marangoni force decreases the interfacial velocity, the droplet becomes more rigid. It is like if the the droplet were more viscous. This also explains why the droplet becomes more align to the flow direction as β_{eq} increases.

Figures 5.8(e) and 5.8(f) also show that as β_{eq} increases the droplet tends to bulge in the middle and stretch at the ends provided the capillary number is large (larger than 1). Van Puyvelde *et al.*[37] has observed this type of morphology for a

compatibilized immiscible polymer blend with both fluids A and B being nearly Newtonian for $Ca_{eq} \approx 6$.

Effect of the viscosity ratio p

Figure 5.9 illustrates the influences of the viscosity ratio p on the droplet deformations. We see that a large p leads to smaller deformations and smaller orientational angles θ and thus to the morphology of surfactant-free droplets. In contrast to the influence of β_{eq}, as p increases both ρ and Γ become more uniformly distributed. The viscosity of the droplet fluid (i.e. the fluid B) tends to suppress the effect of the surfactant. Figures 5.9(e) and 5.9(f) show that the smaller is p the easier it is for the droplet to form bulge wrists and tip ends. Predictions of the microhydrodynamics theories[2,38,39] and results of experimental observations[35] also show that the effect of the surfactant is more pronounced for less viscous fluid B.

Effect of κ_{eq}

The value of κ_{eq} calculated from (5.43) with α being the inverse of the mass density of the fluid A is in the range $10^2 - 10^{10}$. Numerical solutions of Eqs.(5.40) show that if κ_{eq} varies in the range $10 < \kappa_{eq} < 10^{16}$ the morphology remains essentially unchanged.

Rheology

Now we turn to the rheology. On the three Figures 5.10, 5.11 and 5.12 we show: (a) the interfacial shear stress, (b) the total shear stress, (c) the interfacial first normal stress difference, and (e) the interfacial second normal stress difference. All the stresses are normalized by the shear stress of the matrix fluid A ($\eta_m \dot{\gamma}$). Figures 5.10 and 5.11 display the influences of the transport number χ_{eq}, the capillary number Ca_{eq} and the elasticity number β_{eq} on the steady-state stress with p and κ_{eq} fixed. The same values of the parameters are used also on Figures 5.7 and 5.8. The total shear stress is calculated by Eq.(5.67) and Eq.(5.71). Figure 5.12 examines the effect of the viscosity ratio on the steady-state shear stress as

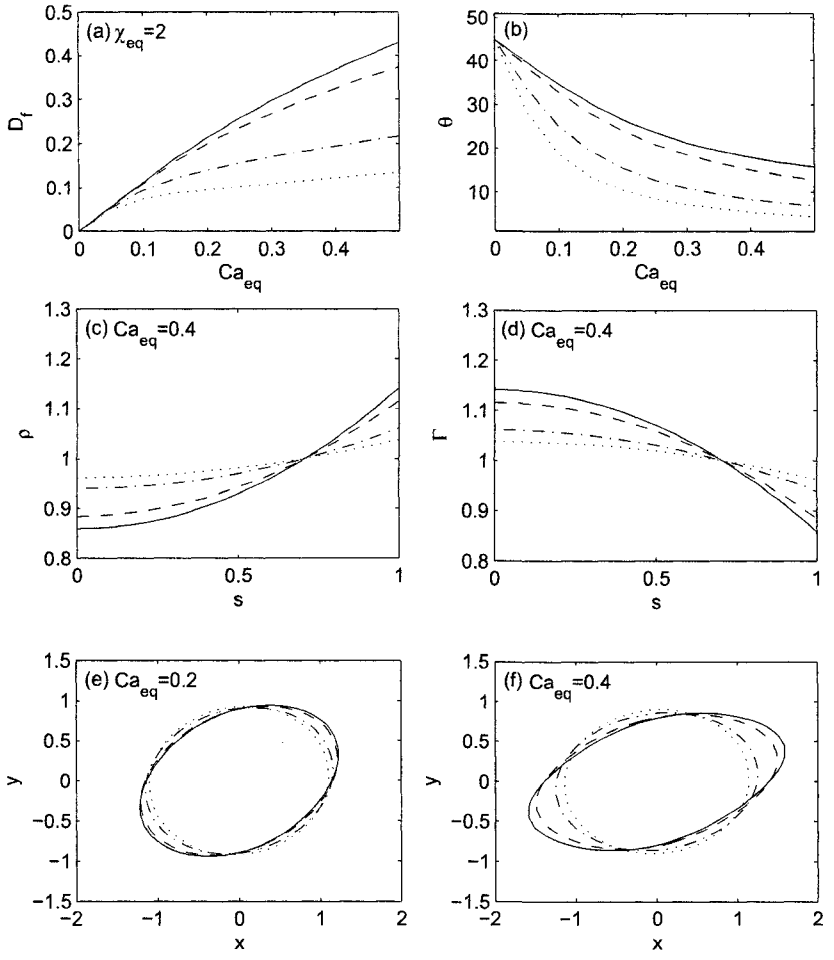

Figure 5.9: Influence of the viscosity ratio p on the steady-state morphology of a droplet covered with a surface active agent with $\beta_{eq} = 1$ and $\chi_{eq} = 2$. (—) corresponds to $p = 0.2$, (- -) corresponds to $p = 1$, (-.-) corresponds to $p = 5$, and (...) corresponds to $p = 10$. (a) D_f vs Ca_{eq}, (b) θ vs Ca, (c) ρ vs s for $Ca_{eq} = 0.4$, (d) Γ vs s at $Ca_{eq} = 0.4$. (e) Droplet with $Ca_{eq} = 0.2$, and (f) with $Ca_{eq} = 0.4$.

a function of Ca_{eq} with $\chi_{eq} = 2$ and $\beta_{eq} = 1$. The volume fraction is $\phi = 0.1$ in all the calculations.

Effect of χ_{eq} and Ca_{eq}

Figures 5.10 and 5.11 reveal the impact of χ_{eq} and Ca_{eq} on the rheology. We see that when $\beta_{eq} \neq 0$ then the larger is χ_{eq} the smaller is the interfacial shear stress and the larger is the total shear stress. This is because the motion of the interface is inhibited by the gradient of the interfacial tension. This finding is displayed on Figures 5.7(c) and 5.8(c).

On the other hand, the first normal stress difference decreases as χ_{eq} increases. For large χ_{eq} the droplet thus starts to behave like if the fluid B were more viscous and no elastic deformations took place. This observation is consistent with the observation that we made about the morphology.

For the second normal stress difference, shown on Figures 5.7(d) and 5.8(d), the influence of β_{eq} is reversed. We have no direct explanation for this observation.

As Ca_{eq} increases, the decreased shear stress and increased first normal stress difference demonstrate the shear thinning and elasticity enhancing phenomena.

Effect of the elasticity number β_{eq}

Figures 5.10 and 5.11 also display the influence of the elasticity number β_{eq} on the rheology of a dilute emulsion. When $\beta_{eq} = 0$ then the surfactant has no effect on the interfacial tension and consequently the rheology of the blend is the same as if the surface active agent were absent. When β_{eq} increases, the Marangoni stress causes the interfacial velocity to decrease and thus the effective viscosity of the droplet increases. This leads then to a decrease in the interfacial shear stress and in the first normal stress difference and to an increase in the total viscosity. The experiments of Velankar *et al.*[40] and Riemann *et al.*[41] show that the compatibilized blends have higher viscosity than uncomptibilized ones. Van Hemelrijck *et al.*[42] also observed in their experiments that highly compatibilized (large β_{eq}) blends behave as suspensions with solid spheres, and its viscosity can be approximated by Einstein's formula, i.e. by $\sigma_{12} \approx 1 + 0.25\phi$.

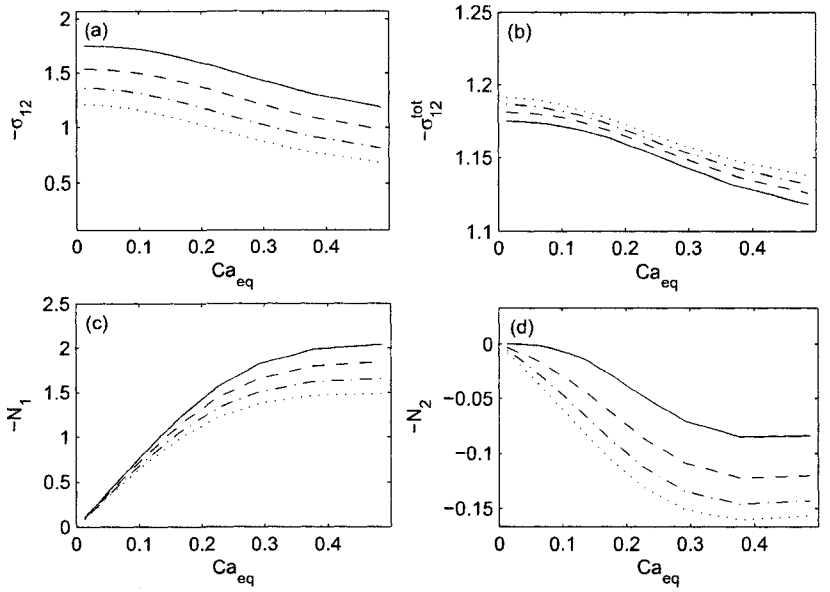

Figure 5.10: Influence of β_{eq} on the steady-state shear stress as a function of Ca_{eq} for an immiscible blend with a surface active agent with $\chi_{eq} = 0.3$. (—) corresponds to $\beta_{eq} = 0$, (- -) corresponds to $\beta_{eq} = 0.5$, (-.-) corresponds to $\beta_{eq} = 1$, and (...) corresponds to $\beta_{eq} = 1.5$. (a) the interfacial shear stress $-\sigma_{12}$, (b) the total shear stress $-\sigma_{12}^{tot}$ for the viscosity ratio $p = 1$ and the volume fraction $\phi = 0.1$, (c) the interfacial first normal stress difference $-N_1$, (d) the interfacial second normal stress difference $-N_2$.

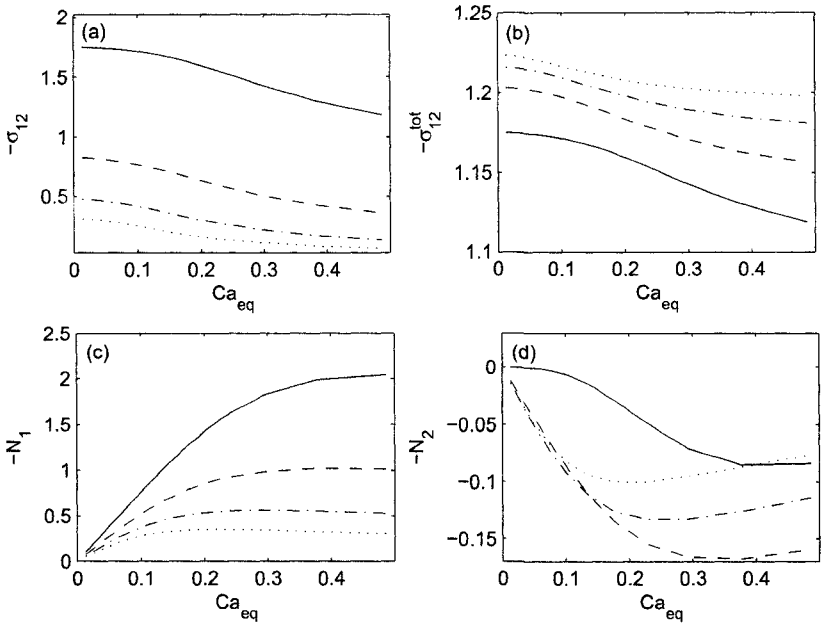

Figure 5.11: The same as Fig.(5.10) except that $\chi_{eq} = 2$.

Effect of the viscosity ratio p

Figure 5.12 examines the effect of the viscosity ratio p on the steady-state shear stress. When p increases, all the interfacial stresses decrease except for the total shear stress. The shear thinning effect is also diminished as p reaches a high value. This is because the droplets become stiffer. This results is in accordance with the experimental observations of Valenkar *et al.*[40] .

5.5 Conclusion

Instead of using microhydrodynamics to investigate immiscible blends (as it is done for example in Refs.1-7) we follow in this paper the mesoscopic viewpoint[8–12] leading to governing equations that can be solved relatively easily. Our objective is to extend the Maffettone-Minale model[9] to blends involving a surface active agent residing mainly on the interface (assumed to be the surface of droplets). The most important new physics that arises in this type of blends is the transport, induced by the imposed flow, of the surface active agent. As a result, its

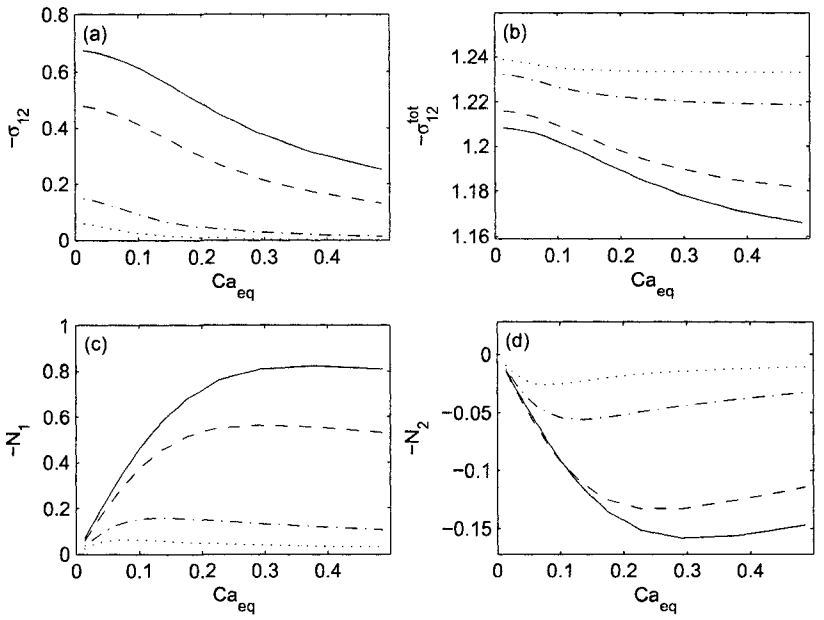

Figure 5.12: Influence of the viscosity ratio p on the steady-state shear stress as a function of Ca_{eq} for an immiscible blend with a surface active agent with $\chi_{eq} = 2$, $\beta_{eq} = 1$ and $\phi = 0.1$. (—) corresponds to $p = 0.2$, (- -) corresponds to $p = 1$, (-.-) corresponds to $p = 5$, and (...) corresponds to $p = 10$. (a) The interfacial shear stress $-\sigma_{12}$, (b) the total shear stress $-\sigma_{12}^{tot}$, (c) the interfacial first normal stress difference $-N_1$, (d) the interfacial second normal stress difference $-N_2$.

distribution as well as the distribution of the surface tension on the surface of droplets become nonuniform. Such nonuniformity then brings about new forces (Marangoni forces) and large deviations from the ellipsoidal shape of droplets. The features that remain outside the scope of this paper include the droplet breakup and coalescence. We also do not investigate the effect of nonlinearity of the surface equation of state (the dependence of the surface tension on the concentration of the surface active agent).

In order to be able to discuss nonuniform distributions on the droplet surface, we have to introduce on it some coordinates. For the sake of simplicity, we use in this paper only one such coordinate (denoted s), namely the coordinate that follows the principal axis of the droplet. The morphology is characterized by a family (parametrized by s) of ellipsoids. The family is referred to as a "necklace". The transport on the surface of the droplet becomes the transport along the backbone of the necklace. Alternatively, we can interpret the necklace characterization of the morphology as a polydispersity in the distribution of droplets. Each droplet has, in general, a different amount of the surface active agent uniformly distributed on it and a corresponding to it different ellipsoidal shape. From the mathematical point of view, an ellipsoid is characterized by a symmetric positive definite matrix $\boldsymbol{c}$ and thus the necklace morphology is characterized by a one parameter family $\boldsymbol{c}(s)$ of such matrices.

With this type of state variables, we then construct a dynamical model. We do it by following the GENERIC formulation[20]. The overall structure of the governing equations is implied by requiring the compatibility of dynamics with thermodynamics. The overall structure is then filled by the physics of immiscible blends expressed in terms of kinematics, free energy and dissipation potential.

From solutions of the governing equations of the model we extract rheology, morphology, and distribution of the surface active agent. In this paper we simplify the process of solving the governing equations by assuming that the transport equation for the surface active agent is decoupled from the remaining equations. Following Ref.1, we solve a simplified form of the transport equation analytically. The remaining equations become then a system of ordinary differential equations that can be readily solved. The phenomenological parameters entering the model are specified by comparing closed form particular solutions of the governing equations of the model with corresponding closed form particular

solutions of governing equations of other types of models. The rheology and the morphology calculated from the model developed in this paper compare well with results implied by other models and with results of experimental observations.

Acknowledgment

This research has been partially supported by the Natural Sciences and Engineering Research Council of Canada

5.6 Appendix: Concentration of the surface active agent on the interface

An approximative analytical expression for the mass density distribution $\rho(s,t)$ of the surface active agent is derived in this appendix from considerations that lie outside the mesoscopic level of description followed in this paper. The basis for the derivation is microhydrodynamics, in particular then the analysis reported in Refs. 1 and 36.

In the setting of microhydrodynamics, the time evolution of ρ is governed by the transport equation derived by Stone and Leal[2]. Let $\rho(s,t) = 1+\rho_1(s,t)$ where we use the dimensionless variables introduced in (5.40). We regard ρ_1, together with its first and the second derivatives with respect to s, as small perturbations. If we neglect diffusion along the interface then the transport equation (to the first order in ρ_1) takes the form[1]

$$\frac{\partial \rho_1}{\partial t} = -\frac{\partial v^{(interface)}}{\partial l} - \frac{\rho_1}{N_M} \tag{5.75}$$

The initial condition is: $\rho_1(s,0) = 0$ *for all* s. By $v^{(interface)}$ we denote the averaged velocity, tangent to the interface, of the surface active agent residing on the interface, l is the coordinate along the interface in the direction of the longest principal axis, and

$$N_M = \frac{\dot{\gamma}}{\frac{mK}{1+mK/h} + \frac{\hat{m}\hat{K}}{1+\hat{m}\hat{K}/\hat{h}}} \tag{5.76}$$

where $\dot{\gamma}$ is the shear rate of the imposed flow, h and $\hat{h}$ are the adsorptio/desorption rate constants, m,$\hat{m}$ are the mass transfer coefficients associated with the bulk phase transfer processes, and K,$\hat{K}$ are the equilibrium constants between interface and bulk phases. If $v^{(interface)}$ is independent of ρ_1 then the solution to (5.75) is

$$\rho_1 = -\left(1 - \exp(-\frac{t}{N_M})\right) N_M \frac{\partial v^{(interface)}}{\partial l} \tag{5.77}$$

If we assume that the interface is spherical then Flumerfelt at al. arrive at the following expression[1,36]: $v^{(interface)} = \frac{1}{\pi(p_{eff}+1)}(p_{eff} + 2(1-s^2))$. If this velocity is inserted into (5.77), the expressions (5.34) and (5.35) are obtained. Flumerfelt has shown that the presence of the surface active agent influences the flow field on and near the droplet surface only by changing p into p_{eff}.

In order to see more the physical interpretation of the effective viscosity ratio p_{eff}, we rewrite it (see (5.36)) in a new form

$$p_{eff} = p + \frac{6}{5}\frac{\tau_\rho}{\tau_c}\beta \tag{5.78}$$

where

$$\tau_\rho = \frac{1}{\left(\frac{mK}{1+mK/h} + \frac{\hat{m}\hat{K}}{1+\hat{m}\hat{K}/h}\right)} \tag{5.79}$$

and

$$\tau_c(s) = \frac{\eta_m a}{\Gamma(s)} \tag{5.80}$$

Both τ_ρ and τ_c are relaxation times: τ_ρ is the relaxation time of the transport of the surface active agent (assumed to be constant over the entire interface), and τ_c is the local relaxation time of the interface. The ratio of these two times controls the strength of the influences of the surface active agent. We note that when $\beta\tau_\rho \ll \tau_c$, the surface active agent has a little effect on the effective viscos-

ity ratio and consequently the droplet behaves as if it has a clean interface with a reduced interfacial tension. On the other hand, when $\beta\tau_\rho \gg \tau_c$ the effective viscosity ratio tends to infinity and the droplet behaves like a solid sphere.

References

[1]R. W. Flumerfelt, "Effects of dynamic interfacial properties on drop deformation and orientation in shear and extensional flow fields," J. Colloid Interface Sci. **76**, 330 (1980).

[2]H. A. Stone and L. G. Leal, "The effects of surfactants on drop deformation and breakup," J. Fluid Mech. **220**, 161 (1990).

[3]P. M. Vlahovska, M. Loewenberg, and J. Blawzdziewicz, "Deformation of a surfactant-covered drop in a linear flow," Phys. Fluids **17**, 103103 (2005).

[4] Y. Pawar and K.J. Stebe, "Marangoni effects on drop deformation in an extensional flow: The role of surfactant physical chemistry. I. Insoluble surfactants" Phys. Fluids **8**, 1738 (1996)

[5] C.D. Eggleton and K.J. Stebe, "An Adsorption-Desorption-Controlled Surfactant on a Deforming Droplet", J. Colloid Interface Sci. **208**, 68 (1998)

[6] C.D. Eggleton, Y.P. Pawar, K.J. Stebe, " Insoluble surfactants on a drop in an extensional flow: a generalization of the stagnated surface limit to deforming interfaces" J.Fluid Mech. **385**, 79 (1999)

[7] I.B. Bazhlekov, P.D. Anderson, H.E.H. Meijer, " Numerical Investigation of the Effect of Insoluble Surfactants on Drop Deformation and Breakup in Simple Shear Flow" J. Colloid Interface Sci. **298**, 369 (2006)

[8] M. Doi and T. Ohta, "Dynamics and rheology of complex interfaces," J. Chem. Phys. **95**, 1242 (1991).

[9] P. L. Maffettone and M. Minale, "Equation of change for ellipsoidal drops in viscous flow," J. Non-Newtonian Fluid Mech. **78**, 227 (1998).

[10] M. Grmela, M. Bousmina, and J. F. Palierne, "On the rheology of immiscible blends," Rheol. Acta **40**, 560 (2001).

[11] W. Yu and M. Bousmina, "Ellipsoidal model for droplet deformation in emulsions," J. Rheol. **47**, 1011 (2003).

[12] N. E. Jackson and C. L. Tucker III, "A model for large deformation of an

ellipsoid droplet with interfacial tension," J. Rheol. **47**, 659 (2003).

[13] M.R. Booty and M. Siegel, " Steady deformation and the tip-streaming of a slender bubble with surfactant in an extensional flow" J.Fluid Mech. **544**,243-275 (2005)

[14] W.J. Milliken and L.G. Leal, "The influence of surfactant on the deformation and breakup of a viscous drop: The effect of surfactant solubility" J. Colloid Interface Sci. **166**, 275 (1994)

[15] Y.T. Hu, D.J. Pine and L.G. Leal, " Drop deformation, breakup, and coalescence with compatibilizer" Phys. Fluids **12**, 484 (2000)

[16]J. D. Eshelby,"The determination of the elastic field of an ellipsoidal inclusion, and related problems" Proc. R. Soc. London, Ser. A **241**, 376 (1957); J. D. Eshelby, "The elastic field outside an ellipsoidal inclusion" Proc. R. Soc. London, Ser. A **252**, 561 (1959).

[17] J. F. Gu and M. Grmela, "GENERIC Model of Active Advection," J. Non-Newtonian Fluid Mech. (2007) in press.

[18]J. E. Marsden and A. Weinstein, " Coadjoint orbits, vortices, and Clebsch variables for incompressible fluids" Physica D **7**, 305 (1983)

[19]B. J. Edwards, M. Dressler, M. Grmela, and A. Ait-Kadi, "Rheological models with microstructural constraints," Rheol. Acta **42**, 64 (2003)

[20]M. Grmela and H. C. Ottinger, "Dynamics and Thermodynamics of Complex Fluids. Part I: Illustration of a General Formalism," Phys. Rev. E **56**, 6620 (1997); H. C. Ottinger and M. Grmela, "Dynamics and Thermodynamics of Complex Fluids. Part II: Development of a General Formalism," Phys. Rev. E **56**, 6633 (1997)

[21]J. W. Cahn and J. E. Hilliard, "Free energy of a nonuniform system. I. Interfacial free energy," J. Chem. Phys. **28**, 258 (1958)

[22]M. Dressler and B. J. Edwards, "The influence of matrix viscoelasticity on the rheology of polymer blends," Rheol. Acta **43**, 257 (2004).

[23] G. I. Taylor, "The formation of emulsions in definable field of flow," Proc. R. Soc. London, Ser. A **146**, 501 (1934).

[24]R. J. Gordon and W.R. Schowalter, "Anisotropic fluid theory: A different approach to the dumbbell theory of dilute polymer solutions," Trans. Soc. Rheol. **16**, 79 (1972).

[25]J. M. Rallison, "Note on the time-dependent deformation of a viscous drop

which is almost spherical," J. Fluid Mech. **98**, 625 (1980).

[26]S. J. Choi and W.R. Schowalter, "Rheological properties of non-dilute suspensions of deformable particles," Phys. Fluids **18**, 420 (1975).

[27]J. F. Palierne, "Linear rheology of viscoelastic emulsions with interfacial tension," Rheol. Acta **29**, 204 (1990); Erratum **30**, 497 (1991).

[28]D. Graebling, R. Muller, and J. F. Palierne, "Linear viscoelastic behavior of some incompatible polymer blends in the melt. Interpretation of data with a model of emulsion of viscoelastic liquids," Macromolecules **26**, 320 (1993).

[29]W. Yu, M. Bousmina, M. Grmela, J. -F. Palierne, and C. Zhou, "Quantitative relationship between rheology and morphology in emulsions," J. Rheol. **46**, 1381 (2002).

[30]G. I. Taylor, "The viscosity of a fluid containing small drops of another fluid," Proc. R. Soc. London, Ser. A **138**, 41 (1932).

[31]R. G. Cox, "The deformation of a drop in a general time-dependent fluid flow," J. Fluid Mech. **37**, 601 (1969).

[32]S. Guido and M. Villone, "Three-dimensional shape of a drop under simple shear flow," J. Rheol. **42**, 395 (1998)

[33]S. Torza, R. G. Cox, and S. G. Mason, "Particle motions in sheared suspensions. XVII. Transient and steady deformation and burst of liquid drops," J. Colloid Interface Sci. **38**, 395 (1972).

[34]T. Jansseune, I. Vinckier, P. Moldenaers, and J. Mewis, "Transient stresses in immiscible model polymer blends during start-up flows," J. Non-Newtonian Fluid Mech. **99**, 167 (2001).

[35]D. Megias-Alguacil, P. Fischer, and E. J. Windhab, "Determination of the interfacial tension of low density difference liquid-liquid systems containing surfactants by droplet deformation methods," Chem. Eng. Sci. **61**, 1386 (2006).

[36]W. J. Phillips, R. W. Graves, and R. W. Flumerfelt, "Experimental studies of drop dynamics in shear fields: role of dynamic interfacial effects," J. Colloid Interface Sci. **76**, 350 (1980).

[37]P. Van Puyvelde, S. Velankar, J. Mewis, and P. Moldenaers, "Effect of marangoni stresses on the deformation and coalescence in compatibilized immiscible polymer blends," Polym. Eng. Sci., **42**, 1956 (2002).

[38]X. Li and C. Pozrikidis, "The effect of surfactants on drop deformation and on the rheology of dilute emulsions in Stokes flow," J. Fluid Mech. **341**, 165

(1997).

[39] W, J. Milliken, H. A. Stone and L. G. Leal, "The effect of surfactant on transient motion of newtonian drops," Phys. Fluids A **5**, 69 (1993).

[40]S. Velankar, P. Van Puyvelde , J. Mewis, and P. Moldenaers, "Steady shear rheological properties of model compatibilized blends," J. Rheol. **48**, 725 (2004).

[41]R. -E. Riemann, H, -J. Cantow, and C. Friedrich, "Rheological investigation of form relaxation and interface relaxation processes in polymer blends," Polymer Bulletin. **36**, 637 (1996).

[42]E. Van Hemelrijck,P. Van Puyvelde, and P. Moldenaers, "Rheology and morphology of highly compatibilized polymer blends," Macromol. Sym. **233**, 51 (2006).

Chapter 6

Mesohydrodynamics of Membrane Suspensions

Jian Feng Gu[1], Miroslav Grmela[1,3] , Mosto Bousmina[2]

[1] Ecole Polytechnique de Montreal, C.P.6079 suc. Centre-ville, Montreal, H3C 3A7, Quebec, Canada

[2] Hassan II Academy of Sciences and Technology, Rabat, Marocco

Submitted to J. Non-Newtonian Fluid Mech. (2008)

[3]corresponding author: e-mail: miroslav.grmela@polymtl.ca

abstract

A new mesoscopic rheological model of human blood is developed. The blood is regarded as a suspension of elastic membranes whose morphology is described by a set of fields extending the fields used as morphological state variables in mesoscopic rheological models of immiscible blends. The predicted rheological behavior is qualitatively in agreement with experimental observations. The inferred material properties of the membranes are also found to be close the ones seen in direct experimental measurements.

6.1 Introduction

Our objective in this paper is to investigate theoretically rheological properties of human blood. The key question that we have to address at the outset of the investigation is of how to describe its complex morphology. We require the description to be simple enough (in order to allow us to arrive at governing equations that can be solved with a standard software) but still sufficiently rich to catch the features that are of essential importance in determining the flow properties. We make the choice in Section 6.2.2. Roughly speaking, we suggest to regard blood as a suspension of elastic membranes whose morphology is described by several scalar and tensor fields extending the set of fields used as the morphological state variables in mesoscopic rheological modeling of immiscible blends. In order to motivate the choice we recall below some well known facts about human blood. The final judgement about the pertinence of our morphological description has to come however from the comparison (made in Section 6.5) of model predictions with results of experimental observations.

Human blood is composed of blood cells suspended in a liquid called blood plasma. The blood cells are mainly red blood cells (also called RBCs or erythrocytes) and white blood cells, including leukocytes and platelets (also called thrombocytes). Red blood cells normally occupy about 42-45% of the blood volume. Plasma, comprising 55% of blood fluid, is mostly water (90% by volume). Although the plasma is a Newtonian fluid, the overall rheological behavior of the blood is non-Newtonian. The measured viscosity usually shows a shear thinning phenomenon. The complexity of the blood rheology is mainly caused by the high

deformability of the membranes of red blood cells. The deformations are constrained by keeping the volume and surface area of the cells constant (or almost constant). In the absence of externally applied forces, these two constraints give the red blood cells the characteristic biconcave shape.

The membrane of red blood cells can be roughly seen as a cytoskeleton network covered by a lipid bilayer. The cytoskeleton is a two-dimensional network of spectrin filaments [1]. The bilayer behaves like a surface fluid with negligible change in area per lipid [2]. The cytoskeleton controls the shear elasticity (deformations of the membrane with keeping the surface are unchanged). The lipid bilayer controls the surface changing deformations, bending, and the surface viscosity within the membranes. Evans and Hochmuth [3] found that the dissipation caused by this viscosity is about two order greater than the dissipation in the internal hemoglobin solution. It also plays a dominant role in resisting the recovery process of membranes.

The experimental techniques used to investigate the morphology include: (1) Aspiration of the cell membrane into a micropipette; (2) Observation through rheoscope; (3) The extensional recovery of red blood cells; (4) Rheological measurement of a suspension of RBCs. The first three are microscopic measurements, which usually need special instruments and great care. The last one is a macrorheological measurement which is much easier to carry out. It needs however a rheological model to translate the rheological results into morphological results. Its accuracy can be improved by improving the rheological models. This is one of the motivations for developing the models.

On the theoretical side, suspensions or emulsion containing solid or liquid dispersions have already been studied for a long time. Among the well known models we mention the microhydrodynamic models [4, 5, 6, 7] and the mesohydrodynamic models [8, 18, 20, 21]. Much smaller number of rheological models have been developed for RBCs suspensions. The difficult questions that arise when dealing with blood rheology are the following: (1) How to describe mathematically (in a simple yet sufficiently complete way) the complex shape of red blood cells. (2) How to correctly express the macroscopic bulk rheology of the suspension via the microscopic local material properties of membranes.

The microhydrodynamic viewpoint of treating these questions consists of writing down the microhydrodynamic governing equations (the Navier-Stokes equa-

tion) together with boundary conditions (on the bulk membrane interface and at infinity) and then solving them. The governing equations are usually straightforward to write down but very difficult to solve. Moreover, their solutions only address the morphology. There is still another step and other approximations to make in order to arrive at rheological consequences.

An analytical solution of the microhydrodynamic equations has been obtained by Barthès-Biesel and Rallison [22] by using a perturbation analysis . They represent the biconcave-shape red blood cell by a initially spherical capsule or vesicle, i.e., a droplet of Newtonian fluid enclosed by a deformable membrane which is modeled as a pure elastic skin. In the limiting case of small deformations the governing equations are linearized and an analytical solution can be found. To get an expression for the extra stress tensor, the Batchelor's equation [23] for dilute suspensions was used. Recently, also in the case of small deformations, Danker et.al. [24] studied the rheology of a dilute suspension of vesicles. Instead of starting from a sphere as Bathès-Biesel and Rallison, their point of departure is an ellipsoid. With the constraint of keeping constant the surface area, a nonlinear solution of deformations at the leading order is obtained. Again, the stresses of the suspension are calculated by using Batchelor's expression [39]. Pal [25] has developed a model for the viscosity of concentrated suspensions of deformable elastic particles using the differential effective medium approach (DEMA).

Numerical solutions of the microhydrodynamic governing equations have been found in [26], [28] (by using the boundary integral method), in [32] (by using the immersed boundary method), and in [33] (by using the boundary element method).

As for the experimental investigation of rheology, RBC suspensions have received less attention than liquid dispersions. Carr and Cokelet [29] made an attempt to relate bulk rheological measurements to the intrinsic membrane properties. Later, Drochon et.al. [30] successfully obtained the elastic modulus of the membranes from the apparent shear viscosity. They used the microrheological model of Barthès-Biesel and Rallison's model. Later, a more accurate data and a refined method were proposed by Drochon [31]. The shear moduli that they obtain are in good agreement with those obtained in direct observations of the morphology. Altered or pathological cells can be recognized in these rheological observations.

A new rheological model of suspensions of RBCs is developed in this paper. Unlike the models based on microhydrodynamics, this model is formulated from the outset on a mesoscopic level. The focus is put on rheology, the treatment of the morphology does not allow to reconstruct shapes of individual cells. The model is constructed as an appropriate extension of the Doi-Ohta model of immiscible blends. Predictions of the model are compared with experimental data of Drochon [31] and with predictions of other models. We also calculate material properties of the cell membranes and compare them with existing data.

6.2 Mesoscopic model

We begin with a mesoscopic picture of the physics taking place in blood subjected to a flow. We then translate it into governing equations of our rheological model by using the thermodynamic (GENERIC) framework. We shall now briefly present the framework and illustrate its use (in Section 6.2.1) on the derivation of the familiar governing equations of simple fluids. The same steps are then made in Section 6.2.2 to arrive at new governing equations of our rheological model of human blood.

Let the macroscopic system under consideration be kept at a constant temperature T. Let x denote the state variables and $\Phi(x,T)$ the free energy. It has been shown in [9, 10, 11, 13, 14, 15, 17] that solutions to

$$\frac{dx}{dt} = \left(\frac{dx}{dt}\right)_{nondiss} + \left(\frac{dx}{dt}\right)_{diss} \tag{6.1}$$

$$\left(\frac{dx}{dt}\right)_{nondiss} = L\Phi_x \tag{6.2}$$

$$\left(\frac{dx}{dt}\right)_{diss} = -\frac{\partial \Xi}{\partial \Phi_x} \tag{6.3}$$

satisfy the conservation laws, compatibility with thermodynamics and compatibility with mechanics provided the the operator L and the potential Ξ satisfy certain properties. By Φ_x we denote derivative of the free energy (a real valued function of x) with respect to x. From the physical point of view, the operator L, transforming a covector Φ_x into a vector, expresses the kinematics of the state

variables x. For example, let $x = \begin{pmatrix} q \\ p \end{pmatrix}$, where q is the position vector and p momentum of a particle, then $L = \begin{pmatrix} 0 & 1 \\ -1 & 0 \end{pmatrix}$. The potential Ξ, a real valued function of Φ_x, is called a dissipation potential.

The compatibility with thermodynamics is mathematically expressed by the inequality

$$\begin{aligned} \left(\frac{d\Phi}{dt}\right)_{nondiss} &= 0 \\ \left(\frac{d\Phi}{di}\right)_{diss} &\leq 0 \end{aligned} \tag{6.4}$$

(i.e. the free energy does not grow during the time evolution). The compatibility with mechanics is expressed by requiring the time evolution governed by

$$\frac{dx}{dt} = L\Phi_x \tag{6.5}$$

be Hamiltonian. This means that the bracket $\{A, B\}$ defined as $\{A, B\} =< A_x, LB_x >$, where $<,>$ denotes the scalar product, is a Poisson bracket. The conservation laws are expressed mathematically by

$$\frac{dE}{dt} = 0; \quad \frac{dM}{dt} = 0; \quad \frac{d\boldsymbol{U}}{dt} = 0 \tag{6.6}$$

where $E(x), M(x), \boldsymbol{U}(x)$ denote respectively the energy, mass, and momentum. All three properties (6.4), (6.5), and (6.6) can be guaranteed by requiring L and Ξ to possess certain properties. Instead of presenting them in the general context (see [13, 14]), we shall show below the specific forms of L and Ξ that they acquire in the familiar context of simple fluids. The new time evolution equations are introduced in Section 6.2.2 by modifying appropriately x, L and Ξ.

6.2.1 Simple fluids

Let the fluid under investigation be a simple fluid (e.g. water) kept at a constant temperature $T \sim \textit{room temperature}$ and assumed to be incompressible. The familiar Navier-Stokes equation governing its time evolution is introduced as

follows.

State variables

We choose to describe states of simple fluids by the momentum field

$$x = (\boldsymbol{u}(\boldsymbol{r})) \tag{6.7}$$

where $\boldsymbol{r}$ denotes the position coordinate.

Kinematics

In order to derive kinematics of (6.7), we recall that the motion of continuum is a continuous family of transformations $\mathbf{R}^3 \to \mathbf{R}^3$. These transformations form a Lie group; the momentum field is an element of the dual of the Lie algebra corresponding to the group. A canonical relation [16] between Lie algebras and Poisson structures then leads directly to the following Poisson bracket

$$\{A, B\}^{(u)} = \int d\boldsymbol{r} u_i (\partial_j (A_{u_i}) B_{u_j} - \partial_j (B_{u_i}) A_{u_j}) \tag{6.8}$$

We use the summation convention, A and B are sufficiently regular real valued functional of $\boldsymbol{u}(\boldsymbol{r})$, $A_{u_j} = \frac{\delta A}{\delta u_j(\boldsymbol{r})}$, by δ/δ we denote the Volterra functional derivative, $\partial_j = \partial/\partial r_j$.

Dissipation potential

The Navier-Stokes dissipation can be cast it the form of the second term on the right hand side of (6.1) by choosing

$$\Xi(\Phi_u) = \int d\boldsymbol{r} D_{ij} \frac{1}{2} \eta D_{ij} \tag{6.9}$$

where $D_{ij} = \frac{1}{2}(\Phi_{u_i} + \Phi_{u_j})$, $\eta > 0$ is the shear viscosity coefficient.

Free energy

For incompressible isothermal fluids we shall simply take the free energy to be the kinetic energy

$$\Phi(\boldsymbol{u}) = \int d\boldsymbol{r} \frac{\boldsymbol{u}^2}{2\rho} \tag{6.10}$$

where ρ denotes the constant mass density. Note that $\Phi_u = \frac{\boldsymbol{u}}{\rho}$ is the velocity field.

Governing equations

If we now put (6.7),(6.8),(6.9), and (6.10) into (6.1) we arrive at the Navier-Stokes equation

$$\left(\frac{\partial u_i}{\partial t}\right)_{nondiss} = -\partial_j(u_i \Phi_{u_j}) - \partial_i p - \partial_j \sigma_{ij} \tag{6.11}$$

$$\left(\frac{\partial u_i}{\partial t}\right)_{diss} = \partial_j(\eta D_{ij}) \tag{6.12}$$

where $p = -\phi(\boldsymbol{r}) + u_j \Phi_{u_j}$; $\phi(\boldsymbol{r})$ is defined by $\Phi = \int d\boldsymbol{r}\phi(\boldsymbol{r})$, i.e. $\phi(\boldsymbol{r}) = \boldsymbol{u}^2/2\rho$; and $\boldsymbol{\sigma} = 0$.

6.2.2 Suspensions of membranes

We shall now follow the steps made in Section 6.2.1 but modify them appropriately in order to express the physics of human blood instead the physics of simple fluids.

State variables

The overall flow of suspensions of elastic membranes will again be characterized by the momentum field (6.7). However, now the fluid under consideration is complex. It possesses an internal structure that evolves in time on the scale comparable with the scale on which (6.7) evolves. Inspired by the choice of the internal state variables made in the context of immiscible blends in [8], we choose

$$x = (\boldsymbol{u}(\boldsymbol{r}), Q, \boldsymbol{q}, \boldsymbol{c}) \tag{6.13}$$

$$\frac{1}{2}\left[(tr\boldsymbol{c})^2 - tr(\boldsymbol{c}\cdot\boldsymbol{c})\right] = \frac{3}{4\pi}\frac{Q}{Q_0} \tag{6.14}$$

as microstructural state variables. By Q we denote the surface area of the membranes per unit volume. We assume that the membranes are uniformly distributed throughout the suspension so that Q is independent of $\boldsymbol{r}$; Q_0 is the surface area of undeformed membranes at equilibrium states. The symbol $\boldsymbol{q}$ denotes a symmetric traceless tensor characterizing the orientation of the membranes. The isotropic distribution corresponds to $\boldsymbol{q} = 0$. The state variables $(Q, \boldsymbol{q})$ have been introduced by Doi and Ohta in their mesoscopic investigation of immiscible blends. The membrane in this case is the interface between two immiscible fluid. In the case of human blood, the membranes of red cells have in addition their own internal structure. In order to be able to describe the intramembrane deformations, we introduce a conformation tensor (symmetric and positive definite) $\boldsymbol{c}$. The deformations characterized by $(Q, \boldsymbol{q})$ and the intramembrane deformations characterized by $\boldsymbol{c}$ cannot be however completely independent. We shall relate them by requiring that the surface area associated with $\boldsymbol{c}$ (characterized by the second invariant of $\boldsymbol{c}$) equals a normalized area Q. This requirement is expressed by the constraint appearing in (6.14)(we shall see below that the equilibrium value of $\boldsymbol{c}\ \frac{\boldsymbol{\delta}}{2\sqrt{\pi}}$).

Kinematics

To determine the kinematics of (6.13),(6.14), we combine the kinematics of the momentum field (6.8), the kinematics of $(Q, \boldsymbol{q})$ found in [18] (see also [37]), and [19] where the kinematics of the conformation tensor $\boldsymbol{c}$ subjected to constraints is investigated:

$$\begin{aligned}\{A,B\} &= \{A,B\}^{(u)} + \{A,B\}^{(Qq)} \\ &\quad + \int d\boldsymbol{r}\left[c_{\alpha\beta}A_{c_{\beta\gamma}}\partial_\alpha(B_{u_\gamma}) + c_{\alpha\gamma}A_{c_{\beta\gamma}}\partial_\alpha(B_{u_\beta})\right. \\ &\quad \left. -\frac{4\pi}{3Q^*}(c_{\varepsilon\varepsilon}c_{\alpha\gamma} - c_{\alpha\beta}c_{\beta\gamma})c_{\eta\mu}A_{c_{\eta\mu}}\partial_\alpha(B_{u_\gamma})\right] - (A \leftrightarrow B)\end{aligned} \tag{6.15}$$

where $(A \leftrightarrow B)$ means the same as above with A and B exchanged. The Poisson bracket $\{A,B\}^{(u)}$ is given in (6.8), and $\{A,B\}^{(Qq)}$ in [18](Note the coefficient of

the fourth term should be changed from 2 to 1).

Dissipation potential

The thermodynamic forces that drive the fluid to equilibrium are chosen as follows:

$$\Phi_Q \tag{6.16}$$

$$\Phi_{\boldsymbol{q}} \tag{6.17}$$

$$\Phi_{c_{ij}} - \frac{1}{3}(\delta_{ij} tr\boldsymbol{c} - c_{ij}) tr\left[(\boldsymbol{\delta} tr\boldsymbol{c} - \boldsymbol{c})^{-1} \cdot \Phi_{\boldsymbol{c}}\right] \tag{6.18}$$

The first two are the same as in the Doi-Ohta theory. It has been shown in [19] that the choice (6.18) of the third thermodynamic force guarantees the satisfaction of the constraint (6.14) in the dissipative time evolution (i.e. the time evolution governed by the second term on the right hand side of (6.1)).

If we restrict ourselves to states at which the thermodynamic forces are not too large (they disappear at equilibrium), then it suffices to consider the following quadratic dissipation potential potential:

$$\begin{aligned} \Xi \;=\; & \int d\boldsymbol{r} \Phi_Q \frac{1}{2} \Lambda_1 \Phi_Q + \int d\boldsymbol{r} \Phi_{q_{ij}} \frac{1}{2} \Lambda_2 \Phi_{q_{ij}} \\ & + \int d\boldsymbol{r} R_{ij} \frac{1}{2} \Lambda_3 c_{jk} R_{ki} \end{aligned} \tag{6.19}$$

where $\boldsymbol{R}$ is the thermodynamic force introduced in (6.18) and $\Lambda_1 > 0, \Lambda_2 > 0$ and $\Lambda_3 > 0$ are material parameters specified later.

Free energy

The following free energy

$$\Phi = \Phi^{(Qq)} + \Phi^{(c)} \tag{6.20}$$

where

$$\Phi^{(c)} = \int d\boldsymbol{r} \frac{H}{2} (tr\boldsymbol{c} - \frac{1}{2\sqrt{\pi}} ln det\boldsymbol{c}) \tag{6.21}$$

extends the free energy

$$\Phi^{(Qq)} = \int d\boldsymbol{r} \left[\frac{\boldsymbol{u}^2}{2\rho} + \Gamma Q + \frac{1}{2} K \left(\frac{Q}{Q_0} - 1 \right)^2 + C_2 \frac{\boldsymbol{q} : \boldsymbol{q}}{Q^2} \right] \tag{6.22}$$

used in the Doi-Ohta model (see [18, 37]) to suspension of elastic membranes. By Γ we denote the interfacial tension, K is the dilation modulus corresponding to the relative area variation of membranes, C_2 is the elastic modulus conjugating to the out-plane deformation of the membrane, and H is the extensional modulus corresponding to the in-plane shear or elongation of the membrane. The first term in Eq.(6.22) is the kinetic energy, the second term is the interfacial energy due to the interfacial tension of a liquid surface, the third and forth terms are the dilation and out-plane deformation elastic energy. The two terms in (6.21) represent the free energy associated with the in-plane shearing of a viscoelastic membrane. To express it, we use the free energy of a Hookean dumbbell. With the free energies specified in Eq.(6.21) and (6.22), the thermodynamic force that drive the system to equilibrium state can be written as

$$\Phi_{\boldsymbol{u}} = \boldsymbol{v} \tag{6.23}$$

$$\begin{aligned} \Phi_Q &= \Gamma + \frac{K}{Q_0} \left(\frac{Q}{Q_0} - 1 \right) - 2C_2 \frac{\boldsymbol{q} : \boldsymbol{q}}{Q^3} \\ \Phi_{\boldsymbol{q}} &= 2C_2 \frac{\boldsymbol{q}}{Q^2} \\ \Phi_{\boldsymbol{c}} &= \frac{H}{2} (\boldsymbol{\delta} - \frac{1}{2\sqrt{\pi}} \boldsymbol{c}^{-1}) \end{aligned} \tag{6.24}$$

Governing equations

By inserting x, L, Ξ specified above into (6.2) we obtain

$$\begin{aligned} \left(\frac{dQ}{dt} \right)_{nondiss} &= -tr \left(\boldsymbol{q} \cdot \nabla \Phi_{\boldsymbol{u}}^T \right) \\ \left(\frac{d\boldsymbol{q}}{dt} \right)_{nondiss} &= \left(\frac{\boldsymbol{q}}{Q} + \frac{2}{3} \boldsymbol{\delta} \right) tr \left(\boldsymbol{q} \cdot \nabla \Phi_{\boldsymbol{u}}^T \right) \end{aligned}$$

$$
\begin{aligned}
& - \left(\boldsymbol{q} + \frac{Q}{3}\boldsymbol{\delta}\right) \cdot \nabla \Phi_{\boldsymbol{u}}^T - \nabla \Phi_{\boldsymbol{u}} \cdot \left(\boldsymbol{q} + \frac{Q}{3}\boldsymbol{\delta}\right) \\
\left(\frac{d\boldsymbol{c}}{dt}\right)_{nondiss} &= \boldsymbol{c} \cdot \Phi_{\boldsymbol{u}} + \Phi_{\boldsymbol{u}}^T \cdot \boldsymbol{c} - \frac{4\pi}{3Q^*}\left((\boldsymbol{c} tr \boldsymbol{c} - \boldsymbol{c} \cdot \boldsymbol{c}) : \Phi_{\boldsymbol{u}}\right) \boldsymbol{c} \qquad (6.25)
\end{aligned}
$$

together with (6.11) in which

$$
p = \boldsymbol{u} \cdot \Phi_{\boldsymbol{u}} + \frac{Q}{3}\Phi_Q - \frac{2}{3}\boldsymbol{q} : \Phi_{\boldsymbol{q}} + \frac{2}{9}Q \mathrm{tr}\Phi_{\boldsymbol{q}} \qquad (6.26)
$$

and

$$
\begin{aligned}
\boldsymbol{\sigma} &= \Phi_Q \boldsymbol{q} + 2\left(\boldsymbol{q} + \frac{Q}{3}\boldsymbol{\delta}\right) \cdot \Phi_{\boldsymbol{q}} - \left[\Phi_{\boldsymbol{q}} : \left(\frac{\boldsymbol{q}}{Q} + \frac{2}{3}\boldsymbol{\delta}\right)\right] \boldsymbol{q} \\
& -2\Phi_{\boldsymbol{c}} \cdot \boldsymbol{c} + \frac{4\pi}{3Q^*}(\boldsymbol{c} : \Phi_{\boldsymbol{c}})(\boldsymbol{c} tr \boldsymbol{c} - \boldsymbol{c} \cdot \boldsymbol{c}) \qquad (6.27)
\end{aligned}
$$

where $\boldsymbol{b} : \boldsymbol{c}$ is defined as $b_{ij}c_{ij}$. The equations governing the dissipative time evolution (obtained by inserting x, Ξ into (6.3)) take the form:

$$
\begin{aligned}
\left(\frac{dQ}{dt}\right)_{diss} &= -\Lambda_1 \Phi_Q \\
\left(\frac{d\boldsymbol{q}}{dt}\right)_{diss} &= -\Lambda_2 \Phi_{\boldsymbol{q}} \\
\left(\frac{d\boldsymbol{c}_{ij}}{dt}\right)_{diss} &= -\frac{1}{2}\Lambda_3 \left(R_{\boldsymbol{c}} \cdot \boldsymbol{c} + \boldsymbol{c} \cdot R_{\boldsymbol{c}}\right)_{kl} \\
& \qquad \left[\delta_{ki}\delta_{lj} - \frac{1}{3}(\boldsymbol{\delta} tr \boldsymbol{c} - \boldsymbol{c})_{kl}(\boldsymbol{\delta} tr \boldsymbol{c} - \boldsymbol{c})^{-1}_{ij}\right] \qquad (6.28)
\end{aligned}
$$

These equations extend the Doi-Ohta equations introduced in [8]. Indeed, by choosing the free energy corresponding to nonstructural liquid interfaces (i.e. we put $K = 0$, $H = 0$ and $\Gamma \neq 0$ in Eq.(6.22), Eqs.(6.25) and (6.28) become the governing equations of the Doi-Ohta model provided the coefficients Λ_1 and Λ_2 are appropriately chosen (see [37]).

In the context of human blood, we choose the free energy (6.20) with $\Gamma = 0$ (i.e. we are not including the surface tension contribution), $K \neq 0$ and $H \neq 0$.

Before continuing with an analysis of solutions of Eqs.(6.25) (6.28), we shall comment about the material parameters entering them.

Three moduli K, H, and C_2 are introduced in the free energy (6.20). K is the

dilation modulus defined as the ratio of the energy stored in the membrane over the normalized area expansion. The larger the K the smaller the area changes attained under the driven of the applied flow. For the RBC membrane, the total area can be looked as being conserved because of the very larger value of K measured.

H is a mesoscopic Young modulus associated with the measure of strain characterized by $(\boldsymbol{q} : \boldsymbol{q})^{1/2}/Q$. It has the dimension [Pa] of the stress. The counterpart of this modulus in the context of microhydrodynamics has the dimension of $[Pam]$, and is usually called the shear modulus E_s. These two form of moduli can be related by $E_s = Ha$, where a is a characteristic length in membrane suspensions. For a red blood cell with an initial discoidal shape, its deviation from the sphere can be describe by the reduced volume $\nu = [V/(4\pi/3)]/[A/4\pi]^{3/2}$. Here V and A are the volume and surface area of a red blood cell. The characteristic length a can be defined as the diameter of a sphere that has the same area of a red blood cell. It relates to the radius of a sphere which has the same volume of a RBC, r_s, by the expression

$$a = 2r_s\nu^{-1/3} \tag{6.29}$$

If the volume fraction of red blood cells in the suspension, ϕ, is known, the initial area density can be written as

$$Q_0 = \frac{3\phi}{r_s}\nu^{-2/3} \tag{6.30}$$

Consequently, the relationship between the two shear moduli writes

$$H = \frac{E_s\nu^{\frac{1}{3}}}{2r_s} \tag{6.31}$$

Another modulus, C_2, called here $\boldsymbol{q}$-modulus here, embraces both the bending and shearing effects. The aspiration experiments made on the RBC show that the bending modulus is relatively small comparing to the shearing modulus. Consequently, the free energy stored in the membrane is dominated by the extensional part rather than the bending part when the deformation and curvature is not very large. We shall assume here that C_2 is proportional to H: $C_2 = \beta_q H$, where β_q is a coefficient that will be determined below.

As for the material parameters entering the dissipation potential, the dimensional analysis suggests the following form:

$$\begin{aligned} \Lambda_1 &= d_1 \frac{Q^2}{\eta_m} \\ \Lambda_2 &= d_2 \frac{Q^2}{\eta_m} \\ \Lambda_3 &= \frac{8}{\zeta} \end{aligned} \tag{6.32}$$

where d_1 and d_2 are Doi-Ohta's (c_1 and c_2 in the notation used in their paper) nondimensional scalars expressing respectively the relaxation rates of the area density (Q) and orientation of the membrane ($\boldsymbol{q}/Q$); ζ is the friction coefficient appearing in the context of the Maxwell model (looked at as the intramembrane friction coefficient here). As we have already mentioned, the viscosity for a red blood cell membrane is related to the dissipation within the bilayer. It is caused by the interaction between lipid-lipid, lipid-cytoskeleton and fibril-fibril in the cytoskeletal network.

The fully explicit form of the equations governing the dissipative part of the time evolution is obtained by inserting (6.24) (with $\Gamma = 0$ and $C_2 = \beta_q H$) into (6.28):

$$\begin{aligned} \left(\frac{dQ}{dt}\right)_{diss} &= 2\Lambda_1 \beta_q H \frac{\boldsymbol{q}:\boldsymbol{q}}{Q^3} - \frac{\Lambda_1 K}{Q_0}\left(\frac{Q}{Q_0} - 1\right) \\ \left(\frac{d\boldsymbol{q}}{dt}\right)_{diss} &= -2\Lambda_2 \beta_q H \frac{\boldsymbol{q}}{Q^2} \\ \left(\frac{d\boldsymbol{c}}{dt}\right)_{diss} &= -\frac{1}{2}\Lambda_3 H \left[\boldsymbol{c} - \frac{\boldsymbol{\delta}}{2\sqrt{\pi}} - T_1(\boldsymbol{c}tr\boldsymbol{c} - \boldsymbol{c}\cdot\boldsymbol{c}) - \frac{T_2}{3}(\boldsymbol{\delta}tr\boldsymbol{c} - \boldsymbol{c})^{-1}\right] \end{aligned} \tag{6.33}$$

where

$$T_1 = \frac{1}{3}(\boldsymbol{\delta}tr\boldsymbol{c} - \boldsymbol{c})^{-1} : (\boldsymbol{\delta} - \frac{\boldsymbol{c}^{-1}}{2\sqrt{\pi}}) \tag{6.34}$$

and

$$T_2 = (\boldsymbol{c} - \frac{\boldsymbol{\delta}}{2\sqrt{\pi}}) : (\boldsymbol{\delta}tr\boldsymbol{c} - \boldsymbol{c}) - T_1(\boldsymbol{c}tr\boldsymbol{c} - \boldsymbol{c}\cdot\boldsymbol{c}) : (\boldsymbol{\delta}tr\boldsymbol{c} - \boldsymbol{c}) \tag{6.35}$$

Altogether, the full set of the equations serving as governing equations of our rheological model of human blood is the following:

$$\begin{aligned}
\frac{dQ}{dt} &= -tr\left(\boldsymbol{q}\cdot\nabla v^T\right)+2\frac{d_1\beta_q H}{\eta_m Q}\boldsymbol{q}:\boldsymbol{q}-\frac{d_1 K Q^2}{\eta_m Q_0}\left(\frac{Q}{Q_0}-1\right)\\
\frac{d\boldsymbol{q}}{dt} &= \left(\frac{\boldsymbol{q}}{Q}+\frac{2}{3}\boldsymbol{\delta}\right)tr\left(\boldsymbol{q}\cdot\nabla v^T\right)-\left(\boldsymbol{q}+\frac{Q}{3}\boldsymbol{\delta}\right)\cdot\nabla v^T-\nabla v\cdot\left(\boldsymbol{q}+\frac{Q}{3}\boldsymbol{\delta}\right)\\
&\quad -2\frac{d_2\beta_q H}{\eta_m}\boldsymbol{q}\\
\frac{d\boldsymbol{c}}{dt} &= \boldsymbol{c}\cdot\nabla\boldsymbol{v}+\nabla\boldsymbol{v}^T\cdot\boldsymbol{c}-\frac{4\pi}{3Q^*}\left((\boldsymbol{c}tr\boldsymbol{c}-\boldsymbol{c}\cdot\boldsymbol{c}):\nabla\boldsymbol{v}\right)\boldsymbol{c}\\
&\quad -\frac{4H}{\zeta}\left[\boldsymbol{c}-\frac{\boldsymbol{\delta}}{2\sqrt{\pi}}-T_1(\boldsymbol{c}tr\boldsymbol{c}-\boldsymbol{c}\cdot\boldsymbol{c})-\frac{T_2}{3}(\boldsymbol{\delta}tr\boldsymbol{c}-\boldsymbol{c})^{-1}\right]\\
\boldsymbol{\sigma}^{int} &= \left[\frac{K}{Q_0}\left(\frac{Q}{Q_0}-1\right)-4\beta_q H\frac{\boldsymbol{q}:\boldsymbol{q}}{Q^3}\right]\boldsymbol{q}+4\beta_q H\left(\boldsymbol{q}+\frac{Q}{3}\boldsymbol{\delta}\right)\frac{\boldsymbol{q}}{Q^2}\\
&\quad +H\left[\frac{\boldsymbol{\delta}}{2\sqrt{\pi}}-\boldsymbol{c}+\frac{4\pi}{6Q^*}(tr\boldsymbol{c}-\frac{3}{2\sqrt{\pi}})(\boldsymbol{c}tr\boldsymbol{c}-\boldsymbol{c}\cdot\boldsymbol{c})\right]
\end{aligned}\tag{6.36}$$

To arrive at a dimensionless form of these equations, we introduce the following dimensionless quantities:

$$Q^*=\frac{Q}{Q_0},\quad \boldsymbol{q}^*=\frac{\boldsymbol{q}}{Q_0},\quad t^*=\frac{t}{\tau_H},\quad \nabla\boldsymbol{v}^*=\frac{\nabla\boldsymbol{v}}{\dot\gamma},\quad \sigma^*=\frac{\sigma}{\eta_m\dot\gamma}\tag{6.37}$$

where $\tau_H=\eta_m/H$ is the characteristic time relating to the relaxation of the in-plane shearing of the membranes. In terms of these quantities, the dimensionless time evolution equations become (for the sake of clarity, the symbol * is hereafter omitted)

$$\begin{aligned}
\frac{dQ}{dt} &= -Ca\,tr\left(\boldsymbol{q}\cdot\nabla v^T\right)+d_1\left[2\beta_q\frac{\boldsymbol{q}:\boldsymbol{q}}{Q}-\xi Q^2(Q-1)\right]\\
\frac{d\boldsymbol{q}}{dt} &= Ca\left[\left(\frac{\boldsymbol{q}}{Q}+\frac{2}{3}\boldsymbol{\delta}\right)tr\left(\boldsymbol{q}\cdot\nabla v^T\right)-\left(\boldsymbol{q}+\frac{Q}{3}\boldsymbol{\delta}\right)\cdot\nabla v^T-\nabla v\cdot\left(\boldsymbol{q}+\frac{Q}{3}\boldsymbol{\delta}\right)\right]\\
&\quad -2d_2\beta_q\boldsymbol{q}\\
\frac{d\boldsymbol{c}}{dt} &= Ca\left[\boldsymbol{c}\cdot\nabla\boldsymbol{v}+\nabla\boldsymbol{v}^T\cdot\boldsymbol{c}-\frac{4\pi}{3Q}\left((\boldsymbol{c}tr\boldsymbol{c}-\boldsymbol{c}\cdot\boldsymbol{c}):\nabla\boldsymbol{v}\right)\boldsymbol{c}\right]\\
&\quad -4\kappa\left[\boldsymbol{c}-\frac{\boldsymbol{\delta}}{2\sqrt{\pi}}-T_1(\boldsymbol{c}tr\boldsymbol{c}-\boldsymbol{c}\cdot\boldsymbol{c})-\frac{T_2}{3}(\boldsymbol{\delta}tr\boldsymbol{c}-\boldsymbol{c})^{-1}\right]
\end{aligned}$$

$$\boldsymbol{\sigma}^{int} = Ca^{-1}\left[\left(\xi(Q-1) - 4\beta_q\frac{\boldsymbol{q}:\boldsymbol{q}}{Q^3}\right)\boldsymbol{q} + 4\beta_q\left(\boldsymbol{q}+\frac{Q}{3}\boldsymbol{\delta}\right)\frac{\boldsymbol{q}}{Q^2} + \frac{\boldsymbol{\delta}}{2\sqrt{\pi}} - \boldsymbol{c} + \frac{4\pi}{6Q}(tr\boldsymbol{c} - \frac{3}{2\sqrt{\pi}})(\boldsymbol{c}tr\boldsymbol{c} - \boldsymbol{c}\cdot\boldsymbol{c})\right] \tag{6.38}$$

These equations will be solved with the initial condition

$$Q(0) = 1; \quad \boldsymbol{q}(0) = 0; \quad \boldsymbol{c}(0) = \frac{\boldsymbol{\delta}}{2\sqrt{\pi}} \tag{6.39}$$

The dimensionless equations (6.38) involve three parameters: Ca, ξ, and κ. They are dimensionless and have the following physical meaning:

(1)$Ca = \eta_m\dot{\gamma}/H$ is the capillary number. It expresses the ratio of the external driven force to the elastic strain force of the membrane. It can also be interpreted as the ratio of the relaxation time of the deformed membrane emerged in surrounding fluids to the characteristic time of flow. Ca can be looked as the counterpart of capillary number in emulsions with fluid interfaces if H is replace by Γ/a. It is worthwhile to note that in original Doi-Ohta model, the capillary number can not be defined because there not exists a characteristic length scale in immiscible blends with complex interfaces. However in present model in the case of vesicles, like RBCs, since the area density Q does not change much from its initial value Q_0, the length scale can be feasibly defined by Eqs.(6.29, 6.30).

(2)$\xi = K/H$ expresses the ratio of the elastic expansion force of membrane to the in-plane elastic shearing or extensional force. It can also be interpreted as the ratio of the two relaxation times: $\xi = \tau_H/\tau_K$, where τ_H is the relaxation time of the in-plane shearing and τ_K is the relaxation time of area variation.

(3)$\kappa = \eta_m/\zeta$ is the ratio of fluid viscosity to the membrane viscosity.

6.3 Determination of the material parameters

d_1, d_2 and β_q are the parameters through which the individual nature of the membrane suspension under consideration is expressed in the present model. In this section we shall first investigate the influence of the parameters d_1 and d_2 on the model predictions. Then, we shall show how to approximately determine these parameters.

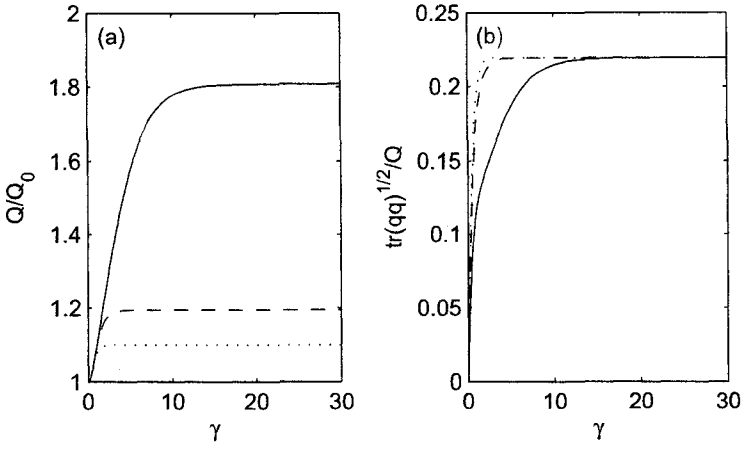

Figure 6.1: The influences of d_1 on the time evolution of the normalized area density $\frac{Q}{Q_0}$ (a) and the deformation $(\boldsymbol{q} : \boldsymbol{q})^{1/2}/Q$ (b) of the membrane under a start-up simple shear flow. The curves (—), (- -) and (...) correspond to $d_1 = 0.1$, $d_1 = 1$ and $d_1 = 10$ respectively.

d_1 and d_2 are parameters which describe the relaxation rate of the membrane area per unit volume (Q) and of the membrane anisotropy ($\boldsymbol{q}$/Q) respectively. Fig.6.1 and Fig.6.2 illustrate the influence of d_1 on the behavior of a membrane suspension for a start-up of a simple shear flow. t/τ_c is the normalized time, Q/Q_0 is the normalized area density, $(\boldsymbol{q} : \boldsymbol{q})^{1/2}/Q$ describes the averaged deformation of the interface, σ_{12}^{int} and N_1^{int} are the interface contributions to the normalized (i.e. divided by $\eta_m\dot{\gamma}$) shear stress and the first normal stress difference. The calculations are made by choosing $d_2 = 1$, $Ca = 1$, $\xi = 1$, $\kappa = 0.1$, $\beta_q = 1$ and d_1 takes three different values: 0.1, 1 and 10.

As shown in Fig.6.1, an increase in d_1 leads to an decrease in area density, Q, and no effect on the steady value of average deformation $(\boldsymbol{q} : \boldsymbol{q})^{1/2}/Q$. A larger d_1 means that a smaller time is needed to attain the steady value of Q and $(\boldsymbol{q} : \boldsymbol{q})^{1/2}/Q$. Fig.6.2 indicates that both the shear stress and the first normal stress difference decrease as d_1 increases.

As to the influences of d_2, Fig.6.3 and Fig.6.4 show that d_2 has the similar but more pronounced effects on the model predictions than d_1 does. The calculations are made by choosing $d_1 = 1$, $Ca = 1$, $\xi = 1$, $\kappa = 0.1$, $\beta_q = 1$, and d_2 takes three different values: 0.1, 1 and 10.

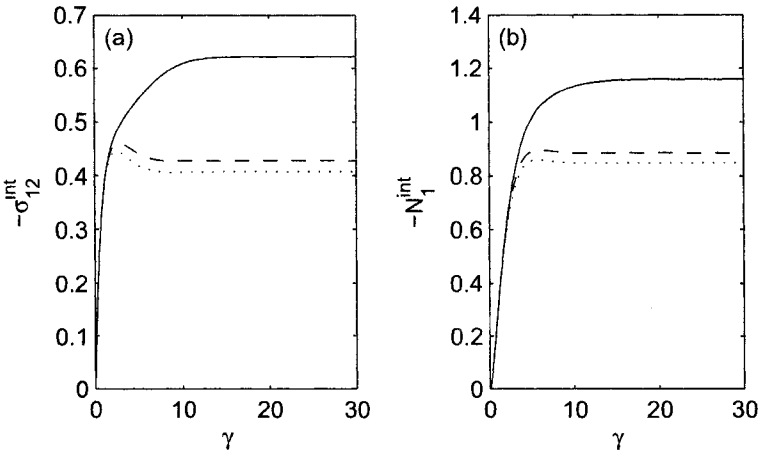

Figure 6.2: The influences of d_2 on the time evolution of the normalized shear stress $-\sigma_{12}^{int}$ (a) and the normalized first normal stress difference $-N_1^{int}$ (b) of the membrane under a start-up simple shear flow. The curves (—), (- -) and (...) correspond to $d_1 = 0.1$, $d_1 = 1$ and $d_1 = 10$ respectively.

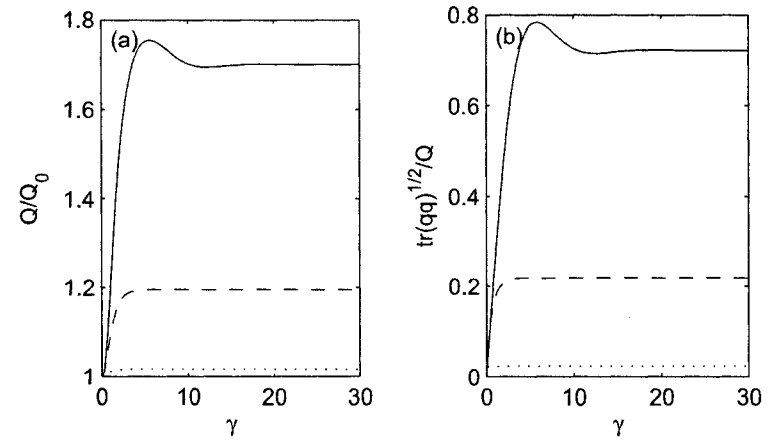

Figure 6.3: The influences of d_2 on the time evolution of the normalized area density $\frac{Q}{Q_0}$ (a) and the deformation $(\boldsymbol{q} : \boldsymbol{q})^{1/2}/Q$(b) of the membrane under a start-up simple shear flow. The curves (—), (- -) and (...) correspond to $d_2 = 0.1$, $d_2 = 1$ and $d_2 = 10$ respectively.

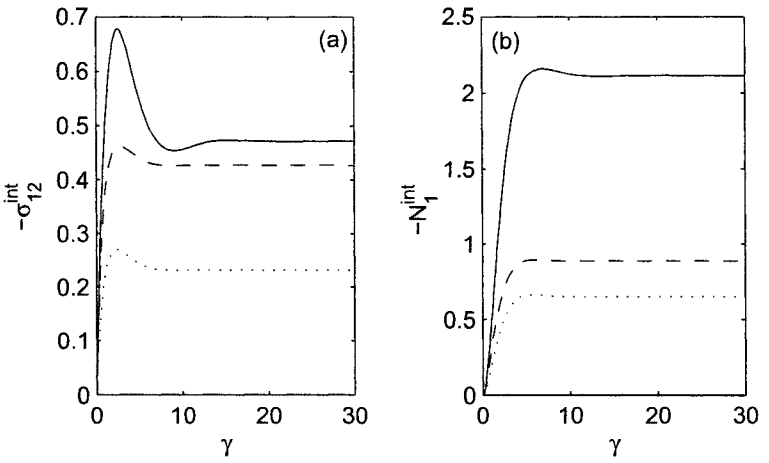

Figure 6.4: The influences of d_2 on the time evolution of the normalized shear stress $-\sigma_{12}^{int}$ (a) and the normalized first normal stress difference $-N_1^{int}$ (b) of the membrane under a start-up simple shear flow. The curves (—), (- -) and (...) correspond to $d_2 = 0.1$, $d_2 = 1$ and $d_2 = 10$ respectively.

Now, we proceed to provide an approximate analytical expressions for d_1 and d_2. The method used is similar to the one used already in [38] and [36]. Our starting point is the perturbation analysis of suspensions under a simple shear flow with

$$\nabla \boldsymbol{v}^T = \begin{pmatrix} 0 & 1 & 0 \\ 0 & 0 & 0 \\ 0 & 0 & 0 \end{pmatrix} \tag{6.40}$$

We assume that Ca is a small parameter and look for solutions of Eqs.(6.38) in the form:

$$Q = 1 + Ca\, Q^{(1)} + O(Ca^2) \tag{6.41}$$

$$\boldsymbol{q} = Ca\, \boldsymbol{q}^{(1)} + O(Ca^2) \tag{6.42}$$

and

$$\boldsymbol{c} = \boldsymbol{\delta} + Ca\, \boldsymbol{c}^{(1)} + O(Ca^2) \tag{6.43}$$

To the first order in Ca, Eqs.(6.38) become

$$\frac{dQ^{(1)}}{dt} = -d_1 \xi Q^{(1)}$$

$$\begin{aligned}
\frac{d\boldsymbol{q}^{(1)}}{dt} &= -\frac{1}{3}\left(\nabla\boldsymbol{v}^T + \nabla\boldsymbol{v}\right) - 2d_2\beta_q\boldsymbol{q}^{(1)} \\
\frac{d\boldsymbol{c}^{(1)}}{dt} &= \frac{1}{2\sqrt{\pi}}(\nabla\boldsymbol{v}^T + \nabla\boldsymbol{v}) - 4\kappa\left(\boldsymbol{c}^{(1)} - \frac{1}{3}tr\boldsymbol{c}^{(1)}\boldsymbol{\delta}\right) \\
\sigma &= \frac{4}{3}\beta_q\boldsymbol{q}^{(1)} - \boldsymbol{c}^{(1)} + \frac{4\pi}{3}tr\boldsymbol{c}^{(1)}\boldsymbol{\delta} + O(Ca)
\end{aligned} \tag{6.44}$$

Now, we determine the coefficients by considering two effects: the relaxation time and zero shear viscosity. The normalized relaxation time for Q, $\boldsymbol{q}$, and $\boldsymbol{c}$ can be easily found from Eq.(6.44) to be $1/d_1\xi$, $1/2d_2\beta_q$ and $1/4\kappa$ respectively. For RBCs, $d_1\xi$ should be very large to make the membrane stiff in area expansion. Since the area of the membrane is almost conserved, the changes in in-plane extension should result in the overall shape changes. This means that the deformation expressed in $\boldsymbol{q}$ and $\boldsymbol{c}$ should be correlated and of the same order. By equating the relaxation time of $\boldsymbol{q}$ and $\boldsymbol{c}$ we obtain the following expression:

$$d_2 = 2\kappa/\beta_q \tag{6.45}$$

The normalized (divided by η_m) zero-shear viscosity, i.e., the plateau value of the steady state shear stress at Ca tending to zero can also be obtained:

$$-\left[\sigma_{12}\right]_{Ca\to 0} = \frac{8\sqrt{\pi}\beta_q + 9}{72\sqrt{\pi}\kappa} \tag{6.46}$$

If we want the present model to recover Batchelor's results [39] for the viscosity of suspension of spheres, i.e., $-\left[\sigma_{12}\right]_{Ca\to 0} = 2.5\phi + 5.5\phi^2$, we get

$$\kappa = \frac{8\sqrt{\pi}\beta_q + 9}{72\sqrt{\pi}(2.5\phi + 5.5\phi^2)} \tag{6.47}$$

However, the experimental data often show that suspensions of red blood cells do not obey the Batchelor's results. In such situations we let κ to be free to vary and use the measured values of the zero-shear viscosity to determine its value. It is also interesting to note that according to the present model the zero-shear viscosity of the RBC suspensions is determined by the viscosity not the elasticity of the membrane.

6.4 Results

6.4.1 Effects of Ca, ξ, and κ on model predictions

Now, we shall investigate the effects of material parameters on the rheological behaviors of a suspensions of red blood cells. The applied flow is an simple shear flow field. The properties of membranes and the flow field are condensed on three nondimensional numbers, Ca, ξ, and κ. the capillary number Ca describes the relative strongness of the external flow to the membrane elasticity. The two ratios ξ, and κ describe respectively the intrinsic elastic and viscous properties of the membrane suspension.

A larger elastic ratio ξ means that the membrane is more rigid in its area changes, thus more difficulty to expand the surface area when it is driven by the external flow. The influences of ξ to the model predictions are displayed in Fig.6.5 and Fig.6.6. The calculation are made on: $d_1 = 1$, $\beta_q = 1$, $\kappa = 0.5$ and $d_2 = 2\kappa/\beta_q$. Not surprisingly we can see that the surface area is decreased by choosing larger value of ξ. ξ has no influence on the deformation of membrane, which is indicated by the coincidence of all the curves. It can also be found that ξ almost has no effect on the shear stress and first normal stress difference. As exhibited in the figures, even when the membrane area is doubled, the shear stress still changes very little. This is indicates that the stress is mostly determined by the orientation and in-plane deformation of the membranes.

Fig.6.5 and Fig.6.6 also illustrate the influence of Ca. As Ca, i.e., shear rate grows, the area density and deformation of membrane tend to reach a constant value. Shear stress shows a zero shear plateau followed by a shear thinning. The first normal stress difference increase with Ca, and has a maximum followed by a decreasing.

The influence of the viscosity ratio κ is displayed in Fig.6.7 and Fig.6.8. The calculations are made for: $d_1 = 1$, $\beta_q = 5$, $\xi = 100$ and $d_2 = 2\kappa/\beta_q$. As presented in Fig.6.7a, the effect of κ on the area density depends on the capillary number. For weak flow fields, i.e. when Ca is small, the increase of the viscosity of the membrane, i.e. of κ, results in a decrease in the surface area at the steady state. On the other hand, for a strong flow field, the viscosity of the membrane facilitates the flow to enlarge surface area against the area elasticity. this is displayed in

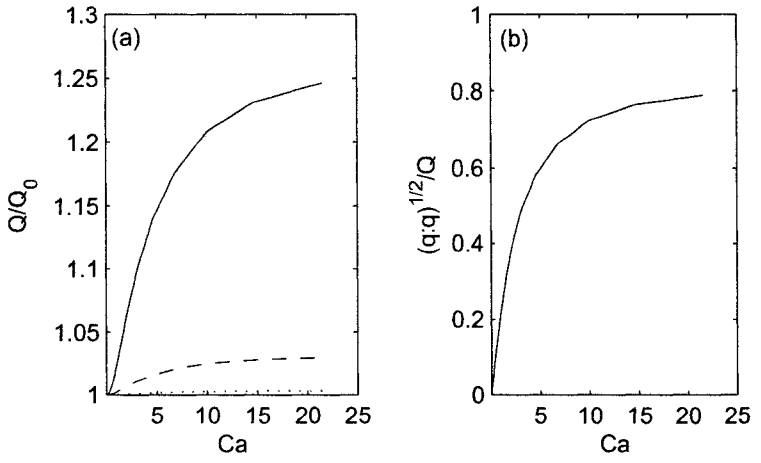

Figure 6.5: The influences of ξ on the steady state value of the normalized area density $\frac{Q}{Q_0}$ (a) and the deformation $(\boldsymbol{q} : \boldsymbol{q})^{1/2}/Q$ (b) of the suspension of RBC membrane submitted to a simple shear flow. The curves (—), (- -) and (...) and correspond to $\xi = 10$, $\xi = 100$ and $\xi = 1000$ respectively.

Fig.6.7b. A larger viscosity of the membrane leads to its smaller deformation. As to the shear stress and first normal stress difference, larger κ, i.e. smaller viscosity of the membrane, always leads to smaller values of σ_{12}^{int} and N_1^{int}.

6.5 Comparison with experimental data and with other models

In the last part of the analysis of predictions of the model, we compare the predicted results with experimental data collected on RBC suspensions and also with predictions of Barthès-Biesel and Rallison (BBR) model on suspensions of deformable capsules. The experimental data are taken from Drochon [31] for dilute suspensions of red blood cells. To study the effects of the rigidity of membranes, RBCs were artificially treated by different concentration of diamide or glutaraldehyde treatment. The suspending liquids were solutions of Dextran T70 in Sodium Trisaminomethan buffer having the viscosity of 18.5 $mPas$. The apparent radius of a sphere that has the same volume as the red blood cell is $r_s = 2.8\mu m$. The haematocrit (volume fraction) of the RBCs in suspensions is 9%. All the blood

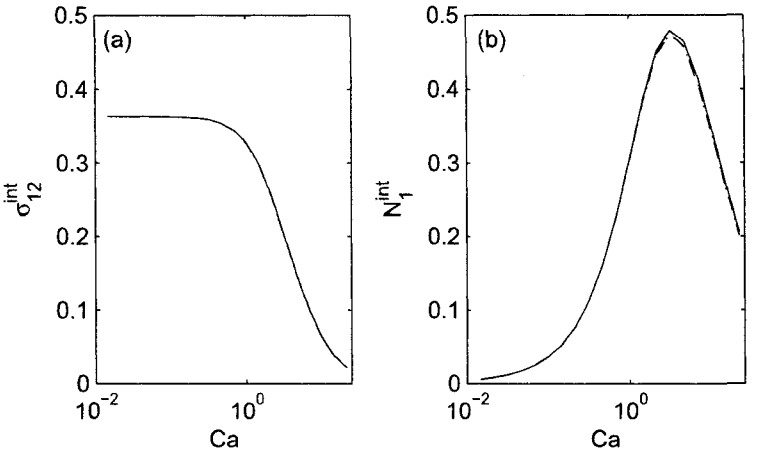

Figure 6.6: The influences of ξ on the steady state value of the normalized shear stress $-\sigma_{12}^{int}$ (a) and the normalized first normal stress difference $-N_1^{int}$ (b) of the suspension of RBC membrane submitted to a simple shear flow. The curves (—), (- -) and (...) and correspond to $\xi = 10$, $\xi = 100$ and $\xi = 1000$ respectively.

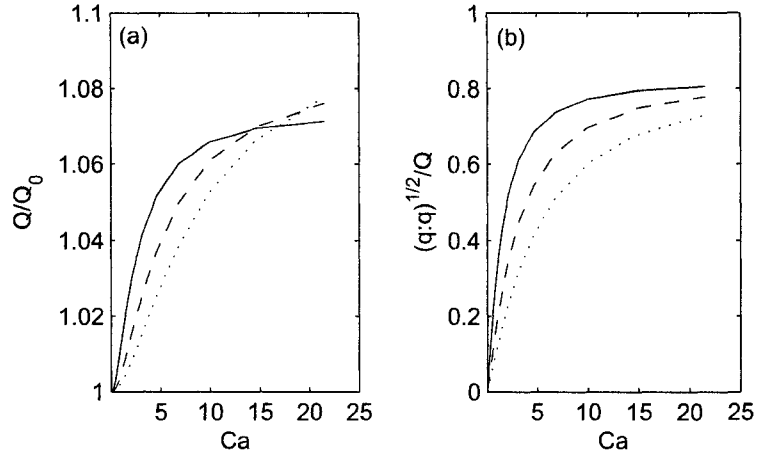

Figure 6.7: The influences of κ on the steady state value of the normalized area density $\frac{Q}{Q_0}$ (a) and the deformation $(\boldsymbol{q} : \boldsymbol{q})^{1/2}/Q$ (b) of the suspension of RBC membrane submitted to a simple shear flow. The curves (—), (- -) and (...) and correspond to $\kappa = 0.3$, $\kappa = 0.6$ and $\kappa = 1$ respectively.

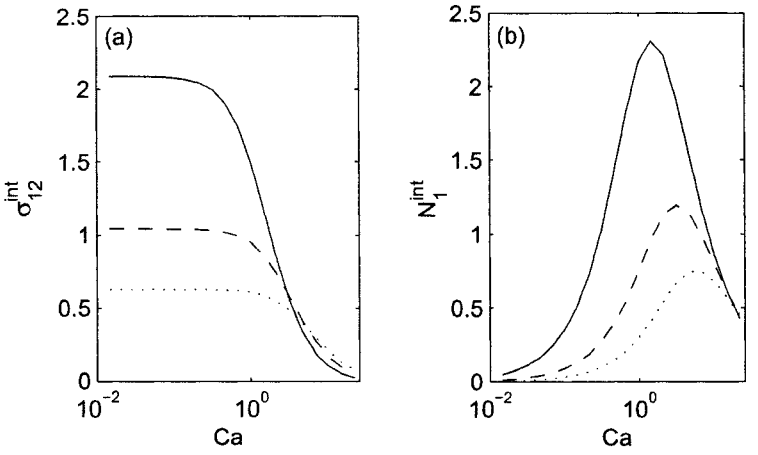

Figure 6.8: The influences of κ on the steady state value of the normalized shear stress $-\sigma_{12}^{int}$ (a) and the normalized first normal stress difference $-N_1^{int}$ (b) of the suspension of RBC membrane submitted to a simple shear flow. The curves (—), (- -) and (...) and correspond to $\kappa = 0.3$, $\kappa = 0.6$ and $\kappa = 1$ respectively.

cells were kept in their normal discoidal shape before experiments. In Fig.6.9, $\eta_m\dot{\gamma}$ denotes the applied shear stress. The filled symbols are measured intrinsic viscosity defined as $[\eta] = (\eta^{tot} - 1)/\phi$. The curves represent the intrinsic viscosity predicted by the present model. If we use the linear mixing rule to calculate the total stress, i.e., $\sigma^{tot} = 1 + \sigma^{int}$. This leads to $[\eta] = \sigma^{int}/\phi$. Predictions of BBR model are represented by blank symbols.

Suspension of RBCs exhibits a shear thinning behavior due to the orientation and deformation of the membranes of red blood cells. As the rigidity of membrane (E_s) increases, the viscosity curves shift to higher shear stress region. A constant zero-shear viscosity can be inferred from the curves. Its value is somewhat higher than Einstein's result of 2.5. These phenomena are qualitatively captured by the present model as well as BBR model. Although there are quantitative deviations between the predictions of both models and experimental data both at zero shear and high shear rates, predictions of both model are very close over the entire shear rates. The deviations may caused by the linear mixing assumption used to subtract the membrane contributions from the total stress and also due to the complex, non ellipsoidal, shape of the red blood cell. Nevertheless, the present model gives a better results than BBR model at low shear region.

Table 6.1: Parameters used to fit the experimental data of Drochon (2003) for the dilute suspensions of red blood cells

d_1	$K[Pa]$	$E_s[10^{-6}N/m]$	β_q
10	7×10^4	0.9, 3, 6	1×10^{-2}

In calculations of the present model, the parameters are chosen as follows. The area density of a suspension is calculated by Eq.(6.30) with $r_s = 2.8\mu m$ and ν taking the value of 0.64. The area modulus K is taken to be 7×10^4 ($K = aK_s$, with $K_s = 450mN/m$ proposed in [40] and [41]). d_1, chosen in such a way that $d_1\xi$ is a larger number, has a very small effect on the shear stress provided it is large enough (see Fig.6.2). d_2 is calculated by Eq.(6.45) and β_q or κ are determined by Eq.(6.47). H is related to the shear modulus E_s by Eq.(6.31). Finally, E_s and β_q are parameters need to be specifies by fitting experimental data. The parameters chosen are displayed in Tab.6.1. The values of E_s obtained in this way are around 0.9×10^{-6} for normal cells, 3×10^{-6} and 6×10^{-6} (N/m), for diamide treated cells with 0.1mM, and 0.3mM respectively. The predicted values for E_s are smaller than, but of the same order as, Drochon's results. The difference may partially be caused by the different measure of strain. The relative magnitude of the three moduli is very close to Drochon's predictions.

Besides the elastic modulus, we can also obtain the viscosity coefficient of membranes. The membrane viscosity relates to the fraction coefficient ζ by $\eta_{mem} = a\zeta/4$, i.e.,

$$\eta_{mem} = \frac{\zeta r_s}{2\nu^{\frac{1}{3}}} \tag{6.48}$$

The value obtained by the best fit is $\zeta = 0.07Pa \cdot s$ which implies the viscosity coefficient $\eta_{mem} = 1.1 \times 10^{-4} poise \cdot cm$. This value is of the same order as, but smaller than, the value of $6 \sim 8 \times 10^{-4} poise \cdot cm$ measured by Hochmuth *et.al* [42] from the recovery experiments of red blood cells. An excellent agreement is found for the relaxation time. The value $\tau_c = \frac{\eta_{mem}}{E_s} = 0.12s$ is exactly in the range of $0.1 - 0.13s$, measured by Hochmuth et al. [42].

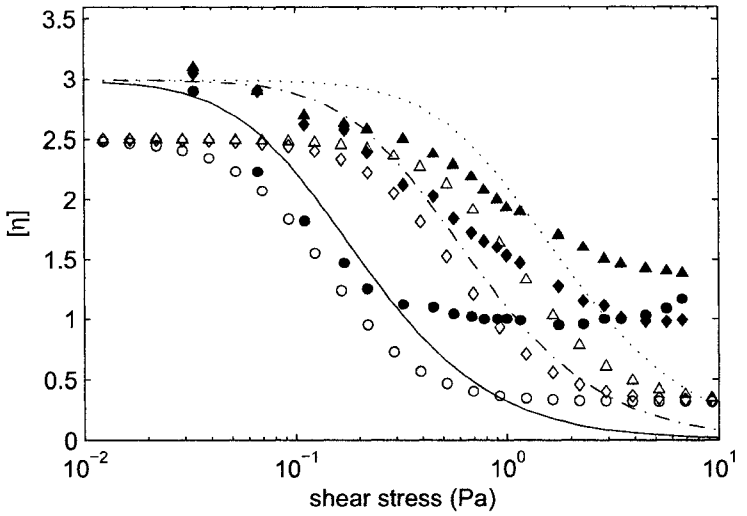

Figure 6.9: The comparison of model predictions with experimental data. Symbols (•), (♦) and (▲) correspond to experimental data of normal cells, diamide treated cells with 0.1mM, and 0.3mM respectively. The curves (—), (- -) and (...) correspond to the present model with $E_s = 0.9 \times 10^{-6}$, $E_s = 3 \times 10^{-6}$ and $E_s = 6 \times 10^{-6}$ respectively. The symbols (○), (◇) and (△) correspond to BBR model with $E_s = 2.7 \times 10^{-6}$, $E_s = 11.1 \times 10^{-6}$ and $E_s = 22.0 \times 10^{-6}$ respectively.

6.6 Conclusion

Fluids involving vesicles or living cells are widely encountered in biological engineering. Since a membrane is the most important component of such fluids, we suggest in this paper to regard the biological fluids as suspensions of membranes. The specific biological fluid that we investigate in this paper is the suspension of red blood cells. The previous rheological modeling of the membrane suspension has been mostly carried out on the microhydrodynamic level, which uses the localized velocity field $\boldsymbol{v}(\boldsymbol{r},t)$, localized stress field $\sigma(\boldsymbol{r},t)$ and the position of membranes $Y(\boldsymbol{r},t)$ to describe states of the suspensions. Because of the enormous complexity of the governing equations, their solutions, and thus predictions of the model, can be found only with the assistance of very powerful computer and numeric technology. Even with such enormous effort, the results remain to be limited to a single or a few vesicles and lacking the rheological predictions.

In this paper we are introducing a more macroscopic (mesoscopic) viewpoint leading to a simpler mathematical formulation that does not require extensive numerical calculation to arrive at predictions of the model. In contrast to the microhydrodynamic modeling, the mesohydrodynamic modeling introduced in this article uses three state variables, the scalar Q, the traceless symmetric tensor $\boldsymbol{q}$, and symmetric positive definite tensor $\boldsymbol{c}$, corresponding to the surface area per unit volume, out-plane deformation and in-plane deformation respectively, as the microstructural state variables. The out and in plane character of the deformations is mathematically expressed by a constraint relating Q and $\boldsymbol{c}$. The modeling is done by following the thermodynamic (GENERIC) framework.

The present model can be looked upon as an extension of the Doi-Ohta model from the case of liquid interfaces to the case of viscoelastic membranes. Both the elasticity and viscosity of the membrane are taken into account in the modeling. The model predicts that upon increasing the rigidity of the membranes, the viscosity-stress curve shifts towards the higher stress (Fig.6.9). This phenomenon is in agreement with the experimental observations and the microhydrodynamic model predictions. The calculated shear modulus, viscosity of membrane and relaxation time are of the same order as those obtained in microscopic measurements.

Bibliography

[1] T. J. Byers and D. Branton, Visualization of the protein associations in the erythrocyte membrane skeleton, Proc. Natl. Acad. Sci. USA 82 (1985) 6153-6157.

[2] E. A. Evans and D. Needham, Cohesive properties of lipid bilayer membranes containing cholestrol, J. Phys. Chem. 91 (1987) 4219-4228.

[3] E. A. Evans and R. M. Hochmuth, Membrane viscoelasticity, Biophys. J. 16 (1976) 1-11.

[4] G. I. Taylor, The viscosity of a fluid containing small drops of another fluid, Proc. Roy. Soc. A 138 (1932) 41-48.

[5] R. G. Cox, The deformation of a drop in a general time-dependent fluid flow, J. Fluid Mech. 37 (1969) 601-623.

[6] S. J. Choi and W. R. Schowalter, Rheological properties of non-dilute suspensions of deformable particles, Phys. Fluids 18 (1975) 420- 427.

[7] J. F. Palierne, Linear rheology of viscoelastic emulsions with interfacial tension, Rheol. Acta 29 (1990) 204-214; Erratum 30 (1991) 497.

[8] M. Doi and T. Ohta, Dynamics and rheology of complex interfaces, J. Chem. Phys. 95 (1991) 1242-1248.

[9] M. Grmela, Particle and bracket formulations of kinetic equations, Contemp Math 28 (1984) 125-132.

[10] M. Grmela, Bracket formulation of diffusion-convection equations, Physica D 21 (1986) 179-212.

[11] M. Grmela, Mesoscopic Dynamic and Thermodynamic: Application to Polymer Fluids, Lecture Notes in Physics 381 (1991) 99-125.

[12] A. N. Beris and B. J. Edwards, Thermodynamics of flowing systems. 1 st edn. Oxford University Press, New York (1994)

[13] M. Grmela and H. C. Ottinger, Dynamics and thermodynamics of complex fluids. I. Development of a general formalism, Phys Rev E 56 (1997) 6620-6632.

[14] H. C. Ottinger and M. Grmela, Dynamics and thermodynamics of complex fluids. II. Illustrations of a general formalism, Phys. Rev.E 56 (1997) 6633-6655.

[15] M. Grmela, Reciprocity relations in thermodynamics. Physica A 309 (2002) 304-328.

[16] J. E. Marsden, A. Weinstein, Coadjoint orbits, vortices, and Clebsch variables for incompressible fluids, Physica D 7 (1983) 305-323.

[17] H. C. Ottinger, Beyond Equilibrium Thermodynamics. Wiley (2005)

[18] M. Grmela, A. Ait-Kadi, Comments on the Doi-Ohta theory of blends, J. Non-Newtonian Fluid Mech. 55 (1994) 191-195.

[19] B. J. Edwards M. Dressler M. Grmela A. Ait-Kadi, Rheological models with microstructural constraints, Rheol. Acta 42 (2003) 64-72.

[20] P. L. Maffettone and M. Minale, Equation of change for ellipsoidal drops in viscous flow, J.Non-Newtonian Fluid Mech., 78 (1998) 227-241.

[21] W. Yu, M. Bousmina, M. Grmela, J. -F. Palierne, and C. Zhou, Quantitative relationship between rheology and morphology in emulsions, J. Rheol. 46 (2002) 1381-1399.

[22] D. Barthès-Biesel and J. M. Rallison, The time-dependent deformation of a capsule freely suspended in a linear shear flow, J. Fluid Mech. 113 (1981) 251-256.

[23] G. K. Batchelor, The stress system in a suspension of force-free particles, J. Fluid Mech. 41 (1970) 515-570.

[24] G. Danker, C. Verdier, C. Misbah, Rheology and dynamics of vesicle suspension in comparison with droplet emulsion, J. Non-Newtonian Fluid Mech. 152 (2008) 156-167.

[25] R. Pal, Rheology of concentrated suspensions of deformable elastic particles such as human erythrocytes, J.Biomech. 32 (2003) 601-608.

[26] C. Pozrikidis, Finite deformation of liquid capsules enclosed by elastic membranes in simple shear flow, J. Fluid Mech. 297 (1995) 123-152.

[27] S. Ramanujan and C. Pozrikidis, Deformation of liquid capsules enclosed by elastic membranes in simple shear flow: large deformations and the effect of fluid viscosities, J. Fluid Mech. 361 (1998) 117-143.

[28] C. Pozrikidis, numerical simulation of the flow-induced deformation of red bllod cells, Annals of Biomedical Enginnering 31 (2003) 1194-1205.

[29] R. Carr and G. R. Cokelet, Rheology of Suspensions of Normal and Hardened Erythrocytes and their Mixtures, J. Rheol. 25 (1981) 67-82.

[30] A. Drochon, D. Barthès-Biesel, C. Lacombe, and L. C. Lelievre, Determination of the Red Blood Cell Apparent Membrane Elastic Modulus From Viscometric Measurements, J. Biomech. Eng.112 (1990) 241-249; Erratum, 113 (1991) 103.

[31] A. Drochon, Rheology of dilute suspensions of red blood cells: Experimental and theoretical approaches, Eur. Phys. J.: Appl. Phys. 22 (2003) 155-162.

[32] C. D. Eggleton and A. S. Popel, Physics of fluids, Large deformation of red blood cell ghosts in a simple shear flow, Physics of fluid 10 (1998) 1834-1845.

[33] H. Zhou and C. Pozrikidis, Deformation of capsules with incompressible interfaces in simple shear flow, J. Fluid Mech. 283 (1995) 175-200.

[34] A. N. Beris and B. J. Edwards. Poisson bracket formulation of viscoelastic flow equations of differential type: A unified approach, J. Rheol. 34 (1990) 503-538.

[35] C. Lacroix, M. Grmela, P. J. Carreau, Relationships between rheology and morphology for immiscible molten blends of polypropylene and ethylene copolymers under shear flow, J. Rheol. 42 (1998) 41-62.

[36] J. F. Gu, M. Grmela, GENERIC Model of Active Advection, J. Non-Newtonian Fluid Mech. 152 (2008) 12-26.

[37] J. F. Gu and M. Grmela, Flow Properties of Immiscible Blends: Doi-Ohta Model with Active Advection, (2008) accepted by Phys. Rev. E.

[38] J. F. Gu, M. Grmela, M. Bousmina, A mesoscopic rheological model of immiscible blends with the interface covered with a surface active agent, Physics of Fluids. 20 (2008) 043102.

[39] G. K. Batchelor, J. T. Green, The determination of the bulk stress in a suspension of spherical particles to order c^2, J. Fluid Mech. 56 (1972) 401-427.

[40] E. A. Evans, R. E. Waugh, Osmotic correction to elastic are compressibility measurements on red cell membrane, Biophys. J. 20 (1977) 307-313.

[41] R. M. Hochmuth, R. E. Waugh, Erythrocyte membrane elasticity and viscosity, Ann. Rev. Physiol. 49 (1987) 209-219.

[42] R. M. Hochmuth, P. R. Worthy, E. A. Evans, Red cell extensional recovery and the determination of membrane viscosity, Biophys. J. 26 (1979) 101-114.

Chapter 7

General Discussion

In this Thesis we consider three types of membrane suspensions: immiscible blends, immiscible blends in the presence of surface active agents, and suspension of red blood cells. Our objective is to model the complex rheological behavior that these suspensions display in experimental observations.

There are two routs that we can follow: microhydodynamics, or mesohydrodynamics. The former puts into focus details of the morphology of small pieces of the membranes (e.g. a single droplet) and requires an extensive expertise in numerical analysis of partial differential equations. The latter concentrates on the rheology and leads to formulations (system of ordinary differential equations in all cases studied in this Thesis) that can be handled with the standard software. We have chosen to follow the route of mesohydrodynamics. The approach based on microhydrodynamics is discussed only in Chapter 4.

In Chapters 2,3,5,6, we proceed as follows. First, we choose a state variable describing morphology of the membranes. In addition to the Doi-Ohta (1991) and Maffettone-Minale (1998) morphological variables, we introduce new ones allowing us to express in a more detail the physics taking place in the suspensions under consideration. In Chapters 2 and 3, we adopt to the set of state variables the gradient of the flow perturbed by the presence of the membranes. In order to be able to deal with the new physics arising when surface active agents are added to the suspensions, we extend in Chapter 5 the Maffettone-Minale state variable to a one parameter family (a necklace) of conformation tensors. The membranes discussed in Chapter 6 (membranes of red blood cells) have a com-

plex mechanical structure. In order to involve their viscoelastic deformations in the rheological model we need a new intra-membrane deformation tensor. The extra state variables introduced in Chapters 2,3,5,6 allow us to obtain certain aspects of the morphology but not all the details seen in the approach based on microhydrodynamics. This is the disadvantage of our approach. Its advantage is that the rheology comes out complete and the governing equations (that have to be solved to derive rheological and morphological predictions of the models) are relatively simple.

Having chosen the state variables, we continue and express the physics by filling the thermodynamic (GENERIC) framework. In particular, we need to specify the free energy and the dissipative thermodynamic forces. In Chapters 2 and 3, the free energy involves new terms addressing the shape of the membranes and the modification of the kinetic energy due to the flow perturbation caused by the presence of the membranes. In Chapter 5, we are including the Marangoni forces arising due to the nonuniformity of the distribution of the surface active agent on membranes. In Chapter 6 we are including mechanical forces inside the red blood cell membranes. As for the dissipative thermodynamic forces, we are using mainly the standard well known forces.

The new physics comes with new material parameters quantifying it. When dealing with a specific suspension, we need to find specific values of the material parameters characterizing it. In all cases discussed in the thesis we were able to establish, for most of the parameters, a relation between the microhydrodynamic material parameters (known from microhydrodynamic measurements) and our mesoscopic material parameters. The relation arises as a result of the comparison of a few particular situations that can be solved analytically and explicitly in both the microhydrodynamic and the mesohydrodynamic approaches.

Comparisons with results of experimental observations show that the meso-hydrodynamic models developed in this thesis can provide improved predictions over the ones reported in the literature. In Chapter 2, the active advection model of emulsions implies predictions that fit well the experimental data and represent an improvement of the Maffettone-Minale (1998) and Cox (1969) results for different values of the capillary number. The extended Doi-Ohta model in Chapter 3 also shows much better predictions than the original Doi-Ohta model, Lee-Park model (1994) and Wagner-Oettinger-Edwards model (1999). The rheology and

the morphology predicted by the model for the system with surface active agents developed in Chapter 5 compare well with results implied by other models and with results of experimental observations. In the case of membranes of red blood cells, the mesohydrodynamic model in Chapter 6 also indicates results that compare favorably with the microhydrodynamic model of Barthès-Biesel and Rallison (1981).

Chapter 8

Conclusion and Recommendations

8.1 Conclusion

This thesis investigates theoretically the rheology and morphology of suspensions involving freely moving soft membranes. Three different approaches have been used: (i) microhydrodynamic perturbation analysis, (ii) numerical boundary integral method of solving the microhydrodynamic governing equations, and (iii) mesoscopic rheological modeling. Several new models have been developed for suspensions with different types of membranes. All these models have been formulated in the thermodynamic (GENERIC) framework. They offer a more profound understanding of the observed flow behavior.

The principal achievements include:

a. The known mesoscopic models (as the Doi-Ohta model and the Maffettone-Minale model) are improved by including the active advection

In both the Doi-Ohta and the Maffettone-Minale models the interface is assumed to be passively advected. The interface however perturbs the flow. The perturbation then transforms the passive advection into a non-passive (i.e. active) advection. In the microhydrodynamic formulation the active advection arises naturally in the solution to the Stokes problem. We have developed an original

mesoscopic formulation of this problem. Predictions of our modified models are in agreement with experimental observations and with models based on microhydrodynamics.

b. A systematic approach was developed to determine the phenomenological coefficients

All mesoscopic models introduce material parameters quantifying the physics put into the models. The individual nature of the fluids under consideration is then expressed in these parameters. For a given fluid, their values can either be found by fitting some selected experimental observations that are regarded as material measurements (for example measurements of the viscosity coefficient in classical hydrodynamics) or by establishing a relation of the mesoscopic model to the microhydrodynamic model (in which the material parameters are assumed to be known). In all models presented in this thesis we have established such relation and used it to determine the values of the mesoscopic material parameters.

c. A Mesoscopic Rheological Model of immiscible blends with the interface covered with a surface active agent was developed

When a surface active agent is added to the immiscible blend, the most important new physics that arises is the transport, induced by the imposed flow, of the surface active agent on the interface. As a result, its distribution as well as the distribution of the surface tension on the surface of droplets become nonuniform. Such nonuniformity then brings about Marangoni forces and large deviations from the ellipsoidal shape of droplets. In order to be able to describe the morphology of the interfaces, we use in this thesis a family (a necklace) of conformation tensors. The transport on the surface of the droplet becomes the transport along the backbone of the necklace. For simplicity, in this thesis, the transport of surface active agent is obtained by the perturbation analysis for small deformed droplets. The model can predict the nonellipsoidal shape of the droplet which is similar to the one observed in experiments. The phenomenological parameters are determined analytically, no fitting parameters are need in the model. The results shows a good agreement with the experimental data and other models.

The strategy to use one parameter family of tensors (a necklace) as a state

variable can also be applied to the modeling of other complex fluids. It therefore widens the applicability of the tensor-type models.

d. A rheological model of suspensions of biological membranes was developed

Finally, we have extended the mesoscopic modeling of complex fluids to a new field, namely to suspensions of biological membranes. We take red blood cells as an example. To describe their morphology, we choose the Doi-Ohta state variables supplement them with an additional conformation tensor addressing the in-plane intramembrane deformations. The free energy is written by using the physical insight acquired in experimental observations. Both the elasticity and viscosity of the membrane are taken into account in the model.

The predicted rheological behavior is found to be qualitatively in agreement with experimental observations. The inferred material properties of the membranes are also found to be close those seen in direct experimental measurements.

8.2 Recommendations

The recommendations for the continuation of this research are as follows:

1. Other mesoscopic rheological models (as for example those arising in the modeling of fiber suspensions) can be extended by adopting the active advection.

2. As to the mesoscopic rheological modeling of immiscible blends with the interface covered with a surface active agent, we can consider the more realistic situations in which the convection of surface active agent is fully coupled with the morphology of the droplet. Another interesting topic is to study the influences of the elasticity of the bulk phases on the rheology of the droplets covered with a compatibilizer.

3. We can also study the effects of the viscosity ratio of the bulk phases and bending elasticity of the membranes on the rheology of the suspensions of red blood cells.

References

Acrivos A., Lo T. S., Deformation and breakup of a single slender drop in an extensional flow, J. Fluid. Mech. 86 (1978) 641-672.
Adamson A. W., Physical Chemistry of Surfaces, 3rd edn. John Wiley & Sons (1967).

Aris R., Vectors, Tensors, and the basic equations of fluid mechanics. Prentice-Hall. (1962).

Ashkin A., Dziedzic J. M., Internal cell manipulation using infrared laser traps, Proc. Natl Acad. Sci. USA 86 (1989) 7914-7918.

Baidakov V. G.,. Boltachev G. Sh, Chernykh G. G., Curvature corrections to surface tension, Phys. Rev. E 70 (2004) 011603.

Barthès-Biesel D., Acrivos A., Deformation and burst of a liquid droplet freely suspended in a linear shear field, J. Fluid Mech. 61 (1973)1-21.

Barthès-Biesel D., Rallison J. M., The time-dependent deformation of a capsule freely suspended in a linear shear flow, J. Fluid Mech. 113 (1981) 251-256.

Batchelor G. K., The stress system in a suspension of force-free particles, J. Fluid Mech. 41 (1970) 515-570.

Batchelor G. K., Green J. T., The determination of the bulk stress in a suspension of spherical particles to order c^2, J. Fluid Mech. 56 (1972) 401-427.

Bazhlekov I. B., Anderson P. D., Meijer H. E. H., Nonsingular boundary integral method for deformable drops in viscous flows, Phys. Fluids 16 (2004) 1064-1081.

Bazhlekov I. B., Anderson P. D., Meijer H. E. H., Numerical investigation of the effect of insoluble surfactants on drop deformation and breakup in simple shear

flow, Journal of Colloid and Interface Science 298 (2006) 369-394.

Beris A. N., Edwards B. J., Poisson bracket formulation of viscoelastic flow equations of differential type: A unified approach, J. Rheol. 34 (1990) 503-538.

Beris A. N., Edwards B. J., Thermodynamics of flowing systems. 1 st edn. Oxford University Press, New York (1994).

Blawzdziewicz J., Vlahovska P., Loewenberg M., Rheology of dilute emulsion of surfactant-covered spherical drops, Physica A 276 (2000) 50-85.

Booty M. R.. Siegel M., Steady deformation and the tip-streaming of a slender bubble with surfactant in an extensional flow, J.Fluid Mech. 544 (2005) 243-275.

Bousmina M., Bataille P., Sapieha S., Schreiber H. P., Comparing the effect of corona treatment and block copolymer addition on rheological properties of polystyrene/polyethylene blends, J. Rheol. 39 (1995) 499-517.

Brahimi B., Ait-Kadi A., Ajji A., Jerome R., Fayt R., Rheological properties of copolymer modified polyethylene/polystyrene blends, J. Rheol. 35 (1991) 1069-1090.

Brooks D. E., Goodwin J. W., Seaman G. V. F., Interactions among Erythrocytes under Shear, J. Appl. Physiol., 28 (1970) 172-177.

Byers T. J., Branton D., Visualization of the protein associations in the erythrocyte membrane skeleton, Proc. Natl. Acad. Sci. USA 82 (1985) 6153-6157.

Cahn J. W., Hilliard J. E., Free energy of a nonuniform system. I. Interfacial free energy, J. Chem. Phys. 28 (1958) 258.

Carr R., Cokelet G. R., Rheology of Suspensions of Normal and Hardened Erythrocytes and their Mixtures, J. Rheol. 25 (1981) 67-82.

Chien S., Usami S., Dellenback R. J., Bryant C. A., Gregersen M. I., Changes of Erythrocyte Deformability During Fixation in Acetaldehyde, in Theoretical and Clinical Hemorheology, H. H. Hartert, A. L. Copley, Eds. Springer-Verlag, Berlin (1971).

Chien S., Usami S., Dellenback R. J., Gregersen M. I., Am. J. Physiol. 219 (1970) 136-142.

Choi S. J., Schowalter W. R., Rheological properties of non-dilute suspensions of deformable particles, Phys. Fluids 18 (1975) 420-427.

Cokelet G. R., The Rheology of Human Blood, in Biomechanics: Its Foundations and Objectiues, Y. C. Fung, N. Perrone, and M. Anliker, Eds., Prentice-Hall, Englewood Cliffs, NY, (1972) 63-104.

Cox R. G., The deformation of a drop in a general time-dependent fluid flow, J. Fluid Mech. 37 (1969) 601-623.

Danker G., Verdier C., Misbah C., Rheology and dynamics of vesicle suspension in comparison with droplet emulsion, J. Non-Newtonian Fluid Mech. 152 (2008) 156-167.

Das N. C., Wang H., Mewis J., Moldenaers P., Rheology and microstructures formation of immiscible model polymer blends under steady state and transient flows, Journal of Polymer Science: Part B: Polymer Physics, 43 (2005) 3519-3533.

de Bruijn R. A., Deformation and breakup of drops in simple shear flows. PhD thesis, Technische Universiteit Eindhoven (1989).

de Bruijn R. A., Tipstreaming of drops in simple shear flows, Chemical Engineering Science 48 (1993) 277-284.

Doi M., Ohta T., Dynamics and rheology of complex interfaces, J. Chem. Phys. 95 (1991) 1242-1248.

Dressler M., Edwards B. J., The influence of matrix viscoelasticity on the rheology of polymer blends, Rheol. Acta 43 (2004) 257-282.

Drochon A., Barthès-Biesel D., Lacombe C., Lelievre L. C, Determination of the Red Blood Cell Apparent Membrane Elastic Modulus From Viscometric Measurements, J. Biomech. Eng. 112 (1990) 241-249; Erratum, 113 (1991) 103.

Drochon A., Rheology of dilute suspensions of red blood cells: Experimental and theoretical approaches, Eur. Phys. J.: Appl. Phys. 22 (2003) 155-162.

Drumright-Clark M. A., Renardy Y., The effect of insoluble surfactant at dilute concentration on drop breakup under shear with inertia. Physics of Fluids 16 (2004) 14-21.

Edwards B. J., Dressler M., Grmela M., Ait-Kadi A., Rheological models with microstructural constraints, Rheol. Acta 42 (2003) 64-72.

Eggleton C. D., Pawar Y. P., Stebe K. J., Insoluble surfactants on a drop in an extensional flow: a generalization of the stagnated surface limit to deforming interfaces. Journal of Fluid Mechanics 385 (1999) 79-99.

Eggleton C. D., Popel A. S., Physics of fluids, Large deformation of red blood cell ghosts in a simple shear flow, Physics of fluid 10 (1998) 1834-1845.

Eggleton C. D., Stebe K. J., An adsorption-desorption-controlled surfactant on a deforming droplet. Journal of Colloid and Interface Science 208 (1998) 68-80.

Eggleton C. D., Tsai T.-M., Stebe K. J., Tip streaming from a drop in the presence of surfactants. Physical Review Letters 87 (2001) 048302.

Elmans P. H. M., Bos H. L., Janssen J. M. H., Meijer H. E. H., Transient Phenomena in dispersive mixing, Chemical Engineering Scince 48 (1993) 267-276.

Eshelby J. D., The determination of elastic field of an ellipsoidal inclusion, and related problems, Proc. R. Soc. London, Ser. A 241 (1957) 376-396.

Eshelby J. D., The elastic field outside of an ellipsoidal inclusion, Proc. R. Soc. London A 252 (1959) 561-569.

Evans E., Bending elastic modulus of red blood cell membrane derived from buckling instability in micropipette aspiration test, Biophys. J. 43 (1983) 27-30.

Evans E., New membrane concept applied to the analysis of fluid shear and micropipette-deformed red blood cells, Biophys. J. 13 (1973) 941-954.

Evans E., Minimum energy analysis of energy deformation applied to pipette aspiration and surface adhesion of red blood cells, Biophys. J. 30 (1980) 265-284.

Evans E. A., Hochmuth R. M., Membrane viscoelasticity, Biophys. J. 16 (1976) 1-11.

Evans E. A., Needham D., Cohesive properties of lipid bilayer membranes containing cholestrol, J. Phys. Chem. 91 (1987) 4219-4228.

Evans E. A., Skalak R., Mechanics and Thermodynamics of Biomembranes, CRC, Boca Raton, FL, (1980).

Evans E. A., Waugh R. E., Osmotic correction to elastic are compressibility measurements on red cell membrane, Biophys. J. 20 (1977) 307-313.

Evans E. A., Waugh R. E., Melnik L., Elastic area compresibility modulus of red cell membrane, Biophys. J. 16 (1976) 585-595.

Evans E. A., Yeung A., Apparent viscosity and cortical tension of blood granulocytes determined by micropipette aspiration, Biophys. J. 56 (1989) 151-160.

Feigl K., Megias-Alguacil D., Fischer P., Windhab E. J., Simulation and experi-

ments of droplet deformation and orientation in simple shear flowwith surfactants, Chemical Engineering Science 62 (2007) 3242-3258.

Filippone G., Netti P. A., Acierno D., Microstructural evolutions of LDPE/PA6 blends by rheological and rheo-optical analyses: Influence of flow and compatibilizer on break-up and coalescence processes, Polymer 48 (2007) 564-573.

Fischer T., Schmid-Schnbein H., Blood Cells, Mol. Dis. 3 (1977) 351-365.

Fischer T., Stohr-Liesen M., Schmid-Schonbein H., The red cell as a fluid drop: Tank treading-like motion of human erythrocyte membrane in shear flow, Science 202 (1978) 894-896.

Flumerfelt R. W., Effects of dynamic interfacial properties on drop deformation and orientation in shear and extensional flow fields, J. Colloid Interface Sci. 76 (1980) 330-349.

Frankel N. A., Acrivos A., The constitutive equation for a dilute emulsion. J. Fluid Mech. 44 (1970) 65-78.

Germain Y., Ernst B., Genelot O., Dhamani L., Rheological and morphological analysis of compatibilized polypropylene/polyamide blends, J. Rheol. 38 (1994) 681-697.

Gordon R. J., Schowalter W. R., Anisotropic fluid theory: A different approach to the dumbbell theory of dilute polymer solutions, Trans. Soc. Rheol. 16 (1972) 79-97.

Grace H. P., Dispersion phenomena in high viscosity immiscible fluid systems and applications of static mixers as dispersion devices in such systems, Chem. Eng. Commun. 14 (1982) 225-277.

Graebling D., Froelich D., Muller R., Viscoelastic properties of polydimethylsiloxane-polyoxyethylene blends in the melt. Emulsion model, J Rheol. 33 (1989) 1283-

1291.

Graebling D., Muller R., Rheological behavior of polydimethylsiloxane/polyoxyethylene blends in the melt. Emulsion model of two viscoelastic liquids, J. Rheol. 34 (1990) 193-205.

Graebling D., Muller R., Palierne J. F., Linear viscoelastic behavior of some incompatible polymer blends in the melt. Interpretation of data with a model of emulsion of viscoelastic liquids, Macromolecules 26 (1993) 320-329.

Gramespacher H., Meissner J., Interfacial tension between polymer melts measured by shear oscillations of their blends, J Rheol. 36 (1992) 1127-1141.

Grizzuti N., Buonocore G., Iorio G., Viscous behavior and mixing rules for an immiscible model polymer blend, J. Rheol. 44 (2000) 149-164.

Grmela M., Particle and bracket formulations of kinetic equations, Contemp. Math. 28 (1984) 125-132.

Grmela M., Hamiltonian dynamics of incompressible elastic fluids, Phys. Lett A 130 (1988) 81-86.

Grmela M., Bracket Formulation of Diffusion-Convection Equation, Physica D 21 (1986) 179-212.

Grmela M., Mesoscopic dynamics and thermodynamics: applications to polymeric fluids, in: J. Casas-Vazquez, D. Jou (Eds.), Rheological Modelling: Thermodynamic and Statistical Approaches, Lecture Notes in Physics, vol. 381, Springer, Berlin, 1991, pp. 99-125.

Grmela M., Stress Tensor in Generalized Hydrodynamics, Phys. Letters A 111 (1985) 41-44.

Grmela M., Reciprocity relations in thermodynamics. Physica A 309 (2002) 304-

328.

Grmela M., Ait-Kadi A., J. Non-Newtonian Fluid Mech. 55 (1994) 191-1994.

Grmela M., Bousmina M., Palierne J. F., On the rheology of immiscible blends, Rheol. Acta 40 (2001) 560-569.

Grmela M., Oettinger H. C., Dynamics and thermodynamics of complex fluids. Part I. Illustration of a general formalism, Phys. Rev. E 56 (1997) 6620-6632.

Gu J. F., Grmela M., GENERIC Model of Active Advection, J. Non-Newtonian Fluid Mech. 152 (2008) 12-26.

Gu J. F., Grmela M., Flow Properties of Immiscible Blends: Doi-Ohta Model with Active Advection, (2008) accepted by Phys. Rev. E.

Gu J. F., Grmela M., Bousmina M., A mesoscopic rheological model of immiscible blends with the interface covered with a surface active agent, Physics of Fluids. 20 (2008) 043102.

Guenther G. K., Baird D. G., An evaluation of the DoiCOhta theory for an immiscible polymer blend, J. Rheol. 40 (1996) 1-20.

Guido S., Villone M., Three-dimensional shape of a drop under simple shear flow, J Rheol. 42 (1998) 395-415.

Ha J. W., Yoon Y., Leal L. G., The effect of compatibilizer on the coalescence of two drops in flow, Phys. Fluids 15 (2003) 849-867.

Henon S., Lenormand G., Richter A., Gallet F., A new determination of the shear modulus of the human erythrocyte membrane using optical tweezers, Biophys. J. 76 (1999) 1145-1151.

Hinch E. J., Acrivos A., Long slender drops in a simple shear flow, J. Fluid.

Mech. 98 (1980) 305-328.
Hochmuth R. M., Waugh R. E., Erythrocyte membrane elasticity and viscosity. Ann. Rev. Physiol. 49 (1987) 209-219.

Hochmuth R. M., Worthy P. R., Evans E. A., Red cell extensional recovery and the determination of membrane viscosity, Biophys. J. 26 (1979) 101-114.

Hu Y. T., A. Lips, Estimating Surfactant Surface Coverage and Decomposing its Effect on Drop Deformation, Physical Review letters, 91 (2003) 044501-1-4.

Hu Y. T., Pine D. J., Leal L. G., Drop deformation, breakup, and coalescence with compatibilizer, Phys. Fluids 12 (2000) 484-489.

Huitric J., Moana M., Carreau P. J., Dufaure N., Effect of reactive compatibilization on droplet coalescence in shear flow, J. Non-Newtonian Fluid Mech. 145 (2007) 139-149.

Huitric J., Moana M.,. Klopffer M. -H, Modelling of the nonlinear behavior of compatibilized polyethylene/polyamide blends in shear and extensional flows, Canadian J. Chem. Eng. 80 (2002) 1051-1056.

Iza M., Bousmina M., Nonlinear rheology of polymer blends: Relaxation result, J. Rheol. 44 (2000) 1363-1384.

Jackson N. E., Tucker C. L., A model for large deformation of an ellipsoid droplet with interfacial tension, J. Rheol. 47 (2003) 659-682.

Jacobs U., Fahrlander M., Winterhalter J., Friedrich C., Analysis of palierne's emulsion model in the case of viscoelastic interfacial properties, J. Rheol. 43 (1999) 1495-1509.

Jafaria S. H., Potschkea P., Stephana M., Warthb H., Alberts H., Multicomponent blends based on polyamide 6 and styrenic polymers: morphology and melt rheology, Polymer 43 (2002) 6985-6992.

Jansen K. M. B.,. Agterof W. G. M, Mellema J., Droplet breakup in concentrated emulsions, J. Rheol. 45 (2001) 227-236.

Janssen J., Dynamics of liquid-liquid mixing, Ph.D. thesis, Eindhoven University (1993).

JanssenJ. J. M., Boon A., Agterof W. G. M., Influence of dynamic interfacial properties on droplet breakup in plane hyperbolic flow, AIChE Journal 43 (1997) 1436-1447.

Jansseune T., Vinckier I., Moldenaers P., Mewis J., Transient stresses in immiscible model polymer blends during start-up flows, J. Non-Newtonian Fluid Mech. 99 (2001) 167-181.

Jeffery G. B., The motion of ellipsoidal particles immersed in a viscous fluid, Proc. R. Soc. Lond. A 102 (1922) 181-179.

Jeon H. K., Macosko C. W., Visualization of block copolymer distribution on a sheared drop, Polymer 44 (2003) 5381-5386.

Junk M., Illner R., A new derivation of Jeffery's equation, J. math, fluid mech. 8 (2006) 1-34.

Kantsler V., Steinberg V., Transition to Tumbling and Two Regimes of Tumbling Motion of a Vesicle in Shear Flow, Phys. Rev. Lett. 96 (2006) 036001.

Khakhar D. V., Ottino J. M., Deformation and breakup of slender drops in linear flows, J. Fluid. Mech. 166 (1986) 265-285.
Kim S., Karilla S. J., Microhydrodynamics, Butterworth-Heinemann (1991).

Kruijt-Stegeman Y. W., van de Vosse F. N., Meijer H. E. H., Droplet behavior in the presence of insoluble surfactants. Physics of Fluids 16 (2004) 2785-2796.

Lacroix C., Grmela M., Carreau P. J., Relationships between rheology and morphology for immiscible molten blends of polypropylene and ethylene copolymers under shear flow, J. Rheol. 42 (1998) 41-62.

Lamb N., Hydrodynamics, 6th ed.,Dover, New York, (1945).
Lee H. M. Park, O. O., Rheology and dynamics of immiscible polymer blends, J. Rheol. 38 (1994) 1405-1425.

Lee J., Pozrikidis C., Effect of surfactants on the deformation of drops and bubbles in Navier-Stokes flow, Computers and Fluids, 35 (2006) 43-60.

Li X., Pozrikidis C., The effect of surfactants on drop deformation and on the rheology of dilute emulsions in Stokes flow. J. Fluid Mech. 341 (1997) 165-149.

Li J. , Renardy Y., Renardy M., Numerical simulation of breakup of a viscous drop in simple shear flow through a volume-of-fluid method, Physics of Fluids 12 (2000) 269-282.

Lyu S., Jones T. D., Bates F. S., Macosko C. W., Role of block copolymers on suppression of droplet coalescence, Macromolecules 35 (2002) 7845-7855.

Macaubas P. H. P., Demarquette N. R., Dealy J. M., Nonlinear viscoelasticity of PP/PS/SEBS blends, Rheol. Acta 44 (2005) 295-312.

Macosko C. W., Guegan P., Khandpur A. K., Nakayama A., Marechal P., Inoue T., Compatibilizers for melt blending: Premade block copolymers, Macromolecules 29 (1996) 5590-5598.

Mader M., Vitkova V., Abkarian M., Viallat A., Podgorski T., Dynamics of viscous vesicles in shear flow, Eur. Phys. J. E. 19 (2006) 389-397.

Maffettone P. L., Minale M., Equation of change for ellipsoidal drops in viscous flow, J. Non-Newtonian Fluid Mech., 78 (1998) 227-241.

Marsden J. E., Ratiu T. S., Introduction to mechanics and symmetry, 2nd ed. in: Texts in Applied Mathematics, vol 17, Springer-Verlag (1999).

Marsden J. E., Weinstein A., Coadjoint orbits, vortices, and Clebsch variables for incompressible fluids, Physica D 7 (1983) 305-323.

Martin J. D., Velankar S. S., Effects of compatibilizer on immiscible polymer blends near phase inversion, J. Rheol. 51 (2007) 669-692.

Megias-Alguacil D., Fischer P., Windhab E. J., Determination of the interfacial tension of low density difference liquid-liquid systems containing surfactants by droplet deformation methods, Chem. Eng. Sci. 61 (2006) 1386-1394.

Mekhilef N., Favis B. D., Carreau P. J., Morphological stability, interfacial tension, and dual-phase continuity in polystyrene-polyethylene blends, Journal of Polymer Science: Part B: Polymer Physics 35 (1997) 293-308.

Milliken W. J., Leal L. G., The influence of surfactant on the deformation and breakup of a viscous drop: the effect of surfactant solubility. Journal of Colloid and Interface Science 166 (1994) 275-285.

Milliken W. J., Stone H. A., Leal L. G., The effect of surfactant on transient motion of newtonian drops, Phys. Fluids A 5 (1993) 69-79.

Minale M., Moldenaers P., Study of the morphological hysteresis in immiscible polymer blend, AIChE J 44 (1998) 943-950.

Minale M., Moldenaers P., Mewis J., Effect of shear history on the morphology of immiscible polymer blends, Macromolecules 30 (1997) 5470-5475.

Moan M., Huitric J., Mederic P., Jarrin J., Rheological properties and reactive compatibilization of immiscible polymer blends, J. Rheol. 44 (2000) 1227-1245.

Oettinger H. C., Beyond Equilibrium Thermodynamics, Wiley-Interscience (2005).

Oettinger H. C.,, Grmela M., Dynamics and thermodynamics of complex fluids. Part II. Development of a general formalism, Phys. Rev. E 56 (1997) 6632-6655.

Pal R., Rheology of concentrated suspensions of deformable elastic particles such as human erythrocytes, J.Biomech. 32 (2003) 601-608.

Palierne J. F., Linear rheology of viscoelastic emulsions with interfacial tension, Rheol. Acta 29 (1990) 204-214; Erratum 30 (1991) 497.

Pawar Y., Stebe K. J., Marangoni effects on drop deformation in an extensional flow: the role of surfactant physical chemistry. I. Insoluble surfactants. Physics of Fluids A 8 (1996) 1738-1751.

Pellicer J., Manzanares J. A., Mafe S., Am. J. Phys. 63 (1995) 542

Phillips W. J., Graves R. W., Flumerfelt R. W., Experimental studies of drop dynamics in shear fields: role of dynamic interfacial effects, J. Colloid Interface Sci. 76 (1980) 350-370.

Potschke P., Paul D. R., Formation of co-continuous structures in melt-mixed immiscible polymer blends, J. Macromol. Sci.-Pol. R. 1 (2003) 87-141.

Pozrikidis C., Boundary Integral and Singularity Methods for Linearized Viscous Flow. Cambridge: Cambridge University Press (1992).

Pozrikidis C., Numerical Computation in Science and Engineering. New York: Oxford Univ. Press (1998).

Pozrikidis C., Finite deformation of liquid capsules enclosed by elastic membranes in simple shear flow, J. Fluid Mech. 297 (1995) 123-152.

Pozrikidis C., numerical simulation of the flow-induced deformation of red bllod cells, Annals of Biomedical Enginnering 31 (2003) 1194-1205.

Puyvelde P. V., Velanker S., Mewis J., Moldenaers P., Effect of Marangoni Stress on the Deformation and Coalescence in compatibiliaed immiscible polymer blends, Polymer Engineering and Sciece. 42 (2002) 1956-1964.

Rallison J. M., Note on the time-dependent deformation of a viscous drop which is almost spherical, J. Fluid Mech. 98 (1980) 625-633.

Rallison J.M., Acrivos A., A numerical study of the deformation and burst of a viscous drop in general shear flows. J. Fluid Mech. 89 (1978) 191-200.

Ramanujan S., Pozrikidis C., Deformation of liquid capsules enclosed by elastic membranes in simple shear flow: large deformations and the effect of fluid viscosities, J. Fluid Mech. 361 (1998) 117-143.

Renardy Y., Renardy M., Cristini V., A new volume-of-fluid formulation for surfactants and simulations of drop deformation under shear at a low viscosity ratio. European Journal of Mechanics B/Fluids 21 (2002) 49-59.

Riemann R. -E., Cantow H. -J., Friedrich C., Rheological investigation of form relaxation and interface relaxation processes in polymer blends, Polymer Bulletin 36 (1996) 637-643.

Riemann R. -E., Cantow H. -J., Friedrich C., Interpretation of a new interface-governed relaxation processes in compatibilized polymer blends, Macromolecules 30 (1997) 5476-5484.

Sailer C., Handge U. A., Melt Viscosity, Elasticity, and Morphology of Reactively Compatibilized Polyamide6/Styrene-Acrylonitrile Blends in Shear and Elongation, Macromolecules 40 (2007) 2019-2028.

Schiesser W. E., The numerical methods of lines. Academic press, Inc. (1991)

Scholz P., Froelich D., Muller R., Viscoelastic properties and morphology of two-

phase polypropylene/polyamide 6 blends in the melt. Interpretation of results with an emulsion model, J. Rheol. 33 (1989) 481-499.

Sheetz M., Laser Tweezers in Cell Biology, Academic Press, San Diego (1998).

Singer S. J., Nicolson G. L., The fluid mosaic model of the structure of cell membranes, Science 175 (1972) 720-731.

Stone H. A., Relaxation and breakup of an initially extended drop in an otherwise quiescent fluid. J. Fluid Mech. 198 (1989) 399-427.

Stone H. A., Leal L. G., The effects of surfactants on drop deformation and breakup, J. Fluid Mech. 220 (1990) 161-186.

Sundararaj U., Macosko C. W., Drop breakup and coalescence in polymer blends-the effects of concentration and compatibilization, Macromolecules 28 (1995) 2647-2657.

Takahashi Y., Kurashima N., Noda I., Doi M., Experimental tests of the scaling relation for textured materials in mixtures of two immiscible fluids, J. Rheol. 38 (1994) 699-712.

Taylor G. I., The viscosity of a fluid containing small drops of another fluid, Proc. Roy. Soc. A 138 (1932) 41-48.

Taylor G. I., The formation of emulsions in definable field of flow, Proc. Roy. Soc. A 146 (1934) 501-523.

Taylor G. I., Conical free surface and fluid interfaces, Proc. 11th Int. congr. Appl. Mech., Munich, (1967) pp.790-796.

Tola R. T., Groeninckxa G., Vinckierb I., Moldenaersb P., Mewis J., Phase morphology and stability of co-continuous (PPE/PS)/PA6 and PS/PA6 blends: effect of rheology and reactive compatibilization, Polymer 45 (2004) 2587-2601.

Torza S., Cox R. G., Mason S. G., Particle motions in sheared suspensions. XVII. Transient and steady deformation and burst of liquid drops, J. Colloid Interface Sci. 38 (1972) 395-411.

Tucker III C. L., Moldenaers P., Microstructural evolution in polymer blends, Annu. Rev. Fluid Mech. 34 (2002) 177-210.

Van Hemelrijck E., Van Puyvelde P., Macosko C. W., Moldenaers P., The effect of block copolymer architecture on the coalescence and interfacial elasticity in compatibilized polymer blends, J. Rheol. 49 (2005) 783-798.

Van Hemelrijck E., Van Puyvelde P., Moldenaers P., Rheology and morphology of highly compatibilized polymer blends, Macromol. Sym. 233 (2006) 51-58.

Van Hemelrijck E., Van Puyvelde P., Velankar S., Macosko C. W., Moldenaers P., Interfacial elasticity and coalescence suppression in compatibilized polymer blends, J. Rheol. 48 (2004) 143-158.

Van Puyvelde P., Velankar S., Mewis J., Moldenaers P., Leuven K. U., Effect of Maragoni stress on deformation and coalescence in compatibilized immiscible polymer blends, Polymer Eng. Sci. 42 (2002) 1956-1964.

Velankar S., Van Puyvelde P., Mewis J., Moldenaers P., Steady shear rheological properties of model compatibilized blends, J. Rheol. 48 (2004) 725-744.

Velankar S., Van Puyvelde P., Mewis J., Moldenaers P., Effect of compatibilization on the breakup of polymeric drops in shear flow, J. Rheol. 45 (2001) 1008-1019.

Verdier C., Rheological Properties of Living Materials. From Cells to Tissues, Journal of Theoretical Medicine 5 (2003) 67-91.

Vinckier I., Laun H. M., Assessment of the Doi-Ohta theory for co-continuous

blends under oscillatory flow, J. Rheol. 45 (2001) 1373-1385.

Vinckier I., Minale M., Mewis J., Moldenaers P., Rheology of semi-dilute emulsions: viscoelastic effects caused by the interfacial tension, Colloids Surf. A: Physicochem. Eng. Aspects 150 (1999) 217-228.

Vinckier I., Moldenaers P., Mewis J., Relationship between rheology and morphology of model blends in steady shear flow, J Rheol 40 (1996) 613-631.

Vinckier I., Moldenaers P., Mewis J., Transient rheological response and morphology evolution of immiscible polymer blends, J. Rheol. 41 (1997) 705-718.

Vlahovska P. M., Loewenberg M., Blawzdziewicz J., Deformation of a surfactant-covered drop in a linear flow, Phys. Fluids 17 (2005) 103103-1-18.

Wagner J., Ottinger H. C., Edwards B. J., Generalized DoiCOhta Model for Multiphase Flow Developed via GENERIC, AIChE. J. 45 (1999) 1169-1181.

Wetzel E. D., Tucket III C. L., Droplet deformation in dispersions with unequal viscosities and zero interfacial tension, J. Flui Mech. 426 (2001) 199-228.

Wieringa J. A., van Dieren F., Janssen J. J. M., AgterofW. G. M., Droplet breakup mechanisms during emulsification in colloid mills at high dispersed phase volume fractions, Trans. Inst. Chem. Eng. 74A (1996) 554-561.

Yeung A., Evans E., Cortical shell-liquid core model for passive flow of liquid-like spherical cells into micropipets, Biophys. J. 56 (1989) 139-149.

Yu W., Bousmina M., Ellipsoidal model for droplet deformation in Newtonian systems. J Rheol 47 (2003) 1011-1039.

Yu W., Bousmina M., Grmela M., Palierne J. -F., Zhou C., Quantitative relationship between rheology and morphology in emulsions, J. Rheol. 46 (2002) 1381-1399.

Zhou H., Pozrikidis C., Deformation of capsules with incompressible interfaces in simple shear flow, J. Fluid Mech. 283 (1995) 175-200.